Title

Interrogating the interplay between hydrogel electrical and physical properties to direct cell behavior and function

Author

Casella, Alena Theresa

Publication Date

2023

Peer reviewed|Thesis/dissertation

Interrogating the interplay between hydrogel electrical and physical properties to direct cell behavior and function

By

ALENA CASELLA
DISSERTATION

Submitted in partial satisfaction of the requirements for the degree of

DOCTOR OF PHILOSOPHY

in

Biomedical Engineering

in the

OFFICE OF GRADUATE STUDIES

of the

UNIVERSITY OF CALIFORNIA

DAVIS

Approved:

J. Kent Leach, Chair

Alyssa Panitch

Erkin Şeker

Tina Jeoh

Committee in Charge

2023

Acknowledgements

I am deeply and sincerely grateful to my advisors, Professor J. Kent Leach and Professor Alyssa Panitch. Not only have they put up with my adverbs for 5.5 years, they have also been immensely supportive mentors and role models. I know co-mentoring me was unconventional, but I thank you both for taking a chance and not giving up on me when I wanted to give up on myself. Kent, thank you for coaching me in creating a bias toward action. You helped me see that trying something builds skills and confidence that no amount of reading and planning can, even in the face of failure. Thank you for your diligent and intentional mentorship and for celebrating the accomplishments of your trainees. Alyssa, thank you for always seeing the big picture, and for reminding me when I lost sight of it. Thank you for creating an environment where research really is an intellectual playground, and for providing a safety net (*i.e.*, a veritable wealth of knowledge about polymers and chemistry and many other subjects) when all turns seemed to be "lefts".

Professor Şeker, thank you, and your students, especially Dr. Jovana Veselinovic, for helping me identify challenges at the beginning of my project. Your patience explaining fundamentals of electrical characterization and your willingness to troubleshoot my first attempts helped me gain early momentum. Thank you for asking challenging questions and offering encouragement during annual data meetings. You have provided a unique perspective about my project that has helped me grow as a researcher.

Professor Tina Jeoh, I am so glad Dr. Sam Tucci introduced me to the STEM for Girls team. Working with you and the other talented students you recruit for the organizing committee has taught me so much about teamwork and leadership, and I had a lot of fun along the way. Thank you for serving on my committee and for your unwavering encouragement.

Graduate school would not have been the same without the intellectual stimulation, emotional support, and friendship of my lab-mates. Dr. Vanessa Franco Carvalho Dartora, Emily Misnick, M.S., Dr. Nelda Vázquez-Portalatín, Dr. Tanaya Walimbe, Dr. Marcus Deloney, Dr. Tima Dehghani, Dr. Hark Sodhi, Dr. Michael Nguyen, and Neona Lowe, M.S., thank you for making the Panitch lab such a fun-loving environment. I am not sure I have ever met a group of people so accepting and bright and willing to dive into the trenches with me. I will always remember my time with you being full of laughter and cheer. To Dr. Ben Hung, Dr. Tomas Gonzalez-Fernandez, Dr. Jenna Harvestine, Dr. Jackie Woods, Dr. Charlotte Vorwald, Takeyah Campbell, M.S., Dr. Marissa Gionet-Gonzales, Nicole Wegrzyniak, B.S., Dr. David H. Ramos-Rodriguez, Katie Griffin, B.S., Bobby Gresham, B.S., Jeremy Lowen, B.S., Vicky Thai, B.S., Nick Johnson, M.S., Sabrina Mierswa, B.S., Shierly Fok Lau, M.S., Andie Filler, B.S., Alex Kermani, M.S., and Erika Wheeler, M.S., I have learned so much by working alongside all of you. Thank you for pushing me to be a better scientist and for answering my many questions as I was getting my sea legs after boarding the tightly run ship that is the Leach lab. Words cannot express how grateful I am to have met and worked with two such wonderful teams.

I must also give thanks to each of my funding sources, without whom I imagine graduate school would have been even more challenging. Being offered the Floyd and Mary Schwall Fellowship in Medical Research and the UC Davis Dean's Distinguished Graduate Fellowship before performing a single experiment was an open-armed welcome from the university for which I will be forever humbled. I am also very grateful to Ms. Barbara Wolfe and the Northern California chapter of the ARCS Foundation for supporting my research efforts and instilling in me a vote of confidence at a time when I was lacking. Many thanks, as well, to the Society of Women Engineers and BMEGG for their scholarships and awards.

For answering my many questions without overt exasperation, I thank Christal Wintersmith, Kristine Pierce, and Ivonne Palma. Christal, thank you for always having an open door and for helping me navigate trying to meet multiple goals simultaneously. The same can be said of Dr. Denneal Jamison-McClung, who I must thank for assuming the mantle of the Biotechnology program, through which I have learned so much and made many great connections. Thank you, Denneal, for connecting me with Dr. Jenna Gallegos and Dr. Sydney Wyatt, too, who were kind enough to let me work alongside them at Samba Scientific as an intern while also trying to finish a PhD. I must also thank the DEB superstar, Dr. Judy Kjelstrom, for being such an inspiration and for bestowing me with her science communication award at the 2022 DEB retreat. Dr. Lyndsey Ruiz, thank you for your dedication to improve graduate student career prospects and directing the Leaders for the Future Program. To this day, I am still amazed by the email of resources and opportunities you sent me about working in life sciences venture capital.

BESA is a crown jewel of BMEGG and I cannot thank the organization enough for creating such a strong sense of community, especially amongst the students. The events BESA organized both on and off campus were such an important vehicle for my engagement throughout graduate school, and all the students who invested time and energy into sustaining the association's mission have my sincere gratitude.

Thank you to Professor Rebecca Willits for welcoming me into her lab at the University of Akron in 2013. It was the start of a journey I never envisioned for myself, but her guidance and mentorship put me on strong path during my undergraduate degree and opened the door to higher education. I must also thank her for fostering a group of scientists who inspire me to this day: Dr. Jessica Stukel Shah, Dr. Sarah Snyder, Dr. Hannah Cebull, and Carli DeJulius, B.S., among others.

To my friends, both in and outside of the lab, I truly don't know what I would have done without you these past years. Tima, Hark, Katie, Bobby, and Takeyah, you are part of so many cherished memories from graduate school that I hope last a lifetime. Dr. Pete Sariano, Dr. Liz Li, Dr. Noah Pacifici, and Dr. Emmet Francis, you all inspired me with your brilliance, hard work, and kindness, and I count myself lucky to have met you. Dr. Christian Silva, I am thrilled we were able to overlap in Davis for a few years. It was a blast reliving memories from our childhood and teenage years, and it was great to make new ones in this chapter of life. Dr. Caroline David, thank you for your well-timed advice and for making it seem like our friendship hadn't missed a beat, even when we were living thousands of miles apart. Also, thank you for sharing many writing and formatting tips that were highly useful for preparing this very document.

To my family, thank you for your love and being my greatest source of inspiration. To my mom and dad, thank you for raising me to be curious, to strive for excellence in everything I do, and for instilling in me that I can achieve anything I set my mind to. Mom, thank you for being my role model, for grounding me when I was distressed, and for never casting a shadow of doubt that I would cross this finish line. Dad, thank you for embodying the engineer who gets their hands dirty and has fun doing it. There were many times in lab when I approached a problem how you I thought you might, and I learned a great deal from those experiences. Steve, thank you for always being willing to share your advice about any- and everything. Thank you, too, for giving me practice answering direct questions – it came in handy for fielding questions from committee members. To Anna and Lucia, your sisterhood and friendship has been such an incredible enrichment in my life, and I am so grateful to have had you both by my side. To Matthew, Shane, Michael, Lexus, Laura, Zach, Monica, Eric, Ian, Kacie, and Reed, thank you for making holidays such a joy and reminding me that there is a bigger world outside academia.

Finally, and with a full heart: Parker, thank you for being my rock during the whirlwind that is graduate school. You made many sacrifices to join me in this journey and, despite those sacrifices, you always cheered me on, even as I continued to say “yes” to too many things. Thank you for reminding me that not everything in life needs to be efficient, that rest is important, and that the future is bright.

Abstract

Tissue engineering aims to combine cells, soluble cues, and biomaterials to repair tissue injuries that surpass the body's innate healing ability. While physical and chemical aspects of regeneration are well-represented in this paradigm, electrical cues are not. This is a significant oversight, as bioelectricity, voltage-mediated communication between cells, plays a critical role in homeostatic and regenerative events *in vivo*. To address this shortcoming, researchers have included electrically conductive additives in biomaterials to mimic the electrical activities and environment cells and tissues experience during healing. Cells grown on conductive substrates frequently demonstrate improved behaviors such as proliferation, differentiation, and maturation, even in the absence of electrical stimulation. While these results are promising, their mechanism of action is not well understood. Additionally, the potential for conductive materials to direct cells has drawn attention away from characterizing how a material's conductivity and biophysical properties influence each other. Examining both characteristics is important since the physical properties of a material are also well-known to orchestrate cell behavior.

For this work, we sought to develop an electrically and mechanically tunable hydrogel platform that could be used to interrogate the relationship between these two properties and understand how their interplay influences cells towards regeneration. The studies conducted for this work involve an electrically conductive, synthetic, conjugated polymer, referred to as PEDOT:PSS, and we mixed it with two well-known hydrogel materials, agarose and polyethylene glycol. We established conditions under which the

electrical and mechanical properties of these hydrogels were decoupled, then demonstrated mesenchymal stromal cells had improved adhesion and spreading on conductive gels over non-conductive ones. To explain this observation, we used solutions of proteins with different isoelectric points (hence different charged in physiological pH) to understand the hydrogels' surface characteristics. More proteins adsorbed to conductive gels, suggesting greater surface charge. These studies begin to fill foundational knowledge gaps by providing a high-level understanding of how electroactive materials improve cell behavior, even in the absence of external stimulation.

We next investigated how the interplay of conductivity and the physical cue, porosity, facilitated myogenic differentiation for muscle tissue engineering applications. Myoblasts grown in conductive microporous scaffolds had markedly greater myosin heavy chain expression at both the gene and protein level. Upregulation of this late myogenic marker is indicative of maturation, suggesting the importance of both electroactivity and microporosity for muscle generation.

These studies help improve our understanding of cell interactions with electrically conductive biomaterials which begin to address important deficits within the field. We hope this work contributes to the development of materials that are intentionally designed to recapitulate the electrical environment of healing or that facilitate communication between endogenous and implanted tissue. We believe such a material would have significant implications for clinical translation and has the potential to improve the quality of life for millions of patients.

Table of Contents

List of Figures

List of Tables

Chapter 1: Introduction

1.1 PROBLEM STATEMENT

Electrically and mechanically tunable biomaterials have great potential to address the clinical challenge of healing critically sized and non-healing wounds, which in addition to diminishing quality of life, can have significant socioeconomic costs. For example, non-healing wounds sustained from volumetric muscle loss or bone non-unions led to striking costs estimated at $400B in 2015[1]. The current gold standard of treatment is autograft, where tissue from a healthy site in the patient's body is removed and transferred to the site of injury. Autograft faces numerous disadvantages, however, including donor site morbidity and pain, and is not a sustainable source for tissue repair. This provides a ripe opportunity for biomaterials scientists and tissue engineers to develop strategies to replace autograft. Progress to engineering tissues has made significant strides over the past 20 years, but the field still faces challenges with replacing tissues in critical wounds and completely restoring tissue function. Tissue engineering strategies generally follow the "Tissue Engineering Triad" in which a scaffold, seeking to replace the extracellular matrix and physical architecture of the *in vivo* environment, delivers cells to an injury site and provides appropriate signals to direct desired behaviors within the cells (*e.g.*, differentiation, proliferation, etc.)[2]. Physical and soluble cues are represented in the conventional Tissue Engineering Triad, but electrical cues are not.

Bioelectricity, voltage-mediated communication inherent to all cells and tissues, plays an important role in cell behavior and tissue modulation, but is rarely considered in tissue engineering research. Bioelectricity originates from the transmembrane potential of each cell and gives rise to endogenous electric fields, which guide cell function and can even override topographical cues[3–5]. On the cellular level, endogenous electric fields are involved in orientation, migration, adhesion, proliferation, and differentiation. On the tissue and organismal level, electric fields play a major role in development, wound healing, and tissue homeostasis[4,6]. Externally applied electrical stimulation is linked to enhanced anatomical and behavioral recovery of tissue injuries and has been used *in vitro* to influence cell behaviors previously listed[7]. However, the parameters of electrical stimulation vary between studies, which hinders scientific reproducibility. Further, mechanisms of how electrical stimulation influences cell behavior are not well characterized, creating a roadblock to clinical translation.

Electrical stimulation is frequently used in conjunction with biomaterials containing conductive additives to augment electrical activity. Conjugated polymers such as polypyrrole (PPy), polyaniline, and poly(3,4-ethylenedioxythiophene) (PEDOT); carbon-based materials such as carbon nanotubes and graphene; and metallic additives like gold and silver nanoparticles have all been used to increase the conductivity of biomaterials[8,9]. In recent years, bio-ionic liquids (bio-ILs), have been used to increase substrate conductivity by facilitating ion movement, rather than electron movement[10,11]. Poly(3,4-ethylenedioxythiophene) polystyrene sulfonate (PEDOT:PSS), which is used in this work, is frequently added to hydrogel materials for nerve and cardiac tissue engineering due to

its high electrical conductivity, low cytotoxicity, and commercial availability[8,14,15]. PEDOT:PSS also boasts the advantage over unmodified PEDOT of being water-dispersible, owing to its $PEDOT^+$ core, PSS^- micellar shell structure that allows it exist as a homogeneous emulsion in aqueous solutes[16]. While electrical stimulation often enhances these effects, multiple studies suggest conductive materials, alone, direct cell differentiation, aid in maturing electroactive cell types, and promote tissue functionality[12,13], though these mechanisms are not well understood, either. Further, despite the increased popularity of using conductive materials in tissue engineering, questions of how electron-conducting materials can influence ion-conducting cells remain unanswered.

Additionally, while some groups investigating the influence of substrate electrical properties on cell behavior also characterize the material's mechanical properties, the practice is not conserved across studies. We believe this is an oversight, as adding components to a material to make it electrically conductive could affect its physical structure and numerous reports highlight the importance of mechanical cues on dictating cell behaviors like differentiation[20,21]. Beyond this, characterizing the interplay between electrical and physical properties could reveal its potential effect on cell behavior. Without thorough material characterization and appropriate experimental controls, it is not possible to elucidate which input has the effect of interest. Therefore, we believe it is crucial to report how inclusion of conductive additives influences material mechanical properties.

Finally, many studies employing electrically conductive materials demonstrate improved cell behaviors when cells are seeded on top of the substrate (*i.e.*, monolayer culture), thereby creating a 2D *in vitro* system. However, cells and tissues are arranged in 3D *in vivo*, and evidence dictates significant differences in cell behavior when cultured in 3D versus 2D[17,18]. Some cells, notably neuronal-type cells, are difficult to culture successfully in 3D, further blunting progress towards 3D composite tissue regeneration[19]. Therefore, narrowing knowledge gaps pertaining to how substrate conductivity may influence cell behavior in 3D is of the utmost importance.

To address the current knowledge gaps pertaining to the relationship between different material properties and their subsequent interplay on cell behavior, I propose the hypothesis and specific aims, described next.

1.2 HYPOTHESIS AND SPECIFIC AIMS

Hypothesis: The interplay of electrical and physical cues, including storage modulus and porosity, improves cell behaviors towards regeneration more than when a physical or electrical cue is provided alone.

Aim 1: Establish the conditions under which hydrogel electrical and physical properties are decoupled.

Aim 2: Evaluate the interplay of scaffold conductivity and biophysical properties on protein adsorption and cell adhesion.

Aim 3: Characterize the interplay of scaffold conductivity and porosity on myogenic differentiation in 3D hydrogels.

1.3 SIGNIFICANCE AND INNOVATION

While the use of conductive materials for tissue engineering is on the rise, several mechanistic knowledge gaps persist regarding how conductivity influences other material properties and cell behavior. This project seeks to perform fundamental materials and *in vitro* research with the following innovations:

1.3.1 Characterizes the interplay between conductivity and biophysical properties

The promise of conductive materials being able to influence cell behavior and differentiation has diverted attention from characterizing how conductivity and substrate biophysical properties influence each other, alter overall properties of a scaffold, and possibly influence cell response.

1.3.2 Elucidates potential biological mechanisms by which electronically conductive substrates influence ion-conducting cells

Despite studies illustrating the positive effects of culturing cells on conductive substrates, the mechanisms dictating how electron-conducting materials influence the behavior of ion-conducting cells have not yet been reported. Some studies postulate that conductive substrates affect protein adsorption, but investigations thus far do not explicitly probe this relationship and how it may influence downstream cell behavior. Addressing knowledge gaps related to the role of material electrical properties in promoting cell behaviors would be a significant contribution to the field of electroconductive biomaterials.

1.3.3 Incorporates electrical properties into an established microporous hydrogel system that improves three-dimensional tissue regeneration

Mounting evidence suggests microporous annealed particle (MAP) scaffolds better promote three-dimensional wound healing[22]. Thus far, most studies using MAP scaffolds focus on tuning the mechanical properties of the annealed scaffolds, but this work introduces electrical properties as an additional input within this modular hydrogel system.

1.3.4 Increases accessibility of conductivity testing for tissue engineering applications

Commonly reported methods for testing conductive substrates for tissue engineering require expensive equipment (*e.g.*, potentiostats, semiconductor parameter analyzers, and four-point probes), which can impair tissue engineering and other biological labs from including conductivity in their experimental design[23]. This work increases accessibility by using inexpensive equipment in a custom setup to measure conductivity of hydrogels.

1.4 THESIS OVERVIEW

Chapter 2 provides background information about electrical signaling within the body and how biomaterials have been used to interface a variety of cells and tissues in an electrical fashion. Chapter 3 presents experimental data in support of Aims 1 and 2, and chapter 4 describes data that relates to Aim 3. Chapter 5 provides an overall conclusion of this dissertation and discusses future directions for this work. The first two appendices document unpublished data that pertain to Aim 1. An additional appendix documents commonly used protocols for this work.

REFERENCES

1. Corona, B. T., Rivera, J. C., Owens, J. G., Wenke, J. C. & Rathbone, C. R. Volumetric muscle loss leads to permanent disability following extremity trauma. J Rehabil Res Dev 52, 785–92 (2015).
2. Vacanti, J. P. & Vacanti, C. A. The history and scope of tissue engineering. in Principles of Tissue Engineering 3–8 (Elsevier, 2014). doi:10.1016/b978-0-12-398358-9.00001-x.
3. Levin, M., Pezzulo, G. & Finkelstein, J. M. Endogenous bioelectric signaling networks: exploiting voltage gradients for control of growth and form. Annu Rev Biomed Eng 19, 353–387 (2017).
4. Funk, R. H. Endogenous electric fields as guiding cue for cell migration. Front Physiol 6, 143 (2015).
5. McLaughlin, K. A. & Levin, M. Bioelectric signaling in regeneration: mechanisms of ionic controls of growth and form. Dev Biol 433, 177–189 (2018).
6. Mathews, J. & Levin, M. The body electric 2.0: recent advances in developmental bioelectricity for regenerative and synthetic bioengineering. Curr Opin Biotechnol 52, 134–144 (2018).
7. Snyder, S., DeJulius, C. & Willits, R. K. Electrical stimulation increases random migration of human dermal fibroblasts. Ann Biomed Eng 45, 2049–2060 (2017).
8. Casella, A., Panitch, A. & Leach, J. K. Endogenous Electric Signaling as a Blueprint for Conductive Materials in Tissue Engineering. Bioelectricity 3, 27–41 (2021).
9. Balint, R., Cassidy, N. J. & Cartmell, S. H. Conductive polymers: towards a smart biomaterial for tissue engineering. Acta Biomater 10, 2341–53 (2014).
10. Noshadi, I. et al. Engineering Biodegradable and Biocompatible Bio-ionic Liquid Conjugated Hydrogels with Tunable Conductivity and Mechanical Properties. Sci. Rep. 7, 4345 (2017).
11. Walker, B. W. et al. Engineering a naturally-derived adhesive and conductive cardiopatch. Biomaterials 207, 89–101 (2019).
12. Zhou, L. et al. Soft conducting polymer hydrogels cross-linked and doped by tannic acid for spinal cord injury repair. ACS Nano 12, 10957–10967 (2018).
13. Ryan, A. J. et al. Electroconductive biohybrid collagen/pristine graphene composite biomaterials with enhanced biological activity. Adv Mater 30, e1706442 (2018).
14. Mawad, D. et al. A conducting polymer with enhanced electronic stability applied in cardiac models. Sci Adv 2, e1601007 (2016).
15. Spencer, A. R. et al. Bioprinting of a Cell-Laden Conductive Hydrogel Composite. ACS Appl. Mater. Interfaces 11, 30518–30533 (2019).
16. Zhang, S. et al. Room-temperature-formed PEDOT:PSS hydrogels enable injectable, soft, and healable organic bioelectronics. Adv Mater 32, e1904752 (2020).
17. Duval, K. et al. Modeling Physiological Events in 2D vs. 3D Cell Culture. Physiology 32, 266–277 (2017).
18. Fontoura, J. C. et al. Comparison of 2D and 3D cell culture models for cell growth, gene expression and drug resistance. Mater. Sci. Eng. C 107, 110264 (2020).

19. Willits, R. K. & Skornia, S. L. Effect of collagen gel stiffness on neurite extension. J Biomater Sci Polym Ed 15, 1521–31 (2004).
20. Engler, A. J., Sen, S., Sweeney, H. L. & Discher, D. E. Matrix elasticity directs stem cell lineage specification. Cell 126, 677–89 (2006).
21. Discher, D. E., Janmey, P. & Wang, Y. Tissue Cells Feel and Respond to the Stiffness of Their Substrate. Science 310, 1139–1143 (2005).
22. Griffin, D. R., Weaver, W. M., Scumpia, P. O., Di Carlo, D. & Segura, T. Accelerated wound healing by injectable microporous gel scaffolds assembled from annealed building blocks. Nat. Mater. 14, 737–744 (2015).
23. Seng, S., Shinpei, T., Yoshihiko, I. & Masakazu, K. Development of a handmade conductivity measurement device for a thin-film semiconductor and its application to polypyrrole. J. Chem. Educ. 91, 1971–1975 (2014).

Chapter 2: Endogenous electric signaling as a blueprint for conductive materials in tissue engineering

2.1 INTRODUCTION

Bioelectricity is a term that describes voltage-mediated communication inherent to all cells and tissues. Bioelectricity plays a major role in cell behavior during development and tissue homeostasis but is understudied within tissue engineering. The development and application of biomaterials for tissue engineering is broadly focused on providing mechanical and chemical cues in their scaffolds to influence cell behavior (*e.g.*, survival, migration, differentiation, etc.), yet few seek to incorporate electrical cues[1]. Bibliometric analysis using PubMed illustrated that, from 2000 to 2019, there were ten times more publications in the field of tissue engineering and regenerative medicine related to the influence of mechanical (greater than 2 million publications) or chemical cues (more than 3 million publications) than those related to electrical cues (200,000 publications). By acknowledging and catering to the electrical aspects of tissues and organs, the potential to improve communication between engineered and endogenous tissue will be increased, which could improve clinical translation.

This chapter is published as Casella A, Panitch A, Leach JK. Endogenous electric signaling as a blueprint for conductive materials in tissue engineering. *Bioelectricity*. 2021 Mar 1;3(1):27-41.

Nerve cells and cardiomyocytes consistently exhibit improved growth and differentiation when seeded on conductive substrates, even in the absence of electrical stimulation (ES)[2–14]. While possible mechanisms for this phenomenon are explained in later sections of this review, it grossly appears that these materials support the function of electroactive cell types by capturing and disseminating electrical signals. Synthetic polymers including polypyrrole (PPy), polyanaline (PANI), and poly(3,4-ethylenedioxythiophene) (PEDOT), or carbon-based materials such as carbon nanotubes and graphene oxide, are frequently used to increase conductivity of biomaterials[15–20]. Although these materials provide at least physiologically relevant, and in some cases, metallic-like[21], conductivity to a system, they also face a number of disadvantages. Most conductive polymers are hydrophobic, which is beneficial for protein adsorption but leads to poor cell adhesion. Some materials (*e.g.*, PANI) trigger an immune response. Also, most synthetic conductive materials are neither degradable nor resorbable, and the effects of their permanent presence in the body is damaging or unknown[3,22–24]. The mechanism of conductivity of these synthetic materials comes from electron transfer, whereas in the body, conductivity arises from the movement of ions. While this has not impeded encouraging results, the gap in mechanistic understanding surrounding these materials is a roadblock for optimal design. Given these drawbacks, there is an important need for approaches that use natural biomaterials to interact with endogenous tissues and confer physiological conductive signals.

This review summarizes recent work using synthetic and naturally derived conductive materials to aid in tissue regeneration. It contextualizes the use of conductive materials in tissue engineering and postulates the future direction of the field.

2.2 ORIGIN AND ENDOGENOUS EFFECTS OF BIOELECTRICITY

2.2.1 Endogenous electric fields

Bioelectricity was first described in the late 1700s by Luigi Galvani while experimenting with frogs. Bioelectricity remains a topic of great importance to biologists, as it is a key player in regulating many cell and tissue behaviors[25]. On the cellular level, bioelectricity is derived from differences in the endogenous membrane potential of each cell. The transmembrane potential is generated by the separation of charges by transmembrane pumps, transporters, and ion channels and results in a resting potential between -90 and -50 mV for most cells[26]. Membrane potentials give rise to endogenous electric fields, which then guide cell behavior and may even override chemical and topographical cues[26–28]. Charge gradients (*i.e.*, electric fields) are also created when ions and other charged molecules pass from cell to cell *via* gap junctions[26]. On the cellular level, endogenous electric fields are involved in orientation, migration, adhesion, proliferation, and differentiation[29,30]. On the tissue and organismal level, electric fields play a major role in development, wound healing, and healthy tissue function (**Fig. 2.1**)[28]. Many literature reviews exist on bioelectricity and provide further detail on its role in development and homeostasis[1,26,27,31]. Given the mounting evidence that electrical

signals can influence cell behavior, there is great interest in developing techniques to electrically stimulate injuries and repair tissue to improve healing.

2.2.2 Electrical stimulation

Electrical stimulation refers to an externally generated electric field applied *via* electrodes to influence cell or tissue response. In tissue injuries, application of an external electric field has enhanced anatomical and behavioral recovery[32,33]. Electrical stimulation can alter cell behaviors such as migration, adhesion, proliferation, and differentiation. However, the specific molecular mechanisms of electrical stimulation on cell behavior remain elusive, preventing optimal design of materials for clinical use[33]. While most electrical stimulation protocols set key parameters including field strength (0.00048 – 6000 mV/mm), current density (0.015-5 A/m^2), and frequency (usually under 100 Hz)[34] within previously reported ranges, the variation in setup between studies limits the ability to directly compare results and draw conclusions about the effects of electrical stimulation as a whole[33].

2.2.3 Bioelectric signaling at the cellular level

Numerous reports describe the role of endogenous or applied electric fields at physiological levels on cellular migration, adhesion, proliferation, and differentiation during development and wound healing[27,35,36]. Generally, applied electric fields affect cell surface receptors, enzyme activity, charge distribution throughout the cell membrane, and membrane protein conformation[28,37,38]. It is believed to trigger similar responses cells

would have to other chemical or physical stressors (*e.g.*, fluid shear stress[39]) that also promote cell survival[40–42]. Upstream signal transduction pathways and calcium ion flux mediate many of the cell behaviors listed, but electric fields also affect cells by stimulating cytoskeletal reorganization, surface receptor redistribution, ATP synthesis, heat shock protein activation, and reactive oxygen species and lipid raft formation[33]. Electrical stimulation elevates the activity of mitogen-activated protein kinase (MAPK), which initiates multiple signaling pathways, each associated with different cell behaviors related to migration, adhesion, proliferation, and differentiation[33,37,43].

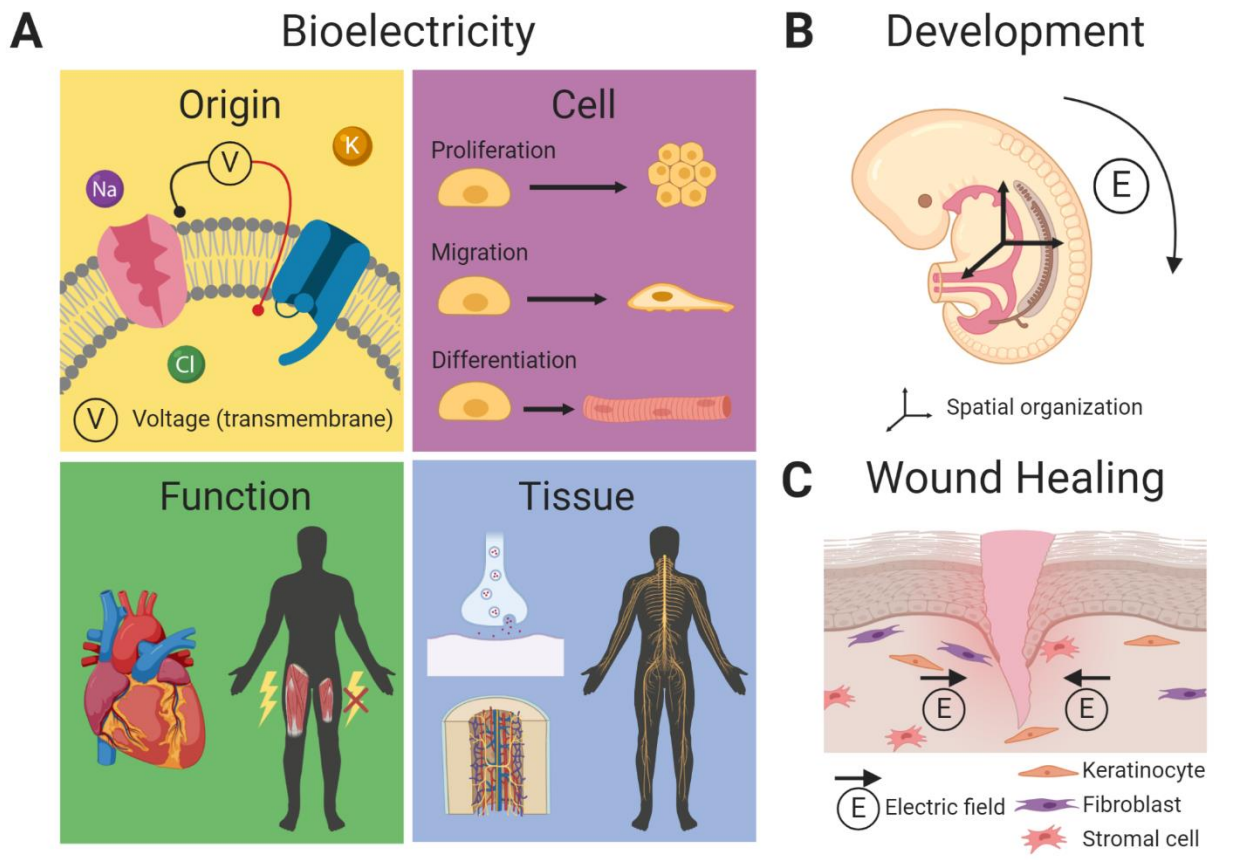

Figure 2.1: Summary of the effects of bioelectricity on the cell, tissue, and organismal level, as well as its role in development and wound healing. (A) Bioelectricity originates

from the separation of charges across the cell membrane, generating a voltage, and can influence cell behaviors including proliferation, migration, and differentiation. Tissue development and homeostasis are also dependent on bioelectric signaling, even if those tissues are outside of the nervous system. Many tissues (*e.g.*, cardiovascular and musculoskeletal) are highly dependent on electrical signals and are disrupted in their absence. **(B)** During development, electric fields are critical for proper morphogenesis and spatial organization of organ systems as well as directing stem cell differentiation. **(C)** Endogenous electric fields arise from wounds and recruit cells to accelerate healing.

2.2.3.1 Migration

Electrical stimulation can also influence cell migration by causing lipids to accumulate into rafts[44]. Lipid rafts are believed to be the principal sensors of electric field within cells, and their formation can activate integrins and other membrane proteins involved in directional cell migration[45]. During development, endogenous electric fields are key players in initial cell polarization and provide cues to guide long-distance migration of neurons and neural stem cells (NSCs) throughout the central and peripheral nervous systems[27,46]. When electrical stimulation is applied, many cell types preferentially travel towards the cathode, while others favor anodal electrotaxis[47], and numerous studies illustrate cell migration changes directions when the field direction is switched[36]. Some cell types exhibit accelerations in migration speed as a function of field strength[35], whereas others do not[36]. In the context of wound healing, endogenous electric fields recruit stem cells to wound sites and direct fibroblasts, keratinocytes, and other cell types

within the wound to promote healing[29,48–50]. When combined with topographical cues, electrical stimulation caused a synergistic directional migration of corneal epithelial cells mediated by upregulated MMP-3 activity[51,52].

2.2.3.2 Adhesion

Cell adhesion is a foundational event that is influenced by electric signals and must be considered when developing new materials for tissue engineering applications. When a cell is triggered by an electric field, cells arrange their cytoskeletal elements to shape to the trigger[33,53]. For example, α2β1 integrins of ligament fibroblasts polarized and clustered after the cells were electrically stimulated. Integrin clustering led to intracellular RhoA polarization which is directly involved in cell membrane protrusion and migration[54]. Conductive materials can also affect cell adhesion, even in the absence of an electric field[55]. One possible explanation of this observation is that increased electrostatic interactions characteristic of conductive substrates cause cells to strongly adhere without forming focal adhesion complexes (FACs). Because this adhesion is not derived from FACs, growth arrest occurs, which ultimately leads to decreased cell proliferation (**Fig. 2.2A**)[56]. Increases in seal resistance that arise between a cell and a conductive substrate may also contribute to increased cell adhesion (**Fig. 2.2B**)[57]. Seal resistance originates from the collection of ionic solution in the cleft between the cell membrane and the surface and can be physically considered as adhesion strength between the cell and the surface. Electrical stimulation may increase extracellular matrix protein adsorption to substrates, providing additional sites for integrin-ligand interactions (**Fig.**

2.2C)[58]. The variation within these explanations and their conjectural nature highlight the need for more mechanistic studies of how cells and conductive substrates interact.

2.2.3.3 Proliferation

Due to changes in ion pump permeability and function throughout the cell cycle, the resting membrane potential of proliferating cells is more depolarized than non-proliferating cells[59]. For example, compared to that of quiescent cells, proliferating cells have a membrane potential between -30 and -10 mV[26]. Potassium and chloride channels are key regulators of ion flow (*i.e.*, endogenous electric fields) that can affect proliferation. This relationship could be used to promote cell growth in tissue engineering applications or leveraged to inhibit cell growth (*e.g.*, developing chemotherapeutics)[27,56,60]. As with other cell behaviors, all cell types may not behave similarly given the same inputs. For example, cardiomyocytes grown on a conductive surface without electrical stimulation showed increased proliferation, yet fibroblasts in the same system exhibited no proliferative response[61]. However, most reports indicate that cells grown on conductive surfaces or treated with ES (or both) experience growth arrest, which is believed to be caused by increased cell adhesion without FAC formation. Other studies contrast these observations by reporting improved proliferation when stimulated with pulsed EFs[62]. In such cases, increased proliferation may be due to electrokinetic flow of media that circulates nutrients and increases their availability to cells[63]. Overall, the presentation of electrical cues, whether through the material substrate or external ES, varies between cell types and is dependent on environmental parameters.

The complexity of such systems necessitates the interrogation of cell proliferation when incorporating electrical elements.

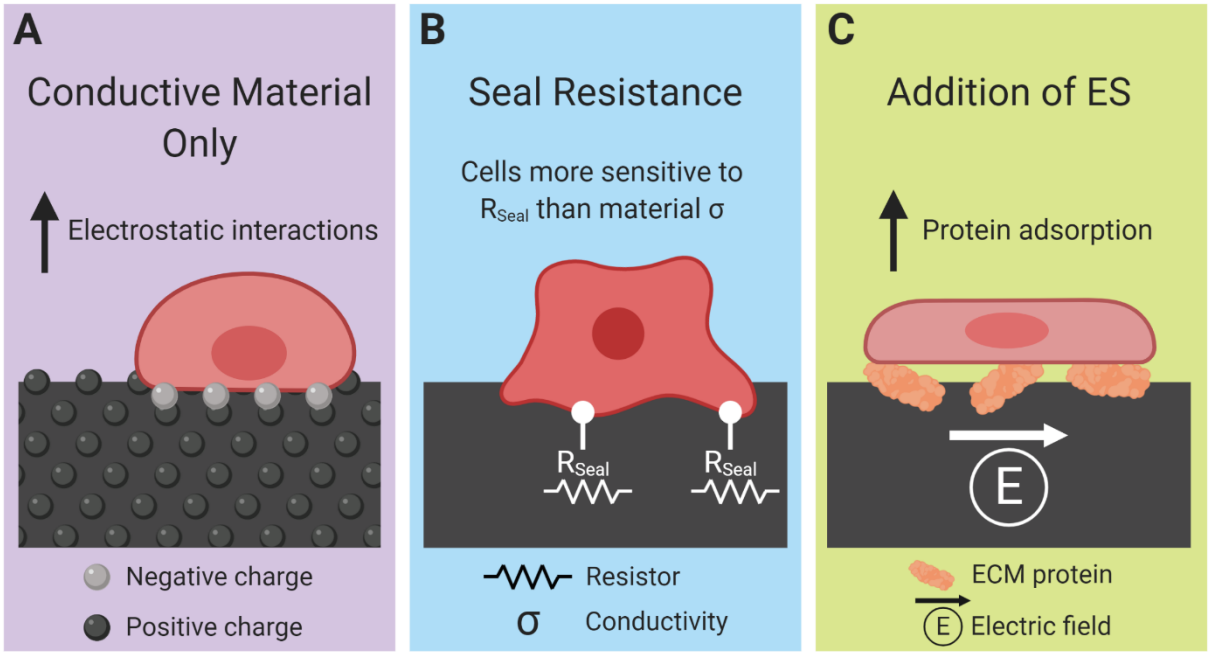

Figure 2.2: Cell interactions with conductive materials with and without electrical stimulation. (A) Conductive materials present more electrostatic charge, which increases electrostatic interaction with cells. **(B)** Conductive materials promote cellular attachment through increased seal resistance (R_{seal}). R_{seal} originates from the collection of ionic solution in the cleft between the cell and the surface and can be considered as adhesion strength between the cell and the substrate. **(C)** Protein adsorption is enhanced by applying an electric current to a conductive substrate, facilitating cell adhesion.

2.2.3.4 Differentiation and maturation

Electrical signaling can initiate differentiation *in vivo* and influence cell fate during development and tissue homeostasis[64]. Endogenous currents also arise from wounds

and signal to begin the differentiation process of depolarized, undifferentiated cells towards a reparative phenotype[27,32]. Altering the transmembrane potential of a variety of stem cells with electrical stimulation can influence their differentiation fate and has been demonstrated in neural, hepatic, and mesenchymal stromal cells (MSCs), as well as in cancer[27]. Applied electric fields can increase cellular uptake of calcium ions and generate reactive oxygen species[65], both of which are linked to stem cell differentiation toward the neurogenic and osteogenic lineage[65–68]. For instance, electrical stimulation caused bone marrow-derived MSCs to express neural markers including *Nestin* and *MAP2*[69,70]. Human neural progenitor cells undergoing electrical stimulation on a conductive substrate showed increased *MMP-9* gene expression and VEGF-A secretion, indicating increased capacity for angiogenesis and survival[71]. Electrical stimulation also induced chondrogenesis of human MSCs without exogenous growth factors[72] and enhanced calcium deposition by adipose-derived human MSCs[73].

2.2.4 Bioelectric signaling at the tissue/organism level

In the developing embryo, endogenous electric fields play an important role in orchestrating organ shape and in anterior/posterior and left/right patterning, which is important for the development of asymmetrically spaced organs such as the heart, organs in the digestive tract, and liver. By de- or hyperpolarizing the membrane potential, electric fields can induce the expression of signaling factors that influence morphological patterns (*e.g.*, folding, proliferation, and migration of cell groups)[74]. Transfer of bioelectric information between cells in both the embryo and adult organism may occur by gap

junctions, tunneling nanotubes, non-synaptic neuronal (*i.e.*, ephaptic) field effects, transepithelial potentials, and transfer of ion channels *via* exosomes[26,28]. Electric field patterns also precede and even pinpoint major morphological events in development such as limb bud development[26,28].

In addition to the cellular processes that are influenced by inherent electrical properties, musculoskeletal tissue is also highly interdependent with nervous tissue during development, adult tissue function, and tissue repair. During development, bone, muscle, ligaments, and tendons all exchange trophic factors with nerves that, when interrupted, can result in less innervation and consequent reduction in tissue volume and function, increased chance of developing osteoporosis in the case of bone tissue, and incomplete development of attachment sites for tendons and ligaments, all of which can result in joint weakness and loss of function[75].

When properly innervated, the signal exchange between nerves and these tissues continues to contribute to proper tissue function. In muscle, the neuromuscular junction is responsible for all skeletal muscle movement, and many sources report that peripheral nerve regeneration is enhanced by brain-derived neurotrophic factor (BDNF), which while largely expressed by the nerves, themselves, is also expressed by myogenic progenitor cells (satellite cells)[76]. In bone, the presence of nerves is believed to play a role in cell migration out of the bone marrow[77], providing regulatory cues for bone metabolism[78], and supporting the hematopoietic stem cell niche[79]. In tendons and ligaments, the main role of nerves is to regulate the vascular system supplying blood to these tissues, though other trophic and nociceptive functions are believed to exist for those nerves ending in

the outermost or synovial layers of these soft tissues[80]. These studies provide sufficient evidence that the role of nerves and their secretions are active players in musculoskeletal tissue development and regulation, and warrant involvement in studies related to musculoskeletal tissue engineering.

Finally, the nervous and vascular systems are closely linked during development and continue to provide key trophic factors to each other during tissue homeostasis. For example, blood vessels supply oxygen and nutrients to nerve networks and neuropeptides secreted by nerve fibers—including neuropeptide Y (NPY), calcitonin gene-related peptide-I (CGRP-I), and substance P (SP)—support angiogenesis[81–85]. Delivery of vascular endothelial growth factor (VEGF) and insulin-like growth factor-1 (IGF-1) supported functional reinnervation in mice after sciatic nerve ligation[86]. On the other hand, MSCs, ECs, and sensory neurons grown on hydrogels containing the laminin-derived IKVAV adhesion peptide showed increased osteogenic, angiogenic, and neuronal markers, respectively[87]. This vascular-nervous supportive interplay has great implication for clinical translation. The dual pursuit of vascularization and innervation gives engineered tissues the best chance of successful integration upon implantation by allowing the systems to support each other during. Given the popularity of materials and protocols designed to improve vascularization, it makes sense to also consider that innervation can also serve to promote blood vessel formation and vice versa.

Endogenous bioelectric signaling plays a key role in many behaviors and functions at both the cell and tissue level. When electrical stimulation is combined with other inputs, whether mechanical or chemical, synergistic effects are generally observed. However,

given conflicting reports about ES[88], the variation in application parameters, and the overall mechanistic knowledge gaps, more studies are necessary before electrical stimulation becomes common clinical practice[33]. There is also great opportunity to use biomaterials as a means to magnify, leverage, or mimic the influence of bioelectric signaling.

2.3 CONDUCTIVE MATERIALS FOR TISSUE ENGINEERING

Synthetic materials with enhanced electrical properties have great potential for numerous biological applications. Comprehensive reviews[89–93] and articles detailing the use of conductive polymers[90,94–97], nanoparticles[98–100], carbon-based[101], and metal-based structures[98,102,103] for use in nerve[94,101,104–106] and cardiac[102,107] tissue engineering have become increasingly prevalent over the last decade. A variety of additives have been used to tune the conductivity of biomaterials (**Fig. 2.3**), and those used in the most recent reports are summarized in **Table 2.1**. Conductive additives incorporated into hydrogels (**Table 2.2**) result in scaffolds that better approximate endogenous tissue (**Table 2.3**). The following sections summarize and provide critical analysis of the most up-to-date research using these materials.

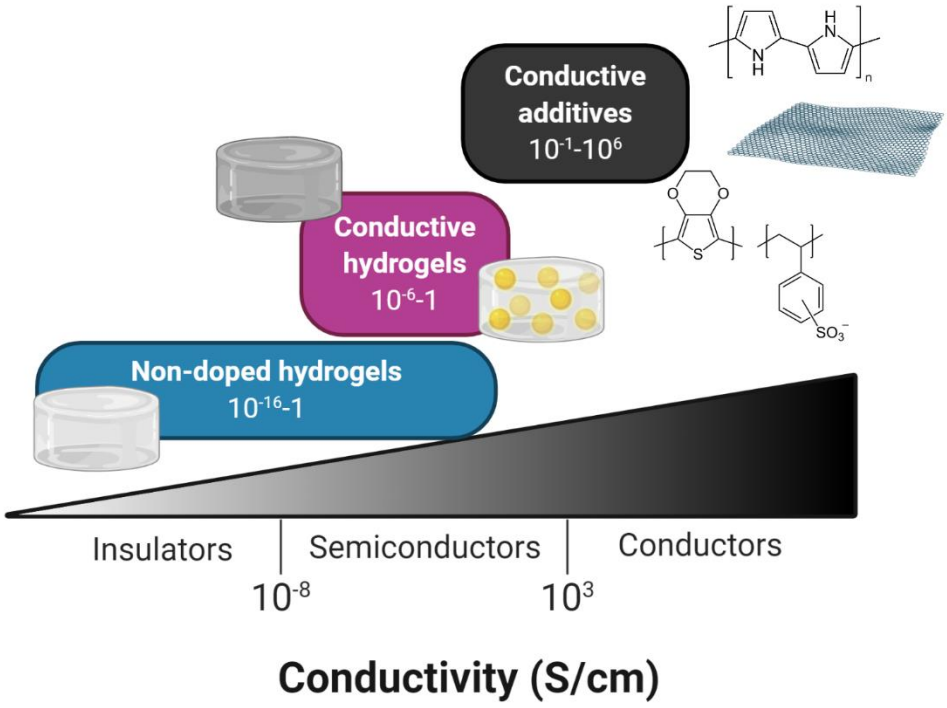

Figure 2.3: Electrical properties of biomaterials with conductive additives used in tissue engineering. Non-doped hydrogels have reduced conductivity, ranging from 10^{-16} S/cm observed in polyacrylamide to 1 S/cm, observed in alginate. Other unmodified hydrogels within this electroconductive range include collagen type I, PEGDA, and chitosan. Conductive additives including polymers like PPy, PANI, and PEDOT, CNTs, and AuNPs have much higher conductivity (~10^{-1}-10^{6} S/cm) and are used to enhance the conductivity of hydrogels.

2.3.1 Synthetic conductive polymers

Electrically conductive synthetic polymers were first reported in 1977 by Heeger, MacDiarmid, and Shirakawa using polyacetylene. Their fabrication of a "conductive plastic" with metallic-like electroactivity was a major breakthrough in the field and

resulted in the 2000 Nobel Prize in Chemistry[108,109]. Since then, over 25 types of conductive polymers have been developed, the most common of which are illustrated in **Fig. 2.4A**[110]. The mode of conductivity for all of these polymers arises from the freedom with which electrons move within and between their polymer chains[111]. Conductive polymers contain moieties that consist of alternating single and double bonds (*i.e.*, conjugated double bonds). The double bonds within the polymer structure are made up of a σ bond and a π bond. Electrons are not as strongly bound to π bonds, which allows them to delocalize. To activate electron movement, the polymer chain must be disrupted by the introduction of a dopant. Oxidation, or *p*-doping, removes electrons from the system and reduction, or *n*-doping, inserts electrons into the system[109]. Charge delocalization can also occur when polymers contain aromatic rings spaced such that their π-orbitals overlap (*i.e.*, π-π stacking). This phenomenon can result in organic materials having metallic-like conductivity[112,113]. Conjugated double bond structures are frequently seen in synthetic materials used for tissue engineering but can also appear in natural conductive materials. Understanding the origin of conductivity can promote purposeful design of materials and aid in understanding material synthesis.

Table 2.1: Electrical characterization and properties of synthetic conductive materials

Material	Conductivity (S/cm)	Reference
PPy	0.02-7.5 × 10^3	Zhou *et al*. 2018[21] & Kaur *et al*. 2015[111]
PANI	0.11-10^5	Min *et al*. 2018[22] & Pan *et al*. 2012[114]
PEDOT	0.4[111]-500[22]	Min *et al*. 2018[22] & Kaur *et al*. 2015[111]

Pristine PEDOT:PSS	0.2-1[115]	Yu Z *et al*. 2016[115] & Sigma Aldrich
Pure PEDOT:SS Hydrogel	20-40	Lu *et al*. 2019[116]
Carbon nanotubes	10^4-10^5	Min *et al* 2018[22] & Wang *et al*. 2018[117]
Single layer Graphene	2000-10^6	Alam *et al*. 2017[17] & Wang *et al*. 2018[117]
Mildly oxidized graphene sheets (MOGS)	675±22	Alam *et al*. 2017[17]

Table 2.2: Electrical characterization and properties of synthetic conductive composites

Composite	Conductivity (S/cm)	Reference
PPy in HA	~1.2-7.3 × 10^{-3}	Yang *et al*. 2016[10]
PPy in Alginate	3.3 × 10^{-5}-1.1 × 10^{-4}	Yang *et al*. 2016[118]
PPy in PCL	~10^{-5}-10^{-1}	Zhang *et al*. 2016[73]
PANI in PCL	~2 × 10^{-4}	Wibowo *et al*. 2020[119]
Poly(glycerol sebacate)-co-aniline	1.4 × 10^{-6} - 8.5 × 10^{-5}	Wu *et al*. 2016[120]
PEDOT-HA nanoparticles in chitosan	~10^{-4}-10^{-2}	Wang *et al*. 2017[121]
PEDOT:PSS in PEG diglycidyl ether	5.22 × 10^2	Solazzo *et al*. 2019[122]
CNTs in PCL + silk fibroin	6.5-8.1 × 10^{-7}	Wu *et al*. 2017[123]
MWCNT in PEG	~10^{-3}-10^{-2}	Imaninezad *et al*. 2018[124]
Carbon nanotubes + rGO sheets in PEG	5.75 × 10^{-5}	Liu *et al*. 2017[15]
Graphene in collagen	6.5 × 10^{-3}	Ryan *et al*. 2018[18]
GO in polydopamine	8 × 10^{-2}	Han *et al*. 2017[125]
AuNPs in chitosan	1.3 × 10^{-3}	Baei *et al*. 2016[19]
Collagen doped with iron oxide nanoparticles	3.7 × 10^{-5}	Bonfrate *et al*. 2017[98]

2.3.1.1 Polypyrrole

Polypyrrole (PPy) is the most studied conductive polymer for biomedical applications following its initial description by Wong *et al*., who tested the stability of conductive polymers in cell culture conditions[126]. When oxidized, PPy exhibits conductivity on the order of 10^3 S/cm, where S is siemens. Its environmental stability, capacity to support adhesion and growth of many cell types, and ease of synthesis make it an attractive additive for biomedical applications[111].

Because PPy is mechanically rigid and brittle after synthesis, it is frequently combined with other polymers to achieve more desirable mechanical properties for tissue engineering applications[93,127]. Peripheral nerve conduits composed of electrospun poly(L-lactic acid-co-ε-caprolactone) (PLCL) coated with PPy were created to facilitate ES. When tested *in vivo* as a nerve conduit, the stimulated conductive scaffolds performed similarly to autograft[55]. These findings not only imply that the presence of a conductive material can influence cell response but also raise questions about how conductivity and other properties (*e.g.*, topography) influence each other[11,52].

PPy has also been used for musculoskeletal tissue engineering. For example, adipose-derived MSCs grown on PPy-PCL composites achieved a 100% increase in calcium deposition when electrically stimulated. The investigators interrogated the role of voltage-gated ion channels to better understand the mechanistic downstream effects of electrical stimulation for bone tissue engineering[73]. Through inhibitory experiments, they determined that voltage-gated Ca^{2+} channels play a more significant role in regulating adipose-derived MSC functions than other ion channels. Additionally, de

Castro *et al*. observed increased alkaline phosphatase (ALP) activity in osteoblasts grown on electrospun scaffolds containing PPy and poly(butylene adipate-*co*-terephthalate) (PBAT) after 21 days compared to PBAT controls, indicating that substrate conductivity can enhance osteogenic potential[128].

Table 2.3: Conductivities of native tissues, unmodified biomaterials, and natural conductive materials

Tissue Type	Conductivity (S/cm)	Reference
Myocardium	~10^{-5} - 10^{-3}	Surowiec *et al*. 1987[129] & Noshadi *et al*. 2017[3]
Nerve/Spinal cord	~10^{-2}-10^{-1}	Zhou L *et al*. 2018[21]
Skeletal muscle (feline, porcine)	~2-8 × 10^{-3}	Surowiec *et al*. 1987[129] & Gabriel *et al*. 2009[130]
Bone	~9.1 × 10^{-5}	Balmer *et al*. 2018[131]
Cartilage (porcine)	~10^{-3}	Binette *et al*. 2004[132]
Skin	~10^{-6} – 10^{-3}	Gabriel *et al*. 2009[130] & Zarrintaj *et al*. 2018[133]
Collagen Type I	2.98 × 10^{-10}	Bonfrate, V *et al*. 2017[98]
	~2.5 × 10^{-3}	Sun, H *et al*. 2017[134]
	3 × 10^{-3}	MacDonald *et al*. 2008[135]
Alginate	~0.1-2	Kaklamani *et al*. 2018[136]
	8.2 × 10^{-6}	Yang *et al*. 2016[118]
PEGDA	7.6 × 10^{-11}	Guarino *et al*. 2013[137]
Polyacrylamide	~10^{-16}	Alam *et al*. 2017[17]

Chitosan	1.91×10^{-10}	Marroquin *et al*. 2013[138]
Wild type *G. sulfurreducens* PilA monomers	$5 \times 10^{-3} – 188 \times 10^{-3}$	Malvankar *et al.* 2011[112] & Adhikari *et al.* 2016[139]
Modified *G. sulfurreducens* PilA monomers	$\sim 10^{-1} - 10^{2}$	Tan *et al*. 2016[140]
Hemin-doped serum albumin	$\sim 10^{-3}$	Amdursky *et al*. 2017[141]
GelMA-Bio-IL	$\sim 10^{-7} – 10^{-5}$	Noshadi *et al*. 2017[3]

2.3.1.2 Polyaniline

Polyaniline (PANI) is another commonly used conjugated polymer, owing to its low cost of production, environmental stability, and greater range of conductive properties over PPy[22,93,142]. Despite these advantages, PANI is used less frequently given multiple conflicting reports of it stimulating an elevated immune response or chronic inflammation[93,142–144]. However, when combined with natural biomaterials such as chitosan, some groups have shown promising scaffolds for cardiac[107], nerve[137], and musculoskeletal tissue engineering. Murine-derived C2C12 myoblasts exhibited increased proliferation and myogenic differentiation markers when grown on silk fibroin combined with a PANI-based material (poly (aniline-*co*-*N*-(4-sulfophenyl)aniline)[145]. In a different study, C2C12s were cultured on aligned, PANI-coated PCL fibers and demonstrated greater capacity towards myotube formation than controls[146]. Endothelial cells better adhered to and proliferated on PANI-coated PCL fibers as well, and proliferation was further improved by ES[147]. Chen *et al*. combined PANI and PCL to make conductive nanofibers, and the addition of PANI caused MSCs to undergo osteogenic

differentiation and deposit higher levels of calcium compared to PCL-only controls, making it a relevant additive for bone tissue engineering. It is important to note that these results were achieved with the material containing an intermediate amount of PANI, which should redirect strategies that are focused on continuously increasing the conductivity of materials they intend to use for similar applications[148].

2.3.1.3 Poly(3,4-ethylenedioxythiophene)

Poly(3,4-ethylenedioxythiophene) (PEDOT) is frequently used as a conductive additive for making electroactive materials, whether alone or in combination with poly(styrene sulfonate) (PSS). PEDOT alone has distinct advantages over other conductive polymers including higher conductivity and better chemical stability[12]. Wang *et al*. incorporated hyaluronic acid (HA)-doped PEDOT nanoparticles into PLLA films, which improved PC12 cell adhesion, spreading, and survival compared to PLLA control films. Electrically stimulated PC12 cells grown on the conductive films exhibited more advanced neurite extension compared to unstimulated controls[149]. When incorporated into chitosan/gelatin gels, these HA-doped PEDOT nanoparticles promoted nerve regeneration[12,13,121].

Despite the positive effects of PEDOT alone, PEDOT:PSS has risen to the forefront in tissue engineering studies. By doping hydrophobic PEDOT with hydrophilic PSS, the conductive agent is easier to disperse and incorporate into hydrogels. Its structure also uniquely provides both electron conduction *via* PEDOT and ionic conduction through PSS, making it a more suitable material for bridging biological and synthetic systems.

PEDOT:PSS is associated with low cytotoxicity, though like many other polymers, its stability in biological applications can be greatly influenced by choice of polymer crosslinker[116,122]. PEDOT:PSS incorporated into collagen-alginate hydrogels at low concentrations improved cardiomyocyte coupling and maturation, even without ES[14]. Multiple groups have used PEDOT:PSS to dope methacrylated gelatin (GelMA) for bioprintable, electroactive materials for tissue engineering[150,151].

Although some novel polymer-based materials address several physical disadvantages of more ubiquitous polymers[5,120], all synthetic conjugated polymers thus far share the limitations of being unable to be degraded or resorbed by the body and having unknown long-term toxic effects, which calls into question their use in tissue replacements.

2.3.1.4 Carbon-based materials

Carbon-based materials such as graphene and carbon nanotubes (CNTs) receive attention for applications in tissue engineering because of their versatility, high conductivity, and ease of synthesis[18]. Many reports also indicate carbon-based materials enhance nerve cell response[15]. These properties make carbon-based materials attractive for use in other tissue engineering applications.

CNTs are perhaps best known for their unique mechanical and thermal properties for applications in non-medical fields, but their high conductivity has resulted in greater attention in recent years for use as electroactive substrates[92]. CNTs also have form and dimensions similar to biological structures such as neurological processes or proteins of

the extracellular matrix that may aid in tissue organization[16,152]. Functionalized CNTs and reduced graphene oxide sheets were incorporated into a poly(ethylene glycol) (PEG)-based hydrogel to create composites providing both electrical conductivity and positive surface charge to serve as a nerve conduit[15]. Compared to unmodified PEG hydrogels, the conductive substrate with positive surface charge resulted in slightly less circular PC12s and an increase in the number of cells bearing neurites, both of which are indicative of neuronal-like behavior. Multi-wall carbon nanotubes (MWCNTs) embedded in PEG gels were used to investigate the synergistic effects of conductivity, mechanical properties, and electrical stimulation on neuronal differentiation and extension[124]. Neuronal outputs were greatest in groups with high PEG concentration (20%), MWCNTs, and exposure to ES. With the removal of ES, this hydrogel still outperformed gels with a lower concentration of PEG, and electrical stimulation further magnified those differences. These data have two major implications. First, a material's conductive properties alone can support significant improvements in cell behavior. Second, desired effects can be significantly enhanced by tuning other material properties and applying ES.

Graphene is another class of carbon-based materials but tends to be easier and less expensive to synthesize compared to CNTs[17]. Graphene oxide (GO) possesses high biocompatibility and promotes cell adhesion in many applications but has restricted conductivity that can be mitigated by chemical reduction, resulting in reduced GO (rGO)[17,153] Pristine graphene has the highest conductivity compared to GO and rGO, but all three variants are frequently used as conductive additives[22]. Balikov and colleagues

used a graphene-based material to investigate how material type, ES, and physical patterns influence human MSCs toward an osteogenic or neurogenic lineage[154]. Physical cues were necessary for expression of late osteogenic markers (*e.g.*, osteopontin) but were unable to influence neuronal markers (*e.g.*, MAP2 and β_3-tubulin), which were only enhanced by ES. Pristine graphene and collagen were combined to stimulate cardiomyocytes, resulting in increased metabolic activity and sarcomeric structures[18]. The conductive material alone brought about significant changes, but the observations were enhanced with the addition of ES.

Overall, carbon-based materials are commonly used in tissue engineering applications to impart electroactivity and are frequently touted for surpassing conductive polymers in their ability to improve the mechanical properties of hydrogels. However, these improvements cannot overshadow the reports that carbon-based materials still face similar drawbacks as synthetic polymers, including cytotoxicity[155,156], hydrophobicity, and being nondegradable[157–159], which reinforces the need for natural conductive materials.

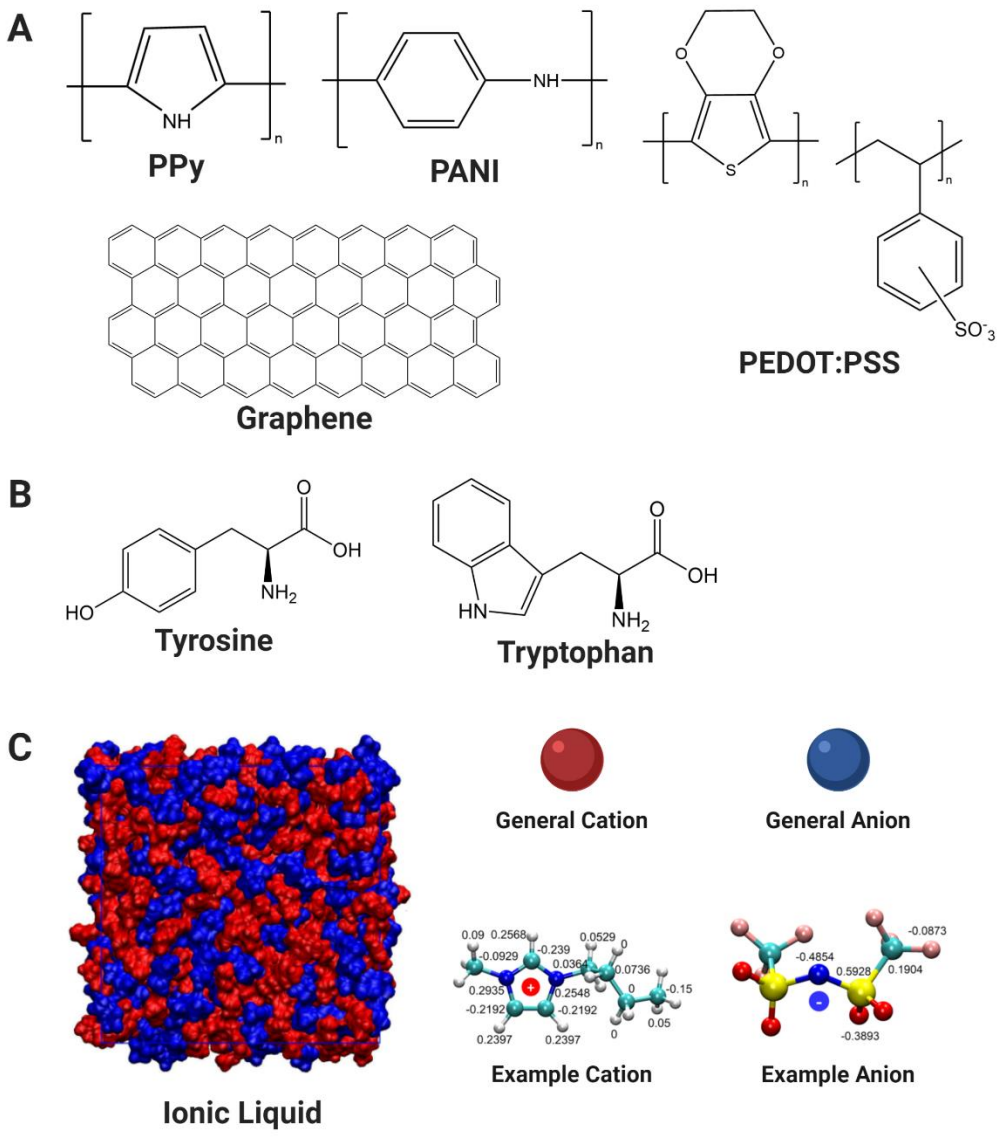

Figure 2.4: Chemical structure of conductive materials used for tissue engineering applications. (A) Synthetic polymers and carbon-based materials have conjugated (alternating single and double bond) structures that facilitate electron movement within and between polymer chains. **(B)** Conjugated structures are present in aromatic amino acids and can give rise to metallic-like conductivity in naturally derived proteins and peptides. Chemical structures recreated with ChemDraw 19.0. **(C)** Other natural conductive materials have charge-dense regions throughout their structure, giving rise to

ionic conductivity. A molecular dynamics simulation applied to a typical example of bio-ionic liquid is reproduced from Feng *et al*. (2019) in which cations and anions are represented in red and blue, respectively. There are many formulations of ionic liquids, but the molecular structures of the cations (1-butyl-3-methylimidazolium) and anions (bis(trifluoromethanesulfonyl)imide) comprising the ionic liquid used by Feng *et al*[160] are provided as an example.

2.3.1.5 Metal-based materials

Metal-based materials, namely nanoparticles, nanorods, and nanowires, are another class of synthetic conductive materials that are under investigation for tissue engineering. Gold is most often used due to its inert behavior in the body, but iron oxide has also been used to modify hydrogels, albeit for applications that have not yet been tested *in vivo*[98]. The use of less common silver, platinum, and zinc nanoparticles have been summarized elsewhere[22]. There is an established history of incorporating gold nanoparticles (AuNPs) into a variety of hydrogel materials and eliciting desired changes in cardiac applications, making them a popular choice as a conductive additive[19].

MSCs incorporated into AuNP-infused chitosan hydrogels exhibited early cardiac markers and enhanced cardiac differentiation compared to unmodified chitosan gels, even in the absence of ES[19]. Cardiomyocytes entrapped in gold-infused GelMA substrates expressed cardiac-specific markers homogeneously throughout the hydrogel, and the gold nanorod groups supported synchronous beating[20]. When electrical stimulation was applied, a lower excitation threshold was observed for the groups containing higher

concentrations of gold nanorods, indicating that the conductive substrates could better promote electrical integration with endogenous tissue.

Although GNPs are considered biocompatible, have high conductivity, and are effective for stimulating cells *in vitro*, gold cannot be resorbed by the body. Long-term studies using well-characterized GNPs confirm that both acute and chronic exposure to GNPs can alter the expression of genes related to cell cycle regulation and damaging oxidative stress[24].

2.3.1.6 Summary

The use of synthetic materials for conductive substrates for tissue engineering is gaining popularity. However, substantial hurdles and disadvantages remain. Synthetic materials conduct electric signals through electrons, which does not mimic the endogenous use of ionic gradients for bioelectricity. Knowledge gaps about the mechanism by which electrically conductive materials and the body interact prevent optimal or significant improvement in material performance. Furthermore, there are conflicting reports about cellular and bodily response to synthetic materials. While most polymeric materials are reported to be biocompatible, synthetic conjugated polymers are unable to be degraded or resorbed by the body and there are numerous reports of elevated immune response when PANI is used. Other conductive polymers, such as PPy and PEDOT, have only recently begun to appear in biomedical engineering applications, which limits knowledge of the long-term toxic effects of these materials on the body. The long-term effects of carbon-based materials and GNPs have been explored and are linked

to cytotoxicity, permanent elevation of stress response in some cell types, and particle accumulation in many organs. Though synthetic conductive materials possess many attractive properties for use in tissue engineering, there is a critical need for conductive materials that can safely interact with the body's native tissues, either in a short-term manner or for permanent implantation.

2.3.2 Natural conductive biomaterials

Whereas the availability of synthetic conductive materials is expansive, the number of natural, conductive biomaterials can be categorized into two types. The first is analogous to conjugated polymers in that charge transport originates from π-π stacking and is most often seen in materials containing aromatic amino acids (*e.g.*, proteins and peptides) **(Fig. 2.4B)**. The other contains charge-dense regions throughout its chemical structure and mainly derives its conductive properties from the movement of ions rather than electrons **(Fig. 2.4C)**.

One of the most prominent models for naturally occurring conjugated conductive "polymers" is the pili proteins of *Geobacter sulfurreducens*[113,139,140,161–167]. These short proteins conduct electrons over μm to cm distances with conductivity around 5×10^{-3} S/cm.[112,139] The mechanism of electron transfer is believed to be electron hopping, made possible by the π-π interchain stacking which occurs when the phenyl rings of aromatic amino acids are in appropriate proximity (*d*-spacing, the distance between atomic planes, of ~3.5 Å)[112]. However, not all aromatic amino acids are equally conductive. The conductivity of the wild type PilA monomer (the precursor to the *G. sulfurreducens* pili)

was increased by 2000-fold by genetically substituting one tyrosine and one phenylalanine for tryptophan[140]. Kalyoncu *et al.* synthesized peptides and films based on *E. coli* secretions with added aromatic amino acids and observed increased conductivity of those materials when compared to controls. In agreement with previous observations, the materials containing tryptophan had higher conductivity compared to those containing phenylalanine or tyrosine. This study suggests that, in addition to conductive motifs, charged amino acids are also critical to conductivity[168,169]. Using peptides to make conductive materials is a recent development in the field[170–172], leaving much room to explore how peptides can be designed to mimic synthetic conductive polymers used for tissue engineering.

Beyond peptide structures, other natural conductive materials for tissue engineering have risen to the forefront. Amdursky and Hsu doped materials with the iron-based hemin for use in flexible bioelectronic interfaces[141] and neural tissue engineering[173], respectively. Hemin is a type of porphyrin, a class of compounds containing pyrrole subunits, making it a natural corollary to the frequently used PPy. Other groups have completely deviated from metallic mimics and embraced the conductivity associated with ionic charges. A new class of conductive hydrogels incorporates choline-based “bioionic liquids” (Bio-ILs)[3]. Ionic liquids generally possess high ionic conductivity along with other desirable features for material synthesis (thermal and electrochemical stability), and biologically based ionic liquids have the preferential property of being naturally derived, non-cytotoxic, and biodegradable. The conductivity of ionic liquids is believed to originate from ions “hopping” from one ion-dense site in the molecule to

another rather than through π-π stacking[160]. When conjugated to GelMA, the addition of Bio-IL increased conductivity of the hydrogels and supported the adhesion, proliferation, and maturation of primary cardiomyocytes. These hydrogels also provided sufficient conductive signaling to cardiomyocytes without ES, as evidenced by the cells' synchronous beating and upregulated connexin 43 protein expression[2]. When probing *in vivo* degradation, the results indicated that cells were able to enzymatically degrade GelMA-Bio-IL hydrogels *via* hydrolysis[3]. While these results are promising for using natural and ionically conductive materials for tissue engineering, additional research is warranted to establish whether ionically conducting materials can be incorporated into a variety of biomaterials and have similar effects on different cell and tissue types.

2.4 PROGRESS IN CONDUCTIVE MATERIALS FOR TISSUE ENGINEERING

The following section briefly summarizes goals of engineering specific tissues, describes how conductive materials have improved tissue engineering, and proposes an outlook for incorporating electroactive elements into tissue engineering.

2.4.1 Conductive materials for nerve tissue engineering

Nervous tissue has limited, or in the case of the central nervous system, no ability to regenerate on its own upon injury. Therefore, the restoration of nervous tissue after injury remains a significant medical challenge. One of the major goals when using neuronal cells to regenerate tissue is directing their differentiation down the neuronal line, rather than supporting cell types such as astrocytes and oligodendrocytes. Electroactive

materials have been repeatedly shown to be supportive of neuronal differentiation[12,21,174]. PPy, PEDOT:PSS, and carbon-based materials have been used frequently. Mass ratios of PPy greater than 0.2 in chitosan-alginate hydrogels led to substrates with conductivity on the order of 10^{-3} S/cm. When used as a nerve conduit, this concentration resulted in tissues with similar histological characteristics as autograft[6]. Adding 0.1 w/v% MWCNTs to PEG resulted in conductivity around 10^{-2} S/cm and greatest PC12 neurite outgrowth and mean length[124]. The addition of electrical stimulation promotes the generation of action potentials which improves synaptic function and is linked to increased secretion of neurotrophic factors, supporting functional recovery *in vivo*[55]. Conductive substrates have also been associated with increased expression of genes associated with Schwann cell myelination[120]. In light of their capacity to support multiple nerve cell types and functions, electroactive materials are promising tools for nerve regeneration.

Conductive substrates have been used as conduits for regeneration in both nervous systems, but the biosafety of and lack of biological mechanistic knowledge surrounding synthetic materials remain important issues to be addressed in future studies[175]. Few recent studies have investigated the action potential profile of neuronal cells grown on conductive substrates to confirm that they behave similarly to uninjured cells[176]. This information is important to consider, because while conductive hydrogels can significantly improve functional recovery, they are yet unable to recapitulate uninjured or autograft tissue.

2.4.2 Conductive materials for cardiac tissue engineering

Because cardiac tissue is electroactive, conductive materials are frequently used for cardiac tissue engineering and have successfully recapitulated the conductivity of native myocardium[129]. Synthetic polymers, carbon-based materials, and gold-based materials are most often used as conductive additives. Conductive substrates are also supportive of induced pluripotent stem cell (iPSC), endothelial stem cell (ESC), and embryoid body differentiation toward cardiomyocytes. The number of myotubes, myofibrils, and sarcomeres increases when cardiomyocytes are grown on electroconductive surfaces[177]. When seeded with cardiomyocytes, conductive materials aid in cell maturation, alignment, communication (*e.g.,* gap junction formation), synchronous beating, and physiological pacing[4]. Hydrogel composites containing CNTs resulted in more aligned cardiomyocyte organization, but it is unclear if this result was due to the mechanical or electrical features of CNTs[152,178]. Navaei *et al.* observed a similar effect using their hydrogel containing gold nanorods. Cardiomyocytes were more organized into the microgrooves of constructs containing gold nanorods than those of the non-doped construct[179]. These characteristics are critical for clinical translation, where development of arrhythmias remains a risk in cardiac tissue engineering. While conductive materials have improved synchronous beating, it remains to be explored whether the improved communication leads to phenotype changes related to cellular growth[92].

When fabricating cardiac patches, material elasticity and durability are of critical importance for proper organ function and longevity. Synthetic conductive substrates are

rarely characterized as highly elastic, nor have there been many reports of patches being cyclically tested to mimic *in vivo* performance. Elastic cardiac patches made from 10 w/v% GelMA and 66 v/v% Bio-IL exhibited conductivity around 1.5×10^{-3} S/cm and upregulated connexin 43 expression[2]. Despite promising preliminary results, the long-term performance of conductive substrates after MI and their potential for developing co-morbidities such as constrictive pericarditis and arrhythmia remains to be evaluated[2].

2.4.3 Conductive materials for muscle tissue engineering

Muscle tissue is efficient at regenerating small injuries, but critically sized injuries (*e.g.*, volumetric muscle loss) require intervention. The main goals of muscle tissue engineering are to promote differentiation of satellite cells or MSCs down the myogenic lineage, create a tissue with anisotropy to allow myoblasts to fuse into myotubes, and to develop vascularized, innervated constructs for functional and electrophysiological recovery. Tissue elasticity is also critical to support muscle contraction. Conductive materials have been effective at differentiating C2C12 myoblasts, upregulating myogenic genes and proteins, and promoting cell fusion[177]. Silk fibroin and a PANI-based polymer were combined to make scaffolds with conductivity on the order of 10^{-4} S/cm. When C2C12 myoblasts were seeded on scaffolds with 2 w/v% polymer, myogenic genes such as myogenic differentiation 1 (*MyoD1)*, myogenin, and troponin T1 (*TNNT1)* were upregulated, though the elasticity of these materials was not tested[145]. While elastic conductive materials have been developed, their material choice (*e.g.*, PA) does not

facilitate cell attachment or encapsulation, a factor which can be addressed in future studies[17].

In addition to supporting myogenic differentiation, the future of conductive materials can also be used to support the electroactivity of muscle tissue at large by encouraging innervation and neuromuscular junction (NMJ) formation[180]. Multiple studies have probed the cellular interplay between muscle and nerve and have reported spontaneous NMJ development. However, the majority of studies using conductive substrates for muscle tissue engineering do not explore co-culture systems. While many studies investigate how electrical stimulation and physical exercise influence muscle repair after injury, the possible synergy when using conductive substrates as a tissue scaffold remains uninvestigated[181].

2.4.4 Conductive materials for bone tissue engineering

The primary goal of bone tissue engineering is to replace critically sized defects unable to spontaneously heal, whether caused by trauma, bone-related diseases, or surgical excision. Strategies for bone tissue engineering focus on making a mechanically stable, osteoinductive, and osteoconductive material to promote bone formation. Bone is considered piezoelectric, meaning it generates electric potentials as it is mechanically loaded[182]. While this phenomenon occurs on the tissue level, the mechanosensitivity of osteocytes creates a connection between electroactive environments and bone remodeling[183,184]. Piezoelectric polymers, most commonly polyvinylidene fluoride (PVDF), have been used to for bone tissue engineering[177,185]. Dynamic mechanical loading of

osteoblasts on piezoelectric scaffolds improved growth and proliferation of osteoblasts[186] and osteogenic differentiation of adipose-derived MSCs[187]. Even in the absence of mechanical loading, the association of cells with conductive substrates and electrical stimulation enhances osteogenic activity[188]. PLA scaffolds with 10 wt% PANI possessed conductivities around 9×10^{-3} S/cm and promoted osteogenic gene expression and ALP activity of bone marrow-derived MSCs[148]. Graphene outperformed non-conductive groups in treating critically sized calvarial defects *in vivo*[189]. These findings indicate that substrate electroactivity is an important contributor to the regenerative capacity of bone cells.

Many bone tissue engineering strategies to date have recapitulated the mechanical environment of native bone and demonstrated efficacy *in vitro* and *in vivo*. Because bone is piezoelectric, it is important to confirm electrical functional outcomes in future studies[190]. Conductive substrates have been used as scaffold materials to improve osteogenic behavior. However, few studies have evaluated critical mechanical properties (*e.g.*, Young's modulus) as a function of substrate modification with electroactive polymers, which may lead to discrepancies in reproducibility. Possible synergies between electroactivity, mechanical cues, and chemical signals for bone tissue engineering are largely unexplored and provide great opportunity to expand foundational knowledge of bone regeneration.

2.5 CONCLUSION

Cells rely on mechanical, chemical, and electrical information to properly function during development and homeostasis. The field of tissue engineering has focused on the composition and mechanical properties of engineered substrates to instruct cell fate. Evidenced-based advances in bioelectricity motivate the pursuit of novel strategies that cater to cells' electrical needs. Despite the promising reports that conductive synthetic substrates influence cell behavior and promote engineered tissue function, these materials have several drawbacks that may be mitigated by the design of conductive natural biomaterials.[188] Additionally, the mismatch in conducting mechanism between electrically conductive substrates and bioelectric tissues has revealed gaps in understanding in how to design materials for the most relevant and significant clinical outcomes. Finally, variations across conductivity studies, whether in electrical stimulation parameters, methods to measure conductivity, and the lack of positive control groups prevent reproducibility within the field and hinder progress toward clinical translation.[189] In particular, foundational experiments to understand of the effects of altering the many parameters of studies using conductive materials (*e.g.*, level of conductivity, seal resistance, type of material or mechanism of conduction, or how electrical properties interplay with other properties within cell- and materials-based therapies) will be important to propel the field forward. The results of such foundational studies could then be used to design studies with more translational outputs both *in vitro* and *in vivo*. They also establish general fundamental understanding that allow for extension of using conductive materials for a variety of biomedical applications (*e.g.*,

improving *in vitro* modeling systems). The field of tissue engineering has evolved far beyond combining cells with materials and implanting in hopes of growing neotissues or promoting repair. There are many examples of pre-implantation characterization of cell adhesion, proliferation, migration, and differentiation in response to engineered materials. In contrast, the application of conductive materials in tissue engineering is only now emerging. The use of conductive materials for this purpose provides new opportunities to promote cellular organization *in vitro* prior to implantation, enabling the implantation of more advanced, functional tissues that possess greater therapeutic potential. Thus, there is tremendous opportunity on the horizon for developing materials that better recapitulate endogenous electrical signaling and support tissue engineering applications.

REFERENCES

1. Funk, R. H., Monsees, T. & Ozkucur, N. Electromagnetic effects - from cell biology to medicine. Prog Histochem Cytochem 43, 177–264 (2009).
2. Walker, B. W. et al. Engineering a naturally-derived adhesive and conductive cardiopatch. Biomaterials 207, 89–101 (2019).
3. Noshadi, I. et al. Engineering Biodegradable and Biocompatible Bio-ionic Liquid Conjugated Hydrogels with Tunable Conductivity and Mechanical Properties. Sci. Rep. 7, 4345 (2017).
4. Cui, Z. et al. Polypyrrole-chitosan conductive biomaterial synchronizes cardiomyocyte contraction and improves myocardial electrical impulse propagation. Theranostics 8, 2752–2764 (2018).
5. Yang, B. et al. Development of electrically conductive double-network hydrogels via one-step facile strategy for cardiac tissue engineering. Adv Heal. Mater 5, 474–88 (2016).
6. Bu, Y. et al. A conductive sodium alginate and carboxymethyl chitosan hydrogel doped with polypyrrole for peripheral nerve regeneration. RSC Adv. 8, 10806–10817 (2018).
7. Mihic, A. et al. A conductive polymer hydrogel supports cell electrical signaling and improves cardiac function after implantation into myocardial infarct. Circulation 132, 772–84 (2015).
8. Shastri, V. R., Schmidt, C. E., Kim, T. H., Vacanti, J. P. & Langer, R. Polypyrrole - a potential candidate for stimulated nerve regeneration. MRS Proc. 414, (2011).
9. Xu, H. et al. Conductive PPY/PDLLA conduit for peripheral nerve regeneration. Biomaterials 35, 225–35 (2014).
10. Yang, J., Choe, G., Yang, S., Jo, H. & Lee, J. Y. Polypyrrole-incorporated conductive hyaluronic acid hydrogels. Biomater Res 20, 31 (2016).
11. Zhou, X. et al. Enhancement of neurite adhesion, alignment and elongation on conductive polypyrrole-poly(lactide acid) fibers with cell-derived extracellular matrix. Colloids Surf B Biointerfaces 149, 217–225 (2017).
12. Wang, S. et al. 3D culture of neural stem cells within conductive PEDOT layer-assembled chitosan/gelatin scaffolds for neural tissue engineering. Mater Sci Eng C Mater Biol Appl 93, 890–901 (2018).
13. Wang, S. P. et al. Chitosan/gelatin porous scaffolds assembled with conductive poly(3,4-ethylenedioxythiophene) nanoparticles for neural tissue engineering. J. Mater. Chem. B 5, 4774–4788 (2017).
14. Roshanbinfar, K. et al. Electroconductive biohybrid hydrogel for enhanced maturation and beating properties of engineered cardiac tissues. Adv. Funct. Mater. 28, 1803951 (2018).
15. Liu, X. et al. Functionalized carbon nanotube and graphene oxide embedded electrically conductive hydrogel synergistically stimulates nerve cell differentiation. ACS Appl Mater Interfaces 9, 14677–14690 (2017).
16. Scapin, G. et al. Enhanced neuronal cell differentiation combining biomimetic peptides and a carbon nanotube-polymer scaffold. Nanomed. 11, 621–32 (2015).

17. Alam, A., Kuan, H. C., Zhao, Z. H., Xu, J. & Ma, J. Novel polyacrylamide hydrogels by highly conductive, water-processable graphene. Compos. Part Appl. Sci. Manuf. 93, 1–9 (2017).
18. Ryan, A. J. et al. Electroconductive biohybrid collagen/pristine graphene composite biomaterials with enhanced biological activity. Adv Mater 30, e1706442 (2018).
19. Baei, P. et al. Electrically conductive gold nanoparticle-chitosan thermosensitive hydrogels for cardiac tissue engineering. Mater Sci Eng C Mater Biol Appl 63, 131–41 (2016).
20. Navaei, A. et al. Gold nanorod-incorporated gelatin-based conductive hydrogels for engineering cardiac tissue constructs. Acta Biomater 41, 133–46 (2016).
21. Zhou, L. et al. Soft conducting polymer hydrogels cross-linked and doped by tannic acid for spinal cord injury repair. ACS Nano 12, 10957–10967 (2018).
22. Min, J. H., Patel, M. & Koh, W. G. Incorporation of conductive materials into hydrogels for tissue engineering applications. Polymers 10, 1078–1078 (2018).
23. Guiseppi-Elie, A. Electroconductive hydrogels: synthesis, characterization and biomedical applications. Biomaterials 31, 2701–16 (2010).
24. Falagan-Lotsch, P., Grzincic, E. M. & Murphy, C. J. One low-dose exposure of gold nanoparticles induces long-term changes in human cells. Proc. Natl. Acad. Sci. 113, 13318–13323 (2016).
25. Piccolino, M. Luigi Galvani and animal electricity: two centuries after the foundation of electrophysiology. Trends Neurosci. 20, 443–448 (1997).
26. Levin, M., Pezzulo, G. & Finkelstein, J. M. Endogenous bioelectric signaling networks: exploiting voltage gradients for control of growth and form. Annu Rev Biomed Eng 19, 353–387 (2017).
27. McLaughlin, K. A. & Levin, M. Bioelectric signaling in regeneration: mechanisms of ionic controls of growth and form. Dev Biol 433, 177–189 (2018).
28. Funk, R. H. Endogenous electric fields as guiding cue for cell migration. Front Physiol 6, 143 (2015).
29. Snyder, S., DeJulius, C. & Willits, R. K. Electrical stimulation increases random migration of human dermal fibroblasts. Ann Biomed Eng 45, 2049–2060 (2017).
30. Kojima, J. et al. Electrically promoted protein production by mammalian cells cultured on the electrode surface. Biotechnol Bioeng 39, 27–32 (1992).
31. Mathews, J. & Levin, M. The body electric 2.0: recent advances in developmental bioelectricity for regenerative and synthetic bioengineering. Curr Opin Biotechnol 52, 134–144 (2018).
32. Reid, B., Song, B. & Zhao, M. Electric currents in Xenopus tadpole tail regeneration. Dev Biol 335, 198–207 (2009).
33. Thrivikraman, G., Boda, S. K. & Basu, B. Unraveling the mechanistic effects of electric field stimulation towards directing stem cell fate and function: a tissue engineering perspective. Biomaterials 150, 60–86 (2018).
34. Balint, R., Cassidy, N. J. & Cartmell, S. H. Electrical stimulation: a novel tool for tissue engineering. Tissue Eng Part B Rev 19, 48–57 (2013).
35. Cao, L. et al. Endogenous electric currents might guide rostral migration of neuroblasts. EMBO Rep 14, 184–90 (2013).

36. Yao, L., Shanley, L., McCaig, C. & Zhao, M. Small applied electric fields guide migration of hippocampal neurons. J Cell Physiol 216, 527–35 (2008).
37. Nie, K. & Henderson, A. MAP kinase activation in cells exposed to a 60 Hz electromagnetic field. J Cell Biochem 90, 1197–206 (2003).
38. Wolf-Goldberg, T., Barbul, A., Ben-Dov, N. & Korenstein, R. Low electric fields induce ligand-independent activation of EGF receptor and ERK via electrochemical elevation of H(+) and ROS concentrations. Biochim Biophys Acta 1833, 1396–408 (2013).
39. Hart, F. X. Integrins may serve as mechanical transducers for low-frequency electric fields. Bioelectromagnetics 27, 505–8 (2006).
40. Delle Monache, S. et al. Inhibition of angiogenesis mediated by extremely low-frequency magnetic fields (ELF-MFs). PLoS One 8, e79309 (2013).
41. Zrimec, A., Jerman, I. & Lahajnar, G. Alternating electric fields stimulate ATP synthesis in Escherichia coli. Cell Mol Biol Lett 7, 172–4 (2002).
42. Tarasov, A. I. et al. Frequency-dependent mitochondrial Ca(2+) accumulation regulates ATP synthesis in pancreatic beta cells. Pflugers Arch 465, 543–54 (2013).
43. Sheikh, A. Q. et al. Regulation of endothelial MAPK/ERK signalling and capillary morphogenesis by low-amplitude electric field. J R Soc Interface 10, 20120548 (2013).
44. Lozano, M. M., Hovis, J. S., Moss, F. R., 3rd & Boxer, S. G. Dynamic reorganization and correlation among lipid raft components. J Am Chem Soc 138, 9996–10001 (2016).
45. Lin, B.-J. et al. Lipid rafts sense and direct electric field-induced migration. Proc. Natl. Acad. Sci. 114, 8568–8573 (2017).
46. Feng, J. F. et al. Guided migration of neural stem cells derived from human embryonic stem cells by an electric field. Stem Cells 30, 349–55 (2012).
47. Chen, C., Bai, X., Ding, Y. & Lee, I.-S. Electrical stimulation as a novel tool for regulating cell behavior in tissue engineering. Biomater. Res. 23, 25 (2019).
48. Guo, A. et al. Effects of physiological electric fields on migration of human dermal fibroblasts. J Invest Dermatol 130, 2320–7 (2010).
49. Zimolag, E. et al. Electric field as a potential directional cue in homing of bone marrow-derived mesenchymal stem cells to cutaneous wounds. Biochim Biophys Acta Mol Cell Res 1864, 267–279 (2017).
50. Long, Y. et al. Effective wound healing enabled by discrete alternative electric fields from wearable nanogenerators. ACS Nano 12, 12533–12540 (2018).
51. Gao, J. et al. Biomimetic stochastic topography and electric fields synergistically enhance directional migration of corneal epithelial cells in a MMP-3-dependent manner. Acta Biomater 12, 102–112 (2015).
52. Tian, L. et al. Synergistic effect of topography, surface chemistry and conductivity of the electrospun nanofibrous scaffold on cellular response of PC12 cells. Colloids Surf. B Biointerfaces 145, 420–429 (2016).
53. Cho, M. R., Thatte, H. S., Lee, R. C. & Golan, D. E. Reorganization of microfilament structure induced by ac electric fields. FASEB J 10, 1552–8 (1996).

54. Tsai, C. H., Lin, B. J. & Chao, P. H. alpha2beta1 integrin and RhoA mediates electric field-induced ligament fibroblast migration directionality. J Orthop Res 31, 322–7 (2013).
55. Song, J. et al. Polymerizing pyrrole coated poly (l-lactic acid-co-epsilon-caprolactone) (PLCL) conductive nanofibrous conduit combined with electric stimulation for long-range peripheral nerve regeneration. Front Mol Neurosci 9, 117 (2016).
56. Choi, W. J. et al. Effects of substrate conductivity on cell morphogenesis and proliferation using tailored, atomic layer deposition-grown ZnO thin films. Sci Rep 5, 9974 (2015).
57. Wu, Y. & Guo, L. Enhancement of intercellular electrical synchronization by conductive materials in cardiac tissue engineering. IEEE Trans Biomed Eng 65, 264–272 (2018).
58. Kotwal, A. & Schmidt, C. E. Electrical stimulation alters protein adsorption and nerve cell interactions with electrically conducting biomaterials. Biomaterials 22, 1055–64 (2001).
59. Blackiston, D. J., McLaughlin, K. A. & Levin, M. Bioelectric controls of cell proliferation: Ion channels, membrane voltage and the cell cycle. Cell Cycle 8, 3527–3536 (2009).
60. Lei, K. F., Hsieh, S. C., Goh, A., Kuo, R. L. & Tsang, N. M. Proliferation arrest, selectivity, and chemosensitivity enhancement of cancer cells treated by a low-intensity alternating electric field. Biomed Microdevices 20, 90 (2018).
61. Martinelli, V. et al. Carbon nanotubes promote growth and spontaneous electrical activity in cultured cardiac myocytes. Nano Lett 12, 1831–8 (2012).
62. Frelinger, A. L., 3rd et al. Platelet-rich plasma stimulated by pulse electric fields: platelet activation, procoagulant markers, growth factor release and cell proliferation. Platelets 27, 128–35 (2016).
63. Yan, D., Yang, C., Miao, J., Lam, Y. & Huang, X. Enhancement of electrokinetically driven microfluidic T-mixer using frequency modulated electric field and channel geometry effects. Electrophoresis 30, 3144–52 (2009).
64. Cao, L. et al. Endogenous bioelectric currents promote differentiation of the mammalian lens. J Cell Physiol 233, 2202–2212 (2018).
65. Diaz-Vegas, A. et al. ROS Production via P2Y1-PKC-NOX2 Is Triggered by Extracellular ATP after Electrical Stimulation of Skeletal Muscle Cells. PLoS One 10, e0129882 (2015).
66. Yamada, M. et al. Electrical stimulation modulates fate determination of differentiating embryonic stem cells. Stem Cells 25, 562–70 (2007).
67. Tonelli, F. M. P. et al. Stem Cells and Calcium Signaling. in Calcium Signaling (ed. Islam, M.) vol. 740 891–916 (Springer, Dordrecht, 2012).
68. Sauer, H., Wartenberg, M. & Hescheler, J. Reactive oxygen species as intracellular messengers during cell growth and differentiation. Cell Physiol Biochem 11, 173–86 (2001).

69. Manthey, A. L. et al. Using electrical stimulation to enhance the efficacy of cell transplantation therapies for neurodegenerative retinal diseases: concepts, challenges, and future perspectives. Cell Transpl. 26, 949–965 (2017).
70. Matsumoto, M. et al. Electrical stimulation enhances neurogenin2 expression through beta-catenin signaling pathway of mouse bone marrow stromal cells and intensifies the effect of cell transplantation on brain injury. Neurosci Lett 533, 71–6 (2013).
71. George, P. M. et al. Electrical preconditioning of stem cells with a conductive polymer scaffold enhances stroke recovery. Biomaterials 142, 31–40 (2017).
72. Kwon, H. J., Lee, G. S. & Chun, H. Electrical stimulation drives chondrogenesis of mesenchymal stem cells in the absence of exogenous growth factors. Sci Rep 6, 39302 (2016).
73. Zhang, J., Li, M., Kang, E. T. & Neoh, K. G. Electrical stimulation of adipose-derived mesenchymal stem cells in conductive scaffolds and the roles of voltage-gated ion channels. Acta Biomater 32, 46–56 (2016).
74. Pitcairn, E. et al. Coordinating heart morphogenesis: a novel role for hyperpolarization-activated cyclic nucleotide-gated (HCN) channels during cardiogenesis in Xenopus laevis. Commun Integr Biol 10, e1309488 (2017).
75. Bannerman, P. & James, M. A. Molecular Mechanisms to Improve Nerve Regeneration Following Damage to the Immature Peripheral Nervous System. 91, 87 (2009).
76. Clow, C. & Jasmin, B. J. Brain-derived neurotrophic factor regulates satellite cell differentiation and skeltal muscle regeneration. Mol Biol Cell 21, 2182–90 (2010).
77. Kuntz, A. & Richins, C. A. Innervation of the bone marrow. J. Comp. Neurol. 83, 213–222 (1945).
78. Togari, A. Adrenergic regulation of bone metabolism: Possible involvement of sympathetic innervation of osteoblastic and osteoclastic cells. Microsc. Res. Tech. 58, 77–84 (2002).
79. Aerts-Kaya, F. et al. Neurological regulation of the bone marrow niche. in Advances in Experimental Medicine and Biology (Springer US, 2019). doi:10.1007/5584_2019_398.
80. Ackermann, P. W., Li, J., Finn, A., Ahmed, M. & Kreicbergs, A. Autonomic innervation of tendons, ligaments and joint capsules. A morphologic and quantitative study in the rat. J. Orthop. Res. 19, 372–378 (2001).
81. Marrella, A. et al. Engineering vascularized and innervated bone biomaterials for improved skeletal tissue regeneration. Mater. Today 21, 362–376 (2018).
82. Tuo, Y. et al. The biological effects and mechanisms of calcitonin gene-related peptide on human endothelial cell. 33, 114–123 (2013).
83. Fan, J.-J., Mu, T.-W., Qin, J.-J., Bi, L. & Pei, G.-X. Different Effects of Implanting Sensory Nerve or Blood Vessel on the Vascularization, Neurotization, and Osteogenesis of Tissue-Engineered Bone In Vivo. 2014, 1–10 (2014).
84. Feng, L., Lingling, E. & Liu, H. The effects of separating inferior alveolar neurovascular bundles on osteogenesis of tissue-engineered bone and vascularization. (2014) doi:10.5507/bp.2014.050.

85. Jia, S. et al. Calcitonin gene-related peptide enhances osteogenic differentiation and recruitment of bone marrow mesenchymal stem cells in rats. Exp. Ther. Med. (2019) doi:10.3892/etm.2019.7659.
86. Raimondo, T. M. et al. Combined delivery of VEGF and IGF-1 promotes functional innervation in mice and improves muscle transplantation in rabbits. Biomaterials 216, 119246–119246 (2019).
87. Dos Santos, B. P. et al. Development of a cell-free and growth factor-free hydrogel capable of inducing angiogenesis and innervation after subcutaneous implantation. Acta Biomater 99, 154–167 (2019).
88. Grossemy, S., Chan, P. P. Y. & Doran, P. M. Electrical stimulation of cell growth and neurogenesis using conductive and nonconductive microfibrous scaffolds. Integr. Biol. 11, 264–279 (2019).
89. Hardy, J. G., Lee, J. Y. & Schmidt, C. E. Biomimetic conducting polymer-based tissue scaffolds. Curr Opin Biotechnol 24, 847–54 (2013).
90. Balint, R., Cassidy, N. J. & Cartmell, S. H. Conductive polymers: towards a smart biomaterial for tissue engineering. Acta Biomater 10, 2341–53 (2014).
91. Yuk, H., Lu, B. & Zhao, X. Hydrogel bioelectronics. Chem Soc Rev 48, 1642–1667 (2019).
92. Burnstine-Townley, A., Eshel, Y. & Amdursky, N. Conductive scaffolds for cardiac and neuronal tissue engineering: governing factors and mechanisms. Adv. Funct. Mater. 1901369 (2019) doi:10.1002/adfm.201901369.
93. Ning, C., Zhou, Z., Tan, G., Zhu, Y. & Mao, C. Electroactive polymers for tissue regeneration: developments and perspectives. Prog Polym Sci 81, 144–162 (2018).
94. Anderson, M. et al. Peripheral nerve regeneration strategies: electrically stimulating polymer based nerve growth conduits. Crit Rev Biomed Eng 43, 131–59 (2015).
95. Abidian, M. R. et al. Hybrid conducting polymer-hydrogel conduits for axonal growth and neural tissue engineering. Adv Heal. Mater 1, 762–7 (2012).
96. Green, R. A., Baek, S., Poole-Warren, L. A. & Martens, P. J. Conducting polymer-hydrogels for medical electrode applications. Sci Technol Adv Mater 11, 014107 (2010).
97. Guimard, N. K., Gomez, N. & Schmidt, C. E. Conducting polymers in biomedical engineering. Prog Polym Sci 32, 876–921 (2007).
98. Bonfrate, V. et al. Enhanced electrical conductivity of collagen films through long-range aligned iron oxide nanoparticles. J Colloid Interface Sci 501, 185–191 (2017).
99. Broda, C. R., Lee, J. Y., Sirivisoot, S., Schmidt, C. E. & Harrison, B. S. A chemically polymerized electrically conducting composite of polypyrrole nanoparticles and polyurethane for tissue engineering. J Biomed Mater Res A 98, 509–16 (2011).
100. Gan, D. et al. Conductive and tough hydrogels based on biopolymer molecular templates for controlling in situ formation of polypyrrole nanorods. ACS Appl Mater Interfaces 10, 36218–36228 (2018).
101. Liu, X. et al. Covalent crosslinking of graphene oxide and carbon nanotube into hydrogels enhances nerve cell responses. J. Mater. Chem. B 4, 6930–6941 (2016).

102. Feiner, R., Fleischer, S., Shapira, A., Kalish, O. & Dvir, T. Multifunctional degradable electronic scaffolds for cardiac tissue engineering. J Control Release 281, 189–195 (2018).
103. Pena, B. et al. Gold nanoparticle-functionalized reverse thermal gel for tissue engineering applications. ACS Appl Mater Interfaces 11, 18671–18680 (2019).
104. Mobini, S., Spearman, B. S., Lacko, C. S. & Schmidt, C. E. Recent advances in strategies for peripheral nerve tissue engineering. Curr. Opin. Biomed. Eng. 4, 134–142 (2017).
105. Song, S. & George, P. M. Conductive polymer scaffolds to improve neural recovery. Neural Regen Res 12, 1976–1978 (2017).
106. Spearman, B. S. et al. Tissue-engineered peripheral nerve interfaces. Adv. Funct. Mater. 28, 1701713–1701713 (2018).
107. Mawad, D. et al. A conducting polymer with enhanced electronic stability applied in cardiac models. Sci Adv 2, e1601007 (2016).
108. MacDiarmid, A. G. 'Synthetic metals': a novel role for oganic polymers (Nobel lecture). Angew Chem Int Ed 40, 2581–2590 (2001).
109. NobelPrize.org. Popular information. https://www.nobelprize.org/prizes/chemistry/2000/popular-information (2000).
110. Tandon, B., Magaz, A., Balint, R., Blaker, J. J. & Cartmell, S. H. Electroactive biomaterials: vehicles for controlled delivery of therapeutic agents for drug delivery and tissue regeneration. Adv Drug Deliv Rev 129, 148–168 (2018).
111. Kaur, G., Adhikari, R., Cass, P., Bown, M. & Gunatillake, P. Electrically conductive polymers and composites for biomedical applications. RSC Adv. 5, 37553–37567 (2015).
112. Malvankar, N. S. et al. Tunable metallic-like conductivity in microbial nanowire networks. Nat Nanotechnol 6, 573–9 (2011).
113. Malvankar, N. S. et al. Structural basis for metallic-like conductivity in microbial nanowires. mBio 6, e00084 (2015).
114. Pan, L. et al. Hierarchical nanostructured conducting polymer hydrogel with high electrochemical activity. PNAS 109, 9287–92 (2012).
115. Yu, Z., Xia, Y., Du, D. & Ouyang, J. PEDOT:PSS films with metallic conductivity through a treatment with common organic solutions of organic salts and their application as a transparent electrode of polymer solar cells. ACS Appl Mater Interfaces 8, 11629–38 (2016).
116. Lu, B. et al. Pure PEDOT:PSS hydrogels. Nat Commun 10, 1043 (2019).
117. Wang, Y. & Weng, G. J. Electrical conductivity of carbon nanotube- and graphene-based nanocomposites. in Micromechanics and Nanomechanics of Composite Solids (eds. Meguid, S. & Weng, G.) 123–156 (Springer, Cham., 2018). doi:10.1007/978-3-319-52794-9_4.
118. Yang, S. et al. Polypyrrole/Alginate Hybrid Hydrogels: Electrically Conductive and Soft Biomaterials for Human Mesenchymal Stem Cell Culture and Potential Neural Tissue Engineering Applications. Macromol. Biosci. 16, 1653–1661 (2016).
119. Wibowo, A. et al. 3D printing of polycaprolactone-polyaniline electroactive scaffolds for bone tissue engineering. Mater. Basel 13, 512 (2020).

120. Wu, Y., Wang, L., Guo, B., Shao, Y. & Ma, P. X. Electroactive biodegradable polyurethane significantly enhanced Schwann cells myelin gene expression and neurotrophin secretion for peripheral nerve tissue engineering. Biomaterials 87, 18–31 (2016).
121. Wang, S. et al. Hyaluronic acid doped-poly(3,4-ethylenedioxythiophene)/chitosan/gelatin (PEDOT-HA/Cs/Gel) porous conductive scaffold for nerve regeneration. Mater Sci Eng C Mater Biol Appl 71, 308–316 (2017).
122. Solazzo, M. et al. PEDOT:PSS interfaces stabilised using a PEGylated crosslinker yield improved conductivity and biocompatibility. J Mater Chem B 7, 4811–4820 (2019).
123. Wu, Y., Wang, L., Guo, B. & Ma, P. X. Interwoven aligned conductive nanofiber yarn/hydrogel composite scaffolds for engineered 3D cardiac anisotropy. ACS Nano 11, 5646–5659 (2017).
124. Imaninezhad, M. et al. Directed and enhanced neurite outgrowth following exogenous electrical stimulation on carbon nanotube-hydrogel composites. J Neural Eng 15, 056034 (2018).
125. Han, L. et al. A mussel-inspired conductive, self-adhesive, and self-healable tough hydrogel as cell stimulators and implantable bioelectronics. Small 13, 1601916 (2017).
126. Wong, J. Y., Langer, R. & Ingber, D. E. Electrically conducting polymers can noninvasively control the shape and growth of mammalian cells. Proc Nati Acad Sci USA 91, 3201–3204 (1994).
127. Brahim, S. & Guiseppi-Elie, A. Electroconductive hydrogels: electrical properties of polypyrrole-poly(HEMA) and electrochemical composites. Electroanalysis 17, 556–570 (2005).
128. de Castro, J. G. et al. Designing a novel nanocomposite for bone tissue engineering using electrospun conductive PBAT/polypyrrole as a scaffold to direct nanohydroxyapatite electrodeposition. RSC Adv. 6, 32615–32623 (2016).
129. Surowiec, A., Stuchly, S. S., Eidus, L. & Swarup, A. In vitro dielectric properties of human tissues at radiofrequencies. 32, 615–621 (1987).
130. Gabriel, C., Peyman, A. & Grant, E. H. Electrical conductivity of tissue at frequencies below 1 MHz. Phys. Med. Biol. 54, 4863–4878 (2009).
131. Balmer, T. W., Vesztergom, S., Broekmann, P., Stahel, A. & Buchler, P. Characterization of the electrical conductivity of bone and its correlation to osseous structure. Sci Rep 8, 8601 (2018).
132. Binette, J. S., Garon, M., Savard, P., McKee, M. D. & Buschmann, M. D. Tetrapolar measurement of electrical conductivity and thickness of articular cartilage. J Biomech Eng 126, 475–84 (2004).
133. Zarrintaj, P. et al. Agarose-based biomaterials for tissue engineering. Carbohydr Polym 187, 66–84 (2018).
134. Sun, H. et al. Carbon nanotube-incorporated collagen hydrogels improve cell alignment and the performance of cardiac constructs. Int J Nanomedicine 12, 3109–3120 (2017).

135. MacDonald, R. A., Voge, C. M., Kariolis, M. & Stegemann, J. P. Carbon nanotubes increase the electrical conductivity of fibroblast-seeded collagen hydrogels. Acta Biomater 4, 1583–92 (2008).
136. Kaklamani, G. et al. On the electrical conductivity of alginate hydrogels. Regen Biomater 5, 293–301 (2018).
137. Guarino, V., Alvarez-Perez, M. A., Borriello, A., Napolitano, T. & Ambrosio, L. Conductive PANi/PEGDA macroporous hydrogels for nerve regeneration. Adv Heal. Mater 2, 218–27 (2013).
138. Marroquin, J. B., Rhee, K. Y. & Park, S. J. Chitosan nanocomposite films: enhanced electrical conductivity, thermal stability, and mechanical properties. Carbohydr Polym 92, 1783–91 (2013).
139. Adhikari, R. Y., Malvankar, N. S., Tuominen, M. T. & Lovley, D. R. Conductivity of individual Geobacter pili. Rsc Adv. 6, 8363–8366 (2016).
140. Tan, Y. et al. Synthetic Biological Protein Nanowires with High Conductivity. Small 12, 4481–4485 (2016).
141. Amdursky, N. et al. Electron hopping across hemin-doped serum albumin mats on centimeter-length scales. Adv Mater 29, (2017).
142. Solazzo, M., O'Brien, F. J., Nicolosi, V. & Monaghan, M. G. The rationale and emergence of electroconductive biomaterial scaffolds in cardiac tissue engineering. APL Bioeng. 3, 041501 (2019).
143. Humpolicek, P. et al. The biocompatibility of polyaniline and polypyrrole: A comparative study of their cytotoxicity, embryotoxicity and impurity profile. Mater Sci Eng C Mater Biol Appl 91, 303–310 (2018).
144. Qazi, T. H., Rai, R. & Boccaccini, A. R. Tissue engineering of electrically responsive tissues using polyaniline based polymers: a review. Biomaterials 35, 9068–86 (2014).
145. Zhang, M. & Guo, B. Electroactive 3D scaffolds based on silk fibroin and water-bornepolyaniline for skeletal muscle tissue engineering. Macromol Biosci 17, 1700147 (2017).
146. Chen, M.-C., Sun, Y.-C. & Chen, Y.-H. Electrically conductive nanofibers with highly oriented structures and their potential application in skeletal muscle tissue engineering. Acta Biomater. 9, 5562–5572 (2013).
147. Li, Y. et al. Enhanced adhesion and proliferation of human umbilical vein endothelial cells on conductive PANI-PCL fiber scaffold by electrical stimulation. Mater Sci Eng C Mater Biol Appl 72, 106–112 (2017).
148. Chen, J., Yu, M., Guo, B., Ma, P. X. & Yin, Z. Conductive nanofibrous composite scaffolds based on in-situ formed polyaniline nanoparticle and polylactide for bone regeneration. J Colloid Interface Sci 514, 517–527 (2018).
149. Wang, S. et al. Fabrication and characterization of conductive poly (3,4-ethylenedioxythiophene) doped with hyaluronic acid/poly (l-lactic acid) composite film for biomedical application. J Biosci Bioeng 123, 116–125 (2017).
150. Spencer, A. R. et al. Bioprinting of a Cell-Laden Conductive Hydrogel Composite. ACS Appl. Mater. Interfaces 11, 30518–30533 (2019).

151. Heo, D. N. et al. Development of 3D printable conductive hydrogel with crystallized PEDOT:PSS for neural tissue engineering. Mater Sci Eng C Mater Biol Appl 99, 582–590 (2019).
152. Shin, S. R. et al. Carbon-nanotube-embedded hydrogel sheets for engineering cardiac constructs and bioactuators. ACS Nano 7, 2369–80 (2013).
153. Li, D., Muller, M. B., Gilje, S., Kaner, R. B. & Wallace, G. G. Processable aqueous dispersions of graphene nanosheets. Nat Nanotechnol 3, 101–5 (2008).
154. Balikov, D. A. et al. Directing lineage specification of human mesenchymal stem cells by decoupling electrical stimulation and physical patterning on unmodified graphene. Nanoscale 8, 13730–9 (2016).
155. Jia, G. et al. Cytotoxicity of carbon nanomaterials: single-wall nanotube, multi-wall nanotube, and fullerene. Env. Sci Technol 39, 1378–83 (2005).
156. Lam, C. W., James, J. T., McCluskey, R. & Hunter, R. L. Pulmonary toxicity of single-wall carbon nanotubes in mice 7 and 90 days after intratracheal instillation. Toxicol Sci 77, 126–34 (2004).
157. Di Giorgio, M. L. et al. Effects of single and multi walled carbon nanotubes on macrophages: cyto and genotoxicity and electron microscopy. Mutat Res 722, 20–31 (2011).
158. Principi, E. et al. Systemic distribution of single-walled carbon nanotubes in a novel model: alteration of biochemical parameters, metabolic functions, liver accumulation, and inflammation in vivo. Int J Nanomedicine 11, 4299–316 (2016).
159. Prajapati, S. K., Malaiya, A., Kesharwani, P., Soni, D. & Jain, A. Biomedical applications and toxicities of carbon nanotubes. Drug Chem Toxicol 1–16 (2020) doi:10.1080/01480545.2019.1709492.
160. Feng, G. et al. Free and bound states of ions in ionic liquids, conductivity, and underscreening paradox. Phys. Rev. X 9, (2019).
161. Bond, D. R. & Lovley, D. R. Electricity production by Geobacter sulfurreducens attached to electrodes. Appl Env. Microbiol 69, 1548–55 (2003).
162. Ing, N. L., Nusca, T. D. & Hochbaum, A. I. Geobacter sulfurreducens pili support ohmic electronic conduction in aqueous solution. Phys Chem Chem Phys 19, 21791–21799 (2017).
163. Malvankar, N. S. & Lovley, D. R. Microbial nanowires: a new paradigm for biological electron transfer and bioelectronics. ChemSusChem 5, 1039–46 (2012).
164. Reardon, P. N. & Mueller, K. T. Structure of the type IVa major pilin from the electrically conductive bacterial nanowires of Geobacter sulfurreducens. J Biol Chem 288, 29260–6 (2013).
165. Vargas, M. et al. Aromatic amino acids required for pili conductivity and long-range extracellular electron transport in Geobacter sulfurreducens. mBio 4, e00105-13 (2013).
166. Xiao, K. et al. Low energy atomic models suggesting a pilus structure that could account for electrical conductivity of Geobacter sulfurreducens pili. Sci Rep 6, 23385 (2016).
167. Yates, M. D. et al. Measuring conductivity of living Geobacter sulfurreducens biofilms. Nat. Nanotechnol. 11, 910–913 (2016).

168. Kalyoncu, E., Ahan, R. E., Olmez, T. T. & Seker, U. O. S. Genetically encoded conductive protein nanofibers secreted by engineered cells. RSC Adv. 7, 32543–32551 (2017).
169. Sepunaru, L. et al. Electronic transport via homopeptides: the role of side chains and secondary structure. J Am Chem Soc 137, 9617–26 (2015).
170. Ing, N. L., Spencer, R. K., Luong, S. H., Nguyen, H. D. & Hochbaum, A. I. Electronic Conductivity in Biomimetic α-Helical Peptide Nanofibers and Gels. ACS Nano 12, 2652–2661 (2018).
171. Hayamizu, Y. et al. Bioelectronic interfaces by spontaneously organized peptides on 2D atomic single layer materials. Sci Rep 6, 33778 (2016).
172. Hauser, C. A. E. & Zhang, S. Peptides as biological semiconductors. http://nobelprize.org/nobel_prizes/chemistry/ (2010).
173. Hsu, C. C., Serio, A., Amdursky, N., Besnard, C. & Stevens, M. M. Fabrication of hemin-doped serum albumin-based fibrous scaffolds for neural tissue engineering applications. ACS Appl Mater Interfaces 10, 5305–5317 (2018).
174. Niu, Y. et al. Enhancing neural differentiation of induced pluripotent stem cells by conductive graphene/silk fibroin films. J Biomed Mater Res A 106, 2973–2983 (2018).
175. Yang, M., Liang, Y., Gui, Q., Chen, J. & Liu, Y. Electroactive biocompatible materials for nerve cell stimulation. Mater. Res. Express 2, 042001–042001 (2015).
176. Acosta-Garcia, M. C. et al. Simultaneous recording of electrical activity and the underlying ionic currents in NG108-15 cells cultured on gold substrate. Heliyon 4, e00550 (2018).
177. da Silva, L. P., Kundu, S. C., Reis, R. L. & Correlo, V. M. Electric phenomenon: a disregarded tool in tissue engineering and regenerative medicine. Trends Biotechnol 38, 24–49 (2020).
178. Mostafavi, E. et al. Electroconductive Nanobiomaterials for Tissue Engineering and Regenerative Medicine. Bioelectricity 2, 120–149 (2020).
179. Navaei, A. et al. Electrically conductive hydrogel-based micro-topographies for the development of organized cardiac tissues. RSC Adv. 7, 3302–3312 (2017).
180. Freeman, J. W. & Browe, D. P. Bio-Instructive Scaffolds for Skeletal Muscle Regeneration. in Bio-Instructive Scaffolds for Musculoskeletal Tissue Engineering and Regenerative Medicine 187–199 (Elsevier, 2017). doi:10.1016/b978-0-12-803394-4.00008-2.
181. Gilbert-Honick, J. & Grayson, W. Vascularized and innervated skeletal muscle tissue engineering. Adv Heal. Mater 9, e1900626 (2020).
182. Marino, A. A., Becker, R. O. & Soderholm, S. C. Origin of the piezoelectric effect in bone. Calcif. Tissue Res. 8, 177–180 (1971).
183. Ahn, A. C. & Grodzinsky, A. J. Relevance of collagen piezoelectricity to “Wolff’s Law”: A critical review. Med. Eng. Phys. 31, 733–741 (2009).
184. van Oers, R. F. M., Wang, H. & Bacabac, R. G. Osteocyte Shape and Mechanical Loading. Curr. Osteoporos. Rep. 13, 61–66 (2015).
185. Ribeiro, C., Sencadas, V., Correia, D. M. & Lanceros-Mendez, S. Piezoelectric polymers as biomaterials for tissue engineering applications. Colloids Surf B Biointerfaces 136, 46–55 (2015).

186. Ribeiro, C. et al. Enhanced proliferation of pre-osteoblastic cells by dynamic piezoelectric stimulation. Rsc Adv. 2, 11504–11509 (2012).
187. Ribeiro, C. et al. Dynamic piezoelectric stimulation enhances osteogenic differentiation of human adipose stem cells. J Biomed Mater Res A 103, 2172–5 (2015).
188. Guex, A. G. et al. Highly porous scaffolds of PEDOT:PSS for bone tissue engineering. Acta Biomater. 62, 91–101 (2017).
189. Wang, W. et al. Engineered 3D printed poly(varepsilon-caprolactone)/graphene scaffolds for bone tissue engineering. Mater Sci Eng C Mater Biol Appl 100, 759–770 (2019).
190. Saberi, A., Jabbari, F., Zarrintaj, P., Saeb, M. R. & Mozafari, M. Electrically conductive materials: opportunities and challenges in tissue engineering. Biomolecules 9, 448 (2019).

Chapter 3: Electroconductive agarose hydrogels modulate mesenchymal stromal cell adhesion and spreading through protein adsorption

3.1 INTRODUCTION

Bioelectricity is involved in tissue homeostasis and plays a critical role in developmental processes such as embryonic development and tissue regeneration. Bioelectricity directs cell migration, adhesion, and proliferation[1,2] and aids in the maturation of electroactive cell types. For example, bioelectric signaling promotes neuronal cell differentiation and synchronous beating of cardiomyocytes[3,4]. Unlike other biophysical properties of hydrogels such as stiffness and viscoelasticity, the potential of electrical cues to influence cell behavior is less investigated. Electrically conductive materials can promote nerve[5,6], cardiac[7,8], muscle[9,10], and bone[11,12] regeneration, and numerous reports indicate that conductive materials can alter cell behavior towards desired outcomes even in the absence of external electrical stimulation[13,14]. However, the mechanism of how conductive materials promote these outcomes is not well

---

This chapter is composed from data published in Casella A, Panitch A, Leach JK. Electroconductive agarose hydrogels modulate mesenchymal stromal cell adhesion and spreading through protein adsorption. *J Biomed Mater Res*. 2023;1-13. doi:10.1002/jbm.a.37503

understood, thereby limiting our capacity to design new materials for tissue regeneration[15].

Many studies investigating electrically conductive hydrogels report both electrical and mechanical characterization of their materials, and some demonstrate synergistic effects between physical and electrical cues on cell behavior[16,17]. However, few report whether they can be decoupled and how their interplay affects cell behavior. Thus, there is a significant need to develop an effective model system to interrogate these basic relationships. There is a substantial body of evidence that demonstrates the importance of directing cell behavior *via* biophysical properties[18–20] that may be tuned using multiple approaches (*e.g.*, increasing polymer concentration, varying crosslinker type or strength, modulating adhesivity[14,20,21]). For electrically conductive hydrogels, the conductive properties are commonly tuned by doping with electrically or ionically[13] conductive additives such as carbon- or metal-based materials and synthetic polymers with conjugated bond structures. These materials all face drawbacks of being nondegradable[22,23] and are poorly soluble, making them difficult to incorporate into hydrogels without further modification[24]. PEDOT:PSS is commonly added to hydrogel biomaterials owing to its commercial availability, water-dispersibility, and non-cytotoxicity[25,26].

Here, we used poly(3,4-ethylenedioxythiophene) polystyrene sulfonate (PEDOT:PSS) to manipulate the conductivity of hydrogels and interrogate the interplay of substrate stiffness and conductivity on cell behavior. We developed a mechanically and electrically tunable hydrogel system using widely available materials and methods that

are accessible for most research groups. We interrogated the contribution of protein adsorption to these hydrogels as a potential mechanism of action. We then investigated human MSC response to physical and electrical cues and hypothesized that cells cultured on conductive hydrogels would have increased cell adhesion regardless of biophysical properties.

3.2 MATERIALS AND METHODS

3.2.1 Fabrication of PEDOT:PSS agarose hydrogels

Agarose (Thermo Fisher Scientific, Waltham, MA) was dissolved in ultrapure water to 2.5 wt% and mixed with PEDOT:PSS (PH1000, Ossila, Sheffield, UK) and water in various ratios to make hydrogels with final concentrations of 0.5 or 1.0 wt% agarose and 0.0, 0.2 or 0.6 wt% PEDOT:PSS (**Table 3.1**). PEDOT:PSS was sonicated for 15 min prior to hydrogel fabrication, and water was warmed to extend gelation time, allowing for adequate mixing. Hydrogel pre-polymer was deposited into glass-mounted PDMS molds (1.5 mm thick × 8 mm I.D.) and allowed to set at room temperature for at least 10 min to make 80 µL gels. After complete gelation, hydrogels were transferred to 24 well plates containing 1 mL of either αMEM (Invitrogen, Waltham, MA) supplemented with 10% FBS (GenClone, San Diego, CA) and 1% penicillin-streptomycin (Gemini Bio Products, West Sacramento, CA) or ultrapure water to remove any unreacted reagents. Gels stored in αMEM were maintained in standard cell culture conditions (*i.e.*, 37°C, 5% CO_2), whereas gels stored in water were kept at room temperature. Pure PEDOT:PSS gels were fabricated by mixing PEDOT:PSS and 4-dodecylbenzenesulfonic acid (Sigma, St. Louis,

MO) at 3 v/v% according to Zhang et al.[27] and used as controls for some biochemical assays (**Fig. 3.1A**).

Table 3.4: Mechanically and electrically tunable hydrogel formulations

Final wt% agarose	Final wt% PEDOT:PSS	Volume of 2.5 wt% agarose (µL)	Volume of 1.0 wt% PEDOT:PSS (µL)	Volume of water (µL)
0.5	0.0	100	0.0	400
	0.2		100	300
	0.6		300	100
1.0	0.0	200	0.0	300
	0.2		100	200
	0.6		300	0.0

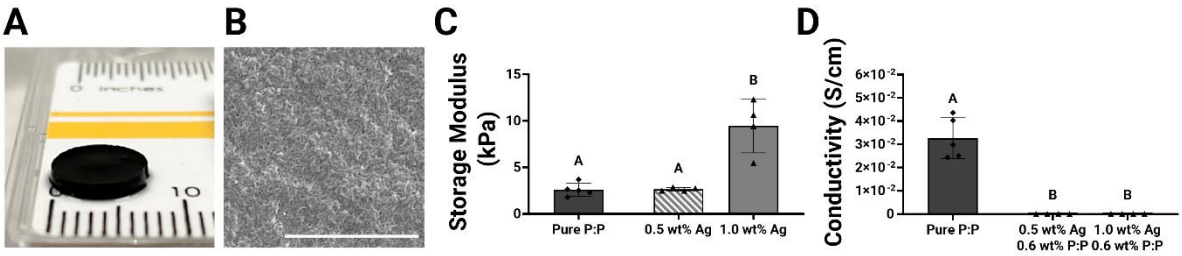

Figure 3.5: Characterization of pure PEDOT:PSS gels. **(A)** Gross image of a pure PEDOT:PSS hydrogel post-fabrication. **(B)** Scanning electron micrograph of a pure PEDOT:PSS hydrogel illustrating formation of a dense, fibrillar network (60,000X objective; scale bar = 1 µm). **(C)** Storage modulus of pure PEDOT:PSS hydrogels compared to 0.5 and 1.0 wt% agarose gels with 0.6 wt% P:P stored in water, measured on 1d ($p \leq 0.001$; n=4-5). **(D)** Conductivity of pure PEDOT:PSS gels was 4 orders of magnitude higher than the agarose-based gels ($p \leq 0.0001$; n=4-5).

3.2.2 Characterization of PEDOT:PSS elution and hydrogel degradation

Fifty µL samples of the solution used to store hydrogels (αMEM or ultrapure water) were removed daily in triplicate into clear, flat 96-well plates. Absorbance was measured at 550 nm. The remaining storage solution was aspirated and replaced with fresh solution.

At 1, 3, 7, and 10d, hydrogel wet mass was measured using a standard lab scale after blotting away excess fluid. Gels were then frozen and lyophilized for at least 24 h or until dry. The dry mass of hydrogels was measured with a Mettler Toledo XPR2 Microbalance (Mettler Toledo, Columbus, OH). Swelling ratio (Q) was calculated using **Equation 3.1**, as described previously[28].

Equation 3.1: $$Q = \frac{\left(\frac{W_{Swollen} - W_{Dry}}{\rho_{Water}}\right) + \frac{W_{Dry}}{\rho_{Polymer}}}{\frac{W_{Dry}}{\rho_{Polymer}}}$$

where ρ is density and ρ_{Water} is 1 g/mL and $\rho_{Polymer}$ is 1.64 g/mL for agarose[29,30].

3.2.3 Mechanical characterization of hydrogels

At 1, 3, 7 and 10d, we measured the gel shear storage modulus using a Discovery HR2 Hybrid Rheometer (TA Instruments, New Castle, DE) with a stainless steel, cross-hatched, 8-mm plate geometry. After pre-loading each gel with approximately 0.03-0.04 N of axial force in compression, an oscillatory strain sweep ranging from 0.004% to 4% strain was applied to each gel to obtain a linear viscoelastic region (LVR)[31]. At least 5 data points were collected for each LVR and averaged to obtain shear storage modulus.

3.2.4 Scanning electron microscopy of hydrogels

Eighty µL hydrogels were prepared as described above and immediately transferred to a 35% ethanol solution to initiate critical point drying. Gels were stored in increasing concentrations of ethanol (35%, 50% 75%, 100%) for 15 min each. Then gels were stored in a 1:1 solution of hexamethyldisilazane (HMDS, Sigma) and 100% ethanol and stored for 1 h. Finally, pure HMDS was added to the gels for 5 min. To complete the dehydration process, HMDS was removed, and gels were allowed to air dry for at least 1 h. Gels were then mounted to aluminum stubs with double-sided carbon tape. Prior to imaging, samples were sputter-coated with gold/palladium. Micrographs were taking using a Thermo Fisher Quattro S Environmental SEM.

3.2.5 Qualitative evaluation of hydrogel hydrophobicity

The hydrophobic or hydrophilic properties of 80 µL gels were assessed qualitatively using solvents with varying surface tension and polarity. A drop of ultrapure water (γ = 72.8 dyn/cm), glycerol (γ = 64.0 dyn/cm; USB Corp., Cleveland, OH), hexane (γ = 18.4 dyn/cm; EMD), or cottonseed oil (γ = 14.9 dyn/cm[32]; Sigma) were applied to the surface of a hydrogel and an image of the beading or spreading of the drop was captured using a Nikon D3300 DSLR camera with an APO 180 mm F2.8 EX macro lens (Sigma Corporation, Japan).

3.2.6 Electrical characterization of hydrogels

The electrical properties of hydrogels were measured using a custom two-point setup depicted in **Figure 3.7A**. Hydrogels were constrained by a PDMS mold (I.D. 10 mm, thickness 1.0 mm) and sandwiched between two brass plates. The sandwich was then stabilized between the jaws of a tabletop angle vise using PDMS blocks as a barrier between the plate and the jaw. One brass plate was connected to a power supply (BK Precision 1735A, Yorba Linda, CA) using alligator clips. One lead of a multimeter (SparkFun Electronics, Niwot, CO) was connected to the other brass plate and the second lead was connected to the power supply to create a complete circuit through which current could be measured. Voltages ranging from 100 to 500 mV, a range selected to avoid electrolysis of water, were applied to the gels to obtain current-voltage curves. After testing, hydrogel thickness and diameter were measured with calipers. Current-voltage curves were analyzed for linearity, and datasets with an R^2 value of ≥0.9 were accepted for resistance calculations. Conductivity was calculated using Pouillet's law (**Equation 3.2)**.

Equation 3.2: $$\sigma = \frac{t}{RA}$$

where σ is conductivity in S/cm, t is thickness of the hydrogel (cm), R is resistance (Ω), and A is cross-sectional area (cm^2). Hydrogels for conductivity testing were stored in ultrapure water to eliminate the confounding effects of ions in PBS and αMEM.

3.2.7 Adsorption of fibronectin to acellular gels

Acellular gels for protein adsorption studies were stored in 1X PBS. After aspirating the storage solution, 1 mL of a 40 µg/mL fibronectin solution in PBS (FN, EMD Millipore, Burlington, MA) was added and allowed to incubate at 37°C for 24 h. FN was added to wells without gels to calculate protein adsorption to the plate. After incubation, the solution in each well was collected and analyzed for protein content using the Micro Bicinchoninic Acid (MicroBCA) Protein Assay Kit (Thermo Fisher Scientific). To characterize the kinetics of FN adsorption, this experiment was repeated with incubation times of 10 s and 30 min.

Protein concentration was calculated using the Assayfit Pro online software (https://www.assayfit.com) with a 2° polynomial curve fit. Concentrations were divided by an absorbance ratio to account for protein-to-protein variation, since bovine serum albumin (BSA) was used for the standard curve. The absorbance ratio was calculated by dividing the concentration of protein reported by the assay by the known concentration of protein (**Equation 3.3**).

Equation 3.3: $$Absorbance\ Ratio = \frac{C_{Assay}}{C_{Known}}$$

The concentration of FN adsorbed to the gels (C_{Gel}) was calculated by subtracting the concentration of FN adsorbed to the plate (C_{Plate}) and the concentration of FN in solution (C_{Sol}) from the concentration of protein initially delivered to each gel (C_{Tot}), as shown in

Equation 3.4. The percent of FN solution retained by the gel was calculated by dividing C_{Gel} by C_{Tot} and multiplying by 100.

Equation 3.4: $$C_{Gel} = C_{Tot} - (C_{Plate} + C_{Sol})$$

3.2.8 Adsorption of charged proteins to acellular gels

To study the influence of conductive polymer on protein adsorption more broadly, gel formulations (100 µL from **Table 3.1**) were pipetted into 96-well plates and stored in ultrapure water. After aspirating the storage water, 200 µL of protein solution were pipetted on top of gels and allowed to incubate for 24 h. Charged protein solutions were PBS containing 1 mg/mL of BSA (Gemini Bio Products), which takes on a negative charge in neutral solution; lysozyme from chicken egg (EMD) which takes on a positive charge in neutral solution; or myoglobin from equine heart (EMD), which is neutral in neutral solution. After 24 h, the protein solutions were analyzed using a BCA Protein Assay Kit (Thermo Fisher Scientific) and analyzed as described above, but with a four-parameter logistic curve fit, per the manufacturer's instructions.

3.2.9 Cell culture

Human MSCs (RoosterBio, Frederick, MD) were cultured in complete media (αMEM, 10% FBS, 1% P/S) in standard culture conditions. MSCs were used at passage 4-6 for all experiments.

Eighty µL gels were fabricated as described above and stored in sterile ultrapure water in a cell culture incubator. Prior to cell seeding, storage water was changed three times, with at least 4 h between changes, to allow for PEDOT:PSS elution. MSCs were trypsinized, pelleted, and resuspended with fresh media at 5×10^5 cells/mL. After aspirating the storage water from the gels, 10 µL of cell suspension were pipetted onto one side of the gel followed by a 10 min incubation in standard culture conditions. Next, gels were flipped and 10 µL of the same cell suspension were added to the other side of the gel. After 10 min, 1 mL of αMEM was added to each well. Media was changed every 2-3 days, and gels were analyzed after 1, 3, and 7d.

3.2.10 Assessment of viability, proliferation, and metabolic activity

Metabolic activity from the cells was measured with the alamarBlue assay (Thermo Fisher Scientific) according to the manufacturer's instructions. Results were normalized to DNA content measured using the Quant-iT PicoGreen™ dsDNA Assay Kit (Thermo Fisher Scientific). Viability of the cells on gels was determined using a LIVE/DEAD stain where viable cells were stained green with calcein AM (Invitrogen) and dead cells were stained red with propidium iodide (Millipore Sigma, St. Louis, MO). Cell adhesion and spreading was visualized by fixing the gels in 4% paraformaldehyde in PBS and staining the cells with Alexa Fluor 488 Phalloidin and DAPI (both from Invitrogen). Cells on gels were imaged using a Nikon Eclipse T32000U microscope.

3.2.11 Statistical analysis

Data are presented as means ± standard deviation. Statistical analysis was performed using GraphPad Prism 9 software using t-tests and one-way or multi-way analysis of variance with Tukey correction for multiple comparison. A mixed-effects analysis model was used for datasets with unequal group sizes. Differences were considered statistically significant at $p \leq 0.05$. Groups that are significantly different are denoted with different letters, while groups that share letters are statistically similar.

3.3 RESULTS

3.3.1 PEDOT:PSS-laden agarose hydrogels maintain their structure over time

Mechanical properties of hydrogels were tuned using two different concentrations of agarose (0.5 or 1.0 wt%), while electrical properties were tuned *via* concentration of PEDOT:PSS (0.0, 0.2, or 0.6 wt%). All hydrogels remained intact for the course of the study (**Fig. 3.2A)**. The incorporation of higher concentrations of PEDOT:PSS, a blue-black polymer, resulted in hydrogels becoming increasingly dark and opaque. While each gel was formulated such that respective groups contained either the same amount of agarose or PEDOT:PSS, the color difference between 0.5 and 1.0 wt% agarose gels containing PEDOT:PSS (both 0.2 and 0.6 wt%) indicates that less electrically conductive polymer was incorporated. This may be due to fewer polymeric entanglements or PSS-agarose crosslinks formed in gels containing less polysaccharide.

After formation, gels were stored in αMEM or ultrapure water to wash away any unincorporated reagents, and storage solution was replaced daily. Storage αMEM did not

grossly appear to change color over time (**Fig. 3.2B**). Absorbance values fluctuated only slightly and did not appreciably deviate from baseline (**Fig. 3.2C**). These data suggest minimal PEDOT:PSS leaching from the gels. Swelling ratio decreased over time for groups containing PEDOT:PSS (**Fig. 3.2D**). With daily replenishment of αMEM, we predict that charged moieties from the cell culture media (*e.g.*, salts and proteins) accumulated within the hydrogel, causing an increase in dry mass over time, which we report in **Fig. 3.3**.

Observations of PEDOT:PSS elution in water contrast strikingly to gels stored in αMEM. Storage water was noticeably gray after 24 h (**Fig. 3.4A**) and absorbance values of the water decreased significantly between 1 and 2 d, indicating PEDOT:PSS elution from the gels. After the initial time point, absorbance values were near zero and gels appeared to reach an equilibrium with the storage water (**Fig. 3.4B**). The dry mass of hydrogels containing PEDOT:PSS also exhibited a decline after 1d, though this may be attributed to the loss of PEDOT:PSS (**Fig. 3.4C**). Hydrogel swelling ratio increased after fabrication but equilibrated after 1d (**Fig. 3.4D**). The 0.5 wt% agarose gels had significantly higher swelling ratios at each time point, regardless of PEDOT:PSS concentration (**Fig. 3.4E**), which may also be attributed to the reduced polymeric entanglements compared to the 1.0 wt% agarose gels.

These data establish the degradation and dissociation properties of the hydrogels used for the remaining studies. Furthermore, these findings illustrate the capacity of conductive additives to elute out of hydrogel materials, emphasizing the importance of material storage prior to characterization.

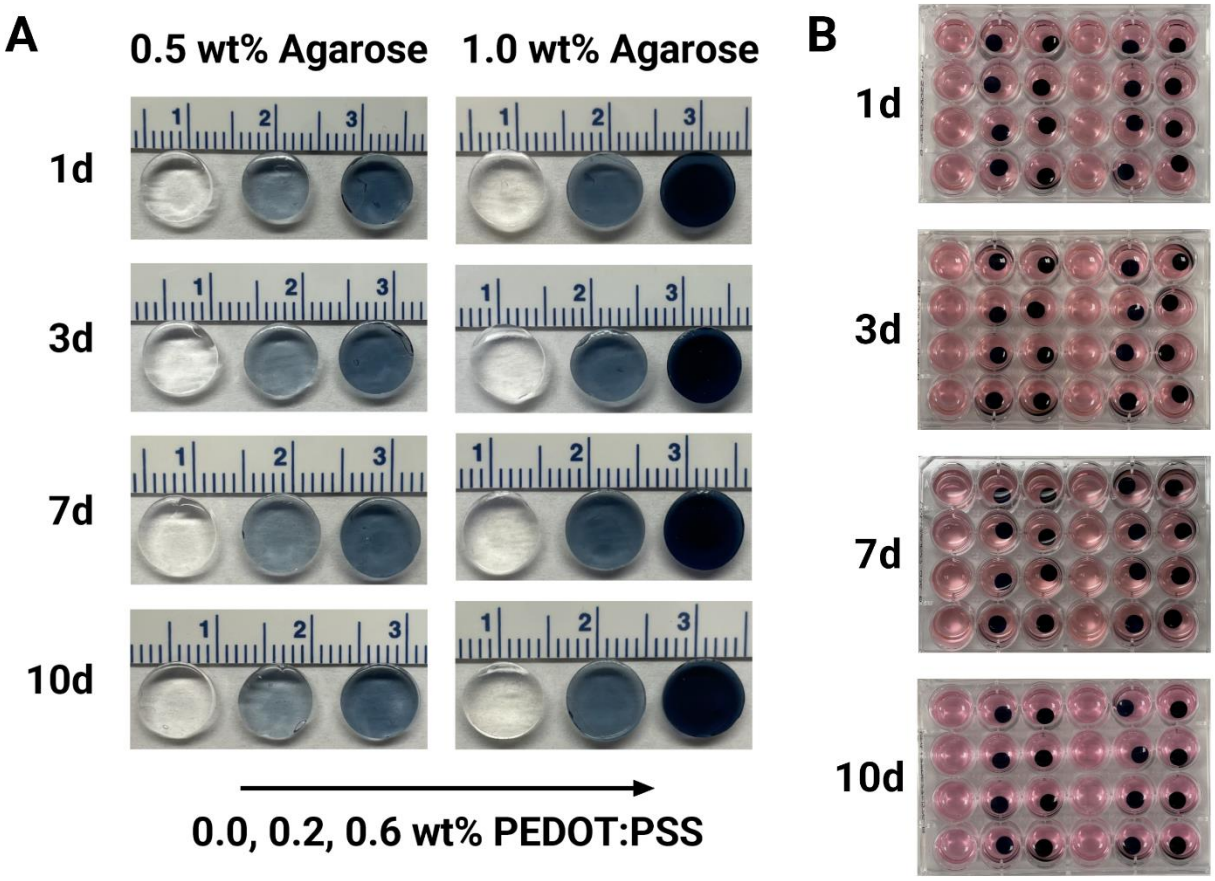
A
0.5 wt% Agarose
1.0 wt% Agarose
1d
3d
7d
10d
0.0, 0.2, 0.6 wt% PEDOT:PSS
B
1d
3d
7d
10d

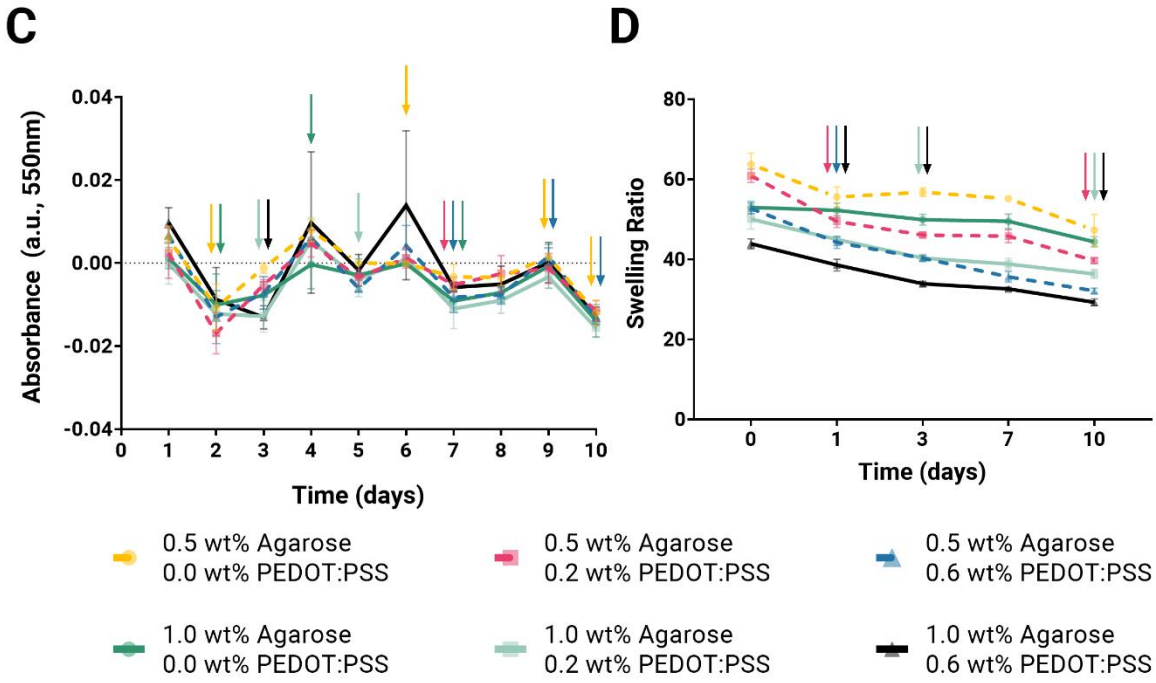
C
Absorbance (a.u., 550nm)
0.04
0.02
0.00
-0.02
-0.04
0 1 2 3 4 5 6 7 8 9 10
Time (days)
D
Swelling Ratio
80
60
40
20
0
0 1 3 7 10
Time (days)
0.5 wt% Agarose
0.0 wt% PEDOT:PSS
0.5 wt% Agarose
0.2 wt% PEDOT:PSS
0.5 wt% Agarose
0.6 wt% PEDOT:PSS
1.0 wt% Agarose
0.0 wt% PEDOT:PSS
1.0 wt% Agarose
0.2 wt% PEDOT:PSS
1.0 wt% Agarose
0.6 wt% PEDOT:PSS

Figure 3.6: Hydrogels stored in αMEM maintain gross structure over 10 days. (A) Gross images of agarose hydrogels with tunable mechanical ([agarose]) and electrical ([PEDOT:PSS]) properties over time. **(B)** Representative images illustrate the lack of color change of gel storage αMEM over time, indicating gel structural integrity. **(C)** Absorbance of hydrogel storage αMEM fluctuated over time but is not appreciably different than baseline. Arrows indicate a significant difference ($p \leq 0.05$) in absorbance between the marked time point and the one preceding it. **(D)** Hydrogel swelling ratio decreased steadily over time. Arrows indicate a significant difference ($p \leq 0.05$) in swelling ratio between the marked time point and the one preceding it.

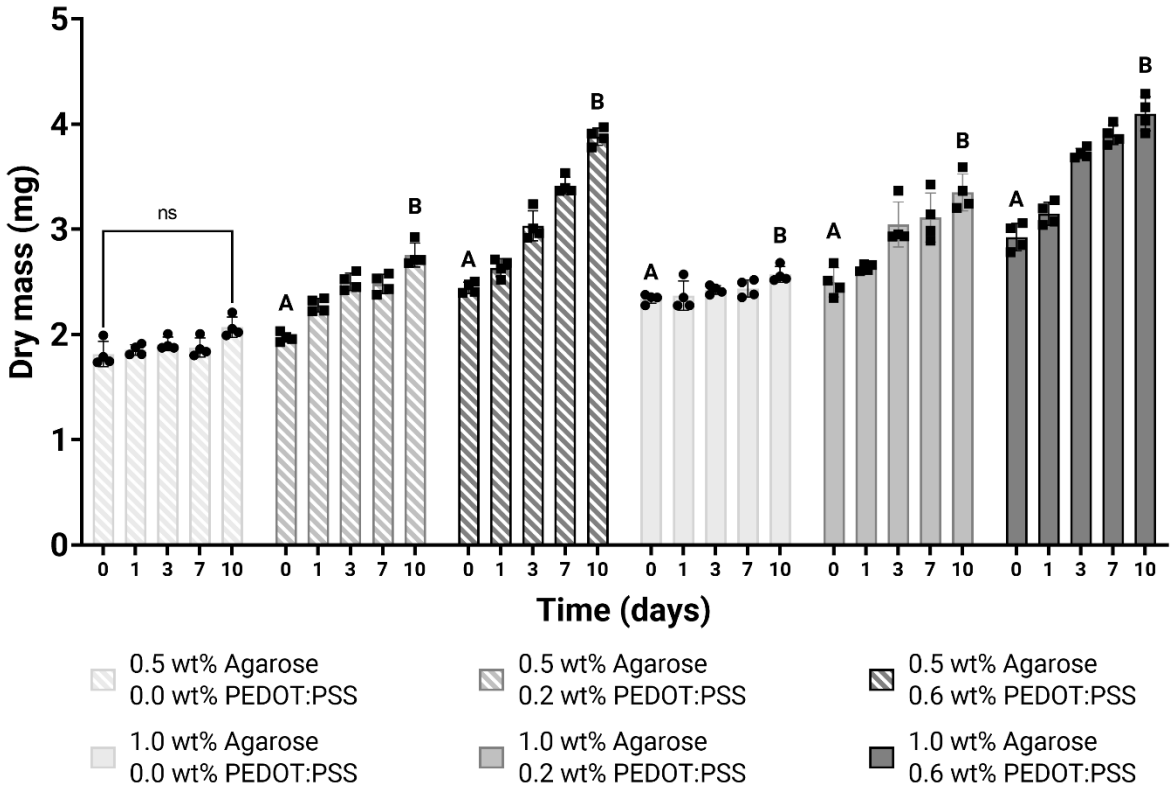

Figure 3.7: Gels stored in αMEM accumulate media components over time. Dry mass of gels increased from 1 to 10d for all groups except the 0.5 wt% agarose, 0.0 wt% PEDOT:PSS gels ($p \leq 0.05$ for 1.0 wt% Ag + 0.0 wt% P:P, $p \leq 0.01$ for 0.5 wt% Ag + 0.2 wt% P:P and 1.0 wt% Ag + 0.6 wt% P:P, $p \leq 0.001$ for 1.0 wt% Ag + 0.2 wt% P:P, and $p \leq 0.0001$ for 0.5 wt% Ag + 0.6 wt% P:P; n=4). Two-way ANOVA for the simple effect of time was used to analyze the differences in dry mass within each group. Only differences between 1 and 10d are displayed. Groups denoted by different letters are statistically significant; ns=not significant.

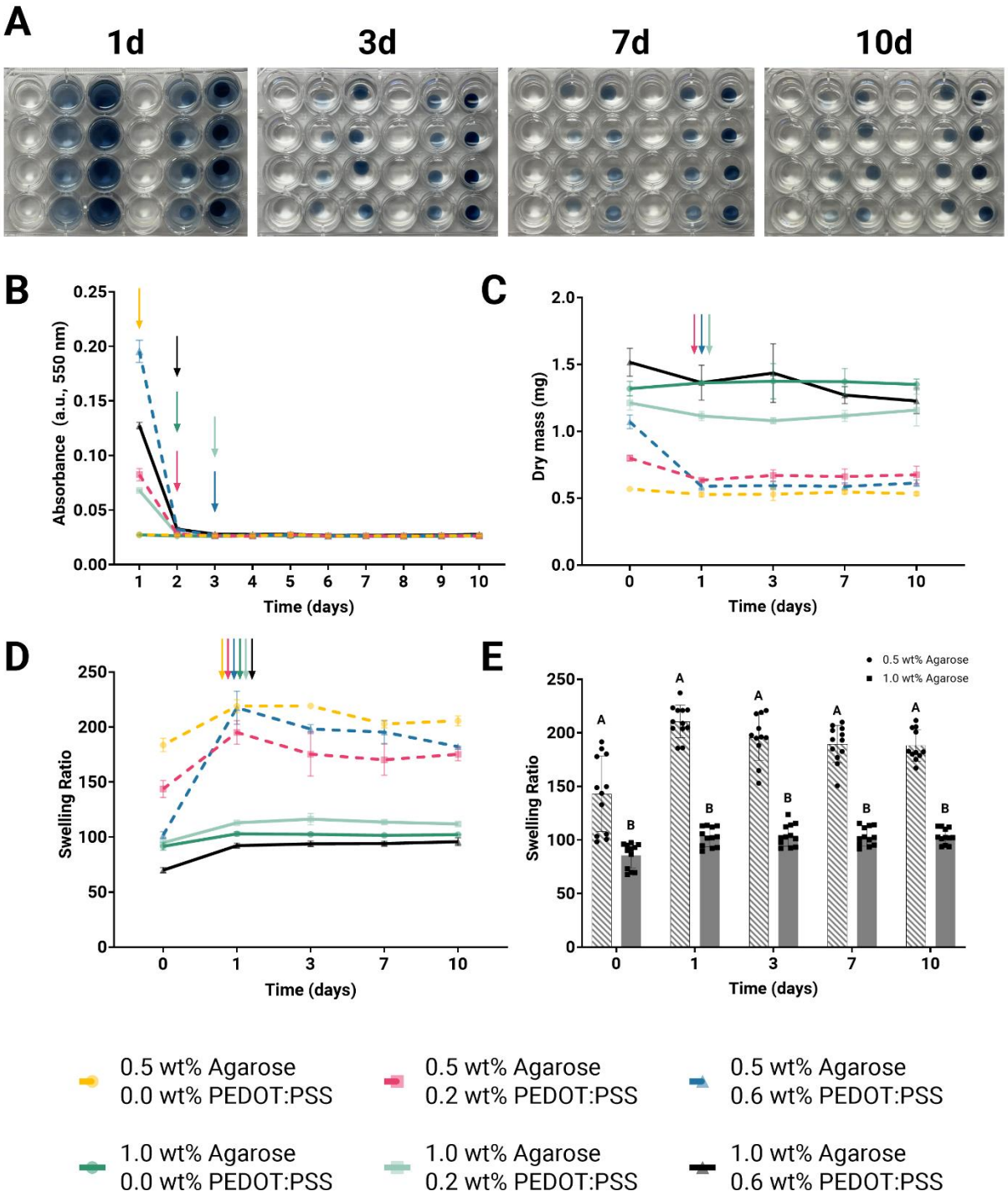

Figure 3.8: Hydrogels maintain gross structure in water over 10 days, despite leached PEDOT:PSS after 1 day. (A) Representative images illustrate the color change of gel storage water over time. **(B)** Absorbance of hydrogel storage water over time decreases

significantly for groups containing PEDOT:PSS after 1d, but begin to equilibrate by 2d. Arrows indicate a significant difference ($p \leq 0.05$) in absorbance between the marked time point and the one preceding it. **(C)** For the hydrogels containing 0.2 or 0.6 wt% PEDOT:PSS, dry mass significantly decreases after 1d. The 1.0 wt% agarose + 0.6 wt% PEDOT:PSS group is an exception, but its dry mass trends in decline over time. After 1d, dry mass does not change in any groups. **(D)** Hydrogel swelling ratio equilibrates after an initial increase on 1d for all groups. These data correspond to the decrease in storage water absorbance, indicative of eluted PEDOT:PSS from **(A)**. **(E)** The 0.5 wt% agarose hydrogels have a significantly higher swelling ratio than the 1.0 wt% agarose gels ($p \leq 0.0001$ for most time points; n=11-12) when the effect of PEDOT:PSS concentration is removed by pooling data. These data indicate that greater agarose content contributes to increased polysaccharide entanglements, which may contribute to changes in PEDOT:PSS elution. Groups denoted by different letters are statistically significant within each time point. Groups that do not contain PEDOT:PSS have unchanging dry mass over time. Arrows indicate a significant difference ($p \leq 0.05$; n=4) in swelling ratio between the marked time point and the one preceding it.

3.3.2 Mechanical and electrical properties of agarose hydrogels can be decoupled

Hydrogel storage modulus was predominantly influenced by wt% agarose when gels were stored in αMEM, though increases ($p \leq 0.05$) were observed in the 0.5 wt% agarose gels when 0.6 wt% PEDOT:PSS was added (**Fig. 3.5A**). To confirm the driving

factor was wt% agarose, we analyzed the storage moduli for all hydrogels at each agarose concentration, regardless of PEDOT:PSS loading. There was a significant increase in storage modulus from approximately 1.75 kPa to 9.5 kPa with increasing agarose content ($p \leq 0.0001$) (**Fig. 3.5B**). While 0.6 wt% PEDOT:PSS caused a significant increase in storage modulus in the 0.5 wt% agarose gels ($p \leq 0.0001$) (**Fig. 3.5C**), the magnitude of this difference was less than the magnitude of the difference in storage modulus between the 0.5 and 1.0 wt% agarose gels (**Fig. 3.5B**). By contrast, when storage modulus was analyzed as a function of PEDOT:PSS content for the 1.0 wt% agarose gels, PEDOT:PSS did not cause a change in mechanical properties (**Fig. 3.5D**). Pure PEDOT:PSS gels had statistically similar mechanical properties to the 0.5 wt% agarose gels, with an average storage modulus of approximately 2.6 kPa (**Fig. 3.1C**).

Gels stored in ultrapure water exhibited similar relationships but were more susceptible to changes with the addition of 0.2 wt% PEDOT:PSS (**Fig. 3.6A,** $p \leq 0.05$). This may be due to more pronounced dissociation over time when gels were stored in water (**Fig. 3.4**). Although both 0.5 and 1.0 wt% agarose gels had higher storage moduli with the addition of PEDOT:PSS, the magnitude of change in storage modulus as a function of wt% agarose (**Fig. 3.6B**, $p \leq 0.0001$) was greater than as a function of wt% PEDOT:PSS (**Fig. 3.6C,D**; $p \leq 0.0001$). These data further highlight the importance of storage conditions on material characterization. Taken together, analysis of storage modulus indicates that below a certain concentration, the addition of PEDOT:PSS does not affect hydrogel biophysical properties. Thus, these data fulfill half of the requirements towards our aim of developing a hydrogel system that is electrically and mechanically decoupled.

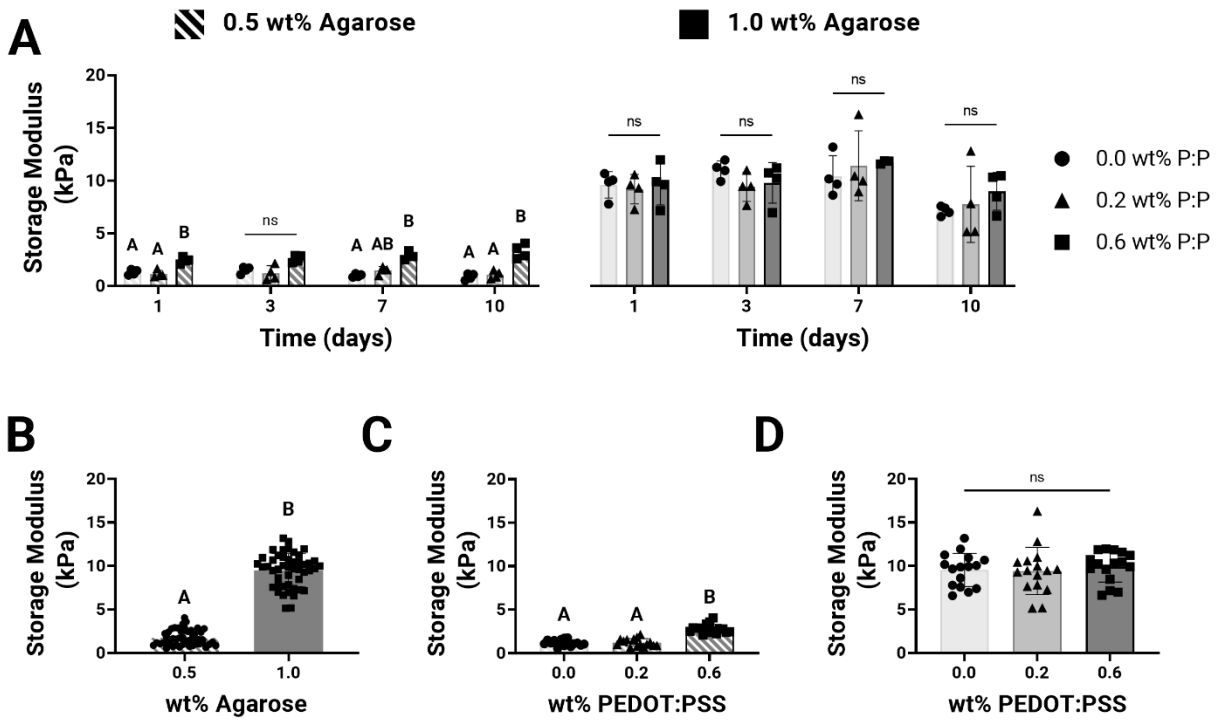

Figure 3.9: Storage modulus of hydrogels stored in αMEM is driven by agarose content. **(A)** Mechanical properties were predominantly affected by wt% agarose, but addition of 0.6 wt% PEDOT:PSS caused significant increases in storage modulus of the 0.5 wt% agarose gels at most time points ($p \leq 0.05$ at 1 and 10d, $p \leq 0.01$ at 7d; n=3-4). Two-way ANOVA for the simple effect of PEDOT:PSS concentration was used to analyze the differences between groups within each time point. Tests were run separately for 0.5 and 1.0 wt% agarose gels. **(B)** Storage moduli of PEDOT:PSS-loaded agarose hydrogels was driven by wt% agarose ($p \leq 0.0001$; n=47-48), calculated with a two-tailed t-test. **(C)** Storage moduli of 0.5 wt% agarose gels increased with addition of 0.6 wt% PEDOT:PSS ($p \leq 0.0001$; n=16). **(D)** The storage moduli of 1.0 wt% agarose gels were unchanged by the addition of PEDOT:PSS ($p \leq 0.0001$; n=16). One-way ANOVA was used to analyze

differences between groups for **(C)** and **(D)**. Groups denoted by different letters are statistically significant, ns=not significant.

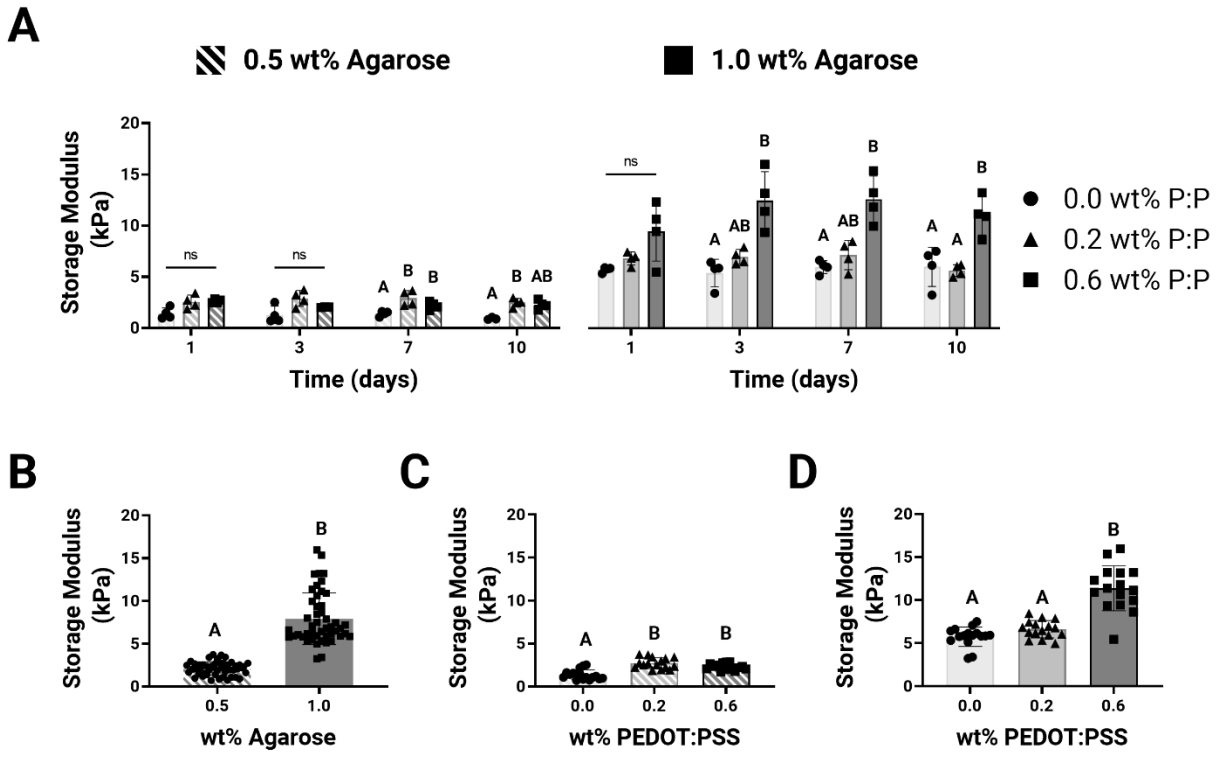

Figure 3.10: Storage modulus of hydrogels stored in water is driven by agarose content. **(A)** Mechanical properties were predominantly affected by wt% agarose, but addition of 0.2 wt% PEDOT:PSS caused significant increases in storage modulus of the 0.5 wt% agarose gels at 7 and 10d ($p \leq 0.05$; n=3-4). Incorporating 0.6 wt% PEDOT:PSS caused significant increases in storage modulus of the 1.0 wt% agarose gels at nearly all time points ($p \leq 0.05$; n=4). Two-way ANOVA for the simple effect of PEDOT:PSS concentration was used to analyze the differences between groups within each time point. Tests were run separately for 0.5 and 1.0 wt% agarose gels. **(B)** Storage moduli of PEDOT:PSS-loaded

agarose hydrogels is driven by wt% agarose ($p \leq 0.0001$; n=48), calculated with a two-tailed t-test. **(C)** Storage moduli of 0.5 wt% agarose gels is affected by the addition of 0.2 wt% PEDOT:PSS, but when more polymer is added, storage modulus does not increase ($p \leq 0.0001$; n=15-16). **(D)** The storage moduli of 1.0 wt% agarose gels are unchanged by the addition of 0.2 wt% PEDOT:PSS. Additional PEDOT:PSS yields stiffer gels ($p \leq 0.0001$; n=16). One-way ANOVA was used to analyze differences between groups for **(C)** and **(D)**. Groups denoted by different letters are statistically significant, ns=not significant.

As expected, electrical conductivity of PEDOT:PSS agarose hydrogels was predominantly driven by PEDOT:PSS content (**Fig. 3.7B**). When conductivity was analyzed as a function of agarose concentration, conductivity increased 1.2-fold with increased agarose concentration ($p \leq 0.05$) (**Fig. 3.7C**). Conductivity measurements of hydrogels formed from each agarose concentration without PEDOT:PSS confirmed that agarose has some intrinsic conductivity (**Fig. 3.7B**), which may contribute to trends of increased conductivity between 0.5 and 1.0 wt% agarose gels for all concentrations of PEDOT:PSS. However, when analyzing conductivity as a function of wt% PEDOT:PSS only, we observed nearly a 2-fold increase in conductivity when increasing PEDOT:PSS concentration from 0 to 0.2 wt% ($p \leq 0.0001$) (**Fig. 3.7D**). Interestingly, we did not detect significant increases in conductivity when PEDOT:PSS concentration was further increased. Conductivities ranged from approximately 2×10^{-6} to 8×10^{-6} S/cm, classifying these materials as semiconductors and appropriate for biological applications. At approximately 3×10^{-2}

S/cm, pure PEDOT:PSS hydrogels had 4 orders of magnitude higher conductivity than the agarose-based gels (**Fig. 3.1D**).

These data provide evidence that the physical and electrical properties of this hydrogel model system can be decoupled. For example, while storage modulus did not change for 1.0 wt% agarose gels doped with 0.0 or 0.2 wt% PEDOT:PSS (**Fig. 3.6**), there was a difference in conductivity between these groups (**Fig. 3.7D**). While not all groups within this hydrogel platform had decoupled electrical and mechanical properties, we studied cell response to all hydrogel conditions. This strategy allowed us to interrogate if cells respond differently to substrates with and without decoupled properties. Additionally, since no differences in storage modulus or conductivity were observed between the gels on 7 and 10d (*data not shown*), the subsequent *in vitro* studies were carried out only to 7d.

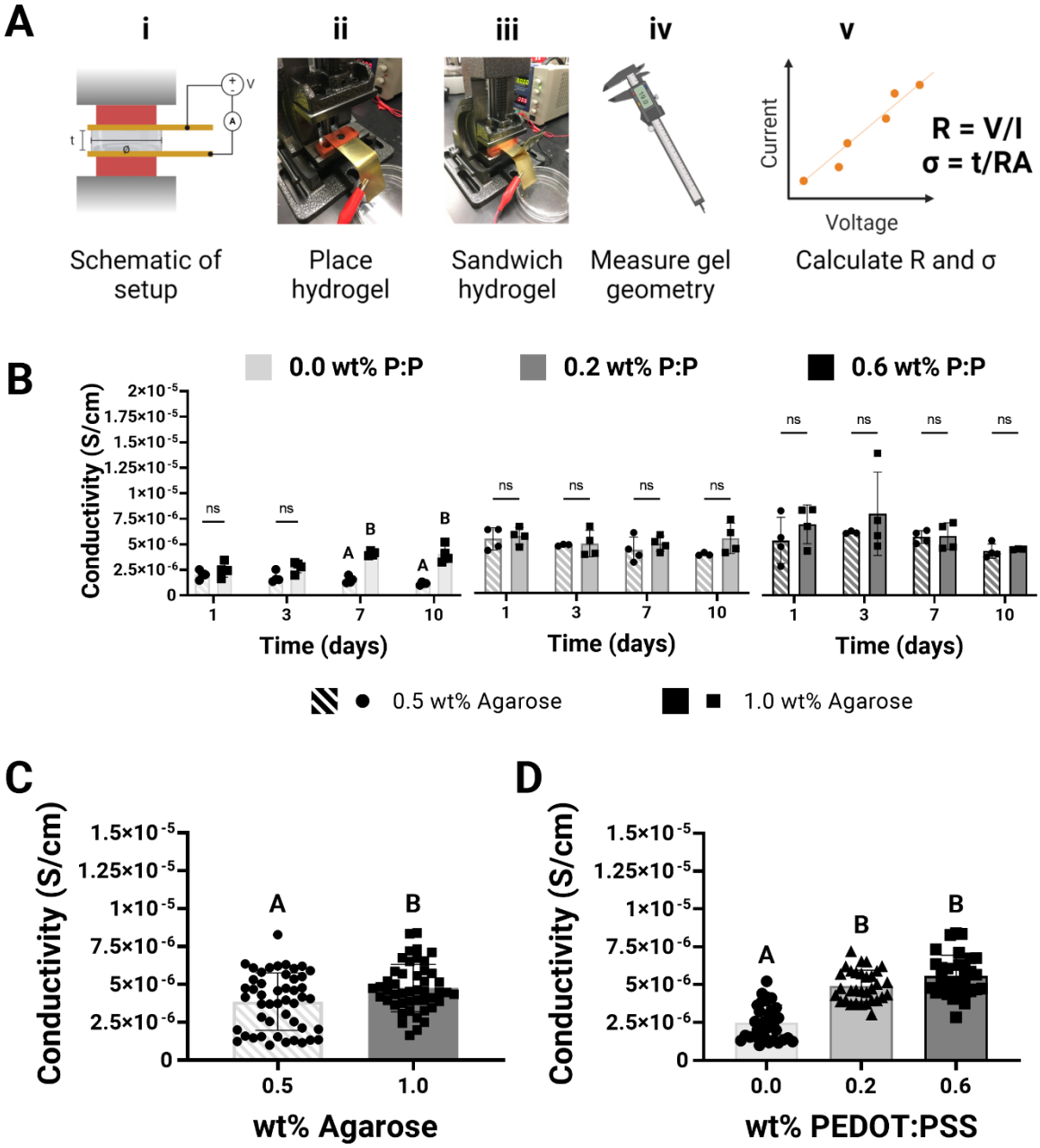

Figure 3.11: Hydrogel conductivity is driven by PEDOT:PSS concentration. **(A)** i: Schematic of conductivity setup, where ii) hydrogels are placed on one brass plate and contained by a PDMS sheet. The hydrogel is then iii) sandwiched between both brass plates. The power supply connected to one plate provides a source of voltage and a multimeter connected to the other plate displays output current. After taking current

measurements, (iv) hydrogel geometric parameters are recorded and (v) current-voltage curves are generated. I-V curves are assessed for linearity and used to calculate resistance. **(B)** Conductivity is predominantly driven by wt% PEDOT:PSS. Differences in the conductivity of 0.5 and 1.0 wt% agarose groups containing no PEDOT:PSS indicate some intrinsic conductivity of agarose ($p \leq 0.01$; n=3-4). The differences due to agarose concentration were not observed in PEDOT:PSS-containing groups. Multiple t-tests for the simple effect of agarose concentration were used to analyze the differences between groups within each time point. Tests were run separately for the 0.0, 0.2, and 0.6 wt% PEDOT:PSS gels. **(C)** Pooled data eliminating the contribution of wt% PEDOT:PSS indicate conductivity of gels increases with increasing agarose content ($p \leq 0.05$; n=47-48), calculated with a two-tailed t-test. **(D)** When conductivity is analyzed as a function of wt% PEDOT:PSS, the level of significance is much greater ($p \leq 0.0001$; n=31-32). One-way ANOVA was used to analyze differences between groups. Groups denoted by different letters are statistically significant; ns=not significant.

3.3.3 Conductive hydrogels support cell viability and metabolic activity at early time points

MSCs cultured on 0.5 and 1.0 wt% agarose exhibited greater viability at 7d when gels were conductive (**Fig. 3.8A,D**). LIVE/DEAD imaging showed the most cell adhesion to substrates containing PEDOT:PSS with little adhesion to non-conductive controls. Minimal cell adhesion was observed at 1d, and cell viability *via* the LIVE/DEAD assay appeared to peak on 3d (**Fig. 3.9**). Of the cells that adhered, most were viable, indicated

by calcein AM staining. Pure PEDOT:PSS supported cell viability through 7d, but cells appeared most viable at 3d (**Fig. 3.10A**).

Metabolic activity *via* alamarBlue was higher for cells cultured on conductive substrates, and raising the concentration of PEDOT:PSS further increased cell activity at 1 and 3d (**Fig. 3.8B,E**). DNA content was nearly constant for all 0.5 wt% agarose groups at each time point, but DNA mass was greatest on 3d ($p \leq 0.0001$), indicating cell proliferation (**Fig. 3.8C**). A similar relationship was observed in the DNA content of cells cultured on 1.0 wt% agarose gels, though conductivity promoted cell proliferation at 3 and 7d over non-conductive controls (**Fig. 3.8F**). While cell metabolic activity decreased over time, conductivity boosted cell behavior compared to the non-conductive controls, which had nearly no cell activity, even at 1d. Pure PEDOT:PSS gels did not consistently promote MSC metabolic activity (**Fig. 3.10B**).

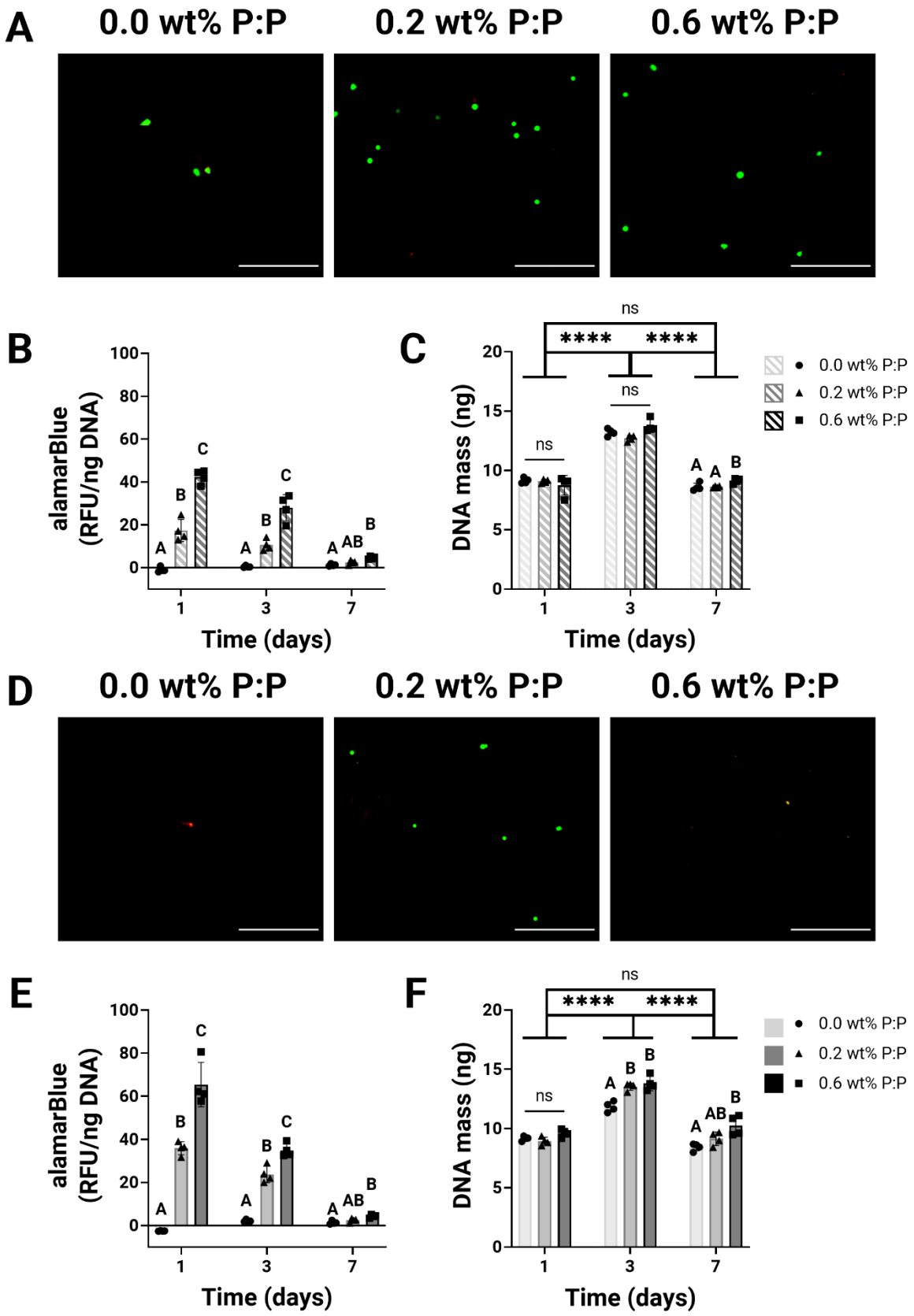
A
0.0 wt% P:P
0.2 wt% P:P
0.6 wt% P:P
B
alamarBlue (RFU/ng DNA)
Time (days)
C
DNA mass (ng)
ns
****
****
0.0 wt% P:P
0.2 wt% P:P
0.6 wt% P:P
D
E
F

Figure 3.12: Conductivity supports cell viability and metabolic activity of MSCs at early time points. (A) LIVE/DEAD images of MSCs on 0.5 wt% agarose gels indicate overall viability of adhered cells at 7d. Gels containing at least 0.2 wt% PEDOT:PSS supported greater cell adhesion compared to non-conductive controls (10X objective, scale bars = 500 μm). **(B)** Metabolic activity of cells cultured on 0.5 wt% agarose gels was significantly greater when the substrate was conductive ($p \leq 0.05$ for 3d, $p \leq 0.01$ for 1 and 7d; n=4). **(C)** DNA mass was nearly constant between groups within each time point ($p \leq 0.05$ for 7d) but was highest overall on 3d ($p \leq 0.0001$). **(D)** LIVE/DEAD staining of MSCs grown on 1.0 wt% agarose gels indicate similar cell behavior, though the 0.2 wt% PEDOT:PSS group supported cell adhesion and viability better than the 0.6 wt% PEDOT:PSS group. **(E)** Metabolic activity of cells cultured on 1.0 wt% agarose gels was also greater when the gel was conductive ($p \leq 0.05$ for 1 and 7d, $p \leq 0.01$ for 3d; n=4). **(F)** DNA mass increased with PEDOT:PSS concentration on 3 and 7d ($p \leq 0.05$), but was highest overall on 3d ($p \leq 0.0001$). Two-way ANOVA for the simple effect of PEDOT:PSS concentration was used to determine differences between groups within each time point for **(B),(C),(E),** and **(F)**. Two-way ANOVA for the main effect of time was used to determine overall differences between time points for **(C)** and **(F)**. Groups denoted by different letters are statistically significant within each time point, ns=not significant.

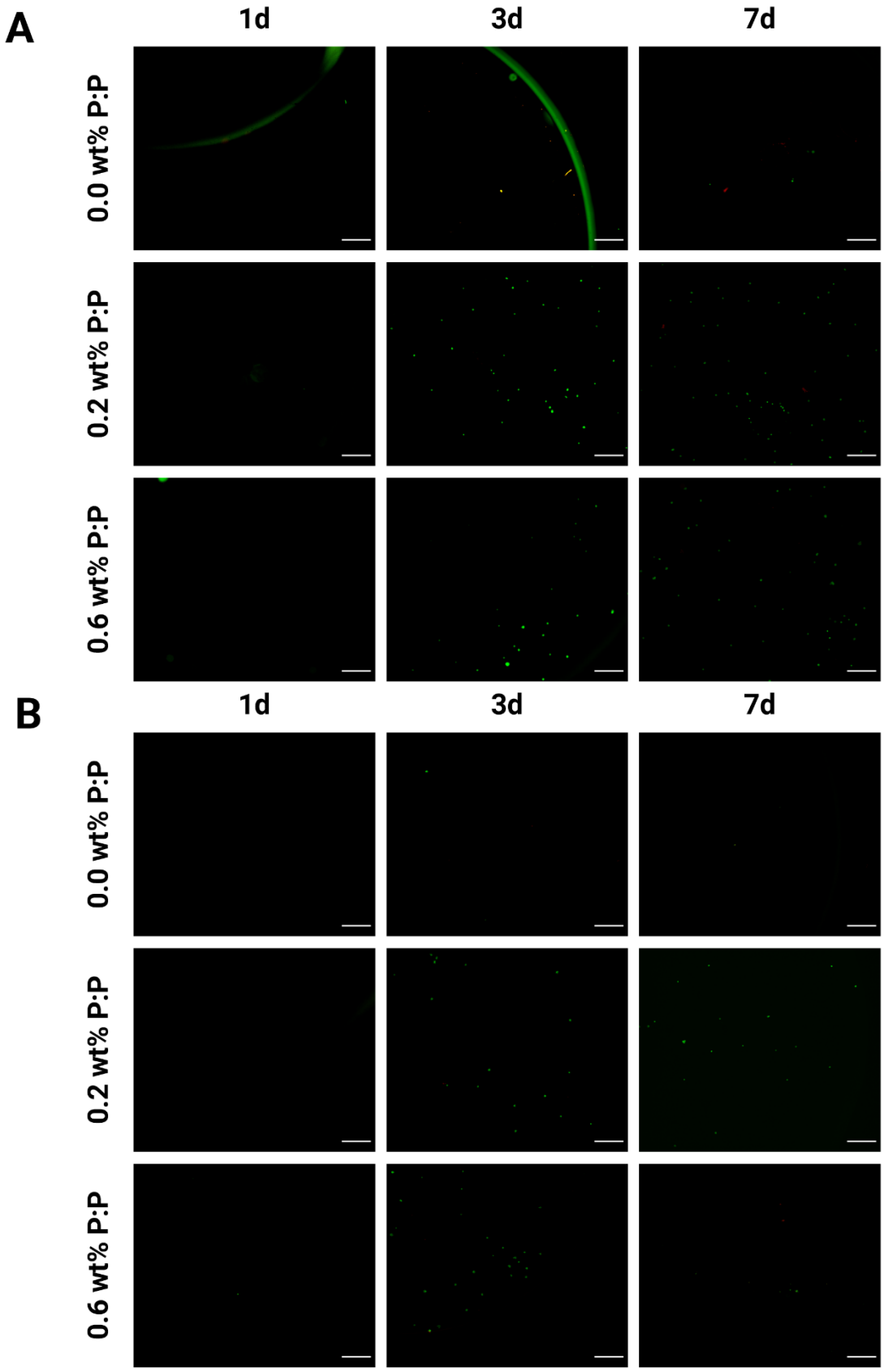
A
1d
3d
7d
0.0 wt% P:P
0.2 wt% P:P
0.6 wt% P:P
B
1d
3d
7d
0.0 wt% P:P
0.2 wt% P:P
0.6 wt% P:P

Figure 3.13: Conductive substrates support cell viability of MSCs at early time points. LIVE/DEAD images of MSCs on **(A)** 0.5 and **(B)** 1.0 wt% agarose gels with increasing conductivity (4X objective, scale bars = 500 μm). Gels containing at least 0.2 wt% PEDOT:PSS supported greater cell adhesion compared to non-conductive controls at all time points. Viability was greatest at 3d. Viable cells were stained green with calcein AM and dead cells were stained red with propidium iodide.

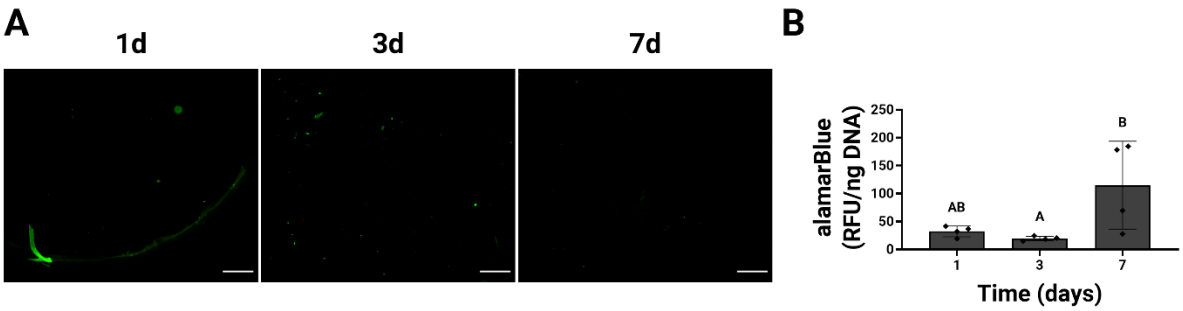

Figure 3.14: *In vitro* properties of pure PEDOT:PSS gels. **(A)** LIVE/DEAD images of MSCs grown on pure PEDOT:PSS gels indicate lack of adhered cells over 7 days (4X objective, scale bars = 500 μm). **(B)** Metabolic activity of cells was not consistently supported by pure PEDOT:PSS gels ($p \leq 0.05$; n=4). One-way ANOVA was used to analyze differences between groups. Groups denoted by different letters are statistically significant, ns=not significant.

3.3.4 Conductive hydrogels support cell adhesion and spreading

MSCs cultured on gels were fixed and stained with DAPI and phalloidin to visualize adhesion and spreading (**Fig. 3.11A**). While some cells adhered to the non-conductive controls, their morphology was rounded. Furthermore, irregular staining on these gels at 7d is indicative of debris. This contrasts strikingly with the cells on gels containing 0.6 wt% PEDOT:PSS, which exhibit cytoskeletal projections and take on the fibroblastic morphology of healthy MSCs. Pure PEDOT:PSS gels were not effective at retaining cells or facilitating spreading (**Fig. 3.12A**). While adhesion to all gels was low overall, the addition of PEDOT:PSS allowed cells to form strong enough bonds to spread, even in the absence of adhesion ligands and external stimulation.

To elucidate possible mechanisms of this observation, we measured the amount of fibronectin (FN) adsorbed to gels as a function of agarose concentration, PEDOT:PSS concentration, and time. We observed more FN in gels with higher PEDOT:PSS concentration ($p \leq 0.05$) starting as early as 30 min, though this may have been due to FN diffusion into the bulk gel. After 24 h of equilibration, FN content was still greater in PEDOT:PSS-containing groups, which we attributed to a combination of diffusion and adsorption (**Fig. 3.11B,C**). This trend was also observed in pure PEDOT:PSS gels (**Fig. 3.12B**). The trending increase in protein adsorption between gels containing 0.2 and 0.6 wt% PEDOT:PSS required further investigation, as there were no significant differences in conductivity between these groups (**Fig. 3.7D**). As such, we performed scanning electron microscopy on dehydrated gels. Hydrogels with 0.0 and 0.2 wt% PEDOT:PSS had clear fibrillar and network-like structures, whereas the 0.6 wt% PEDOT:PSS groups had more

globular structures, leading to increased surface roughness (**Fig. 3.11D**). Surface roughness contributes to protein adsorption, in part by increasing the available surface area. Thus, the 0.6 wt% PEDOT:PSS gels may facilitate more FN interaction due to their topography[33]. We also qualitatively investigated the hydrophobic properties of the hydrogels. We did not observe striking differences in hydrophobicity with presence of PEDOT:PSS, with the exception of the 0.5 wt% agarose gels, where the edges of the water drop are visible on the gels containing PEDOT:PSS (**Fig. 3.13**).

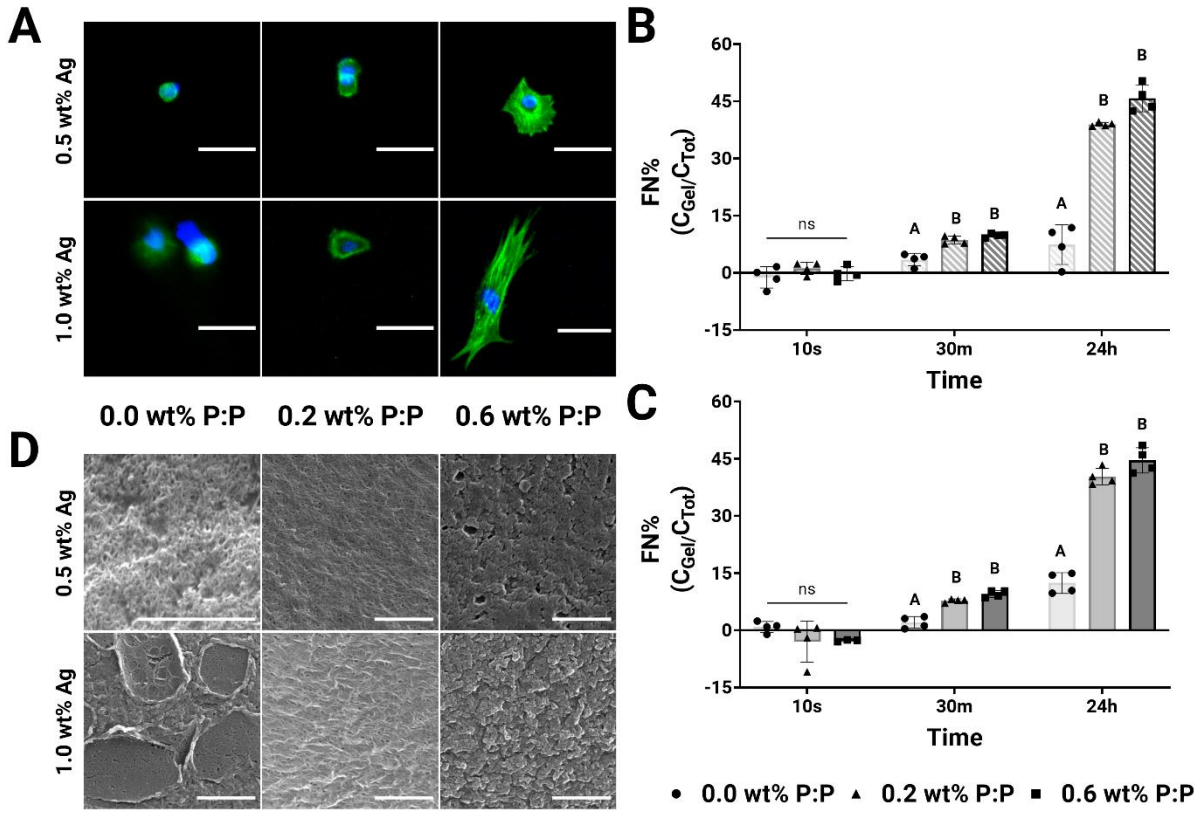

Figure 3.15: Conductive hydrogels support greater cell adhesion and spreading even in the absence of binding sites. (A) Cells adhered to and spread more effectively on conductive substrates compared to non-conductive controls. Cell cytoskeleton was

stained for phalloidin (green), and nuclei were stained with DAPI (blue) (7d, 10X objective, scale bars = 50 μm). **(B)** The concentration of adsorbed fibronectin (FN) to 0.5 wt% agarose gels increased with increasing concentrations of PEDOT:PSS ($p \leq 0.05$ for 30 min, $p \leq 0.01$ for 24 h; n=4). **(C)** Similarly, FN adsorbed better to conductive 1.0 wt% agarose gels ($p \leq 0.05$ for 30 min, $p \leq 0.01$ for 24 h; n=4). **(D)** Scanning electron micrographs of hydrogels demonstrate surface network characteristics (50,000X objective for 0.5 wt% Ag. + 0.0 wt% P:P; 25,000X objective for all other groups; scale bars = 1 μm). Two-way ANOVA for the simple effect of PEDOT:PSS concentration was used to analyze the differences between groups within each time point for **(B)** and **(C)**. Groups denoted by different letters are statistically significant, ns=not significant.

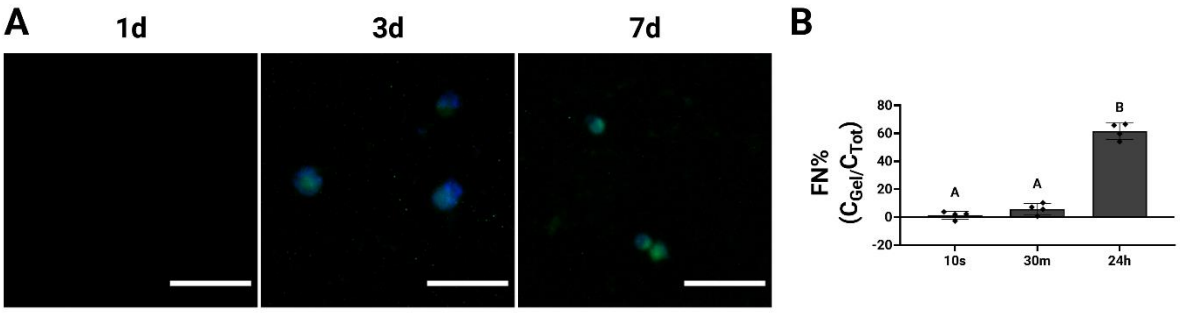

Figure 3.16: Adhesion and adsorption properties of pure PEDOT:PSS gels. **(A)** Cell cytoskeleton was stained for phalloidin (green), and nuclei were stained with DAPI (blue) (10X objective, scale bars = 50 μm). No cells are visible on 1d and irregular and undefined staining on 3 and 7d are indicative of debris. **(B)** The concentration of fibronectin (FN) in the pure PEDOT:PSS gels increased with time ($p \leq 0.0001$; n=4), and was approximately 60% at 24h, exceeding that measured in the 0.5 and 1.0 wt% agarose gels with 0.6 wt%

P:P at 24h (**Fig. 3.11B,C**). One-way ANOVA was used to analyze differences between groups. Groups denoted by different letters are statistically significant, ns=not significant.

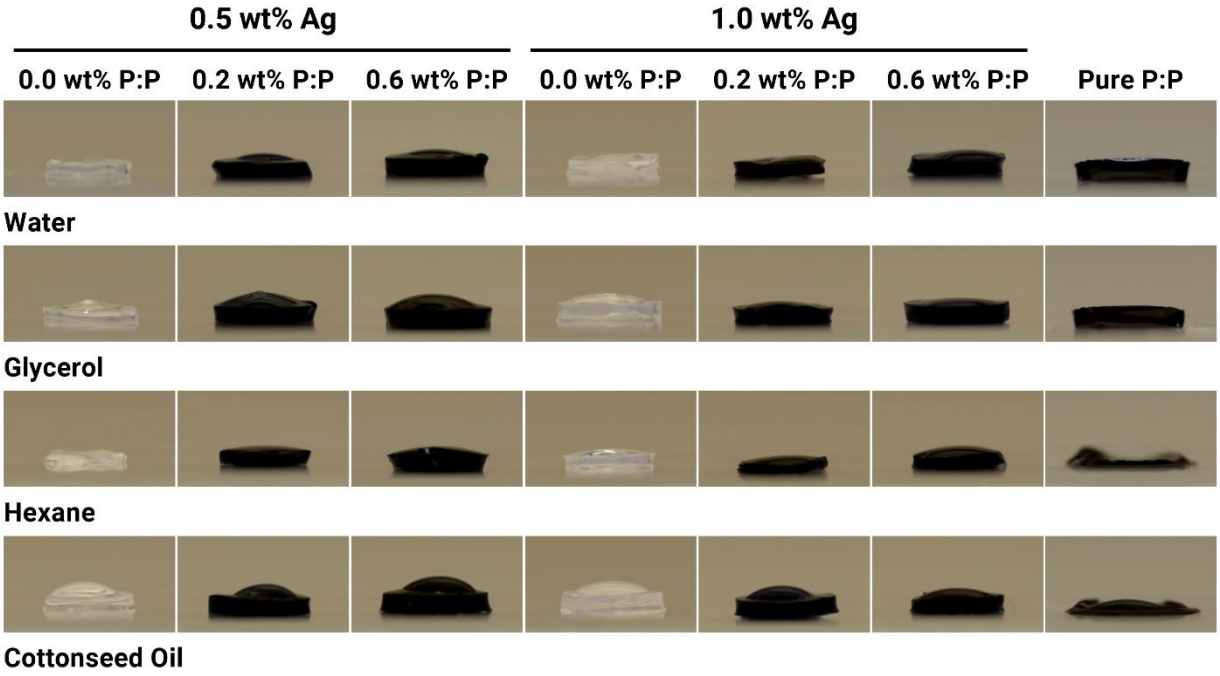

Figure 3.17: Qualitative assessment of hydrophobic properties of hydrogels. Droplet formation did not vary dramatically among groups for all solvents tested. Owing to the phase separation properties of PEDOT:PSS, it is likely that the polymer conformed to minimize contact with the aqueous environment of the hydrogel, thereby masking the hydrophobic properties of PEDOT.

3.3.5 Conductive hydrogels promote adsorption of charged proteins

To further understand how conductive hydrogels facilitated fibronectin adsorption and cell adhesion in the absence of cell-binding ligands, we examined whether

conductivity promoted electrostatically driven protein adsorption. To that aim, we dissolved proteins with varying isoelectric points in PBS, where they took on net charge (BSA (-), lysozyme (+), and myoglobin (neutral)) (**Fig. 3.14A**) and added them to acellular hydrogels. The adsorption of charged proteins (BSA and lysozyme) mostly correlated with PEDOT:PSS concentrations for both 0.5 and 1.0 wt% agarose gels (**Fig. 3.14B,C**). Myoglobin was unaffected by conductivity or storage modulus (*i.e.*, wt% agarose). Interestingly, for the 0.5 wt% agarose gels, there was a lower level of protein adsorption in the conductive groups compared to those in the 1.0 wt% agarose gels. This may be attributed to reduced retention of PEDOT:PSS by the 0.5 wt% agarose gels.

These data indicate that conductive substrates have increased surface charges that electrostatically interact with other charged molecules. Increased cell adhesion to conductive substrates is likely driven by the adsorption of charged proteins in the cell-culture media that facilitate adhesion (*e.g.*, albumin). These findings align with our observation of increased FN adsorption, which takes on a moderately negative charge in PBS and is known to enable cell adhesion.

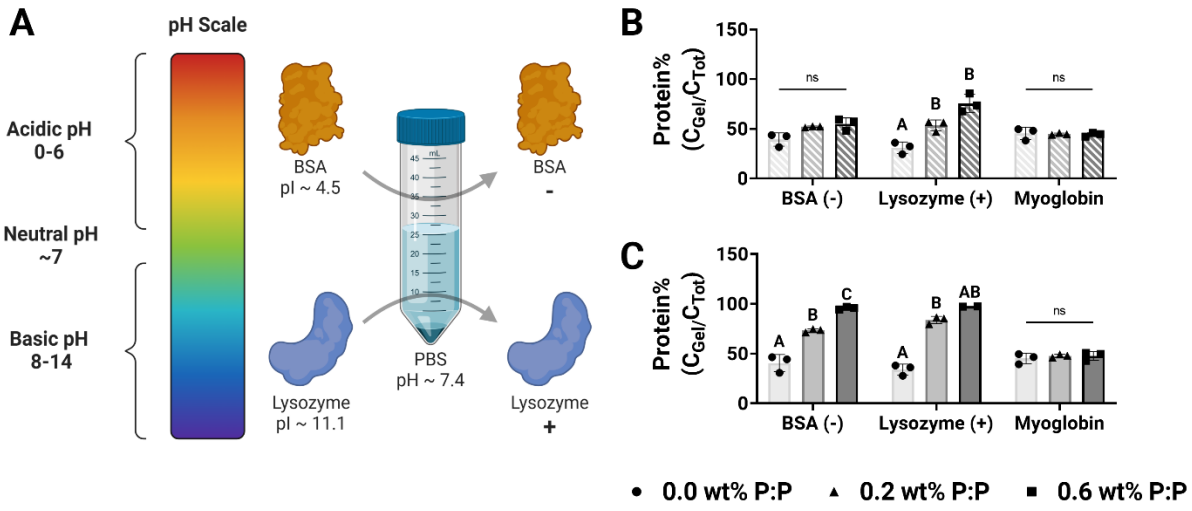

Figure 3.18: Conductivity facilitates the adsorption of charged proteins. **(A)** Schematic illustrating proteins with different isoelectric points become charged when dissolved in a neutral solvent. **(B)** Conductive 0.5 wt% agarose gels facilitate greater adsorption of the positively charged protein, lysozyme, compared to the non-conductive control ($p \leq 0.05$). Further, adsorption of the neutral protein, myoglobin, is unaffected by substrate conductivity (n=3). **(C)** Similar behavior is observed with 1.0 wt% agarose gels, though differences were observed for both charged proteins ($p \leq 0.05$; n=2-3). Two-way ANOVA for the simple effect of PEDOT:PSS concentration was used to analyze the differences between groups within each protein solution. Groups denoted by different letters are statistically significant within each protein group, ns=not significant.

3.4 DISCUSSION

Electrically conductive biomaterials are a promising tool to influence cell behavior given their ability to facilitate bioelectric signaling, which is frequently linked to tissue development and wound healing. While using conductive materials to imbue hydrogels

with electroactive properties is becoming more commonplace, few studies investigate how changing the electrical characteristics of a material affect its other properties. Beyond that, the interplay of electrical and physical properties and how they affect cell behavior is understudied.

In this work, we used agarose and PEDOT:PSS to create an electrically and mechanically tunable hydrogel platform. PEDOT:PSS is frequently used for creating conductive biomaterials and boasts the advantage of being water-dispersible compared to other synthetic polymers which are strongly hydrophobic. Numerous hydrogels and polymers are suitable to make mechanically tunable biomaterials for tissue engineering. Agarose is among the easiest to fabricate, and mechanical tunability is controlled simply by changing the concentration of polysaccharide, thereby reducing variability between samples. While agarose is inherently non-adhesive, cell-binding moieties can be added by incorporating collagen or chemically modifying the agarose backbone to make it amenable to covalent bonding of adhesive peptides[34,35]. This contrasts with other commonly used biomaterials such as collagen, alginate, or GelMA, which have additional variables beyond polymer concentration that affect mechanical properties. Interpenetrating networks[36] and electrospun scaffolds[37] have been formed into conductive substrates but require more complex protocols to fabricate.

With this platform, we interrogated fundamental cell behaviors such as viability, adhesion, and metabolic activity. We observed significant differences in protein adsorption and cell adhesion on conductive substrates. Without the inclusion of adhesive ligands, we did not expect this material to effectively promote cell behavior. However,

given significant differences between the PEDOT:PSS-containing groups and agarose-only controls, this work still illustrates the influence of electrically conductive moieties in hydrogels, even in the absence of external stimulation. Future work will incorporate conductive additives into other hydrogel materials with different tunable mechanical properties (*e.g.*, adhesive ligand concentration, stress-relaxation, etc.) to further probe the relationships between biophysical and electrical properties. Additionally, while synthetic conductive polymers and carbon-based materials are frequently used in biomaterials, emerging studies using naturally derived[38] and ionically conductive[3,13] additives show strong promise for making bioresorbable and clinically translatable biomaterials.

The stiffness and storage moduli of conductive hydrogels vary greatly depending on the application. The storage moduli of our hydrogels ranged from approximately 2-12 kPa, suitable for mimicking the mechanical properties of a variety of soft tissues (*e.g.,* nerve and muscle)[18]. Similar storage moduli have been reported in studies using collagen-based- [39] and fibrin-alginate gels[40]. While storage moduli of our gels was primarily influenced by the concentration of agarose, the addition of PEDOT:PSS also affected their biophysical properties. For the 0.5 wt% agarose gels, addition of 0.6 wt% PEDOT:PSS caused a significant increase in storage modulus, though the magnitude of this increase was less than that observed by increasing the agarose concentration. By contrast, the storage modulus of the 1.0 wt% agarose gels was unaffected by PEDOT:PSS. Other studies have also reported changes in mechanical properties with addition of conductive polymers. Song et al. observed increased Young's modulus and hardness when adding polypyrrole to reduced graphene oxide scaffolds[41]. The addition of polypyrrole to alginate

hydrogels also yielded significantly higher Young's moduli in proportion to polypyrrole concentration[42]. These data demonstrate the importance of testing the influence of conductive additives on material biophysical properties.

The conductive properties of the materials used in this study matched the properties of other electrically conductive hydrogels [11]. Conductivities for electrically conductive hydrogels range from approximately 10^{-6} S/cm for carbon nanotubes incorporated into silk fibroin[43] to 10^{-2} S/cm for PEDOT-hyaluronic acid nanoparticles mixed into a chitosan hydrogel[44]. Most gels fall within the range of 10^{-6}-10^{-3} S/cm, on par with the conductivities of endogenous tissues (10^{-5}-10^{-3} S/cm)[15]. For example, Basurto and colleagues made polypyrrole-containing scaffolds on the order of 10^{-5} S/cm and reported increased myogenic maturation when C2C12s were seeded on conductive scaffolds. Interestingly, the benefits of conductivity are not limitless, as continued increases in conductivity can have detrimental effects on cell metabolic activity[10]. Furthermore, a study by Marzocchi and colleagues illustrates changes in proliferation of different cell lines depending on the oxidation state of PEDOT:PSS, highlighting the need to characterize and control material electrical properties for *in vitro* applications[45]. Collectively, these data emphasize the importance of designing materials with electrical properties that match those of native tissues. However, bioelectricity fluctuates throughout regenerative processes and may serve as a new target for material electrical properties[46].

The positive effects of conductive substrates on cell behavior are frequently attributed to the materials' ability to facilitate protein adsorption[47]. In the seminal paper

by Schmidt et al., the authors postulate that the negative surface charge of polypyrrole led to increased adsorption of positively charged proteins, which led to subsequent PC-12 adhesion and extension[48]. However, studies that demonstrate surface charge properties of conductive biomaterials are rare. Inspired by prior work[49,50], we used proteins with different isoelectric points to interrogate the surface charge properties of agarose and PEDOT:PSS hydrogels. Adsorption of both positively and negatively charged proteins increased with increasing PEDOT:PSS concentrations, particularly for the gels containing a higher concentration of agarose. While PEDOT:PSS has both positive and negative charges in its chemical structure that may contribute to this phenomenon, charged materials also rearrange the distribution of surface charges to accommodate other charged moieties with which they interact in order to achieve electroneutrality[51]. It is possible that proteins change their conformation as they interact with a conductive substrate, which merits future investigation. However, we believe changes observed in the physical properties of the hydrogels corroborate the role of electroneutrality. With increased electrostatically driven protein adsorption to the gel surface and throughout the bulk construct, we predict charges within the polymer network were progressively shielded. Charge shielding limited charge repulsion within the hydrogel, leading to decreased swelling ratio, despite increases in dry mass. We also qualitatively assessed the hydrophobic properties of the gels and observed minimal differences between groups, regardless of PEDOT:PSS presence. We believe that the PSS^- shell, $PEDOT^+$ core structure of PEDOT:PSS is uninterrupted in the aqueous state of hydrogels, rendering similar behaviors between PEDOT:PSS-containing and undoped agarose gels[27]. It is also

possible that, if exposed in a hydrophilic environment, PEDOT will rearrange or phase separate to minimize its exposure to the polar, or more hydrophilic, environment[52]. For this reason, it is not surprising that the hydrogels have minimal change in hydrophobic character. Finally, our conductive gels promoted MSC adhesion and spreading compared to non-conductive control groups. While this may be attributed to increased adsorption of proteins found in the cell culture media, it will be important to investigate cell-binding pathways in response to conductive substrates.

In this work, we illustrate the progression of fabricating an electrically conductive hydrogel system in which mechanics and conductivity can be decoupled, allowing us to study the influence of each on cell behavior. We demonstrate that conductive hydrogels facilitate MSC adhesion and spreading and provide evidence that these improvements in cell behavior may be linked to changes in protein adsorption to conductive hydrogels. These studies fill important knowledge gaps when using electrically conductive materials for biological applications. These findings highlight the importance of thorough material characterization and provide mechanistic insight into how cell behavior is influenced by conductive materials, even when not externally stimulated. Additionally, the methods for incorporating conductive additives and characterizing hydrogel electrical properties are highly accessible for most research groups, providing a means for others to expand into this growing field.

REFERENCES

1. Levin, M., Pezzulo, G. & Finkelstein, J. M. Endogenous bioelectric signaling networks: exploiting voltage gradients for control of growth and form. *Annu Rev Biomed Eng* **19**, 353–387 (2017).
2. Funk, R. H. Endogenous electric fields as guiding cue for cell migration. *Front Physiol* **6**, 143 (2015).
3. Walker, B. W. *et al.* Engineering a naturally-derived adhesive and conductive cardiopatch. *Biomaterials* **207**, 89–101 (2019).
4. Cui, Z. *et al.* Polypyrrole-chitosan conductive biomaterial synchronizes cardiomyocyte contraction and improves myocardial electrical impulse propagation. *Theranostics* **8**, 2752–2764 (2018).
5. Zhou, L. *et al.* Soft conducting polymer hydrogels cross-linked and doped by tannic acid for spinal cord injury repair. *ACS Nano* **12**, 10957–10967 (2018).
6. Zhou, X. *et al.* Enhancement of neurite adhesion, alignment and elongation on conductive polypyrrole-poly(lactide acid) fibers with cell-derived extracellular matrix. *Colloids Surf B Biointerfaces* **149**, 217–225 (2017).
7. Roshanbinfar, K. *et al.* Electroconductive biohybrid hydrogel for enhanced maturation and beating properties of engineered cardiac tissues. *Adv. Funct. Mater.* **28**, 1803951 (2018).
8. Zhang, C. *et al.* A self-doping conductive polymer hydrogel that can restore electrical impulse propagation at myocardial infarct to prevent cardiac arrhythmia and preserve ventricular function. *Biomaterials* **231**, 119672 (2020).
9. Zhang, M. & Guo, B. Electroactive 3D scaffolds based on silk fibroin and water-bornepolyaniline for skeletal muscle tissue engineering. *Macromol Biosci* **17**, 1700147 (2017).
10. Basurto, I. M., Mora, M. T., Gardner, G. M., Christ, G. J. & Caliari, S. R. Aligned and electrically conductive 3D collagen scaffolds for skeletal muscle tissue engineering. *Biomater. Sci.* **9**, 4040–4053 (2021).
11. Guex, A. G. *et al.* Highly porous scaffolds of PEDOT:PSS for bone tissue engineering. *Acta Biomater.* **62**, 91–101 (2017).
12. Chen, J., Yu, M., Guo, B., Ma, P. X. & Yin, Z. Conductive nanofibrous composite scaffolds based on in-situ formed polyaniline nanoparticle and polylactide for bone regeneration. *J Colloid Interface Sci* **514**, 517–527 (2018).
13. Noshadi, I. *et al.* Engineering Biodegradable and Biocompatible Bio-ionic Liquid Conjugated Hydrogels with Tunable Conductivity and Mechanical Properties. *Sci. Rep.* **7**, 4345 (2017).
14. Solazzo, M. *et al.* PEDOT:PSS interfaces stabilised using a PEGylated crosslinker yield improved conductivity and biocompatibility. *J Mater Chem B* **7**, 4811–4820 (2019).
15. Casella, A., Panitch, A. & Leach, J. K. Endogenous Electric Signaling as a Blueprint for Conductive Materials in Tissue Engineering. *Bioelectricity* **3**, 27–41 (2021).
16. Zhao, G. *et al.* Anisotropic conductive reduced graphene oxide/silk matrices promote post-infarction myocardial function by restoring electrical integrity. *Acta Biomater.* **139**, 190–203 (2022).

17. Eftekhari, B. S., Eskandari, M., Janmey, P. A., Samadikuchaksaraei, A. & Gholipourmalekabadi, M. Surface topography and electrical signaling: single and synergistic effects on neural differentiation of stem cells. *Adv Funct Mater* 1907792 (2020) doi:10.1002/adfm.201907792.
18. Engler, A. J., Sen, S., Sweeney, H. L. & Discher, D. E. Matrix elasticity directs stem cell lineage specification. *Cell* **126**, 677–89 (2006).
19. Branco da Cunha, C. *et al.* Influence of the stiffness of three-dimensional alginate/collagen-I interpenetrating networks on fibroblast biology. *Biomaterials* **35**, 8927–8936 (2014).
20. Chaudhuri, O. *et al.* Hydrogels with tunable stress relaxation regulate stem cell fate and activity. *Nat. Mater.* **15**, 326–334 (2016).
21. Leach, J. K. & Whitehead, J. Materials-directed differentiation of mesenchymal stem cells for tissue engineering and regeneration. *ACS Biomater. Sci. Eng.* **4**, 1115–1127 (2018).
22. Falagan-Lotsch, P., Grzincic, E. M. & Murphy, C. J. One low-dose exposure of gold nanoparticles induces long-term changes in human cells. *Proc. Natl. Acad. Sci.* **113**, 13318–13323 (2016).
23. Prajapati, S. K., Malaiya, A., Kesharwani, P., Soni, D. & Jain, A. Biomedical applications and toxicities of carbon nanotubes. *Drug Chem Toxicol* 1–16 (2020) doi:10.1080/01480545.2019.1709492.
24. Humpolicek, P. *et al.* The biocompatibility of polyaniline and polypyrrole: A comparative study of their cytotoxicity, embryotoxicity and impurity profile. *Mater Sci Eng C Mater Biol Appl* **91**, 303–310 (2018).
25. Mawad, D. *et al.* A conducting polymer with enhanced electronic stability applied in cardiac models. *Sci Adv* **2**, e1601007 (2016).
26. Spencer, A. R. *et al.* Bioprinting of a Cell-Laden Conductive Hydrogel Composite. *ACS Appl. Mater. Interfaces* **11**, 30518–30533 (2019).
27. Zhang, S. *et al.* Room-temperature-formed PEDOT:PSS hydrogels enable injectable, soft, and healable organic bioelectronics. *Adv Mater* **32**, e1904752 (2020).
28. Campbell, K. T., Stilhano, R. S. & Silva, E. A. Enzymatically degradable alginate hydrogel systems to deliver endothelial progenitor cells for potential revasculature applications. *Biomaterials* **179**, 109–121 (2018).
29. Laurent, T. C. Determination of the structure of agarose gels by gel chromatography. *Biochim. Biophys. Acta BBA - Gen. Subj.* **136**, 199–205 (1967).
30. Pluen, A., Netti, P. A., Jain, R. K. & Berk, D. A. Diffusion of Macromolecules in Agarose Gels: Comparison of Linear and Globular Configurations. *Biophys. J.* **77**, 542–552 (1999).
31. Ho, S. S., Keown, A. T., Addison, B. & Leach, J. K. Cell migration and bone formation from mesenchymal stem cell spheroids in alginate hydrogels are regulated by adhesive ligand density. *Biomacromolecules* **18**, 4331–4340 (2017).
32. Singleton, W. S. & Benerito, R. R. Surface phenomena of fats for parenteral nutrition. *J. Am. Oil Chem. Soc.* **32**, 23 (1955).

33. Rechendorff, K., Hovgaard, M. B., Foss, M., Zhdanov, V. P. & Besenbacher, F. Enhancement of Protein Adsorption Induced by Surface Roughness. *Langmuir* **22**, 10885–10888 (2006).
34. Yixue, S. *et al.* Modification of agarose with carboxylation and grafting dopamine for promotion of its cell-adhesiveness. *Carbohydr. Polym.* **92**, 2245–2251 (2013).
35. Cambria, E. *et al.* Cell-Laden Agarose-Collagen Composite Hydrogels for Mechanotransduction Studies. *Front. Bioeng. Biotechnol.* **8**, 346 (2020).
36. Spearman, B. S. *et al.* Conductive interpenetrating networks of polypyrrole and polycaprolactone encourage electrophysiological development of cardiac cells. *Acta Biomater* **28**, 109–120 (2015).
37. Chen, M.-C., Sun, Y.-C. & Chen, Y.-H. Electrically conductive nanofibers with highly oriented structures and their potential application in skeletal muscle tissue engineering. *Acta Biomater.* **9**, 5562–5572 (2013).
38. Malvankar, N. S. *et al.* Tunable metallic-like conductivity in microbial nanowire networks. *Nat Nanotechnol* **6**, 573–9 (2011).
39. Walimbe, T., Calve, S., Panitch, A. & Sivasankar, M. P. Incorporation of types I and III collagen in tunable hyaluronan hydrogels for vocal fold tissue engineering. *Acta Biomater* **87**, 97–107 (2019).
40. Vorwald, C. E., Gonzalez-Fernandez, T., Joshee, S., Sikorski, P. & Leach, J. K. Tunable fibrin-alginate interpenetrating network hydrogels to support cell spreading and network formation. *Acta Biomater* **108**, 142–152 (2020).
41. Song, F. *et al.* Room-temperature fabrication of a three-dimensional reduced-graphene oxide/polypyrrole/hydroxyapatite composite scaffold for bone tissue engineering. *RSC Adv.* **6**, 92804–92812 (2016).
42. Yang, S. *et al.* Polypyrrole/Alginate Hybrid Hydrogels: Electrically Conductive and Soft Biomaterials for Human Mesenchymal Stem Cell Culture and Potential Neural Tissue Engineering Applications. *Macromol. Biosci.* **16**, 1653–1661 (2016).
43. Wu, Y., Wang, L., Guo, B. & Ma, P. X. Interwoven aligned conductive nanofiber yarn/hydrogel composite scaffolds for engineered 3D cardiac anisotropy. *ACS Nano* **11**, 5646–5659 (2017).
44. Wang, S. *et al.* Hyaluronic acid doped-poly(3,4-ethylenedioxythiophene)/chitosan/gelatin (PEDOT-HA/Cs/Gel) porous conductive scaffold for nerve regeneration. *Mater Sci Eng C Mater Biol Appl* **71**, 308–316 (2017).
45. Marzocchi, M. *et al.* Physical and electrochemical properties of PEDOT:PSS as a tool for controlling cell growth. *ACS Appl Mater Interfaces* **7**, 17993–8003 (2015).
46. Funk, R. H., Monsees, T. & Ozkucur, N. Electromagnetic effects - from cell biology to medicine. *Prog Histochem Cytochem* **43**, 177–264 (2009).
47. Kotwal, A. & Schmidt, C. E. Electrical stimulation alters protein adsorption and nerve cell interactions with electrically conducting biomaterials. *Biomaterials* **22**, 1055–64 (2001).
48. Schmidt, C. E., Shastri, V. R., Vacanti, J. P. & Langer, R. Stimulation of neurite outgrowth using an electrically conducting polymer. *Proc Nati Acad Sci USA* **94**, 8948–53 (1997).

49. Guo, H. *et al.* Surface charge dominated protein absorption on hydrogels. *Soft Matter* **16**, 1897–1907 (2020).
50. Pasche, S., Voros, J., Griesser, H. J., Spencer, N. D. & Textor, M. Effects of ionic strength and surface charge on protein adsorption at PEGylated surfaces. *J Phys Chem B* **109**, 17545–52 (2005).
51. Hartvig, R. A., Van De Weert, M., Østergaard, J., Jorgensen, L. & Jensen, H. Protein Adsorption at Charged Surfaces: The Role of Electrostatic Interactions and Interfacial Charge Regulation. *Langmuir* **27**, 2634–2643 (2011).
52. Albertsson, P.-Å. Partition of Cell Particles and Macromolecules in Polymer Two-Phase Systems. in *Advances in Protein Chemistry* (eds. Anfinsen, C. B., Edsall, J. T. & Richards, F. M.) vol. 24 309–341 (Academic Press, 1970).

Chapter 4: Conductive microgel scaffolds enhance myogenic potential of myoblasts *in vitro*

4.1 INTRODUCTION

Muscle tissue engineering is an important strategy for repairing large muscle wounds such as cases of volumetric muscle loss (VML) that surpass the body's innate healing ability. VML and other musculoskeletal disorders, which affect over 500 million people worldwide, can result in reduced mobility (and in some cases disability) and significant economic burden on the order of billions of dollars every year[1,2]. The current gold standard of treatment is autologous muscle graft which has negative side effects of donor site morbidity and atrophy. Muscle tissue engineering seeks to address these shortcomings by providing alternative strategies for healing[3,4]. An engineered tissue approach has numerous and specific requirements to recapitulate muscle's hierarchical, anisotropic, elastic, vascularized, and innervated properties, and VML injuries also face the challenge of being irregularly shaped.

Biomaterials are under investigation for use in filling large muscle defects. Synthetic and natural polymers have been developed for specific applications such as aligned structures to recapitulate muscle isotropy, elastic materials to mimic the contractile function of muscle tissue, and hydrogels for use as volume fillers and cell delivery vehicles. Hydrogels are a popular biomaterial for use in cell and drug delivery due to their tunability and viscoelastic behavior which mimics that of native tissues[5].

Microgels are emerging as a promising hydrogel platform due to their modularity and microporosity[6]. Unlike conventional bulk hydrogels which are nanoporous, the inherent void space between microgels permits immediate cell migration without the need to first remodel the local environment. Furthermore, their ability to be injected and cryopreserved increases their accessibility in the clinic[7,8]. A multitude of studies have examined bulk hydrogels for muscle tissue engineering[5], yet there is limited data available on the use of microgels. While microgels have been mixed with silver nanoparticles to form a conductive mixture that conferred electric signals across *ex vivo* tissues, their influence on muscle cell regeneration was not examined[9].

Electrically conductive biomaterials are rapidly gaining popularity within tissue engineering owing to these materials' ability to direct cell differentiation and maturation, particularly for nerve[10] and cardiac tissue repair[11]. Synthetic conductive polymers such as polypyrrole, polyaniline, and PEDOT:PSS (poly(3,4-ethylenedioxythiophene) polystyrene sulfonate)) or carbon-based materials (*e.g.*, carbon nanotubes, graphene, etc.) are frequently used to imbue hydrogels with electroactive properties[12,13]. For example, previous reports have developed synthetic electrospun fibers for muscle tissue engineering which contained either polyaniline blends[14,15] or PEDOT:PSS nanoparticles[16]. Another report used polypyrrole in directionally aligned collagen scaffolds to direct myoblast behavior[17]. While these reports include both electrical and physical cues to promote cell differentiation toward myogenesis, the interplay between conductivity and scaffold porosity has yet to be directly interrogated.

As such, we aim to combine the microporosity of microgels with the conductivity of PEDOT:PSS to enhance myogenic differentiation. Herein, we demonstrate a conductive microgel platform which outperforms both conductive bulk degradable and non-conductive scaffolds in promoting myogenic differentiation. We generate microgel scaffolds with a conductivity ~3.5×10^{-6} S/cm and a compressive modulus ~28 kPa. We show that cell viability and scaffold stiffness is not altered by the addition of PEDOT:PSS, and that microgels can be annealed into a contiguous scaffold. We further show that gene and protein expression indicative of myotube maturation is upregulated in our conductive microgel scaffolds when seeded with murine C2C12 myoblasts, suggesting the importance of both electroactivity and microporosity for muscle regeneration. Future work will investigate the interplay of porosity and conductivity on the myogenesis of clinically relevant, human-derived muscle cells.

4.2 MATERIALS AND METHODS

4.2.1 Microgel synthesis

Microgels were fabricated using a microfluidic device previously described[18] and adapted by our group[7]. For nondegradable microgels, the aqueous phase consisted of 8-arm 10 kDa PEG-VS (JenKem, Plano, TX) and RGD (Ac-RGDSPGERCG-NH_2, Genscript, Piscataway, NJ) in 100 mM HEPES buffer (N-2-hydroxyethylpiperazine-N'-2-ethanesulfonic acid, pH 5.25, Sigma, St. Louis, MO) mixed with 3.5 kDa PEG-DT (JenKem) dissolved in diH_2O with or without PEDOT:PSS (PH1000, Ossila, Sheffield, UK). The final microgel concentrations were 4.5 mM PEG-VS, 10.8 mM PEG-DT, 1 mM RGD, and 0.25

wt% PEDOT:PSS. The oil phase consisted of Novec 7500 Oil and 0.75 wt% Picosurf (Sphere Fluidics, Cambridge, UK). After exiting the device, microgels were combined with a solution of 1 v/v% triethylamine (TEA, Sigma) in Novec 7500 Oil using a Y-junction (IDEX Health and Science, Oak Harbor, WA) and left at room temperature overnight to ensure complete crosslinking. Microgels were cleaned to remove residual oil and surfactant as described.[7]

4.2.2 Annealing microgels

Microgels were annealed as previously described.[7] Briefly, microgels were suspended in an annealing solution consisting of additional crosslinker in HEPES containing 0.4% VA-086 photoinitiator (FUJIFULM Wako Chemicals, Richmond, VA) equal to the volume of microgels. After incubating for 1 min, the microgels were spun down for 3 min at 14,000 × *g*. The supernatant was removed and microgels were optionally mixed with cells before plating in the desired mold. The microgel slurry was then exposed to UV light (20 mW/cm^2, 320-500 nm, Omnicure S2000) for 2 min to form annealed scaffolds.

4.2.3 Bulk degradable gel synthesis

GPQ-A (GCRDGPQGIAGQDRCG, Genscript) was substituted for PEG-DT to permit MMP-mediated degradation. The final concentrations were 8 mM PEG-VS, 19.2 mM GPQ-A, 1 mM RGD, and 0.25 wt% PEDOT:PSS. A precursor solution consisting of PEG-VS, RGD, and optionally PEDOT:PSS in HEPES (25 mM, pH 7.2) at 2X concentration was combined with cells and pipetted into the desired mold. An equal volume of 2X GPQ-A (pH 8.3) in

media was then mixed in by pipetting up and down. The gels were incubated at 37°C for 15 min before being transferred to a well plate.

4.2.4 Conductivity testing

Annealed microgels were electrically characterized as described previously[19]. Briefly, 6 mm scaffolds were constrained by a PDMS mold and sandwiched between two brass plates. The sandwich was then stabilized between the jaws of a tabletop angle vise using PDMS blocks as a barrier between the plate and the jaw. One brass plate was connected to a power supply (BK Precision 1735A, Yorba Linda, CA) using alligator clips. One lead of a multimeter (SparkFun Electronics, Niwot, CO) was connected to the other brass plate and the second lead was connected to the power supply to create a complete circuit through which current could be measured. Voltages ranging from 100 to 500 mV, chosen to avoid the electrolysis of water, were applied to obtain current-voltage curves. After testing, hydrogel diameter and thickness were measured with calipers and hydrogel cross-sectional area was calculated. Current-voltage curves were analyzed for linearity and datasets with an R^2 value ≥0.9 were accepted for resistance calculations. Conductivity was calculated using Pouillet's law (**Equation 5.1**). Hydrogels for conductivity testing were stored in ultrapure water to eliminate the confounding effects of ions in other solutions.

Equation 5.5:

$$\sigma = \frac{t}{RA}$$

where σ is conductivity in S/cm, t is thickness of the hydrogel (cm), R is resistance (Ω), and A is cross-sectional area (cm^2).

4.2.5 Mechanical testing

4.2.5.1 Determination of bulk hydrogel shear storage modulus

Bulk hydrogel scaffolds were loaded onto a Discovery HR2 Rheometer (TA Instruments, New Castle, DE) with a stainless steel, cross hatched, 8 mm plate geometry. An oscillatory strain sweep ranging from 0.004% to 4% strain was performed on each gel to obtain the linear viscoelastic region (LVR) before failure.

4.2.5.2 Determination of microgel compressive elastic modulus

Individual microgels were examined using a MicroTester (CellScale, Waterloo ON, Canada). Microgels were loaded onto an anvil in a water bath filled with PBS. The microgels were then compressed to half their diameter by a stainless-steel platen attached to a tungsten rod over 30 s. Displacement and force were traced *via* MicroTester software. The slope of the linear region of the compressive modulus *versus* nominal strain graph was recorded as the calculated modulus.

4.2.6 Cell culture

C2C12 murine myoblasts (CRL-1772, Lot #70013341, ATCC, Manassas, VA) were cultured in DMEM (Thermo Fisher Scientific, Walham, MA) supplemented with 10% FBS (GenClone, San Diego, CA) and 1% Penicillin-Streptomycin (P/S, Gemini Bio Products,

West Sacramento, CA) (DMEM-G) in standard culture conditions (*i.e.*, 37°C, 5% CO_2). Cultures were maintained until <70% confluent to prevent myoblast differentiation. Differentiation media was prepared by supplementing DMEM with 2% heat-inactivated horse serum (Thermo Fisher Scientific) and 1% FBS (DMEM-D). C2C12s were seeded in tissue culture plastic flasks at 5,000 cells/cm^2. Cells were seeded into microgels at 100,000 cells per gel to account for some cell loss post-annealing. Cells were seeded into bulk degradable gels at 50,000 cells per gel. Cells seeded into gels were handled with DMEM-G and cell-laden scaffolds were cultured in 24-well plates containing DMEM-G for approximately 24 h (0d) before transferring to a fresh well plate containing DMEM-D (1d). Metabolic activity and differentiation of myoblasts in microgel and bulk degradable scaffolds were assessed at 3d and 7d.

4.2.7 Biochemical assessment of metabolic activity and proliferation

Metabolic activity of C2C12s in microgel scaffolds was assessed using the alamarBlue™ Cell Viability Reagent according to the manufacturer's instruction (Thermo Fisher Scientific). In short, cell-laden scaffolds were transferred to fresh DMEM-D with 1:10 alamarBlue reagent™ and incubated at 37°C for 2 h before analysis. Results were normalized to the DNA content measured using the Quant-iT PicoGreen dsDNA Kit (Thermo Fisher Scientific).

4.2.8 Immunostaining

Scaffolds were fixed in 4% paraformaldehyde for 1 h and incubated in blocking buffer composed of 10% goat serum and 10 mg/mL Bovine Serum Albumin (BSA, Gemini Bio Products) for 30 min at room temperature. Constructs were then incubated with myosin heavy chain antibody conjugated with Alexa Fluor 488 (1:50; Santa Cruz Biotechnology, 376157) and myogenin antibody conjugated with Alexa Fluor 680 (1:50, Santa Cruz Biotechnology, 12732). Samples were rinsed with PBS and incubated with DAPI (1:500 in PBS; Thermo Fisher Scientific) for 10 min. Z-stacks were taken on a confocal microscope (Leica Stellaris 5), and max projections were used to illustrate cell morphology throughout the scaffolds.

4.2.9 qPCR

Total RNA was isolated from cells using TRIzol reagent (Thermo Fisher Scientific) according to the manufacturer's instructions. RNA quality and quantity was measured using a Nanodrop One© instrument (Thermo Fisher Scientific) before reverse transcribing to cDNA with the QuantiTect Reverse Transcription kit (Qiagen, Hilden, Germany). All cDNA samples were diluted with PCR-grade ultrapure water to 12.5 ng/µL prior to qPCR. qPCR was performed using Taq PCR Master Mix kit (Qiagen), TaqMan Gene Expression Assay probes (Cat. 4331182, Thermo Fisher Scientific), and a QuantStudio™ 6 instrument (Thermo Fisher Scientific). Samples were activated at 94°C for 3 min, followed by 40 cycles of 94°C for 30 s, 60°C for 30 s, and 72°C for 1 min, and underwent a final annealing step at 72°C for 10 min. All genes were normalized to the

housekeeping gene GAPDH (Mm99999915_g1) and fold change relative to the 0.00% PEDOT:PSS group at the earliest timepoint was calculated using the $2^{-\Delta\Delta Ct}$ method. C2C12 expression of the myogenic differentiation markers MyoD (*Myod1*, Mm00440387_m1), myogenin (*Myog*, Mm00446194_m1) and myosin heavy chain (*Myh7*, Mm00600555_m1) was interrogated at 3 and 7d.

4.2.10 Statistical analysis

Data are presented as means ± standard deviation. GraphPad Prism 9 software was used to plot all graphs and perform statistical testing. Statistically significant groups are denoted by two conventions: asterisks were used to denote differences when using a t-test or 1-way ANOVA, whereas letters were used when a 2-way ANOVA was employed. Groups denoted by different letters are statistically significant. Datasets with additional interactions were analyzed using MATLAB.

4.3 RESULTS

4.3.1 PEG microgels can be annealed into conductive scaffolds with mechanical properties appropriate for muscle tissue engineering

PEG microgels were fabricated as previously described and modified with RGD to facilitate cell adhesion[7]. PEDOT:PSS was optionally introduced into the aqueous phase of microgel fabrication such that the final concentration within each microgel was 0.25 wt% (**Fig. 4.1A**). Microgels could be successfully annealed into 8 mm scaffolds with good retention of PEDOT:PSS, as depicted in **Figure 4.1B**. The addition of PEDOT:PSS caused

a significant increase in annealed scaffold conductivity from 1.584 ± 0.684 × 10^{-6} S/cm to 3.517 ± 0.964 × 10^{-6} S/cm (**Fig. 4.1C**). Next, we assessed if addition of PEDOT:PSS affected the mechanical properties of the microgels and annealed scaffolds. We measured the compressive modulus of individual microgels on a MicroTester (**Fig. 4.1D**) which was ~28 kPa for both groups. Using Hooke's law for isotropic materials and a Poisson's ratio of approximately 0.5, the storage modulus of each microgel is estimated to be 10 kPa[20]. Since cells interact directly with individual microgels, these mechanical properties were considered appropriate for muscle tissue engineering applications[21]. The storage modulus of annealed scaffolds also did not significantly differ between groups, indicating that PEDOT:PSS did not affect annealing ability (**Fig. 4.1E**). Together, these data illustrate successful incorporation of PEDOT:PSS into PEG microgels without altering mechanical properties. The microgels can be annealed to form scaffolds with decoupled electrical and mechanical properties suitable for muscle tissue engineering.

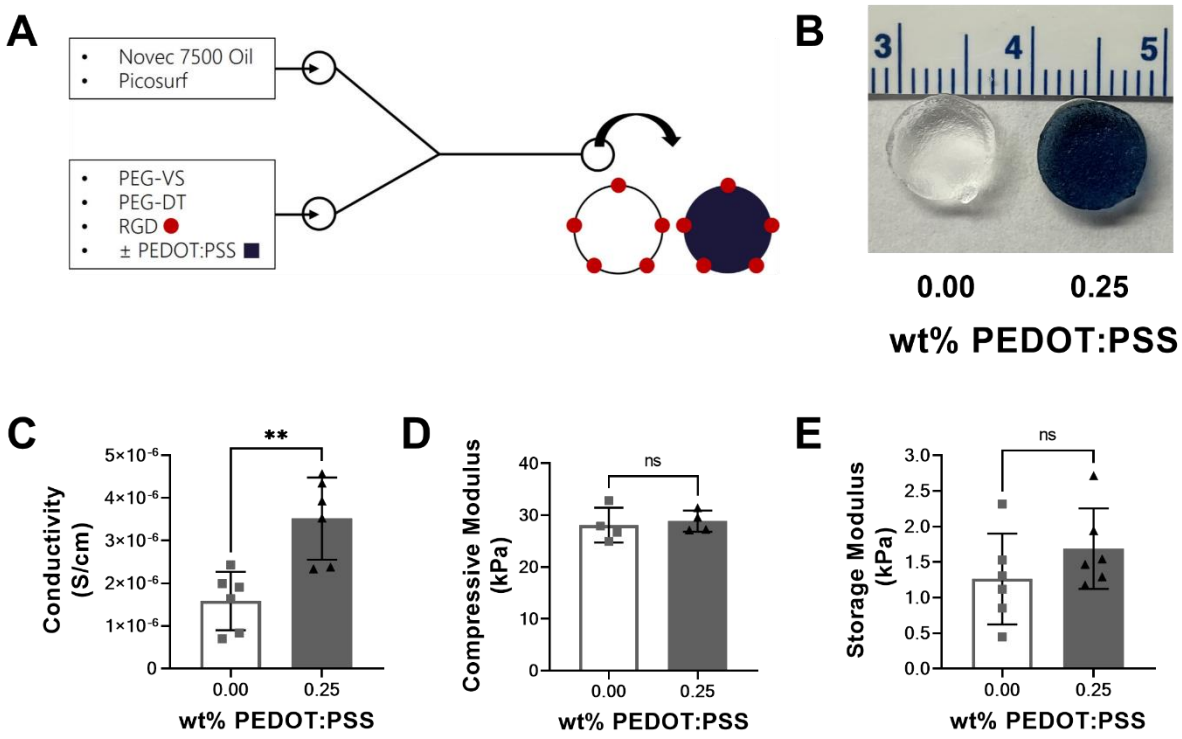

Figure 4.19: Conductive microgels have decoupled electrical and mechanical properties. (A) Schematic of PEG microgel modification and PEDOT:PSS incorporation. **(B)** Gross images of 8 mm scaffolds demonstrate successful annealing with UV light and retention of PEDOT:PSS. **(C)** Scaffolds containing PEDOT:PSS were significantly more conductive than non-conductive controls (n=6). By contrast, PEDOT:PSS did not affect **(D)** the compressive modulus of individual microgels (n=4) or **(E)** the storage modulus of annealed microgel scaffolds (n=6). Groups were compared using a two-tailed t-test where $^{**}p \leq 0.01$ and ns = not significant.

4.3.2 Conductive microgel scaffolds support C2C12 myoblast metabolic activity indicative of differentiation

C2C12 mouse myoblasts were seeded into annealed microgel scaffolds and into bulk degradable gels as a control. After 3 and 7d, metabolic activity of the cells was measured with the alamarBlue assay, the results of which were normalized to DNA content. Cells in conductive annealed microgel scaffolds had significantly greater proliferation at 3d than those than those in the non-conductive control, evidenced by the increase in DNA content (**Fig. 4.2A**). However, the metabolic activity of cells on 3d appeared lower, in the conductive group, though results were not significant (**Fig. 4.2B**). This may indicate the conductive microgels' ability to promote C2C12 differentiation, which is associated with lower metabolic activity[22]. There were no changes in DNA content or metabolic activity of myoblasts in annealed microgel scaffolds at 7d.

Conversely, C2C12s grown on bulk degradable gels had no difference in DNA content or metabolic activity on 3d. On 7d, however, the PEDOT:PSS-containing bulk gels had greater DNA content, indicating that conductive substrates may better support cell viability (**Fig. 4.2C**). Metabolic activity on the bulk degradable gels was low at 3d, and the reduction in activity on the conductive gels at 7d compared to the non-conductive controls is also believed to be suggestive of cell differentiation (**Fig. 4.2D**).

Overall, these data suggest microgels containing PEDOT:PSS support increased proliferation and differentiation of C2C12s compared to microgels without a conductive additive. Furthermore, these data demonstrate the advantage of microporous scaffolds

in supporting cell viability, proliferation, and metabolic activity compared to nanoporous bulk hydrogels that are frequently used for tissue engineering studies.

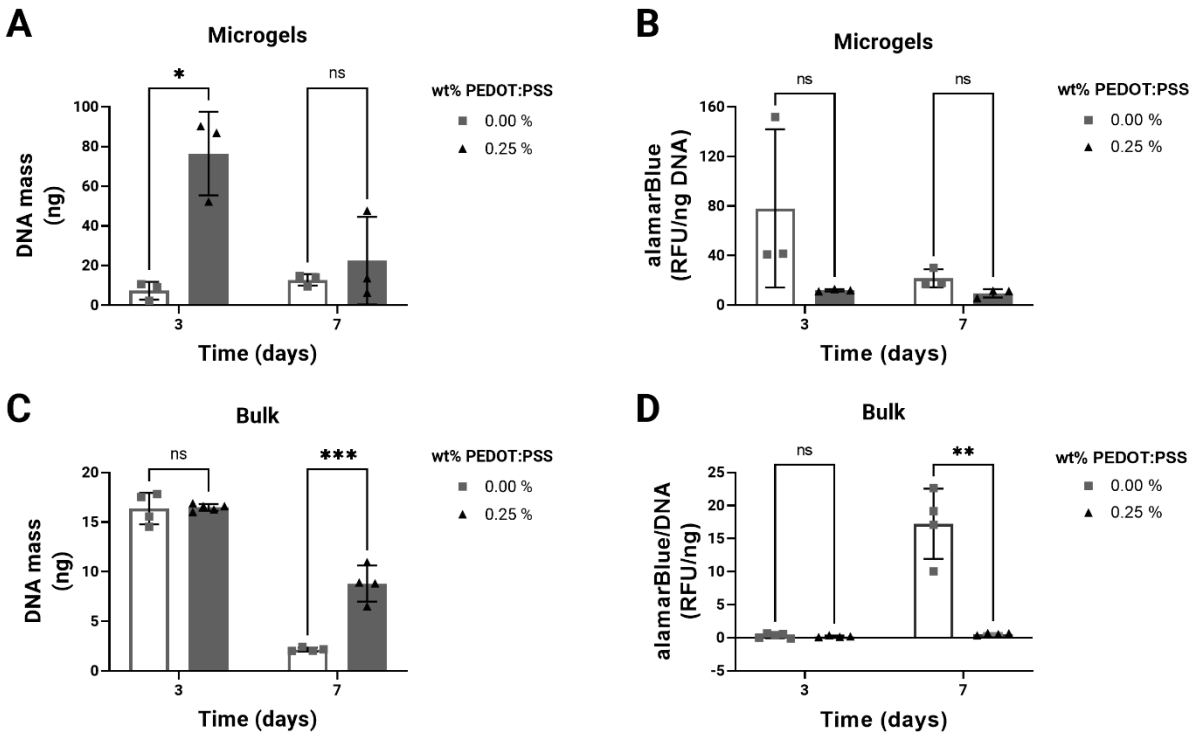

Figure 4.20: Microgel structure promotes C2C12 metabolic activity indicative of differentiation compared to bulk hydrogels. (A) DNA content of C2C12s in annealed microgel scaffolds demonstrate conductive scaffolds promoted myoblast proliferation at 3d (n=3, *$p \leq 0.05$). **(B)** When normalized to DNA content, metabolic activity appears lower in myoblasts on conductive gels at 3d, which may point to cells undergoing differentiation (n=3). **(C)** C2C12s cultured in bulk degradable hydrogels had lower proliferation overall, though the conductive hydrogels supported myoblasts better at 7d than non-conductive controls (n=4, ***$p \leq 0.001$). **(D)** When normalized to DNA content, the metabolic activity of C2C12s on bulk degradable gels was minimal, indicating the

advantage of microporous materials over nanoporous ones (n=4, **$p \leq 0.01$). Groups were compared using multiple, unpaired t-tests where ns = not significant.

4.3.3 C2C12 differentiation is aided by microporous structure and conductivity

The myogenic differentiation of C2C12s seeded in microgel scaffolds was analyzed at 3d and 7d post-seeding. qPCR to interrogate the early myogenic marker, MyoD (*Myod1*), did not offer a conclusive pattern in gene expression response to microgel porosity or conductivity (**Fig. 4.3A**). The expression of the slightly later myogenic marker, myogenin (*Myog*), indicated cell response was unaffected by substrate conductivity, but was sensitive to hydrogel structure and time (**Fig. 4.3B**). While *Myog* expression was generally downregulated compared to the control, it was higher at 3d than at 7d, as expected. When cells were seeded on bulk degradable controls, there was no change in gene expression. Expression of the later myogenic marker, myosin heavy chain (*Myh7*), suggested potential interactions between conductivity, physical structure, and time (**Fig. 4.3C**). Most notably, there was a significant increase in *Mhy7* expression by cells grown in conductive microgel scaffolds compared to the non-conductive group at 7d. Few differences existed between the remaining interactions, though a trend for greater *Myh7* expression was observed in the cells grown in conductive bulk gels at 7d compared to those in their non-conductive counterpart, as well. When the interactions between time, physical properties, and electrical properties were analyzed with a three-way ANOVA, *Myh7* expression was influenced by the combination of time and electrical cues (p=0.0002) as well as time and physical cues (p=0.0073).

Immunostaining for MHC was much more pronounced in conductive microgels at 7d compared to non-conductive controls (**Fig. 4.3D**). Although nuclei staining indicated good cell distribution within the microgel scaffolds, there was no discernable MHC staining at 3d for either microgel group. C2C12s seeded on bulk degradable gels had minimal activity, as evidenced by their rounded morphology and minimal MHC staining. Cells were also stained for myogenin, but signal was limited and only visible when cells were cultured in the conductive microgel scaffolds for 7 days. The immunostaining data corroborates the MHC gene expression analysis and affirms both physical and electrical properties of a material influence cell differentiation.

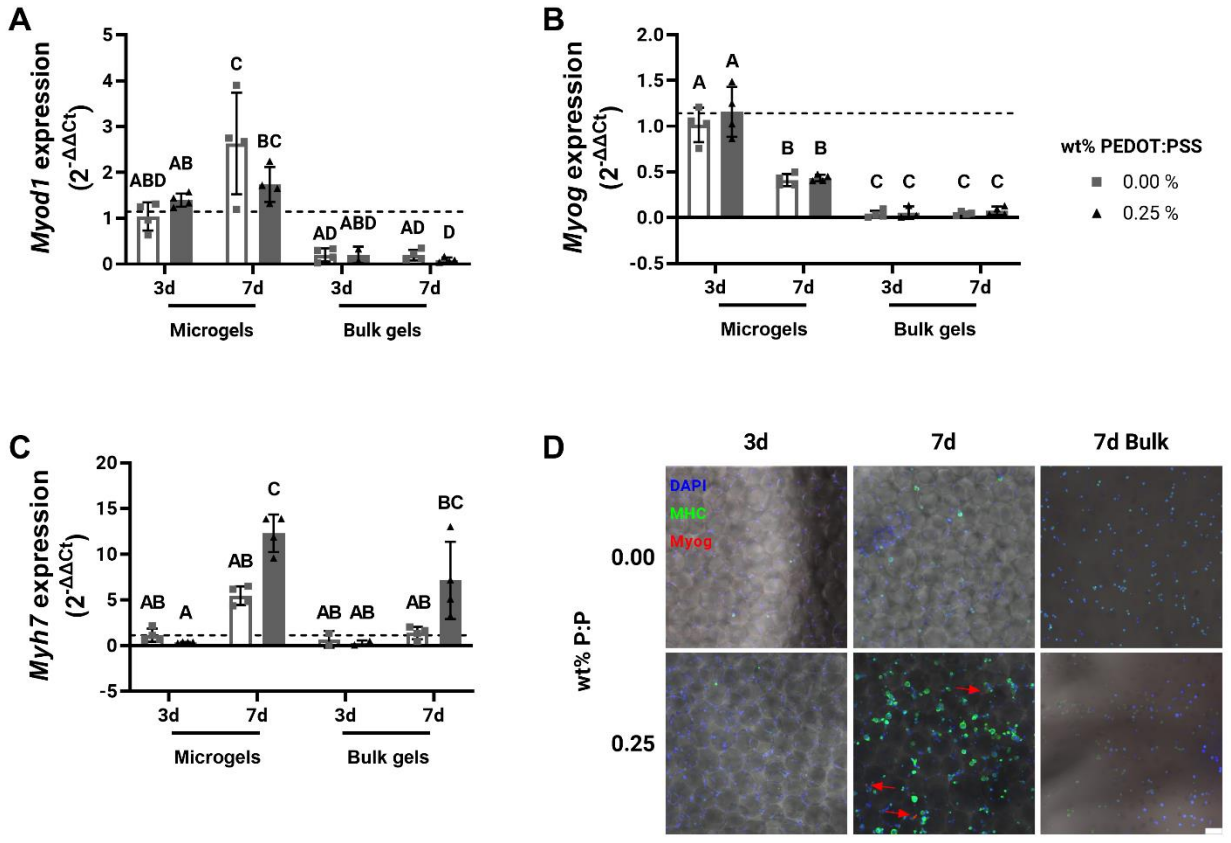

Figure 4.21: Microgel structure aids in expression of early myogenic markers of C2C12s, and conductivity further enhances expression of late myogenic markers. (A)

Expression of the early myogenic gene, *Myod1*, is not significantly affected by either the electrical or physical properties of the microgel annealed scaffolds (n=2-4). **(B)** Myogenin gene expression (*Myog*) was not dependent upon scaffold conductivity but was significantly different in response to scaffold porosity and time (n=3-4). **(C)** Expression of the gene for myosin heavy chain (*Myh7*) suggest conductivity, porosity, and time each contribute to cell response. Notably, *Myh7* expression 7 days after C2C12s were seeded in conductive microgels was significantly higher than those cultured in the non-conductive control and both microgel groups on 3d (n=2-4). The displayed statistics were generated using a two-way ANOVA. Groups denoted with different letters are significantly different. Groups that share letters are statistically similar. **(D)** Immunofluorescence staining of C2C12s demonstrate an upregulation in myosin heavy chain (MHC) protein expression when cultured in conductive microgel scaffolds. Trace myogenin (red arrows) was observed in this group, as well, and was not present in cells grown in the non-conductive gels or bulk gels at both time points. Scale = 100 μm.

4.4 DISCUSSION

Physical and electrical properties are critical for directing cell behavior and can synergistically promote cell differentiation and maturation. In this work we developed conductive microgel scaffolds to interrogate myogenic behavior of C2C12 myoblasts. While microgels have been used for the regeneration of many tissue types[6], to our knowledge no studies have investigated the benefit of combining the microporosity of microgel scaffolds with conductive material. Herein, we demonstrate the ability of

conductive microgels to promote increased myoblast proliferation, differentiation, and maturation compared to bulk conductive hydrogels and non-conductive microgel scaffolds.

When designing a biomaterial, the ability for cells to migrate and proliferate is essential[23,24]. To address this, materials are often designed to be enzymatically or hydrolytically degradable to permit cellular invasion[25]. However, these techniques still require time for material remodeling after cells are implanted. Unlike bulk hydrogels, microgels possess inherent void space in between the particles which permit immediate cell migration. Furthermore, the monodisperse nature of microfluidic-produced microgels ensures consistent, predictable, and tunable void space. PEG-based microgels with defined geometries were used to improve nutrient diffusion and cell dispersal in a 3D scaffold. Other groups have utilized microgel fragments to create materials with highly tunable mechanical properties[26]. While these fragments boast a facile workflow, they face the drawback of not having defined void spaces, which can be specifically optimized to regulate cell behaviors[7].

We used PEDOT:PSS in this work to bestow the PEG microgels with conductive properties. PEDOT:PSS is frequently used for fabricating conductive biomaterials owing to its commercial availability and its relative homogeneity when suspended in water[13]. The hydrophobic $PEDOT^+$ core is surrounded by a shell of PSS^-, which forms micelles that can evenly distribute within a water-based material, such as hydrogels[27]. This contrasts starkly to other commonly used synthetic conductive materials such as polypyrrole, polyaniline, and graphene, which despite possessing high levels of electrical conductivity,

require further chemical processing to overcome their hydrophobic properties and be incorporated into hydrogels. Although addition of PEDOT:PSS into the PEG microgels caused the conductivity of annealed scaffolds to double, it did not affect the compressive modulus of individual microgels or the storage modulus of annealed scaffolds, which contrasts previous work in a related system[19]. In that regard, this hydrogel platform had completely decoupled electrical and mechanical properties, allowing for the interrogation of how these properties individually influence cell behavior.

Others have sought to incorporate electrical elements into hydrogels for muscle tissue engineering with similar electrical properties[12]. The PEDOT:PSS-containing microgel scaffolds' conductivity was approximately 3.5×10^{-6} S/cm, which is comparable to studies conducted by Basurto et. al.[17] and others[28,29]. Though these studies characterize changes in mechanical properties with the inclusion of conductive additives, few specifically interrogate the interplay of biomaterial electrical and physical properties on influencing cell response. Further, as previously mentioned, the novelty of this work is the examination of porosity as a physical property and how it interacts with electroactivity to affect cell behavior.

Ultimately, we found both the microporosity and conductive components of our scaffolds to be critical in directing myoblast differentiation. For example, though we observed significantly greater DNA content of C2C12s cultured in conductive microgel scaffolds compared to non-conductive controls, the metabolic activity of those cells was much lower, suggestive of myoblast differentiation. These results are in agreement with other studies demonstrating lower metabolic activity in differentiating cells[22]. Further,

when probing for myogenic markers, there was a stark increase in myosin heavy chain gene and protein expression in the C2C12s grown in the conductive scaffolds at later time points. Myosin heavy chain is a hallmark indicator for muscle cells that are maturing from myoblasts to more functional myotubes. Markers that define earlier stages of myogenic differentiation include MyoD and myogenin, which we also interrogated[30–32]. The expression of *Myod1* did not have a clear dependence on either microporosity or conductivity, and myogenin was affected mainly by scaffold physical structure and time. Other studies investigating muscle cell differentiation demonstrate strong MyoD expression at time points earlier than we measured. Additionally, since our hypothesis was that conductive microporous materials would promote myogenic differentiation, it is possible that the window in which MyoD and myogenin are expressed was narrowed outside of a feasible detectable limit. To explore this concept, future work could include gene expression studies 24 h post-seeding. Together, these data indicate that physical and electrical cues can effectively differentiate C2C12s without additional soluble cues beyond what is suggested for myoblast culture.

The results of these experiments are promising for recapitulating the porous and electroactive aspects of muscle tissue, but one limitation of this work is the random alignment of porosity found in microgel scaffolds. Surface topography and muscle cell alignment has been shown to be vital in myogenic differentiation due to the highly organized structure of muscle[3,33]. Future work may consider including a mechanism of alignment such as application of an external electric field[34–36] or bioprinting[37–39]. Additionally, while MHC expression was visibly upregulated on conductive microgels on

7d, we did not observe myocyte fusion into myotubes. This may be improved with higher seeding density into the annealed constructs or incorporating mechanisms for the material to degrade and thus make room for myotubes to assemble.

This work is, to the best of our knowledge, the first to demonstrate the utility of conductive, microporous scaffolds for muscle tissue engineering. Both electrical and physical properties were integral for promoting myoblast differentiation at both the gene and protein level. The bioactivity and injectable nature of the microgel scaffolds make them a promising tool for clinical translation to heal muscle wounds. Future work will probe the response of primary human cells to these scaffolds to determine if conductive microgels can support even greater, more clinically translatable myogenic differentiation.

REFERENCES

1. Corona, B. T., Rivera, J. C., Owens, J. G., Wenke, J. C. & Rathbone, C. R. Volumetric muscle loss leads to permanent disability following extremity trauma. J Rehabil Res Dev 52, 785–92 (2015).
2. Manring, H., Abreu, E., Brotto, L., Weisleder, N. & Brotto, M. Novel excitation-contraction coupling related genes reveal aspects of muscle weakness beyond atrophy—new hopes for treatment of musculoskeletal diseases. Front. Physiol. 5, (2014).
3. Jana, S., Levengood, S. K. L. & Zhang, M. Anisotropic Materials for Skeletal-Muscle-Tissue Engineering. Adv. Mater. 28, 10588–10612 (2016).
4. Grasman, J. M., Zayas, M. J., Page, R. L. & Pins, G. D. Biomimetic scaffolds for regeneration of volumetric muscle loss in skeletal muscle injuries. Acta Biomater. 25, 2–15 (2015).
5. Lev, R. & Seliktar, D. Hydrogel biomaterials and their therapeutic potential for muscle injuries and muscular dystrophies. J. R. Soc. Interface 15, 20170380 (2018).
6. Newsom, J. P., Payne, K. A. & Krebs, M. D. Microgels: Modular, tunable constructs for tissue regeneration. Acta Biomater. 88, 32–41 (2019).
7. Lowen, J. M. et al. Multisized Photoannealable Microgels Regulate Cell Spreading, Aggregation, and Macrophage Phenotype through Microporous Void Space. Adv. Healthc. Mater. 2202239 (2023) doi:10.1002/adhm.202202239.
8. Anderson, A. R., Nicklow, E. & Segura, T. Particle fraction is a bioactive cue in granular scaffolds. Acta Biomater. 150, 111–127 (2022).
9. Shin, M., Song, K. H., Burrell, J. C., Cullen, D. K. & Burdick, J. A. Injectable and Conductive Granular Hydrogels for 3D Printing and Electroactive Tissue Support. Adv. Sci. 6, 1901229 (2019).
10. Liu, X. et al. Covalent crosslinking of graphene oxide and carbon nanotube into hydrogels enhances nerve cell responses. J. Mater. Chem. B 4, 6930–6941 (2016).
11. Walker, B. W. et al. Engineering a naturally-derived adhesive and conductive cardiopatch. Biomaterials 207, 89–101 (2019).
12. Dong, R., Ma, P. X. & Guo, B. Conductive biomaterials for muscle tissue engineering. Biomaterials 229, 119584 (2020).
13. Casella, A., Panitch, A. & Leach, J. K. Endogenous Electric Signaling as a Blueprint for Conductive Materials in Tissue Engineering. Bioelectricity 3, 27–41 (2021).
14. Chen, M.-C., Sun, Y.-C. & Chen, Y.-H. Electrically conductive nanofibers with highly oriented structures and their potential application in skeletal muscle tissue engineering. Acta Biomater. 9, 5562–5572 (2013).
15. Hosseinzadeh, S. et al. The nanofibrous PAN-PANi scaffold as an efficient substrate for skeletal muscle differentiation using satellite cells. Bioprocess Biosyst. Eng. 39, 1163–1172 (2016).
16. McKeon-Fischer, K. D., Browe, D. P., Olabisi, R. M. & Freeman, J. W. Poly(3,4-ethylenedioxythiophene) nanoparticle and poly(ε-caprolactone) electrospun scaffold characterization for skeletal muscle regeneration. J. Biomed. Mater. Res. A 103, 3633–3641 (2015).

17. Basurto, I. M., Mora, M. T., Gardner, G. M., Christ, G. J. & Caliari, S. R. Aligned and electrically conductive 3D collagen scaffolds for skeletal muscle tissue engineering. Biomater. Sci. 9, 4040–4053 (2021).
18. de Rutte, J. M., Koh, J. & Di Carlo, D. Scalable High-Throughput Production of Modular Microgels for In Situ Assembly of Microporous Tissue Scaffolds. Adv. Funct. Mater. 29, 1900071 (2019).
19. Casella, A., Panitch, A. & Leach, J. K. Electroconductive agarose hydrogels modulate mesenchymal stromal cell adhesion and spreading through protein adsorption. J. Biomed. Mater. Res. A 111, 596–608 (2023).
20. Mott, P. H. & Roland, C. M. Limits to Poisson's ratio in isotropic materials. Phys. Rev. B 80, 132104 (2009).
21. Gonzalez-Fernandez, T., Sikorski, P. & Leach, J. K. Bio-instructive materials for musculoskeletal regeneration. Acta Biomater. 96, 20–34 (2019).
22. Martinez Villegas, K., Rasouli, R. & Tabrizian, M. Enhancing metabolic activity and differentiation potential in adipose mesenchymal stem cells via high-resolution surface-acoustic-wave contactless patterning. Microsyst. Nanoeng. 8, 1–14 (2022).
23. Loh, Q. L. & Choong, C. Three-Dimensional Scaffolds for Tissue Engineering Applications: Role of Porosity and Pore Size. Tissue Eng. Part B Rev. 19, 485–502 (2013).
24. Annabi, N. et al. Controlling the Porosity and Microarchitecture of Hydrogels for Tissue Engineering. Tissue Eng. Part B Rev. 16, 371–383 (2010).
25. Lutolf, M. P. et al. Synthetic matrix metalloproteinase-sensitive hydrogels for the conduction of tissue regeneration: Engineering cell-invasion characteristics. Proc. Natl. Acad. Sci. 100, 5413–5418 (2003).
26. Muir, V. G. et al. Influence of Microgel and Interstitial Matrix Compositions on Granular Hydrogel Composite Properties. Adv. Sci. n/a, 2206117.
27. Zhang, S. et al. Room-temperature-formed PEDOT:PSS hydrogels enable injectable, soft, and healable organic bioelectronics. Adv Mater 32, e1904752 (2020).
28. Guex, A. G. et al. Highly porous scaffolds of PEDOT:PSS for bone tissue engineering. Acta Biomater. 62, 91–101 (2017).
29. Guo, B., Qu, J., Zhao, X. & Zhang, M. Degradable conductive self-healing hydrogels based on dextran-graft-tetraaniline and N-carboxyethyl chitosan as injectable carriers for myoblast cell therapy and muscle regeneration. Acta Biomater. 84, 180–193 (2019).
30. Hwangbo, H. et al. Photosynthetic Cyanobacteria can Clearly Induce Efficient Muscle Tissue Regeneration of Bioprinted Cell-Constructs. Adv. Funct. Mater. n/a, 2209157.
31. Jang, Y.-N. & Baik, E. J. JAK-STAT pathway and myogenic differentiation. JAK-STAT 2, e23282 (2013).
32. Fortini, P., Iorio, E., Dogliotti, E. & Isidoro, C. Coordinated Metabolic Changes and Modulation of Autophagy during Myogenesis. Front. Physiol. 7, 237 (2016).
33. Gao, H. et al. Regulation of Myogenic Differentiation by Topologically Microgrooved Surfaces for Skeletal Muscle Tissue Engineering. ACS Omega 6, 20931–20940 (2021).

34. Kim, W. et al. A Bioprinting Process Supplemented with In Situ Electrical Stimulation Directly Induces Significant Myotube Formation and Myogenesis. Adv. Funct. Mater. 31, 2105170 (2021).
35. Liao, I.-C., Liu, J. B., Bursac, N. & Leong, K. W. Effect of Electromechanical Stimulation on the Maturation of Myotubes on Aligned Electrospun Fibers. Cell. Mol. Bioeng. 1, 133–145 (2008).
36. Flaibani, M. et al. Muscle Differentiation and Myotubes Alignment Is Influenced by Micropatterned Surfaces and Exogenous Electrical Stimulation. Tissue Eng. Part A 15, 2447–2457 (2009).
37. Ostrovidov, S. et al. 3D Bioprinting in Skeletal Muscle Tissue Engineering. Small 15, 1805530 (2019).
38. Fan, T. et al. Controllable assembly of skeletal muscle-like bundles through 3D bioprinting. Biofabrication 14, 015009 (2021).
39. Yang, G. H., Kim, W., Kim, J. & Kim, G. A skeleton muscle model using GelMA-based cell-aligned bioink processed with an electric-field assisted 3D/4D bioprinting. Theranostics 11, 48–63 (2021).

Chapter 5: Conclusions and future perspectives

This chapter summarizes the results and implications of the work presented in chapters 3 and 4, discusses the challenges faced, and provides a perspective on the future of these studies and the field of electroactive materials for tissue engineering, at large.

5.1 CURRENT STATE OF ELECTROACTIVE BIOMATERIALS FOR TISSUE ENGINEERING

The overall goal of using electrically conductive biomaterials for tissue engineering is to recapitulate the electrical activities cells and tissues experience during endogenous homeostatic or regenerative events. Although evidence of incorporating conductive additives into biomaterials exists as early as 1963, the number of studies was modest until the 1990s (*i.e.*, <100 publications per year), after which there has been an exponential increase in interest (**Fig. 5.1A**). For instance, there were over twelve thousand studies published in the past 5 years alone (*i.e.*, 2018-2022), implying a saturated focus within the field of biomaterials. However, when narrowed to include which of these studies were used for tissue engineering, the number is reduced by nearly 80%. Within these reports, less than half include keywords related to the physical properties of biomaterials, which provides an opportunity for further investigation into how electrical and physical properties influence each other and subsequent cell behavior.

A search for studies published in the past 10 years with “biomaterials” and various conductive additives as keywords indicates a majority (~60%) of experiments used carbon-based materials such as carbon nanotubes and graphene (**Fig. 5.1B**). Gold nanoparticles were also prominently featured (~30%). Synthetic conductive polymers such as PEDOT (poly(3,4-ethylenedioxythiophene)), polypyrrole, and polyaniline made up about 10% of the total count, and each type of polymer was featured in a similar number of papers. Only 0.62% of biomaterials studies used bio-ionic liquids (bio-IL).

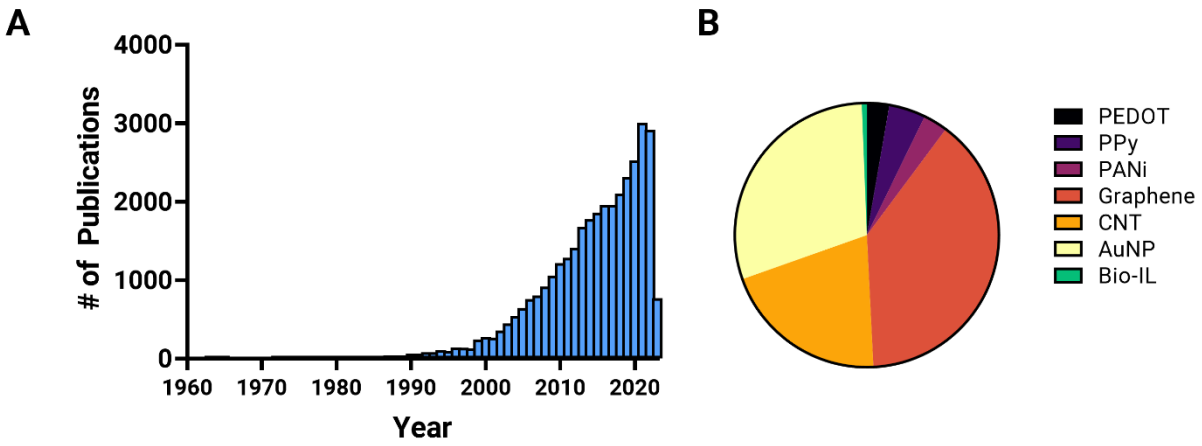

Figure 5.22: PubMed keyword searches indicated trends in electrically conductive biomaterials research. (A) Nearly 30,000 studies published over 60 years result when PubMed was queried for “conducive” and “biomaterial”. An exponential rise in publications on this subject was initiated in the late 1990s and early 2000s. **(B)** The number of studies published between 2012 and 2023 with the keywords “biomaterial” and specific conductive additives (*e.g.*, “PEDOT”) indicate popular use of carbon-based materials such as graphene and carbon nanotubes (CNT) and gold nanoparticles (AuNP). The synthetic polymers PEDOT, polypyrrole (PPy), and polyaniline (PANi) were used in

only about 10% of biomaterials studies. Very few studies investigated bio-ionic liquids (bio-IL) for biomaterials research.

Conductive biomaterials, regardless of their dopant, are being used for a variety of tissue engineering applications. Cardiac tissue engineering is a potent area for use, owing to the heart's well-characterized electroactivity. Numerous studies demonstrate conductive biomaterials facilitate synchronous beating of cardiomyocytes, ameliorating risk of arrhythmia. Greater alignment of cardiac tissue is generally achieved when materials such as electrospun nanofibers are used[1], or when exogenous electric fields are applied to the material[2]. Conductive materials are also frequently used for nerve tissue engineering, and many studies show increased neurite extension or better conferral of nerve signals when used in spinal cord injury models[3]. Using electroactive materials for bone tissue engineering is also popular, given bone's piezoelectric properties[4]. Incorporating electroactivity in engineering other musculoskeletal tissues, however, is still a burgeoning area. For instance, less than 10 publications result from a PubMed search for treating volumetric muscle loss with conductive biomaterials.

Although great strides have been made to engineer tissues and promote regeneration, few hydrogel-based materials have been successfully introduced into the clinic[5]. There are various roadblocks to translation, many of which are due to logistical and financial challenges with scaling up cellular components, growth factors, and materials. By mimicking the electrical events of regeneration, researchers of conductive biomaterials hope to facilitate communication between engineered and endogenous

tissues to speed innate healing[6]. It is also possible that, with their enhanced ability to confer electric signals, conductive biomaterials can bridge critical wounds to promote healing without also delivering cells. If the cell delivery component of tissue engineering could be reduced or eliminated, several hurdles to clinical translation could be removed. The work of this dissertation aims to contribute knowledge to better understand how cells interact with electrically conductive biomaterials in support of this goal.

5.2 RESULTS AND IMPLICATIONS OF THIS WORK

Chapter 3 used agarose hydrogels doped with PEDOT:PSS (poly(3,4-ethylenedioxthiophene) polystyrene sulfonate) to characterize how electrical and mechanical properties can be decoupled. It also provided evidence that conductive substrates can promote cell adhesion and spreading, even in the absence of external electric fields. These observations corroborated other published works, but also proposed a high-level mechanism of action behind the observations. Employing soluble proteins with different isoelectric charges allowed us to establish that conductive hydrogels present increased surface charges that facilitate protein adsorption. We believe this protein adsorption provides a layer on the material that permits cell adhesion and spreading. This hypothesis was supported when we measured increased adsorption of fibronectin and albumin to the conductive hydrogels, as these proteins are well-known to play a role in the interaction between a cell and the extracellular matrix. As such, the results presented in Chapter 3 begin to fill significant knowledge gaps within the field. In support of Aim 1, we provided evidence of certain conditions under which electrical and

mechanical properties of a hydrogel can be decoupled. We also suggested a process by which conductive materials promote cell behavior even in the absence of external stimulation, which satisfies Aim 2.

Chapter 4 provided preliminary data suggesting physical and electrical properties synergistically direct myoblasts down the myogenic lineage, thereby fulfilling Aim 3. When C2C12 mouse myoblasts were incorporated into PEDOT:PSS-containing microporous scaffolds, they had greater differentiation potential, indicated by the increase in myosin heavy chain gene and protein expression. The conductive microgel scaffolds also had decoupled electrical and physical properties, which augments the evidence to support Aim 1. The data from Chapter 4 suggest both porosity and conductivity were integral for promoting myoblast differentiation. Beyond the bioactive implications of these data, the fact that microgels can be injected and cryopreserved make this hydrogel system a promising tool for muscle repair in the clinic.

5.3 LIMITATIONS OF THIS WORK

While the work presented in Chapters 3 and 4 provide insight into how various cell types respond to electrically and mechanically tunable hydrogels, we acknowledge the following limitations:

Although the materials in Chapter 4 contained cell-binding motifs in addition to electrical and physical inputs, the work in Chapter 3 did not. While the conductive properties of the hydrogels contributed to cell adhesion and spreading, there were only a

few cells that adhered to the materials, which is not feasible for clinical translation or rigorous *in vitro* characterization beyond those which we tested. For example, attempts to investigate gene expression did not result in RNA samples with high enough quality to proceed with PCR. We believe this was due mainly to small amounts of available biological data, as our materials were seeded with 10,000 cells per gel and PCR is designed to work for samples with at least 1×10^6 cells per sample.

Cell binding motifs may have been incorporated within the agarose hydrogels by coating the gels with collagen type I or another protein, seeding the gels with a solution of fibronectin, or leveraging previously reported chemistries to covalently attach cell-binding peptides to the backbone of the agarose monomers. Alternatively, while we posit that agarose was an appropriate material to use owing to its singular crosslinking mechanism, we could have tested other materials, such as RGD-modified alginate or methacrylated gelatin (GelMA). However, attempts not reported in this dissertation included mixing PEDOT:PSS into collagen and alginate hydrogels without success, which we anticipate was due to incompatibilities between the strongly acidic conductive polymer and the hydrogels' crosslinking mechanism requiring a neutral pH. We also investigated adding a solution of fibronectin to the agarose gels prior to seeding cells but observed no difference in cell adhesion. Upon reflection, this strategy may have had success if we tested different adsorption times and concentrations of fibronectin, but we felt these experiments were out of scope to support the overarching message of Chapter 3. Further, although measuring adsorption of charged proteins was a positive result for Chapter 3, additional studies are needed to determine how much protein adsorption is

appropriate for cell adhesion. Without determining an effective concentration, there is risk that materials that facilitate protein adsorption may also be susceptible to the formation of biofilms, which is a devastating result for implanted therapeutics[7].

While the results of Chapter 4 were very promising for demonstrating how microporous and conductive hydrogels promote myoblast differentiation, additional studies would need to be done to show restoration of muscle function. Tests that could strengthen the results of our work include, for example, determining if muscle cells were responsive to neurotransmitters or if the cells could contract within the material upon stimulation. The scaffolds used in Chapter 4 also did not recapitulate muscle's hierarchical and aligned structure. As discussed, we hypothesize that making the annealed microgel scaffolds degradable may have facilitated some spontaneous alignment as the muscle cells continued to fuse and differentiate, but this hypothesis requires extensive investigation beyond the scope of what we report.

Overall, the work of this dissertation contributes foundational knowledge of how ionically conducting cells interact with electrically conductive materials. It highlights the importance of the interplay between biomaterial electrical and physical properties and provides an application of leveraging both properties to promote muscle tissue regeneration. Each study has noteworthy limitations, and many additional experiments would be necessary before this technology could be translated into the clinic for patient use.

5.4 CHALLENGES AND FUTURE DIRECTIONS

5.4.1 Promoting accessibility of electrical characterization techniques

A major challenge faced in this work was developing a means to characterize the conductive properties of hydrogels. Standard techniques for electrical characterization, which are largely intended for solid and dry substances, frequently require multiple pieces of expensive equipment. Many commonly used potentiostats, for example, are thousands of dollars, not to mention the additional supplies needed for accurate measurement (*e.g.*, platinum wires, silver paste, etc.). These costs are a significant barrier for research groups looking to break into the field. Additionally, very little literature exists describing setup and techniques of using said instruments and supplies with enough detail to accurately reproduce protocols.

To overcome these challenges, we developed a custom benchtop conductivity setup using inexpensive, accessible supplies and provided detailed instructions for measuring the conductivity of hydrogels. Although the measurements provided by this setup are not as precise as those derived from standard protocols, they were enough to determine differences between groups and are thus sufficient for proof-of-concept studies, such as those presented in this work. Establishing standardized testing protocols for electrical characterization of hydrogel materials would be invaluable for improving the reproducibility of studies fabricating and describing novel electroactive biomaterials.

5.4.2 Overcoming the safety limitations of synthetic conductive materials

There is also the pressing challenge of whether conductive materials are safe and efficacious over time. Although numerous studies claim synthetic conjugated materials such as PEDOT, polypyrrole, polyaniline, carbon nanotubes, and graphene are biocompatible, there are few reports that test safety long term. Most studies demonstrate viability of cells cultured on a material at early time points but provide minimal additional characterization. Further, compatibility testing is complicated by the difficulty in accounting for the effect of material inconsistencies (*e.g.*, surface charge, shape, length, etc.) on toxicity[8]. One study examining the effects of long-term exposure to gold nanoparticles indicated that expression of genes related to oxidative stress, cell cycle regulation, and inflammation are modified in response to the material[9]. Another study found polyaniline to be toxic depending on its molecular weight and concentration[10]. Additionally, given the synthetic nature of these materials, they are not bioresorbable, and are thus not able to be broken down into components that the body can metabolize and clear. As such, particles resultant of degradation or wear are likely to be stored in a patient's tissues. If synthetic conductive materials continue to be used in tissue engineering cases, thorough long-term testing of the effects of both the material and its byproducts are critical to ensure patient safety. However, given the rise of naturally derived and ionically conducting biomaterials, perhaps there will be a shift away from synthetic conjugated materials in the future.

5.4.3 Using naturally derived conductive materials

Given the shortcomings of synthetic conductive materials, there is great motivation to develop strategies using materials the body can readily recognize and metabolize. A significant foundation for naturally conductive materials is the pili protein secreted by *Geobacter sulfurreducens*, the conductivity of which is between 10^{-2} and 10^{-3} S/cm, matching the electrical properties of a variety of tissue types[11]. Modifications of the PilA monomer, the pili protein precursor, suggest that aromatic and charged amino acids can increase a peptide's conductivity by several orders of magnitude[12]. Other groups have enhanced the conductivity of amino acid-based materials with similar methods[13,14], and attempts to develop an electrically conductive peptide are discussed in this work in Appendix A1. Despite clear evidence for tuning the electrical properties of peptides and proteins to have greater electroactivity, there are, to date, no reports of incorporating them into a material for tissue healing.

By contrast, the use of ionically conducting materials for tissue engineering is on the rise. Methacrylated gelatin hydrogels containing a bio-IL had conductivity similar to that measured in materials containing synthetic additives and successfully promoted synchronous beating of cardiomyocytes[15]. Further, the material possessed low immunogenicity and was effectively degraded, which are marked advantages over synthetic materials[16]. This work is an encouraging pathway for the future of conductive materials: not only do ion-conducting materials match the conducting mechanism employed by cells, there is evidence that these materials are also effective for promoting tissue regeneration.

The use of bio-ILs for biomaterials research is highly promising, though attempts made in this work to incorporate bio-IL into alginate hydrogels was met with obstacles, as discussed in Appendix A2. Evoking differences in electroactivity between alginate alone and alginate with bio-IL conjugated to its backbone was a significant challenge. These conductivity results suggested, however, that alginate without bio-IL would be classified as a semiconductor, and thus begs the question of if it could be used as a conductive biomaterial in its unmodified state. Alginate and other polysaccharides have charged hydroxyl groups throughout their chemical structures that may give rise to ionically conductive properties. Other examples in nature illuminate the potential for sulfated materials to be efficient conductors, as well. For instance, the Ampullae of Lorenzini, which are tubular structures found in the snouts of some sharks, skates, and rays, contain a jelly that allow these animals to detect changes in electric fields generated by muscle contractions of prey. Further investigation of the Ampullae of Lorenzini jelly implies it primarily consists of keratan sulfate and has a conductivity of 1.8×10^{-3} S/cm[17]. Another naturally occurring conductive material include eumelanin, the most common form of the melanin pigments in skin, whose conductivity is approximately 10^{-5}–10^{-3} S/cm[18,19]. Despite the semiconductive classification of these natural materials, few studies incorporate them into biomaterials for tissue engineering, which presents a ripe opportunity for future biomaterials researchers. As these studies eventually unfold, a helpful practice for transitioning between material classes may be to directly compare the effectiveness of ionic *versus* electronic conductors[20].

5.4.4 Understanding mechanisms of cellular electrical sensing

One of the most significant challenges when devising strategies to promote the electrical behavior of cells is understanding how cells sense electric materials or external electric fields. Comprehensive reviews exist about the history and physiology of bioelectricity, but even these reports concede a need for better mechanistic understanding of how electric fields direct certain cell behaviors (*e.g.*, actin polymerization, intracellular cyclic AMP levels, and regulation of cytoskeletal molecules)[21]. Although the effects of exposing cells to electric fields and conductive substrates are exciting, there is still a pressing need to better understand how cells receive and interpret these stimuli.

Some groups have hypothesized that materials that conduct electrons engage cells in a capacitance-type coupling, where charges from the scaffold accumulate around a source cell and the lack of charges in the vicinity creates an electric gradient that can stimulate surrounding target cells (**Fig. 5.2**). Ionic conductors are believed to create a current coupling between cells and the substrate. The ionically conductive material offers a more attractive route for ions from a source cell to travel through compared to the surrounding media, which causes charge accumulation around a target cell. This charge accumulation can then trigger an action potential. Changes in cell response to different types of conductive materials have not yet been investigated, but exploring the distinction between these materials could be a first step in understanding how electron-conducting surfaces cause changes in cells, which communicate solely through ionic signaling[6].

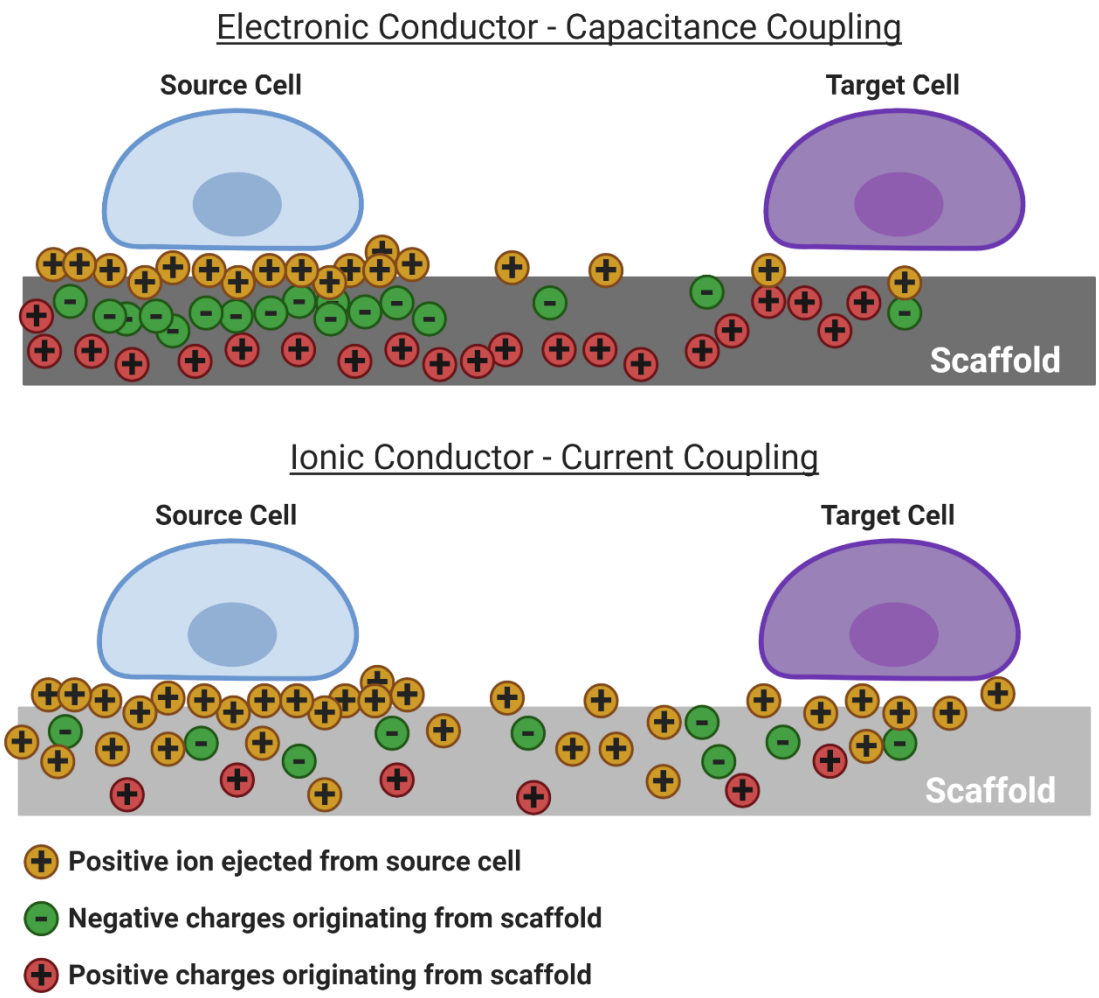

Figure 5.23: Proposed differences in cell sensing mechanisms depending on the electron- or ion-conducting nature of a substrate. Electron-conducting materials are thought to induce a capacitance-type coupling with cells, whereby charges accumulate around a source cell. The lack of charges in the vicinity evokes an electric field that target cell experiences. Ion-conducting materials form a current coupling and offer a more attractive route for charges to travel through. Charges that accumulate around a target cell can thus trigger an action potential. This figure is recreated from Burstine-Townley et al. *Adv. Func Mat*er. 2018. 10.1002/adfm.201901369.

Beyond understanding how cell sense the electrical properties of their substrate, there is also a gap in understanding about what level of conductivity is therapeutic. Endogenous tissues possess a wide range of conductive properties (*e.g.*, ~10^{-6} S/cm for skin[22] and 10^{-1} S/cm for nerve[3]), but it is not well understood how closely an implanted material needs to match a tissue's properties to effectively heal it. Some studies demonstrate that the most conductive materials among a group may, in fact, preclude functional outputs associated with cell differentiation[23]. Experiments that deliberately investigate cell response to a material's level of conductivity, similar to the seminal work measuring cell response to material stiffness[24], would be highly impactful for the future of electroactive biomaterials.

In sum, despite thousands of studies developing electrically or ionically conductive biomaterials that promote cell differentiation and tissue repair, understanding the mechanisms of action behind cell response to electroactive materials continues to present a significant challenge. While we are beginning to define changes in the cell membrane in response to electrical stimulation, there is still vast opportunity to uncover how cells sense electrical environments and how those cues trigger changes in cell genetic regulation and signal transduction. Bioelectricity is well-understood as being critical for homeostasis and regeneration, so having deeper understanding of cellular activity in response to electrical inputs will be instrumental in advancing electroactive biomaterials design.

5.4.5 Applying electroactive materials to form composite tissues

Ultimately, the goal of tissue engineering is to provide a solution to heal large tissue wounds that surpass the body's innate ability to heal. While tissue engineered strategies frequently focus on repair using one or two cell types, native tissue structure is composite and complex. For example, muscle is grossly composed of myocytes, nerves, connective tissue, and vasculature. Very few tissue engineered approaches have successfully recapitulated this complexity, but there has been some success promoting innervation of muscle[25,26], bone[27,28], and corneal tissue[29]. However, none of these reports utilized electroactive biomaterials. Future prospects that combine different cell types within conductive biomaterials or use conductive materials as a scaffold for electrically stimulating *in vitro* composites could be instrumental for enhancing the performance of engineered constructs and thus improve their chance of functionally restoring injured tissues.

In summary, this dissertation contributes foundational knowledge to begin filling the many knowledge gaps about how electrically conductive biomaterials are an effective strategy for tissue engineering. Our findings are applicable for studying a variety of tissue types and can serve as a platform to further investigate the cellular response to electron conducting materials.

REFERENCES

1. Roshanbinfar, K. et al. Nanofibrous Composite with Tailorable Electrical and Mechanical Properties for Cardiac Tissue Engineering. Adv. Funct. Mater. 30, 1908612 (2020).
2. Roshanbinfar, K. et al. Electroconductive biohybrid hydrogel for enhanced maturation and beating properties of engineered cardiac tissues. Adv. Funct. Mater. 28, 1803951 (2018).
3. Zhou, L. et al. Soft conducting polymer hydrogels cross-linked and doped by tannic acid for spinal cord injury repair. ACS Nano 12, 10957–10967 (2018).
4. Guex, A. G. et al. Highly porous scaffolds of PEDOT:PSS for bone tissue engineering. Acta Biomater. 62, 91–101 (2017).
5. Willyard, C. Timeline: Regrowing the body. Nature 540, S50–S51 (2016).
6. Burnstine-Townley, A., Eshel, Y. & Amdursky, N. Conductive Scaffolds for Cardiac and Neuronal Tissue Engineering: Governing Factors and Mechanisms. Adv. Funct. Mater. 30, 1901369 (2020).
7. Cheng, G., Zhang, Z., Chen, S., Bryers, J. D. & Jiang, S. Inhibition of bacterial adhesion and biofilm formation on zwitterionic surfaces. Biomaterials 28, 4192–4199 (2007).
8. Liu, Y., Zhao, Y., Sun, B. & Chen, C. Understanding the Toxicity of Carbon Nanotubes. Acc. Chem. Res. 46, 702–713 (2013).
9. Falagan-Lotsch, P., Grzincic, E. M. & Murphy, C. J. One low-dose exposure of gold nanoparticles induces long-term changes in human cells. Proc. Natl. Acad. Sci. 113, 13318–13323 (2016).
10. Zhang, Y. et al. Synthesis and biocompatibility assessment of polyaniline nanomaterials. J. Bioact. Compat. Polym. 34, 16–24 (2019).
11. Malvankar, N. S. et al. Tunable metallic-like conductivity in microbial nanowire networks. Nat Nanotechnol 6, 573–9 (2011).
12. Tan, Y. et al. Synthetic Biological Protein Nanowires with High Conductivity. Small 12, 4481–4485 (2016).
13. Kalyoncu, E., Ahan, R. E., Olmez, T. T. & Seker, U. O. S. Genetically encoded conductive protein nanofibers secreted by engineered cells. RSC Adv. 7, 32543–32551 (2017).
14. Creasey, R. C. G., Shingaya, Y. & Nakayama, T. Improved electrical conductance through self-assembly of bioinspired peptides into nanoscale fibers. Mater. Chem. Phys. 158, 52–59 (2015).
15. Walker, B. W. et al. Engineering a naturally-derived adhesive and conductive cardiopatch. Biomaterials 207, 89–101 (2019).
16. Noshadi, I. et al. Engineering Biodegradable and Biocompatible Bio-ionic Liquid Conjugated Hydrogels with Tunable Conductivity and Mechanical Properties. Sci. Rep. 7, 4345 (2017).
17. Josberger, E. E. et al. Proton conductivity in ampullae of Lorenzini jelly. Sci. Adv. 2, e1600112 (2016).
18. Bettinger, C. J., Bruggeman, J. P., Misra, A., Borenstein, J. T. & Langer, R. Biocompatibility of biodegradable semiconducting melanin films for nerve tissue engineering. Biomaterials 30, 3050–3057 (2009).

19. Wünsche, J. et al. Protonic and Electronic Transport in Hydrated Thin Films of the Pigment Eumelanin. Chem. Mater. 27, 436–442 (2015).
20. Song, X. et al. A tunable self-healing ionic hydrogel with microscopic homogeneous conductivity as a cardiac patch for myocardial infarction repair. Biomaterials 273, 120811 (2021).
21. McCaig, C. D., Rajnicek, A. M., Song, B. & Zhao, M. Controlling Cell Behavior Electrically: Current Views and Future Potential. Physiol. Rev. 85, 943–978 (2005).
22. Gabriel, C., Peyman, A. & Grant, E. H. Electrical conductivity of tissue at frequencies below 1 MHz. Phys. Med. Biol. 54, 4863–4878 (2009).
23. Chen, J., Yu, M., Guo, B., Ma, P. X. & Yin, Z. Conductive nanofibrous composite scaffolds based on in-situ formed polyaniline nanoparticle and polylactide for bone regeneration. J Colloid Interface Sci 514, 517–527 (2018).
24. Engler, A. J., Sen, S., Sweeney, H. L. & Discher, D. E. Matrix elasticity directs stem cell lineage specification. Cell 126, 677–89 (2006).
25. Liu, G. et al. The effect of urine-derived stem cells expressing VEGF loaded in collagen hydrogels on myogenesis and innervation following after subcutaneous implantation in nude mice. Biomaterials 34, 8617–8629 (2013).
26. Das, S. et al. Pre-innervated tissue-engineered muscle promotes a pro-regenerative microenvironment following volumetric muscle loss. Commun. Biol. 3, 1–14 (2020).
27. Marrella, A. et al. Engineering vascularized and innervated bone biomaterials for improved skeletal tissue regeneration. Mater. Today 21, 362–376 (2018).
28. Fitzpatrick, V. et al. Functionalized 3D-printed silk-hydroxyapatite scaffolds for enhanced bone regeneration with innervation and vascularization. Biomaterials 276, 120995 (2021).
29. Wang, S. et al. In vitro 3D corneal tissue model with epithelium, stroma, and innervation. Biomaterials 112, 1–9 (2017).

APPENDICES

Appendix 1: Designing an electrically conductive collagen-binding peptide to incorporate into hydrogels and a brief survey of conductivity measurement techniques

A1.1 INTRODUCTION

The use of electrically conductive materials for biological applications is becoming more commonplace as the benefits of catering to the electrical needs of biological systems continue to be reported. Studies developing conductive biomaterials frequently combine synthetic conductive additives and hydrogel-based materials, which has resulted in a versatile library of materials with diverse electrical properties suitable for various applications. While metal- and carbon-based materials are featured within this library, many studies also use synthetic polymers with conjugated bond structures. Electrons are not as strongly bound within these alternating single- and double-bond structures, which in some cases, allows for metallic-like conductivity[1]. Despite their effectiveness, these materials face the drawback of not being bioresorbable, which may be a significant hurdle to clinical translation in regenerative medicine applications.

Although the range of synthetic conductive materials is expansive, there is also evidence of naturally derived materials with high conductivity. Most notable for this work is the pili proteins secreted by *Geobacter sulfurreducens*, which have conductivity on the order of 10^{-3}-10^{-2} S/cm[3,4]. The wild-type sequence of the PilA monomer can also be

modified to raise conductivity up to 10^2 S/cm[5]. Other groups have taken inspiration from *G. sulfurreducens* and fabricated shorter peptide sequences with impressive conductive properties as summarized in **Table A1.1**. From these studies, we can ascertain that aromatic amino acids, which contain the same π -π interchain stacking structures as synthetic conjugated polymers, can be leveraged to increase the conductivity of naturally occurring materials that may be significantly more compatible with *in vivo* systems.

Previous work from our lab has reported successful synthesis and application of a peptide derived from a platelet receptor to collagen type I, abbreviated as SILY (RRANAALKAGELYKSILYGC)[6–10]. This peptide sequence binds to collagen with high specificity but can still be functionalized to have specific therapeutic properties. In this work, we aim to utilize the collagen-binding properties of SILY to create a conductive peptide that can be incorporated into a clinically relevant hydrogel without additional crosslinking steps. We hypothesized that a concentrated region of conjugated bond structures within a peptide sequence would enhance its electroactivity and, when incorporated into hydrogels, confer its electrical properties to the bulk material.

Another objective of this study was to identify effective methods for measuring hydrogel electrical properties. A variety of techniques exist within the literature (**Figure A1.5**) and are discussed below. However, most of these techniques are indicated for characterizing either dry materials or materials with immobilized conductive additives (*i.e.*, deposited onto electrodes). Thus, measuring the electrical properties of water-based materials may necessitate parameter optimization or protocol adjustment.

Table A1.5: Published examples of conductive peptide sequences, their method of assembly, electrical characterization technique, and electrical characteristics

Peptide Sequence	Assembly Method	Electrical Characterization
[11]R5T3Y: SVNVTQVGFGYYY	Drop-cast onto electrodes	2-point probe, ±5 V sweep. Qualitative analysis.
[5]W51W57: FTLIELLIVVAIIGILAAIAIPQF SAYRVKAYNSAASSDLRNLK TALESAWADDQTWPPES	Drop-cast onto electrodes	2-point probe, ±0.5 V sweep. Conductivity = 90-977 S/cm.
[12]GFPRFAGFP	Self-assembly into a film	2-point probe, ±2 V sweep. Conductance on the order of 10^{-11} S.
[13]YYACAYY	Annealed into a film	2-point probe. Resistivity decreases with increasing temperature down to 1.2×10^{-2} Ω·cm.
[14]KAAAAAA (KA6) coated DNA nanowires	Drop-cast onto electrodes	2-point probe, ±8 V sweep. Measured current ~40 pA vs. ~ 50 fA for native DNA
[15]ELKAIAQEFKAIAKEFKAIAF EFKAIAQK in nanofiber and gel	Soluble nanofibers (μM) drop-cast Peptides in higher concentrations (mM) form gels	Single nanofiber: Conductive probe AFM Conductivity =1.12 ± 0.77 S/cm Nanofiber sheet: 2-point probe; ± 0.8 V sweep. Resistance = 188 ± 36 Ω Dried gel: Electrical Impedance Spectroscopy Conductance = ~10^{-7} – 5×10^{-3} S

A1.2 METHODS

A1.2.1 Peptide synthesis

The peptide sequence YYYEEYRRANAALKAGELY (YYYGELY) was synthesized on an automated solid phase Liberty Blue peptide synthesizer (CEM, Matthews, NC) with rink amide resin (CEM)[16]. Resin-bound peptide was washed 3 times with dimethylformamide (DMF), 3 times with dichloromethane (DCM), 3 times with DMF, and 3 times with DCM. After thoroughly vacuum drying, peptide was cleaved from the resin by adding a mixture of 88 v/v% TFA, 5 v/v% phenol, 5 v/v% Ultra-pure water (UP H_2O), and 2 v/v% triisopropyl silane (TIPS) and allowing the slurry to mix for 3 h at room temperature (RT) with rotation. Cleaved peptide was precipitated 3 times using cold diethyl ether. Peptide purification was carried out using reverse-phase chromatography on an ÄKTA Explorer FPLC (GE Healthcare, Chicago, IL) using a C18 column (Grace™ Vydac™) and a 0-60% acetonitrile gradient against water. Purity was verified using matrix-assisted laser desorption/ionization-time of flight (MALDI-ToF).

A1.2.2. Electrical characterization of peptides in solution

YYYGELY peptide was dissolved at 0.02 and 0.04 mg/mL in UP H_2O. The leads of a multimeter (SparkFun Electronics, Boulder, CO) were submerged into the peptide-containing solution and resistance was recorded (**Fig. A1.2A**). Multimeter leads were wiped thoroughly with UP H_2O and ethanol and dried between measurements. Resistance was normalized to the resistance of water since the experiment was repeated using a different water source.

A1.2.3 Surface area calculation of platinum wire electrodes

Platinum wires (Cat. 45093, Alfa Aesar, Haverhill, MA) were wrapped five times around a 20G needle (Becton Dickinson, Franklin Lakes, NJ) to form coil electrodes used to test the electrical properties of hydrogels. Electrode surface area (*A*) was calculated according to **Equation A1.1**.

Equation A1.1: $A = \left(\frac{D+t}{2}\right)^2 \pi - \left(\frac{D}{2}\right)^2 \pi$

where *D* is the inner diameter of the needle (*D* = 0.9 mm) and *t* is the thickness (*i.e.*, diameter) of the platinum wire (*t* = 0.25 mm). The surface area calculated with **Equation A1.1** was multiplied by 5 to account for the number of coils in each electrode.

A1.2.4 Hydrogel preparation

Peptide was incorporated into 180 µL collagen type I hydrogels according to **Table A1.2** such that the mass of peptide was defined by the mass of collagen in each gel. Peptide was weighed using a microbalance (Mettler Toledo, Columbus, OH) and transferred to a microcentrifuge tube. The neutralizing solution (NS) within the Rat Tail Collagen Type I kit (RatCol #5133 Advanced Biomatrix, Carlsbad, CA) was added to the peptide-containing tube and vortexed to mix. Sonication for 5 min was required to completely dissolve some samples. Using a positive displacement pipette, collagen (3.8 mg/mL) was mixed with the dissolved peptide solution, taking care to avoid forming bubbles. The collagen and peptide solution was dispensed into glass-mounted PDMS

molds containing platinum wire electrodes as shown in **Figure A1.3A,B.** Samples were stored in a petri dish containing a dampened Kim wipe and incubated at 37°C for 1 h.

Table A1.6: Formulations of collagen (3.8 mg/mL) hydrogels containing conductive peptide or PVP

Component	Volume (µL)
Total construct	180
Collagen Type I	162
Neutralizing solution (1:10)	18
Component	**Mass (µg)**
Collagen Type I	615.6
YYYGELY or PVP (2 w/w%)	12.32
YYYGELY or PVP (20 w/w%)	123.2
YYYGELY (50 w/w%)	307.8

A1.2.5 Electrical characterization

A1.2.5.1 Cyclic voltammetry on collagen hydrogels

YYYGELY was incorporated into collagen gels at 2 and 20 w/w% to collagen according to **Table A1.2**. Polyvinylpyrrolidone (PVP, MW 55000 Da, Sigma Aldrich, St. Louis, MO) was incorporated into collagen gels as a positive control group. Alligator clips were used to connect each electrode to either the reference or working electrode of a potentiostat (Gamry, Warminster, PA) (**Fig. A1.3B**). The potentiostat was programmed

with a ±5 V range, 50 mV/s scan rate, and a 1 mV step size. Curves were assessed for oxidation and reduction peaks to indicate electrical activity.

A1.2.5.2 Conductivity testing with semiconductor parameter analyzer

YYYGELY was incorporated into collagen gels at 50 w/w% collagen type I according to **Table A1.2** and crosslinked around platinum wire electrodes as described above. The gold electrodes of a Keithley HP4155A semiconductor parameter analyzer (Keithley Instruments, Cleveland, OH) were manipulated into place such that they made secure contact with the platinum wire electrodes embedded in the collagen gels (**Fig. A1.4A**). A ±2 V sweep with 10 mV steps were applied to the gels to generate current-voltage curves. Resistance was calculated from current-voltage curves with a linear fit R^2 value ≥ 0.85. Then conductivity was calculated according to Pouillet's law (**Equation A1.2**):

Equation A1.2: $$\sigma = \frac{L}{RA}$$

where σ is conductivity in S/cm, L is the distance between electrodes in cm (**Fig. A1.3A**), R is resistance (Ω), and A is the electrode surface area in cm^2 (**Equation A1.1**). Electrode distance, L, was measured for each gel.

A1.2.6 Statistical analysis

Data are presented as means ± standard deviation. Statistical analysis was conducted using GraphPad Prism 9 software. Groups were compared using t-tests or

one-way analysis of variance (ANOVA) with Tukey correction. Differences were considered statistically significant at $p \leq 0.05$.

A1.3 RESULTS

A1.3.1 Peptides with conjugated bond structures and other charged moieties can be successfully synthesized and purified

Based on prior reports, we sought to design a peptide containing a collagen-binding site, a repeating sequence of amino acids containing conjugated bond structures, and charged amino acids throughout its sequence. The collagen-binding site was based on previous work with the collagen-binding peptide abbreviated as SILY (**Fig. A1.1A**)[6]. Kalyoncu and colleagues demonstrated that including repeats of the aromatic amino acids, tryptophan (W) or tyrosine (Y), within peptide sequences improved nanofiber conductivity[11]. This result was further enhanced by including charged amino acids (*e.g.*, arginine (R) (+), lysine (K) (+), aspartic acid (D) (-), and glutamic acid (E) (-)) throughout peptide sequences, which also mimics the native structure of the *G. sulfurreducens* PilA protein[5]. Thus, we appended the N-terminus of the SILY peptide with a triplicate of tyrosine and glutamic acid. We also removed amino acids at the C-terminus of the SILY peptide to shorten the peptide and thus improve synthesis (**Fig. A1.1B**). The original SILY peptide already contained various charged amino acids throughout its sequence, which were conserved in the YYYGELY peptide. The results of peptide purification *via* mass spectroscopy show a singular predominant peak at approximately 2342 m/z, indicating sufficiently pure peptide for future use (**Fig. A1.1C**).

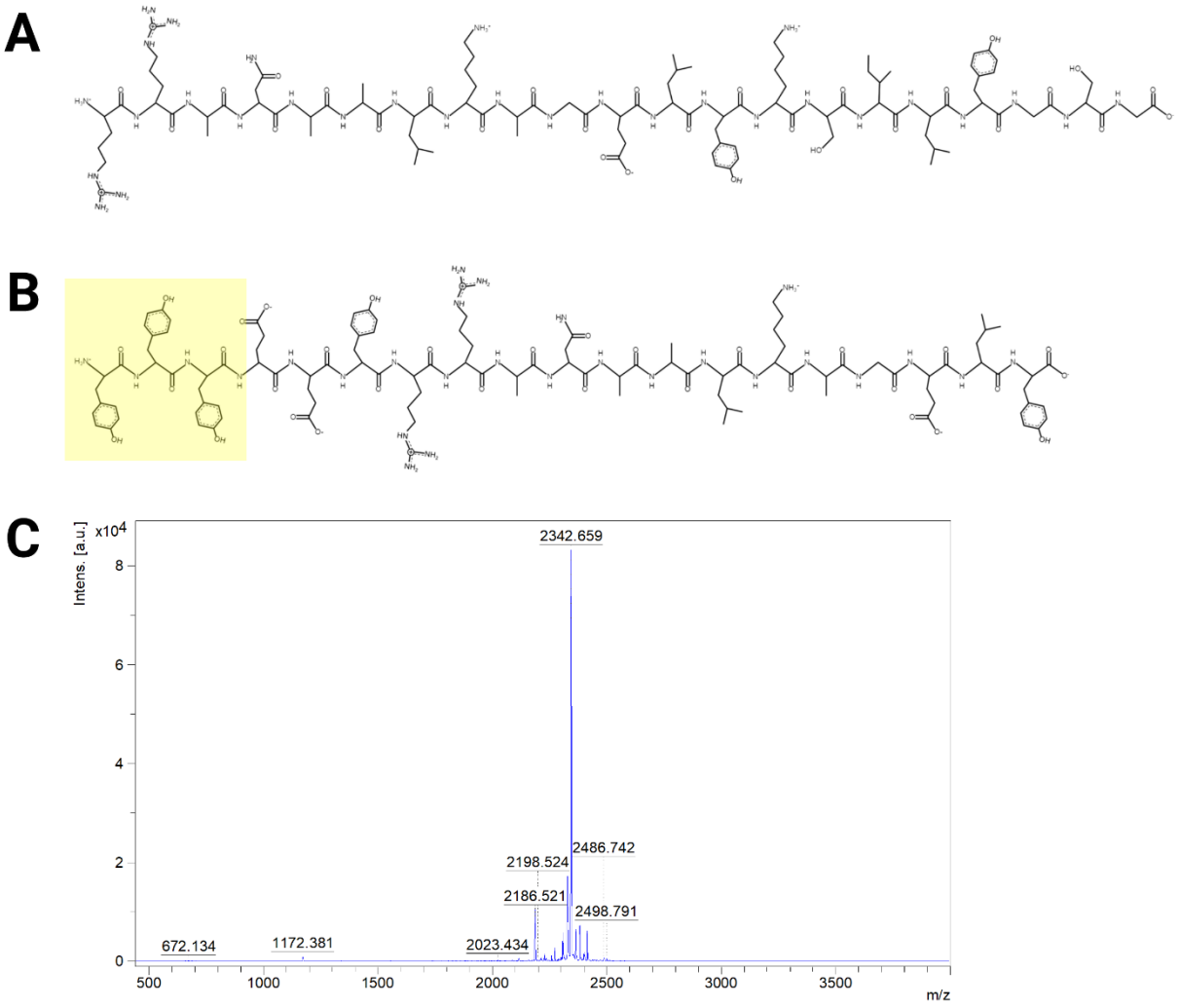

Figure A1.24: Design and purification of a conductive collagen-binding peptide. (A) The sequence of the collagen-binding peptide from previous work nicknamed SILY, upon which the sequence of this novel conductive peptide, **(B)** YYYGELY, is based. The yellow box highlights the triple repeat of tyrosine (Y), an aromatic amino acid believed to bestow this peptide with electron-conducting capabilities. **(C)** The mass spectrum of purified YYYGELY generated using MALDI-ToF reveals a singular, predominant peak at approximately 2342 m/z, indicative of successful peptide purification.

A1.3.2 Conductive peptides improve the electrical properties of solutions

We began characterizing the electrical properties of YYYGELY by measuring how the resistance of UP H_2O changed after incorporating the peptide (**Fig. A1.3A**). Even at 0.02 mg/mL, the resistance of water significantly decreased by approximately half. When the concentration of peptide was doubled to 0.04 mg/mL, the resistance of the solution was again halved (**Fig. A1.3B**). These results suggest the peptide has some electrical properties. The reduction in resistance may also be due to the presence of charged amino acids within the peptide sequence, thereby imparting ions to the solution. Although this peptide was designed to be electronically conductive with the inclusion of aromatic amino acids, the presence of differently charged amino acids throughout the sequence is also important for conferring electrical signals along the entire peptide. Therefore, these data provide important evidence that the peptide sequence was synthesized successfully.

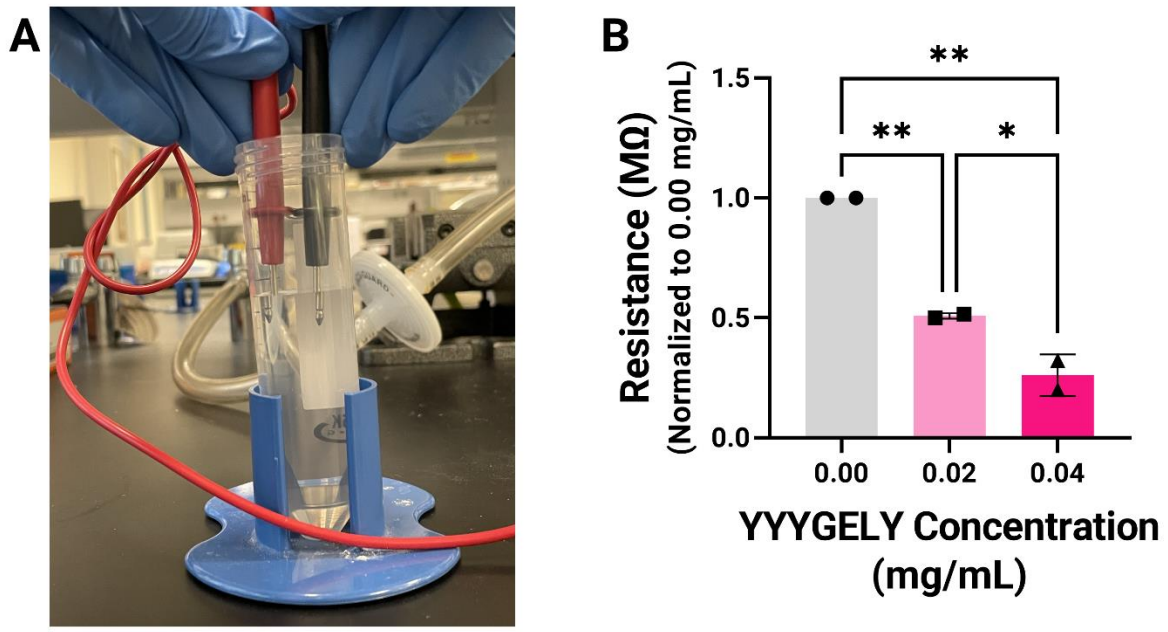

Figure A1.25: Resistance measurements of YYYGELY peptide in UP H_2O. (A) The leads of a multimeter were submerged in a solution of conductive peptide at three concentrations. **(B)** The solution's resistance had an inverse correlation with the concentration of YYYGELY. Solution resistance was normalized to the resistance of water since two sources of UP H_2O were used. Groups were compared using a one-way ANOVA with Tukey correction (n=2, *$p \leq 0.05$, **$p \leq 0.01$).

A1.3.3 Conductive peptides can be incorporated into hydrogels and may demonstrate oxidative and reductive properties with cyclic voltammetry

Collagen Type I gels containing 2 or 20 w/w% YYYGELY or PVP were crosslinked around coil electrodes as depicted in **Fig A1.3A, B**. When tested using cyclic voltammetry, the curves for all groups were relatively flat, indicating minimal electrical activity.

However, a slight peak appeared in the 2 w/w% gel's voltammogram around -1.7 V, indicating possible oxidation or other electrochemical activity.

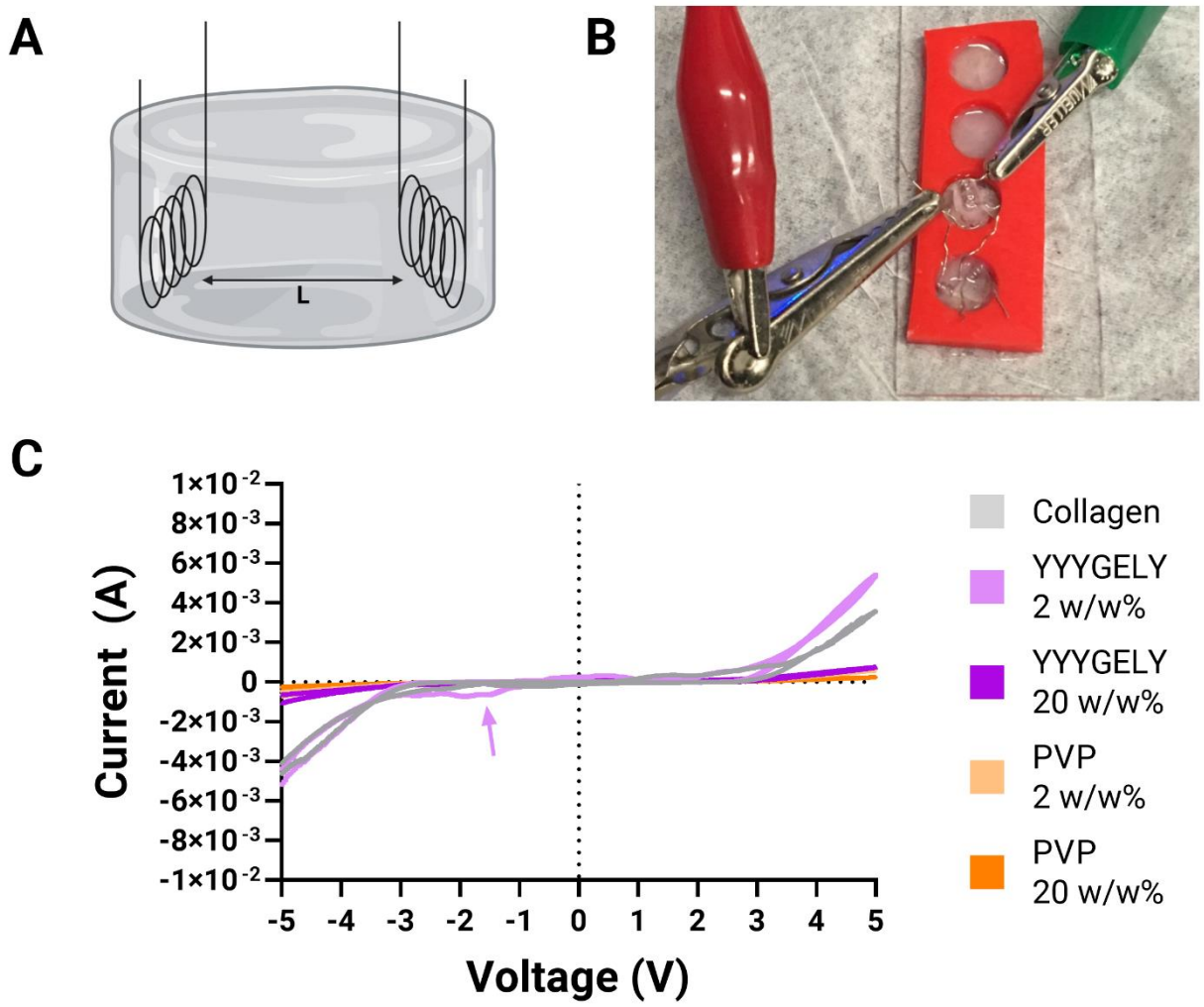

Figure A1.26: Electrical characterization of collagen gels containing YYYGELY using cyclic voltammetry. (A) Schematic for embedding two coil electrodes into each hydrogel, where the length (*L*) between electrodes is used in subsequent conductivity measurements. **(B)** Gross images of hydrogels with embedded electrodes connected to a potentiostat for cyclic voltammetry measurements. **(C)** Voltammograms of each hydrogel formulation containing either YYYGELY or PVP as a positive control. All curves

were flat and not appreciably different than the collagen-only control. However, there was a slight peak around -1.7 V in the 2 w/w% YYYGELY group (light purple arrow) that hints at potential electrical activity in the gel.

A1.3.4 Conductive peptides improve the conductivity of collagen hydrogels when measured in a 2-point probe system

The conductivity of collagen gels containing YYGELY was also tested using a two-probe setup connected to an Keithley HP4155A semiconductor parameter analyzer. The probes of the analyzer were manipulated so they made contact with the protruding ends of the coil electrodes embedded in the collagen gels, as depicted in **Fig. A1.4A**. Only two concentrations of YYYGELY were tested (0 and 50 w/w%, **Table A1.2**). Current-voltage curves for two gels per group were generated from a ±2 V sweep. The collagen-only gels (**Fig. A1.4B**) were not identical, suggesting discrepancies in electrode distance and contact with the hydrogel. The output current measured with these gels was also several orders of magnitude lower than that of the gels containing conductive peptide (**Fig. A1.4C**). Current-voltage curves were analyzed for linearity and used to calculate resistance, which was used in **Equation A1.2** to calculate conductivity. Conductivity measurements were normalized to electrode surface area (**Equation A1.1**). Conductivity was seven orders of magnitude higher in gels containing 50 w/w% YYYGELY ($\sigma = 2.3 \times 10^{-3}$ S/cm) than those with 0.0 w/w% ($\sigma = 3.2 \times 10^{-10}$ S/cm) (**Fig. A1.4D**). These results demonstrate that YYYGELY confers electroactive properties to collagen gels and thus has intrinsic conductive attributes.

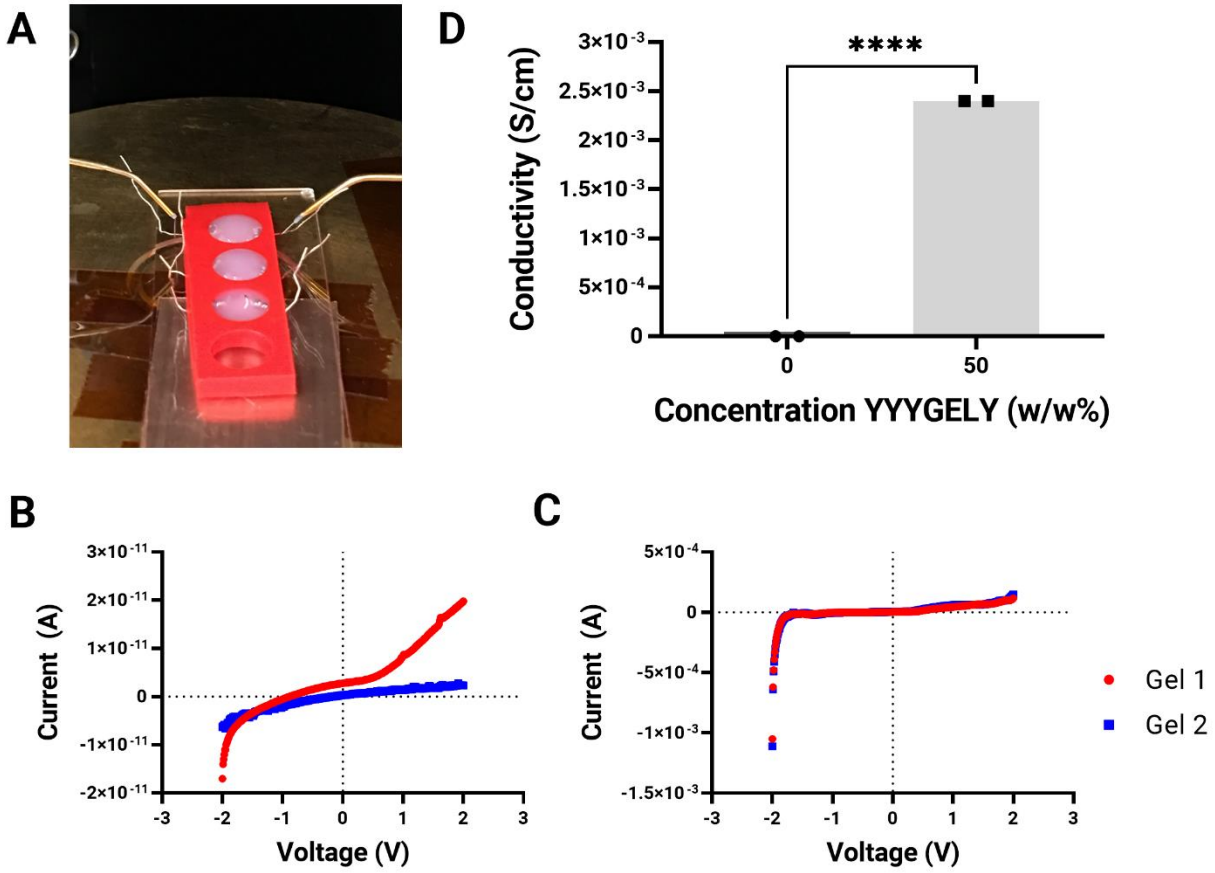

Figure A1.27: Electrical characterization of collagen gels containing YYYGELY using 2-point probe. (A) Image of the conductivity testing setup using a 2-point probe connected to a semiconductor parameter analyzer. The gold probes of the apparatus were manipulated to contact the free ends of the coil electrodes embedded in the gels. **(B)** Current-voltage curves for two collagen-only gels that were used to calculate gel resistance. The output current of these gels was several orders of magnitude less than that of the **(C)** gels containing YYYGELY. **(D)** Calculated conductivity of collagen gels with and without YYYGELY was normalized to electrode surface area. The conductivity of the 50 w/w% YYYGELY hydrogels was several orders of magnitude higher than the collagen-only gels. Groups were compared using a two-tailed t-test (n=2, ****$p \leq 0.0001$).

A1.4 DISCUSSION

In these experiments, we sought to synthesize an electrically conductive peptide that could be incorporated into collagen hydrogels without additional crosslinking steps. Prior work demonstrated successful fabrication of a collagen-binding peptide, and in this work, we adjusted the sequence of the same peptide so that it contained aromatic amino acids for enhanced electrical properties. When tested in water, the addition of the conductive YYYGELY peptide significantly reduced the resistance of the solution, thereby improving its electroactive properties. It is likely this effect was primarily due to the inclusion of charged amino acids within the YYYGELY sequence, and it is unknown if the peptide remained intact after mixing with water. However, including charged amino acids throughout a peptide sequence is necessary for conferring electrical signals across long peptide sequences, as seen in the PilA protein of *G. sulfurreducens*[5,11]. Thus, the reduction of resistance upon addition of conductive peptide is evidence of successful incorporation of charge amino acids into the YYYGELY sequence.

We then incorporated YYYGELY into collagen type I gels and tested conductivity using two methods. Cyclic voltammograms were similar for all groups and not appreciably different than the collagen-only controls. This trend was observed in the groups containing PVP, a polymer known for its electrical conductivity. However, the hydrophobicity of PVP may have caused polymer aggregation within the water-based collagen gel, which would prevent charges from being conferred throughout the gel. Notably, the 2 w/w% YYYGELY group had a slight oxidation-like peak around -1.7 V. Although this peak is minimal and the voltammogram does not follow the “duck” shape

seen in typical curves, this deviation from the other sweeps may indicate slightly elevated electrical activity. The fact that a similar peak was not seen in the 20 w/w% YYYGELY group indicates possible faults in contact between the electrodes and the gels or an anomaly in the 2 w/w% result. One major shortcoming of this study was small sample sizes for all groups, which reduces the reproducibility and robustness of results.

The other method used for conductivity testing involved a 2-point probe setup, which is frequently employed by other studies characterizing electroactive hydrogels. We demonstrated that gels containing 50 w/w% YYYGELY were seven orders of magnitude more conductive than gels containing no peptide. At 2.4×10^{-3} S/cm, the gels containing conductive peptide can also be classified as semiconductors and are comparable to other reported conductive hydrogels[17–19]. However, this study also suffers the limitation of small sample size and could be further improved by testing additional concentrations of peptide. This would be particularly useful in determining the range of peptide concentration that elicits an electroactive effect and thus how versatile this material could be for tissue engineering applications.

The subject of exploring different methods for measuring the electrical properties of water-based materials was secondary to developing an electrically conductive peptide in this work, but it presented a significant challenge. Using electroconductive materials is rapidly expanding within tissue engineering, but issues with reproducibility are prominent and limit the field's ability to make significant strides in developing efficacious electroactive constructs. To improve understanding and repeatability of experiments, this

section summarizes and describes the frequently used techniques for electrically characterization of novel materials.

There are a variety of methods to measure the conductive properties of materials, with ranges in complexity, cost, and resolution, the most common of which are illustrated in **Figure A1.5**. Some techniques, such as 2- and 4-point probe, seek to measure the conductive properties of materials directly. While these techniques are historically used to test solid substrates, 4-point probe is frequently used to test gel formulations[20–22]. Materials can also be incorporated into simple and inexpensive circuits to determine categorically if the material confers electricity (*e.g.*, through an LED)[23]. This technique, however, does not provide quantitative information about the resistance of the material.

Two-point methods measure conductivity by placing the material between two probes that supply voltage and measure current (or *vice versa*). To improve validation of results, detailed descriptions of experimental setups are necessary, as reports using 2-point probe methods have a range of setups, illustrated in **Figure A1.5A**. When using two point probe methods, it is critical to avoid the formation of Schottky barriers, accomplished by using non-rectifying, ohmic contacts[24]. The simplest way to test these materials is to probe the gel directly, rather than connecting the probe tips to other electrodes embedded in the gel, though the ability to consistently measure electrode-gel contact area should be considered.

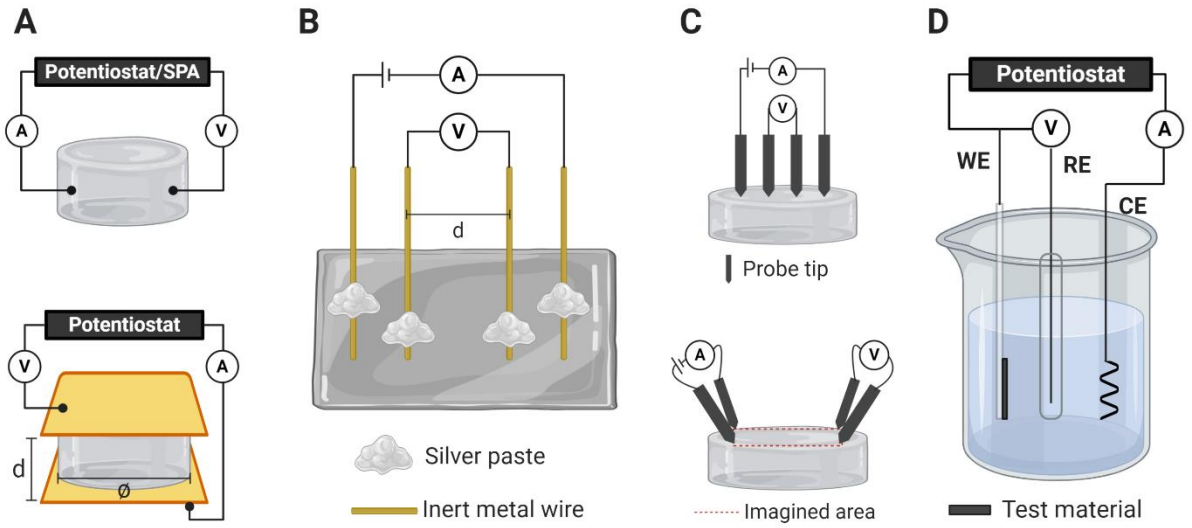

Figure A1.28: Electrical characterization techniques commonly used in tissue engineering studies. (A) Two-point probe techniques use needle-tip probes or sandwich a material between plates of conducting materials (*e.g.*, gold). **(B)** A standard four-point probe technique uses inert metal wires affixed to the experimental material with silver paste. **(C)** Linear four-point probe (top) and one type of van der Pauw setup (bottom). **(D)** Cyclic voltammetry (WE = working electrode, RE = reference electrode, CE = counter electrode).

Similarly, when using 4-point probe setups, the distinction between standard (**Figure A1.5C, top**) and van der Pauw (*e.g.*, used by Xia et. al[25]) (**Figure A1.5C, bottom**) needs to be explicit. Standard (*i.e.*, linear) 4-point probe is most appropriate for determining surface resistivity in the sensing direction, which is relevant for anisotropic materials, whereas van der Pauw is most appropriate for determining average bulk

resistivity of a sample. Another method to measure the conductive properties of materials is to perform electrochemistry using cyclic voltammetry (CV) (**Figure A1.5D**)[26].

While there are numerous ways to measure the conductivity of materials, it is understudied whether the reported properties remain identical when measured with different methods. This lack of understanding is further exacerbated by the observation that conductivity studies frequently lack positive controls, which is critical not only for determining statistical significance between groups, but also in confirming the instrument's accuracy.

In this work, we opted to use cyclic voltammetry and a 2-point probe setup with a semiconductor parameter analyzer. Making consistent contact between the hydrogel and the electrodes was a challenge for both methods. Additionally, the probes were at risk of forming a Schottky barrier, as neither method facilitated probing the gels directly. Furthermore, the voltage ranges selected for this work were likely inappropriate for water-based materials. Water electrolysis can begin when ±1.5 V is applied[27], and the minimum voltage applied in these studies was ±2 V. Future work with this material would adopt the conductivity testing setup described in Chapter 3 and test at a lower voltage range.

CONCLUSION

In this work, we designed a peptide sequence to have electrical properties to confer electrical conductivity to collagen gels. We demonstrated successful fabrication and purification of the peptide and confirmed that charged moieties were present within the sequence. When incorporated into collagen hydrogels, preliminary conductivity

measurements indicated that the conductive peptide could, indeed, make collagen gels more conductive, though several testing parameters would need to be adjusted to reproducibly confirm these observations. Overall, while these data are preliminary, they begin the important work of developing conductive additives that are compatible with *in vivo* systems, thereby addressing a significant shortcoming of frequently used synthetic conjugated polymers.

I gratefully acknowledgement the help of Pr. Erkin Şeker and Dr. Jovana Veselinovic for their guidance and assistance with the cyclic voltammetry measurements, Dr. Yusha Bey and the UC Davis Center for Nano-MicroManufacturing facility (CNM2) for guidance and assistance with the semiconductor parameter analyzer experiments, and Dr. William Jewell and the UC Davis Campus Mass Spectrometry.

REFERENCES

1. MacDiarmid, A. G. 'Synthetic metals': a novel role for oganic polymers (Nobel lecture). Angew Chem Int Ed 40, 2581–2590 (2001).
2. Casella, A., Panitch, A. & Leach, J. K. Endogenous electric signaling as a blueprint for conductive materials in tissue engineering. Bioelectricity (2020) doi:10.1089/bioe.2020.0027.
3. Malvankar, N. S. et al. Tunable metallic-like conductivity in microbial nanowire networks. Nat Nanotechnol 6, 573–9 (2011).
4. Adhikari, R. Y., Malvankar, N. S., Tuominen, M. T. & Lovley, D. R. Conductivity of individual Geobacter pili. Rsc Adv. 6, 8363–8366 (2016).
5. Tan, Y. et al. Synthetic Biological Protein Nanowires with High Conductivity. Small 12, 4481–4485 (2016).
6. Paderi, J. E. & Panitch, A. Design of a Synthetic Collagen-Binding Peptidoglycan that Modulates Collagen Fibrillogenesis. Biomacromolecules 9, 2562–2566 (2008).
7. Scott, R. A., Paderi, J. E., Sturek, M. & Panitch, A. Decorin Mimic Inhibits Vascular Smooth Muscle Proliferation and Migration. PLOS ONE 8, e82456 (2013).
8. Stuart, K., Paderi, J., Snyder, P. W., Freeman, L. & Panitch, A. Collagen-Binding Peptidoglycans Inhibit MMP Mediated Collagen Degradation and Reduce Dermal Scarring. PLOS ONE 6, e22139 (2011).
9. Hao, D. et al. Engineered extracellular vesicles with high collagen-binding affinity present superior in situ retention and therapeutic efficacy in tissue repair. Theranostics 12, 6021–6037 (2022).
10. Walimbe, T. et al. Proangiogenic Collagen-Binding Glycan Therapeutic Promotes Endothelial Cell Angiogenesis. ACS Biomater. Sci. Eng. 7, 3281–3292 (2021).
11. Kalyoncu, E., Ahan, R. E., Olmez, T. T. & Seker, U. O. S. Genetically encoded conductive protein nanofibers secreted by engineered cells. RSC Adv. 7, 32543–32551 (2017).
12. Creasey, R. C. G., Shingaya, Y. & Nakayama, T. Improved electrical conductance through self-assembly of bioinspired peptides into nanoscale fibers. Mater. Chem. Phys. 158, 52–59 (2015).
13. Namgung, S. D. et al. Increased electrical conductivity of peptides through annealing process. APL Mater. 5, 086109 (2017).
14. Nazari, Z. E., Gomez Herrero, J., Fojan, P. & Gurevich, L. Formation of Conductive DNA-Based Nanowires via Conjugation of dsDNA with Cationic Peptide. Nanomaterials 7, 128 (2017).
15. Ing, N. L., Spencer, R. K., Luong, S. H., Nguyen, H. D. & Hochbaum, A. I. Electronic Conductivity in Biomimetic α-Helical Peptide Nanofibers and Gels. ACS Nano 12, 2652–2661 (2018).
16. Zheng, J.-S., Tang, S., Qi, Y.-K., Wang, Z.-P. & Liu, L. Chemical synthesis of proteins using peptide hydrazides as thioester surrogates. Nat. Protoc. 8, 2483–2495 (2013).
17. Yang, J., Choe, G., Yang, S., Jo, H. & Lee, J. Y. Polypyrrole-incorporated conductive hyaluronic acid hydrogels. Biomater Res 20, 31 (2016).
18. Ryan, A. J. et al. Electroconductive biohybrid collagen/pristine graphene composite biomaterials with enhanced biological activity. Adv Mater 30, e1706442 (2018).

19. Baei, P. et al. Electrically conductive gold nanoparticle-chitosan thermosensitive hydrogels for cardiac tissue engineering. Mater Sci Eng C Mater Biol Appl 63, 131–41 (2016).
20. Bonfrate, V. et al. Enhanced electrical conductivity of collagen films through long-range aligned iron oxide nanoparticles. J Colloid Interface Sci 501, 185–191 (2017).
21. Lu, B. et al. Pure PEDOT:PSS hydrogels. Nat Commun 10, 1043 (2019).
22. Wibowo, A. et al. 3D printing of polycaprolactone-polyaniline electroactive scaffolds for bone tissue engineering. Mater. Basel 13, 512 (2020).
23. Alam, A., Kuan, H. C., Zhao, Z. H., Xu, J. & Ma, J. Novel polyacrylamide hydrogels by highly conductive, water-processable graphene. Compos. Part Appl. Sci. Manuf. 93, 1–9 (2017).
24. Pierret, R. F. Semiconductor device fundamentals. (Addison-Wesley, 1996).
25. Xia, Y., Sun, K. & Ouyang, J. Solution-Processed Metallic Conducting Polymer Films as Transparent Electrode of Optoelectronic Devices. Adv. Mater. 24, 2436–2440 (2012).
26. Elgrishi, N. et al. A practical beginner's guide to cyclic voltammetry. J. Chem. Educ. 95, 197–206 (2018).
27. Wrighton, M. S. et al. Strontium titanate photoelectrodes. Efficient photoassisted electrolysis of water at zero applied potential. J. Am. Chem. Soc. 98, 2774–2779 (1976).

Appendix 2: Electroactive alginate hydrogels have enhanced conductivity and support cell basic cell behavior

A2.1 INTRODUCTION

Electrically conductive biomaterials have great potential to advance tissue engineering as reports imply electroactive substrates promote nerve, cardiac, muscle, and bone regeneration[1–3]. Additionally, these studies indicate conductive substrates alter cell behaviors towards desired outcomes (*e.g.*, enhancing gap junction markers in cardiomyocytes), even in the absence of electrical stimulation[4]. Conjugated polymers such as polypyrrole (PPy), polyaniline, and poly(3,4-ethylenedioxythiophene) (PEDOT); carbon-based materials such as carbon nanotubes and graphene; and metallic additives like gold and silver nanoparticles, are all used to increase the conductivity of biomaterials[5]. However, the synthetic nature of such subtrates means they cannot be resorbed by the body, and the long-term safety of these materials has not been established. Some studies even indicate that synthetic conductive materials like gold nanoparticles and graphene may elicit an inflammatory response or be toxic to cells[6,7]. Identifying conductive materials that the body can safely metabolize may aid significant progress toward clinical translation. Unfortunately, many naturally occurring materials, including collagen and chitosan, have low conductivity around 10^{-10} S/cm[8,9].

In recent years, bio-ionic liquids (bio-ILs), have been used to increase substrate conductivity by facilitating ion movement, rather than electron movement. Bio-ILs are

used in a variety of sectors, namely as chemical solvents, but only ~5% of studies using bio-ILs employed them for tissue engineering[10]. Reports leveraging bio-ILs for tissue engineering demonstrate excellent biocompatibility and show promise for facilitating cardiac repair[11,12]. Although these outcomes are exciting, there are still knowledge gaps about cell-scaffold coupling between electron-conducting (*e.g.*, polypyrrole, graphene) and ion-conducting (*e.g*., bio-ionic liquids) materials. Differences in these properties may promote distinct effects on cell behavior, but such comparative studies are lacking[13].

In this work, we used alginate hydrogels to investigate differences in myoblast behavior on ion- versus electron-conducting substrates. We first functionalized alginate with free thiol groups that coordinated covalent binding with a choline-based bio-IL. We also tested alginate gels containing electron-conducting graphene and PEDOT:PSS. Increased bio-IL content offered a modest increase in gel conductivity, but it was still less than conductive properties of gels containing PEDOT:PSS. When seeded with C2C12 myoblasts, the bio-IL- and PEDOT:PSS-containing gels both facilitated cell adhesion and spreading, though metabolic activity was greater on the PEDOT:PSS-containing gels. Cell behavior was poor on pure PEDOT:PSS hydrogels, implying that there is a range of optimal conductivities for biological applications.

A2.2 MATERIALS AND METHODS

A2.2.1 Alginate oxidation and modification with RGD peptide

PRONOVA UltraPure (UP) MVG alginate (>200,000 g/mol, NovaMatrix Sandvika, Norway) was oxidized as previously described[14,15]. Alginate was dissolved at 10 mg/mL

in UP H_2O overnight before adding 1 mM of sodium periodate to achieve 1% oxidation. The reaction was quenched with equimolar ethylene glycol after stirring for 17 h protected from light. The alginate was then dialyzed in UP H_2O, filtered, and lyophilized.

The same oxidized MVG alginate and fresh VLVG alginate (<75,000 g/mol, NovaMatrix Sandvika) were modified with RGD peptides using standard carbodiimide chemistry as previously described[16]. Alginate was dissolved overnight at 10 mg/mL in MES buffer (0.1 M MES, 0.3 M NaCl, pH 6.5). Then *N*-(3-Dimethylaminopropyl)-*N*'-ethylcarbodiimide hydrochloride (EDC) and *N*-Hydroxysuccinimide sodium salt (Sulf-NHS) were added in a 2:1 ratio per gram of alginate. The peptide G4RGDSP (Commonwealth Biotechnologies, Richmond, VA) was added to achieve a degree of substation (DS) of 2. The resulting 1% ox. MVG-RGD and VLVG-RGD were dialyzed against UP H_2O, sterile filtered, and lyophilized[15].

A2.2.2 Alginate thiolation

A separate sample of VLVG alginate was thiolated using two methods described previously, both based on standard carbodiimide chemistry. Alginate was first dissolved at 10 mg/mL in MES buffer (pH 6.5) overnight, then varying amounts of either L-cysteine methyl ester hydrochloride[17] (Sigma-Aldrich, St. Louis, MO) (**Fig. A2.1A**) or 3,3'-dithiobis(propanoic dihydrazide)[18–20] (DTP, Frontier Specialty Chemicals, Logan, UT) were added to achieve 0, 2.5, 5, and 10% thiolation. After dissolving overnight, EDC was incorporated in a 5:1 molar ratio to DTP and Sulfo-NHS was included in a 1:2 ratio to EDC. Effective thiolation, evidenced by gelation *via* formation of disulfide bridges was observed

soon after adding EDC. While the gel loosened into a liquid as rotational mixing proceeded, 1 mL of a molar excess of TCEP was adding the following day to completely sever disulfide bridges (**Fig. A2.2A**). After mixing for 1 day, thiolated alginate (SH-VLVG) solutions were dialyzed against UP H_2O for 3 days to remove any unreacted reagents. SH-VLVG was frozen and lyophilized before being reconstituted for additional modification (**Fig. A2.2B**).

The success of adding free thiol groups to alginate with L-cysteine methyl ester hydrochloride was confirmed using H^{-1} NMR. The molarity of free thiols on VLVG after using DTP was quantified using the Ellman's assay (Thermo Fisher Scientific, Waltham, MA) where L-cysteine hydrochloride monohydrate was used to construct a standard curve and all samples of SH-VLVG were dissolved at 1 mg/mL in Ellman's Reaction Buffer (0.1 M sodium phosphate, containing 1mM EDTA, pH 8.0).

A2.2.3 Synthesis of bio-ionic liquid

Choline bicarbonate (Sigma-Alrich) and acrylic acid (Acros Organics) were mixed in a 1:1 molar ratio as previously described[12] to form choline acrylate, referred here as bio-ionic liquid (bio-IL) (**Fig. A2.3A**). A 100 mL 3-arm mixing flask was attached to a reflex column and submerged in a mineral oil bath set to 50°C according to **Fig. A2.3B**. A stir bar and 10 mL of acrylic acid were added to the flask before beginning reflux and stirring at 400 rpm. One arm of the flask was stoppered to prevent boiling over while adding 20 mL choline bicarbonate dropwise through the open arm of the flask. Once temperature reached 50°C, the reaction proceeded for 5 h, leaving the arm of the flask open. After the

reaction was complete, the solution was transferred to a glass bottle and protect from light. Any remaining bicarbonate groups were purged by storing the open bottle in a vacuum chamber overnight. Synthesis was confirmed using H^{-1} NMR.

A2.2.4 Conjugation of bio-IL to SH-Alg using Michael-type addition

SH-VLVG was reconstituted at 5 mg/mL in 1X PBS for 1 day before adding a molar excess (~10:1) of bio-IL to free thiols, determined *via* the Ellman's assay (**Fig. A2.4A**). The solution was titrated to pH 7.2-7.4 to initiate Michael-type addition. The reaction was quenched after at least 2 h by lowering the pH to approximately 6.5. SH-VLVG+bio-IL solutions were dialyzed against UP H_2O for 3 days before freezing, lyophilizing, and reconstituting. Samples for the Ellman's assay were dissolved at 1 mg/mL in Ellman's Reaction Buffer. Remaining SH-VLVG+bio-IL was dissolved at 25 mg/mL in 1X PBS (**Fig. A2.4B**).

A2.2.5 Fabricating alginate hydrogels with bio-IL

All samples of alginate (1% ox. MVG-RGD, VLVG+RGD, and SH-VLVG+bio-IL) were dissolved at 25 mg/mL in 1X PBS. Hydrogels contained 33% mixes of each type of alginate. In place of SH-VLVG+bio-IL, positive control gels contained 10 mg/mL of either graphene (Sigma-Aldrich) or poly(3,4-ethylenedioyxthiophene) polystyrene sulfonate (PEDOT:PSS; P:P) (PH1000, Ossila, Sheffield, UK) in water (**Fig. A2.5A**). All components were combined by rotational mixing for at least 30 min prior to hydrogel formation. Alginate mixtures (80 µL) were pipetted into 8 mm diameter silicone molds mounted on

a glass slide and sandwiched between dialysis membranes. A solution of 200 mM $CaCl_2$ + 6 mM $BaCl_2$ was added to the top dialysis membrane and allowed to crosslink for 5 min. The system was flipped, the glass plate removed, and additional crosslinking solution was added to the dialysis membrane. After 5 min of crosslinking, both dialysis membranes were removed, and more crosslinking solution was added for 10 min (**Fig. A2.5B**). After formation, gels were stored in UP H_2O to remove trace ionic solution.

A2.2.6 Electrical characterization of hydrogels

The electrical properties of hydrogels were measured using a custom two-point setup described previously[21]. Hydrogels were constrained by a PDMS mold (I.D. 10 mm, thickness 1.0 mm) and sandwiched between two brass plates. The sandwich was then stabilized between the jaws of a tabletop angle vise using PDMS blocks as a barrier between the plate and the jaw. One brass plate was connected to a power supply (BK Precision 1735A, Yorba Linda, CA) using alligator clips. One lead of a multimeter (SparkFun Electronics, Niwot, CO) was connected to the other brass plate and the second lead was connected to the power supply to create a complete circuit through which current could be measured. Voltages ranging from 100 to 300 mV, a range selected to avoid electrolysis of water, were applied to the gels to obtain current-voltage curves. After testing, hydrogel thickness and diameter were measured with calipers. Current-voltage curves were analyzed for linearity, and datasets with an R^2 value of ≥0.9 were accepted for resistance calculations. Conductivity was calculated using Pouillet's law (**Equation A2.1)**.

Equation A2.6:

$$\sigma = \frac{t}{RA}$$

where σ is conductivity in S/cm, t is thickness of the hydrogel (cm), R is resistance (Ω), and A is cross-sectional area (cm^2).

A2.2.7 Cell culture and in vitro characterization of conductive gels

C2C12 murine myoblasts (CRL-1772, Lot #70013341, ATCC, Manassas, VA) were cultured in DMEM (Thermo Fisher Scientific) supplemented with 10% FBS (GenClone, San Diego, CA) and 1% Penicillin-Streptomycin (P/S, Gemini Bio Products, West Sacramento, CA) in standard culture conditions (*i.e.*, 37°C, 5% CO_2). Cultures were maintained until <70% confluent to prevent myoblast differentiation. Cells were seeded on top of alginate hydrogels at 10,000 cells per gel. Pure PEDOT:PSS gels were fabricated as described previously[22] and, after sterilizing with 70% ethanol, were used as a control. At 3d, cell metabolic activity was measured with the alamarBlue assay (Thermo Fisher Scientific) according to the manufacturer's instructions. Results were normalized to DNA content measured using the Quant-iT PicoGreen™ dsDNA Assay Kit (Thermo Fisher Scientific). Viability of the cells on gels was determined using a LIVE/DEAD stain where viable cells were stained green with calcein AM (Invitrogen) and dead cells were stained red with propidium iodide (Millipore Sigma, St. Louis, MO). Cells on gels were imaged using a Keyence BZ-X700 fluorescent microscope at a 4X magnification.

A2.2.8 Statistical analysis

Data are presented as means ± standard deviation. Statistical analysis was conducted using GraphPad Prism 9 software. Groups were compared using one- or two-way analysis of variance (ANOVA) with Tukey correction. Differences were considered statistically significant at $p \leq 0.05$.

A2.3 RESULTS

A2.3.1 Thiolating alginate with cysteine is successful, though not consistent

Based on prior reports, we sought to add increasing numbers of free thiol groups to VLVG alginate using cysteine and carbodiimide chemistry (**Fig. A2.1A**). Purified samples were subject to H^{-1} NMR spectroscopy. The spectra of unmodified alginate (**Fig. A2.1B**) differed from that of alginate mixed with cysteine to a degree of substitution 10 (DS10) by a distinct peak at approximately 2.75 ppm (**Fig. A2.1C**). Other degrees of substitution (*e.g.*, 2.5 and 5) had similar results (*data not shown*). The addition of this peak is evidence that alginate was successfully thiolated using cysteine. However, when free thiols were quantified using the Ellman's assay, results were consistently non-linear (**Fig. A2.1D**), thereby necessitating the need to identify an alternate thiolation strategy.

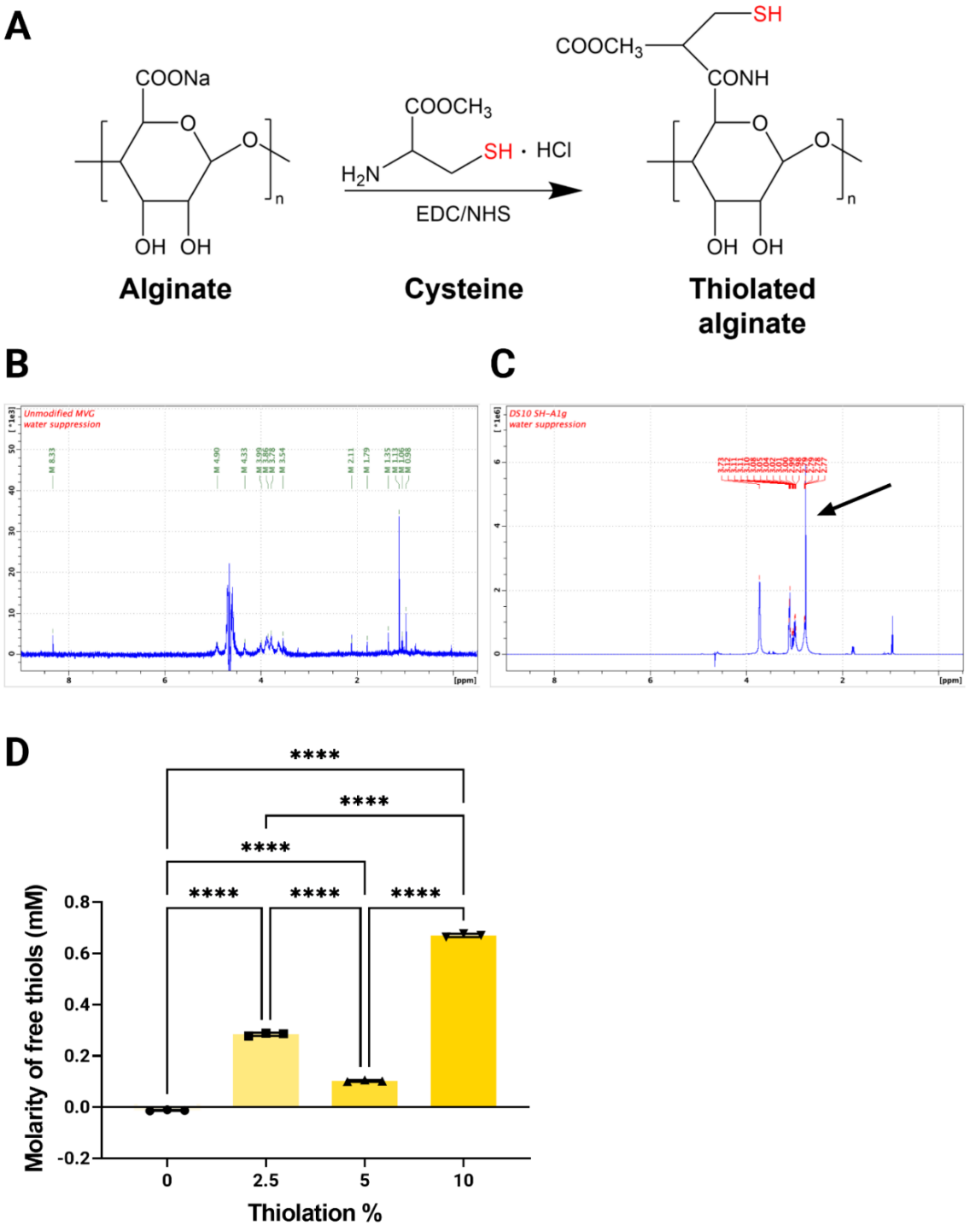

Figure A2.29: Alginate can be successfully thiolated using cysteine. (A) Alginate can undergo carbodiimide chemistry with L-cysteine methyl ester hydrochloride to add free thiol groups to the polysaccharide's backbone. Comparing H^{-1} NMR spectra of **(B)**

alginate alone and **(C)** alginate mixed with cysteine to a degree of substitution 10 (DS10) reveals an additional peak (black arrow) indicative of successful modification. **(D)** The results of the Ellman's assay revealed a non-linear relationship between percent thiolation and molarity of free thiols, rendering a need to thiolate alginate a different way. Groups were compared using a one-way ANOVA with Tukey correction (n=3, ****$p \leq 0.0001$).

A2.3.2 Thiolating alginate with DTP and is effective and consistent

To address the shortcomings observed when thiolating alginate with cysteine, we sought inspiration from previous work that used DTP and carbodiimide chemistry to add free thiols to various glycosaminoglycans[18–20]. Adding EDC and Sulfo-NHS to alginate solutions containing DTP resulted in nearly instant gelation, suggesting DTP acts as a crosslinker between alginate monomers. Although not a desired outcome, gelation is indicative of successful conjugation of DTP to alginate. Gel solutions loosened as mixing continued, owing to the acidic pH of the reaction. However, final treatment with the reducing agent, TCEP, was necessary to cleave any remaining disulfide bridges (**Fig. A2.2A**). Thorough dialysis was required to remove any unreacted reagents prior to characterization *via* the Ellman's assay (**Fig. A2.2B**). The molarity of free thiols increased as thiolation % increased, though there was no difference between the 2.5 and 5.0% groups (**Fig. A2.2C**). However, differences between the other groups were large enough to anticipate changes in electrical activity due to subsequent bio-IL content. Therefore, SH-VLVG generated from reactions containing DTP was used for the remaining experiments.

A

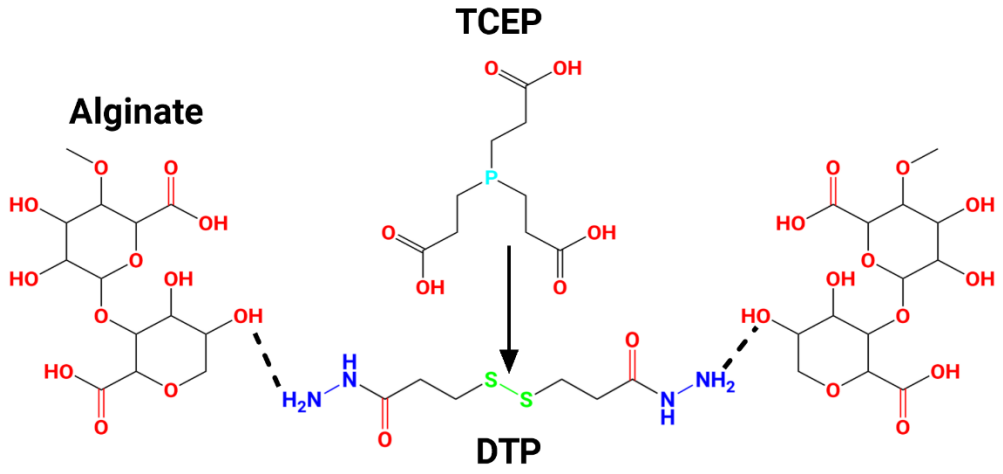
TCEP
Alginate
DTP

B

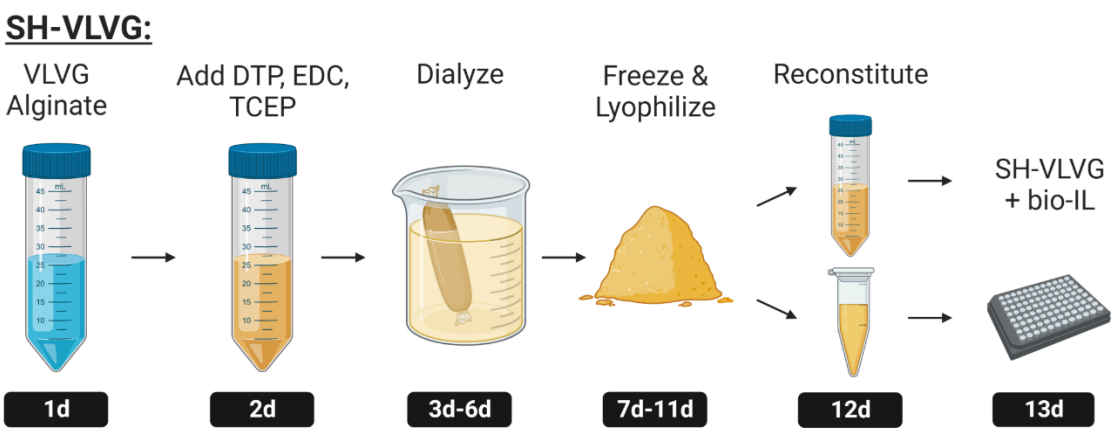
SH-VLVG:
VLVG Alginate
Add DTP, EDC, TCEP
Dialyze
Freeze & Lyophilize
Reconstitute
SH-VLVG + bio-IL
1d
2d
3d-6d
7d-11d
12d
13d

C

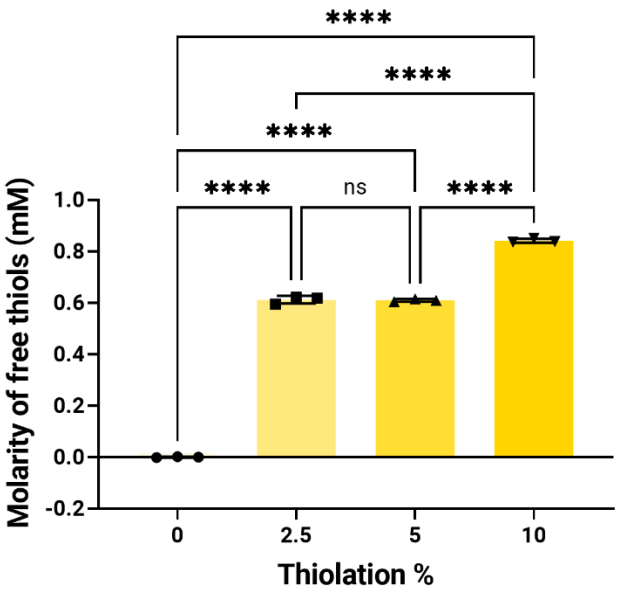
****
****
****
****
ns
****
Molarity of free thiols (mM)
1.0
0.8
0.6
0.4
0.2
0.0
-0.2
0
2.5
5
10
Thiolation %

Figure A2.30: DTP more consistently increases free thiol groups on alginate. (A) Reacting DTP and alginate using carbodiimide chemistry results in crosslinked monomers that can be cleaved using the reducing agent, TCEP, which targets disulfide bridges. Reducing these bridges results in alginate monomers with free thiol groups. **(B)** Thiolated alginate (SH-VLVG) underwent thorough dialysis before freezing, lyophilizing, and reconstituting for the Ellman's assay and downstream use. **(C)** There were significant differences in the molarity of free thiols for groups modified using DTP. Although there were not differences between 2.5 and 5.0%, these results were more linear than those gleaned from using cysteine as a source of thiols. Groups were compared using a one-way ANOVA with Tukey correction (n=3, ****$p \leq 0.0001$, ns = not significant).

A2.3.3 Bio-ionic liquid can be successfully synthesized based on prior reports

Previous studies used choline bicarbonate and acrylic acid to synthesize choline acrylate (**Fig. A2.3A**), which then imparted ionic conductivity to methacrylated gelatin[12]. Adapting this approach to be compatible with alginate hydrogels alginate hydrogels did not require alteration in the bio-IL synthesis. Choline bicarbonate and acrylic acid were reacted at 50°C for 5 h under reflux according to the setup in **Fig. A2.3B**. Synthesis was confirmed using H^{-1} NMR, and the spectrum for choline bicarbonate alone (**Fig. A2.3C**) lacked peaks that were seen in the reaction result (**Fig. A2.3D**). These data illustrate successful synthesis of bio-IL and match the results reported by the study of reference.

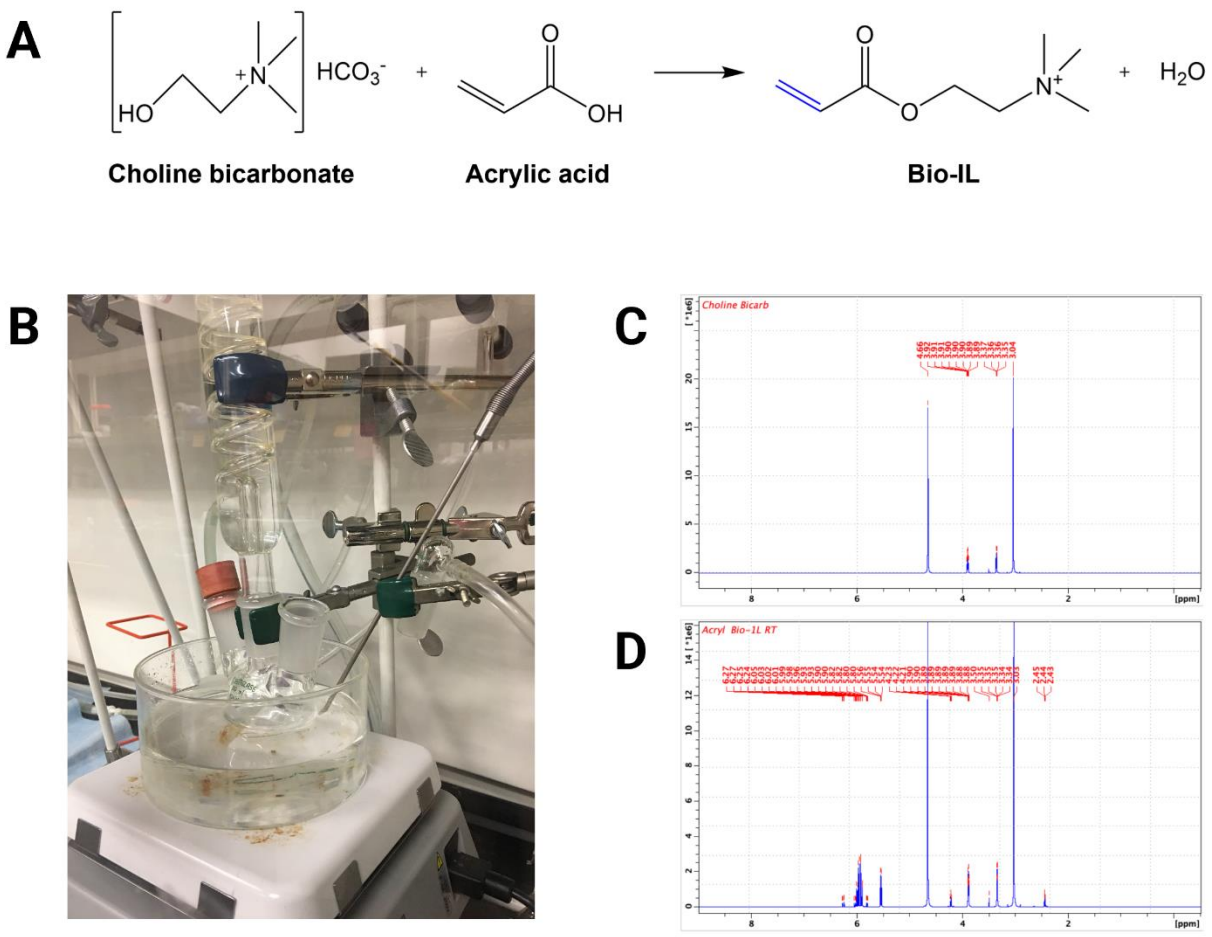

Figure A2.31: Synthesis of bio-ionic liquid can be successfully synthesized from prior studies. (A) The chemical reaction by which choline bicarbonate is mixed with acrylic acid to make choline acrylate, referred to as bio-IL. **(B)** Illustrates the setup of the reaction using heating and reflux. **(C)** The H^{-1} NMR spectrum of choline bicarbonate contrasts that of choline bicarbonate mixed with acrylic acid by a cluster of peaks between 5.5 and 6.5 ppm. The addition of these peaks suggests successful synthesis of bio-IL.

A2.3.4 Bio-IL is conjugated to free thiol groups on SH-VLVG via Michael-type addition

Prior work from our group has demonstrated successful crosslinking of acrylated molecules and those with free thiol groups using Michael-type addition[19]. Therefore, we sought to apply the same strategy to conjugate previously synthesized bio-IL to SH-VLVG (**Fig. A2.4A**). Once SH-VLVG was purified and reconstituted, bio-IL was added in a molar excess of free thiols and the solution was titrated to pH 7.2-7.4 to initiate Michael-type addition. The reaction was quenched by lowering the pH and SH-VLVG+bio-IL was purified for later use (**Fig. A2.4B**). The significant reduction in free thiols measured by the Ellman's assay post-conjugation confirm bio-IL attachment (**Fig. A2.4C**). Incomplete abrogation of the free thiols on 10% SH-VLVG+bio-IL suggests inefficiencies within the reaction, and future work may seek to include an even greater molar excess of bio-IL during Michael-type addition.

A

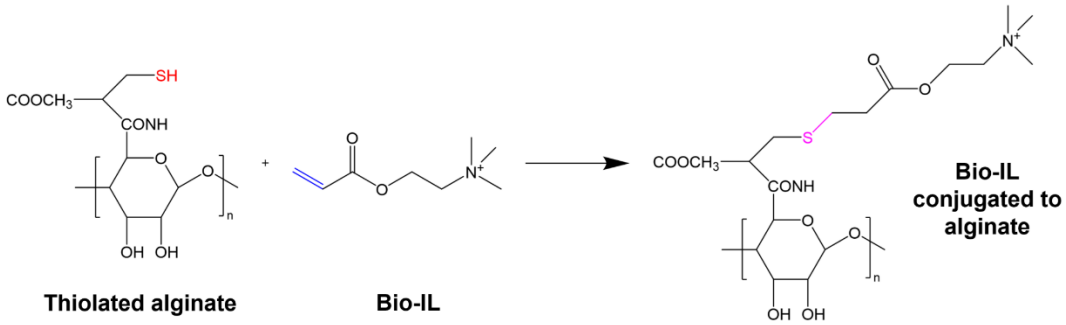
SH
COOCH3
CONH
OH OH
Thiolated alginate
Bio-IL
COOCH3
CONH
OH OH
Bio-IL conjugated to alginate

B

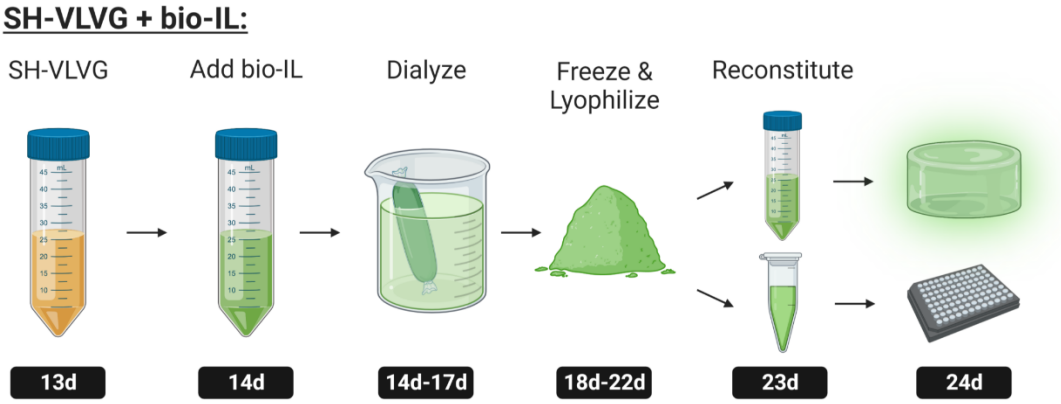
SH-VLVG + bio-IL:
SH-VLVG
Add bio-IL
Dialyze
Freeze & Lyophilize
Reconstitute
13d
14d
14d-17d
18d-22d
23d
24d

C

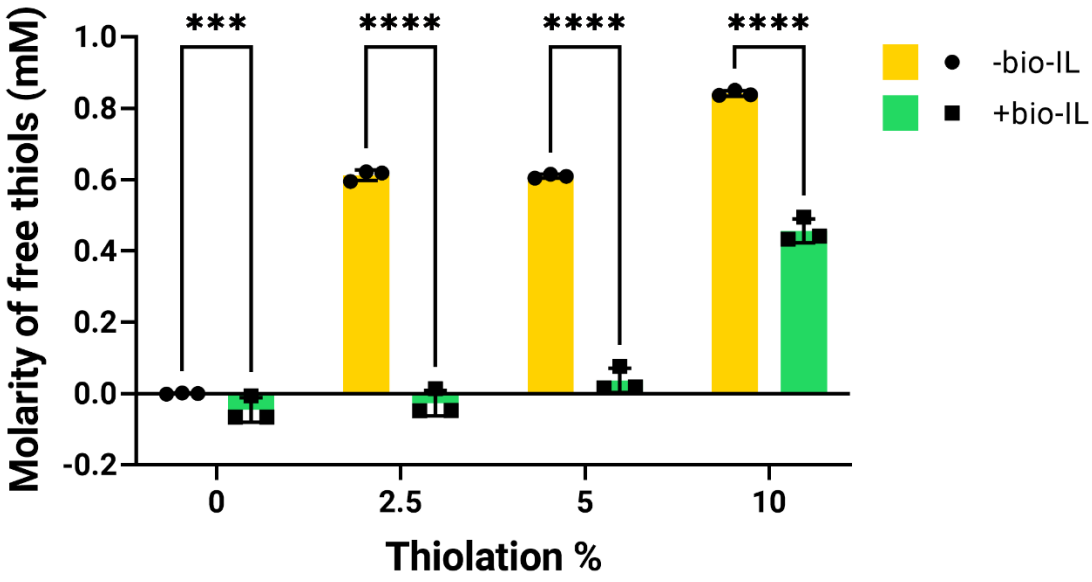
Molarity of free thiols (mM)
1.0
0.8
0.6
0.4
0.2
0.0
-0.2
***
****
****
****
0
2.5
5
10
Thiolation %
-bio-IL
+bio-IL

Figure A2.32: Bio-IL is conjugated to free thiol groups on SH-VLVG *via* Michael-type addition. (A) We sought to utilize a previously reported strategy to bind the acrylate groups of bio-IL to the free thiol groups on thiolated alginate *via* Michael-type addition. **(B)** SH-VLVG+bio-IL required thorough dialysis before freezing, lyophilizing, and reconstituting for the Ellman's assay and downstream use. **(C)** Results of the Ellman's assay pre- and post- conjugation demonstrate significant reduction the molarity of free thiols after bio-IL is added, thereby confirming successful attachment. Incomplete abatement in the 10% SH-VLVG+bio-IL group suggest inefficiencies within the reaction that may be addressed in future work. Groups were compared using a 2-way ANOVA (n=3, ***$p \leq 0.001$, ****$p \leq 0.0001$).

A2.3.5 Bio-IL can be successfully incorporated into alginate gels and improves conductivity over unmodified hydrogels.

After confirming successful conjugation of bio-IL to SH-VLVG, mixtures containing equal parts 1% oxidized MVG alginate, RGD-modified VLVG alginate, and SH-VLVG+bio-IL were formed into hydrogels. Therefore, the total SH-VLVG+bio-IL content reflected 1/3 of the initial percent thiolation (*i.e.*, 0, 0.83, 1.66, and 3.33% from 0, 2.5, 5, and 10%, respectively). Gels containing graphene or PEDOT:PSS instead of SH-VLVG+bio-IL were used as electron-conducting controls (**Fig. A2.5A**). The alginate-based gels were ionically crosslinked using a solution and methods reported by our group previously (**Fig. A2.5B**)[15]. Hydrogels containing SH-VLVG+bio-IL had the most consistent morphology and were optically clear. As an inherently hydrophobic material, graphene was not homogenous

within the hydrogel, though it appeared to be dispersed throughout the entire construct. PEDOT:PSS, as expected, was homogenously distributed throughout the gel, making it opaque (**Fig. A2.5C**). Conductivity testing revealed 3.33 v/v% bio-IL gels were significantly more conductive than the 0 and 0.833% bio-IL gels as well as the graphene-containing gels. The PEDOT:PSS-containing gels were more than twice as conductive as all other groups at approximately 2.4×10^{-5} S/cm, though all gels' conductivity was on a similar order of magnitude (**Fig. A2.5D**). These results suggest that bio-IL has the potential to imbue hydrogels with heightened conductive properties, though these results do not yet outperform electron-conducting synthetic polymers.

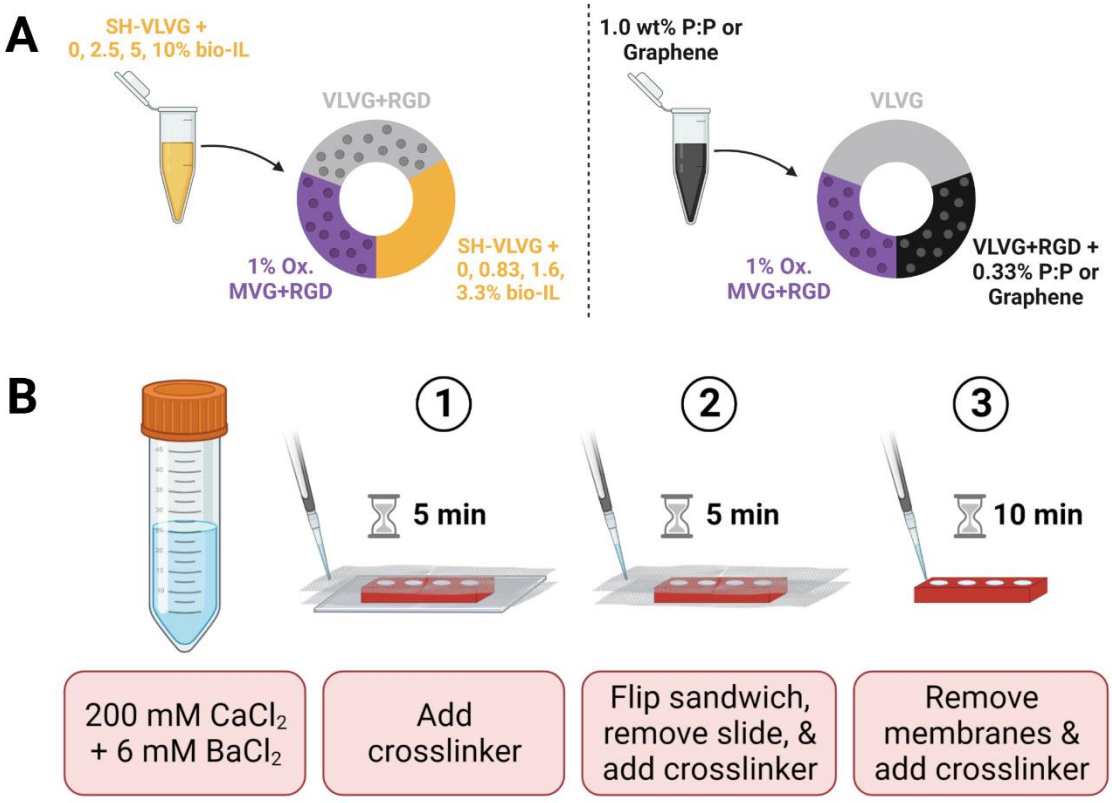
A
SH-VLVG +
0, 2.5, 5, 10% bio-IL
VLVG+RGD
1% Ox.
MVG+RGD
SH-VLVG +
0, 0.83, 1.6,
3.3% bio-IL
1.0 wt% P:P or
Graphene
VLVG
1% Ox.
MVG+RGD
VLVG+RGD +
0.33% P:P or
Graphene
B
1
2
3
5 min
5 min
10 min
200 mM CaCl2
+ 6 mM BaCl2
Add
crosslinker
Flip sandwich,
remove slide, &
add crosslinker
Remove
membranes &
add crosslinker

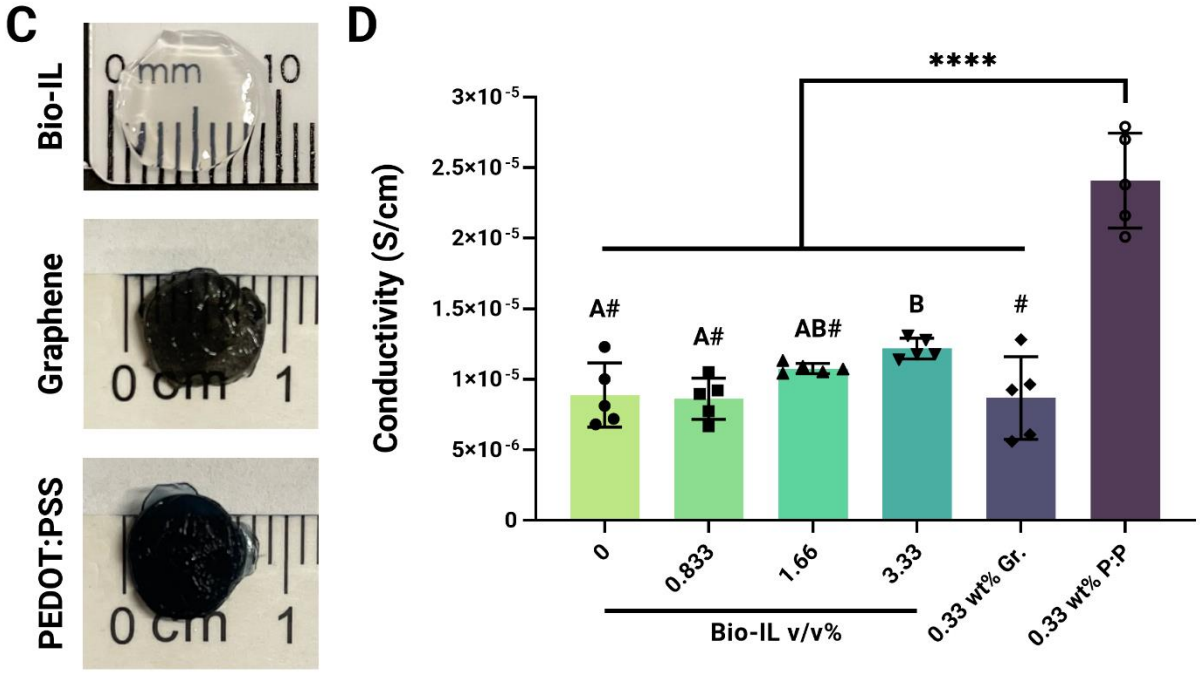
C
Bio-IL
Graphene
PEDOT:PSS
0 mm 10
0 cm 1
0 cm 1
D
****
Conductivity (S/cm)
3×10-5
2.5×10-5
2×10-5
1.5×10-5
1×10-5
5×10-6
0
A#
A#
AB#
B
#
0
0.833
1.66
3.33
0.33 wt% Gr.
0.33 wt% P:P
Bio-IL v/v%

Figure A2.33: Bio-IL can be successfully incorporated into alginate gels and improves conductivity over unmodified hydrogels. (A) Mixtures of SH-VLVG+bio-IL, 1% oxidized MVG+RGD, and VLVG-RGD were used to make hydrogels. Gels containing graphene or PEDOT:PSS instead of SH-VLVG+bio-IL were used as controls. **(B)** Alginate gels were crosslinked using a solution containing Ca^{2+} and Ba^{2+} ions to make 8 mm constructs. **(C)** Gross images of hydrogels illustrate successful crosslinking and consistent morphology of bio-IL-containing gels (3.33% shown, but other bio-IL gels looked similar). Graphene was not homogenously distributed throughout the gel, given its hydrophobic nature, but PEDOT:PSS was evenly dispersed. **(D)** Conductivity testing revealed the 3.33% bio-IL gels were significantly more conductive than the unmodified alginate, 0.83% bio-IL, and graphene-containing groups, though PEDOT:PSS-containing gels were more conductive than all groups (****$p \leq 0.0001$). Bio-IL groups were compared using a 1-way ANOVA. Groups with different letters are statistically significant (n=5). Groups whose conductivity was statistically similar to the gels containing graphene are marked with # (#$p \leq 0.5$, n=5).

A2.3.6 C2C12 myoblast behavior is promoted by electroactive hydrogels within a range of conductivity

Although differences in conductivity between bio-IL containing groups was not profound, efforts to increase bio-IL content in gels would be misplaced if bio-IL was cytotoxic. Thus, we characterized cell viability and metabolic activity after being cultured on conductive gels for 3 days. Only the 0 and 3.33% bio-IL groups and 0.33 wt% PEDOT:PSS gels were utilized for this study and pure PEDOT:PSS gels were used as a

control. Pure PEDOT:PSS gels experienced significant shrinkage after repeat washes with ethanol, but otherwise maintained a circular shape (**Fig. A2.6A**). The conductivity of pure PEDOT:PSS gels was 4 orders of magnitude greater than the other groups at approximately 1.35×10^{-2} S/cm (**Fig. A2.6B**). The conductivity of the other gels was lower in this characterization compared to those in **Figure A2.5D**, which may have been a result of the relative insensitivity of the conductivity testing setup. Additionally, differences between the 0 and 3.33% bio-IL groups were lost in this characterization. The PEDOT:PSS-containing alginate, however, was still significantly more conductive than the other alginate-based gels. Cell metabolic activity was significantly greater in the 0.33 wt% PEDOT:PSS group than all others, including the 100% PEDOT:PSS gels (**Fig. A2.6C**). Additionally, very few cells were visible on the pure PEDOT:PSS gels, indicative of poor adhesion. The unmodified alginate gels also did not facilitate myoblast adhesion, which was unexpected, given that the majority of the gels' composition contained RGD-modified alginate. By contrast, many cells adhered to and spread on the 3.33% bio-IL and 0.33 wt% PEDOT:PSS groups, and most of them were viable, as indicated by the LIVE/DEAD stain (**Fig. A2.6D**). These data suggest that electrical cues can also play a role in support cell behavior, though groups with the most conductivity may not have the best effect.

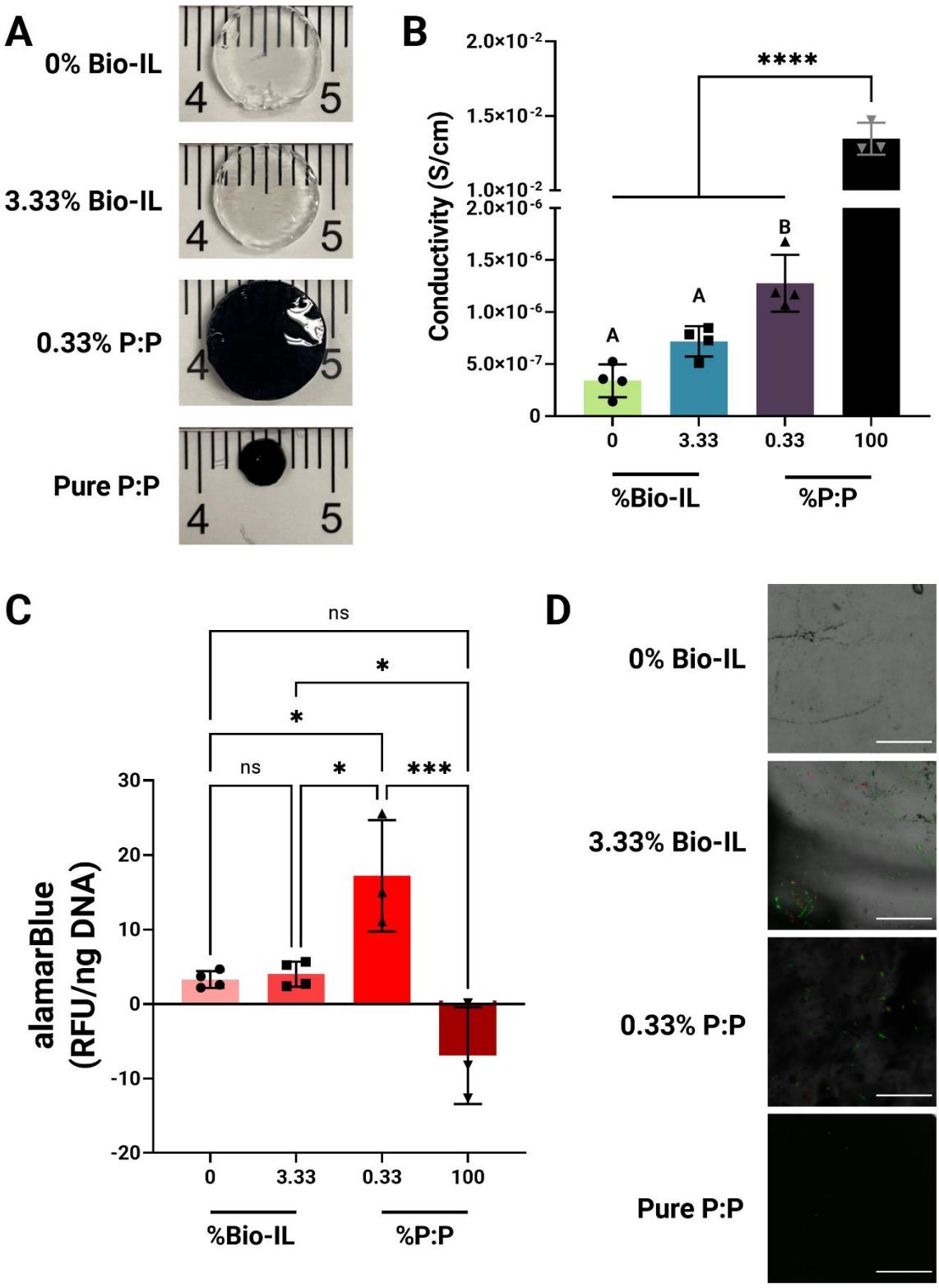
A
0% Bio-IL
3.33% Bio-IL
0.33% P:P
Pure P:P
4
5
B
Conductivity (S/cm)
2.0×10-2
1.5×10-2
1.0×10-2
2.0×10-6
1.5×10-6
1.0×10-6
5.0×10-7
0
****
A
A
B
0
3.33
0.33
100
%Bio-IL
%P:P
C
alamarBlue (RFU/ng DNA)
ns
*
*
ns
*
***
30
20
10
0
-10
-20
0
3.33
0.33
100
%Bio-IL
%P:P
D
0% Bio-IL
3.33% Bio-IL
0.33% P:P
Pure P:P

Figure A2.34: Electroactive hydrogels promote C2C12 myoblast behavior within a certain range of conductivities. (A) Gross images of hydrogels used to interrogate early C2C12 myoblast behavior. Pure PEDOT:PSS gels notably shrank after sterilizing with 70% ethanol, but maintained a circular shape. **(B)** Electrical characterization indicated no difference in conductivity between bio-IL groups, which contrasts previous observations in **Fig. A2.5**. PEDOT:PSS-containing alginate gels were more conductive than the other alginate-based gels, but the pure PEDOT:PSS gels had several orders of magnitude more conductivity than all other gels (n=3-4, ****$p \leq 0.0001$). Groups were compared using a 1-way ANOVA. Direct comparison between alginate-based gels is denoted with letters where groups with different letters are statistically different. **(C)** Myoblasts seeded on gels had the highest metabolic activity on the 0.33 wt% PEDOT:PSS gels. The lowest metabolic activity was observed in the pure PEDOT:PSS gels, and there was no difference in the bio-IL groups (n=3-4, *$p \leq 0.05$, ***$p \leq 0.001$, ns = not significant). **(D)** Results of the LIVE/DEAD stain indicate minimal myoblast adhesion to the 0% bio-IL and pure PEDOT:PSS groups. However, the 3.33% bio-IL and 0.33 wt% PEDOT:PSS gels facilitated cell adhesion and spreading, and most cells were viable, indicated by green calcein AM staining (4X, scale bar = 500 μm).

A2.4 DISCUSSION

In this work, we sought to incorporate a previously reported bio-IL into alginate hydrogels. Alginate hydrogels are physically tunable with a variety of methods (*e.g.*, concentration, crosslinking method, etc.) and was thus considered a promising candidate

for fabricating an electrically and mechanically tunable hydrogel platform. We successfully synthesized a choline-based bio-IL that corroborated the results of other reports. We tested two strategies for thiolating alginate and found DTP more effective than cysteine. Bio-IL was successfully conjugated to the backbone of alginate and did not prevent the alginate from ionically crosslinking into a hydrogel. The conductivity of these gels trended upwards with increasing concentrations of bio-IL. However, when compared to gels containing PEDOT:PSS, the bio-IL gels had significantly lower conductivity. Attempts to raise the degree of thiolation were unsuccessful as, disulfide bridges were unable to be reduced with an excess of TCEP (*data not shown*). When the hydrogel formulation was adjusted so two-thirds of the composition contained conductive additives, there were still no differences between groups (*data not shown*). Therefore, one major limitations of this study was reaching a limit on the amount of bio-IL that could be tethered to the alginate backbone.

When C2C12 myoblasts were seeded on a subset of gels, the cells had the highest metabolic activity on alginate gels containing PEDOT:PSS. Although pure PEDOT:PSS gels had the highest conductivity, very few cells adhered to the material and metabolic activity was poor. These results indicate that, while conductive properties can facilitate improved cell behaviors, there appears to be a window of conductivity outside of which effects can be detrimental. Another study measuring how scaffolds containing polyaniline influenced the osteogenic potential of mesenchymal stromal cells reached a similar conclusion[23]. This has important implications for future research on electroactive

biomaterials, as the optimal level of conductivity for tissue engineering applications has not been specifically addressed.

An intention of this work was to address the knowledge gap of how cell response might differ when they are cultured on electron- versus ion-conducting materials. Although there is a growing body of evidence illustrating electrically conductive biomaterials orchestrate cell behavior, the mechanism behind this effect is not well understood, particularly since cells communicate electrically *via* ion gradients, whereas the majority of electroactive materials conduct electrons. However, because we were not able to generate a bio-IL-containing gel with similar conductivity to the P:P-containing group, we could not interrogate this relationship.

Finally, although thiolated alginate conjugated with bio-IL was not an efficacious ionically conductive material, there are numerous studies using other naturally derived molecules with great potential. For example, peptides inspired by the pili protein secreted by *Geobacter sulfurreducens*, have been designed with charged and aromatic amino acids to have greater conductivity than similar peptide sequences without such moieties[24]. Other examples in nature, namely sulfated materials, also have great promise. In fact, some such materials have conductivities on the order of 10^{-3} S/cm[25,26], which is significantly higher than any of the gels tested in this work, save those made purely of PEDOT:PSS. Our group has previously used sulfated hyaluronic acid[19], chondroitin sulfate[20], and sulfated alginate[15] to make hydrogels, and techniques described in this study could be used to specifically interrogate their electroactive effects on cells in the future.

CONCLUSION

The experiments described in this work illustrate techniques for conjugating choline-based bio-ionic liquids to increase ionic conductivity of hydrogels. Although the electrical properties of the ion-conducting gels did not meet those of alginate gels containing the electron-conductor, PEDOT:PSS, both materials exhibited biocompatible properties *via* cell adhesion and viability. These preliminary insights serve to inform future work that test different techniques to increase bio-IL content in hydrogels or that investigate different ionically conductive materials, completely. This work and related future work help address the need for alternative electroactive substrates for tissue engineering that overcome the safety limitations of synthetic polymers. Validating the long-term safety and efficacy of ionically conductive biomaterials could be instrumental for clinical translation and help heal wounds of millions of patients.

I gratefully acknowledge the assistance of Dr. Ping Yu and the UC Davis Nuclear Magnetic Resonance (NMR) Facility for her assistance collecting H^{-1} NMR data. Chemical structures and schematics were made using ChemDraw and BioRender, respectively.

REFERENCES

1. Zhou, L. et al. Soft conducting polymer hydrogels cross-linked and doped by tannic acid for spinal cord injury repair. ACS Nano 12, 10957–10967 (2018).
2. Wu, Y., Wang, L., Guo, B., Shao, Y. & Ma, P. X. Electroactive biodegradable polyurethane significantly enhanced Schwann cells myelin gene expression and neurotrophin secretion for peripheral nerve tissue engineering. Biomaterials 87, 18–31 (2016).
3. Wang, S. et al. 3D culture of neural stem cells within conductive PEDOT layer-assembled chitosan/gelatin scaffolds for neural tissue engineering. Mater Sci Eng C Mater Biol Appl 93, 890–901 (2018).
4. Thrivikraman, G., Boda, S. K. & Basu, B. Unraveling the mechanistic effects of electric field stimulation towards directing stem cell fate and function: a tissue engineering perspective. Biomaterials 150, 60–86 (2018).
5. Casella, A., Panitch, A. & Leach, J. K. Endogenous Electric Signaling as a Blueprint for Conductive Materials in Tissue Engineering. Bioelectricity 3, 27–41 (2021).
6. Liu, Y., Zhao, Y., Sun, B. & Chen, C. Understanding the Toxicity of Carbon Nanotubes. Acc. Chem. Res. 46, 702–713 (2013).
7. Falagan-Lotsch, P., Grzincic, E. M. & Murphy, C. J. One low-dose exposure of gold nanoparticles induces long-term changes in human cells. Proc. Natl. Acad. Sci. 113, 13318–13323 (2016).
8. Bonfrate, V. et al. Enhanced electrical conductivity of collagen films through long-range aligned iron oxide nanoparticles. J Colloid Interface Sci 501, 185–191 (2017).
9. Marroquin, J. B., Rhee, K. Y. & Park, S. J. Chitosan nanocomposite films: enhanced electrical conductivity, thermal stability, and mechanical properties. Carbohydr Polym 92, 1783–91 (2013).
10. Gomes, J. M., Silva, S. S. & Reis, R. L. Biocompatible ionic liquids: fundamental behaviours and applications. Chem. Soc. Rev. 48, 4317–4335 (2019).
11. Walker, B. W. et al. Engineering a naturally-derived adhesive and conductive cardiopatch. Biomaterials 207, 89–101 (2019).
12. Noshadi, I. et al. Engineering Biodegradable and Biocompatible Bio-ionic Liquid Conjugated Hydrogels with Tunable Conductivity and Mechanical Properties. Sci. Rep. 7, 4345 (2017).
13. Burnstine-Townley, A., Eshel, Y. & Amdursky, N. Conductive Scaffolds for Cardiac and Neuronal Tissue Engineering: Governing Factors and Mechanisms. Adv. Funct. Mater. 30, 1901369 (2020).
14. Bouhadir, K. H. et al. Degradation of Partially Oxidized Alginate and Its Potential Application for Tissue Engineering. Biotechnol. Prog. 17, 945–950 (2001).
15. Gionet-Gonzales, M. et al. Sulfated Alginate Hydrogels Prolong the Therapeutic Potential of MSC Spheroids by Sequestering the Secretome. Adv. Healthc. Mater. 10, 2101048 (2021).
16. Ho, S. S., Keown, A. T., Addison, B. & Leach, J. K. Cell migration and bone formation from mesenchymal stem cell spheroids in alginate hydrogels are regulated by adhesive ligand density. Biomacromolecules 18, 4331–4340 (2017).

17. Xu, G. et al. In situ thiolated alginate hydrogel: Instant formation and its application in hemostasis. J Biomater Appl 31, 721–729 (2016).
18. Shu, X. Z., Liu, Y., Luo, Y., Roberts, M. C. & Prestwich, G. D. Disulfide Cross-Linked Hyaluronan Hydrogels. Biomacromolecules 3, 1304–1311 (2002).
19. Walimbe, T., Calve, S., Panitch, A. & Sivasankar, M. P. Incorporation of types I and III collagen in tunable hyaluronan hydrogels for vocal fold tissue engineering. Acta Biomater 87, 97–107 (2019).
20. Nguyen, M., Liu, J. C. & Panitch, A. Physical and Bioactive Properties of Glycosaminoglycan Hydrogels Modulated by Polymer Design Parameters and Polymer Ratio. Biomacromolecules 22, 4316–4326 (2021).
21. Casella, A., Panitch, A. & Leach, J. K. Electroconductive agarose hydrogels modulate mesenchymal stromal cell adhesion and spreading through protein adsorption. J. Biomed. Mater. Res. A 111, 596–608 (2023).
22. Zhang, S. et al. Room-temperature-formed PEDOT:PSS hydrogels enable injectable, soft, and healable organic bioelectronics. Adv Mater 32, e1904752 (2020).
23. Chen, J., Yu, M., Guo, B., Ma, P. X. & Yin, Z. Conductive nanofibrous composite scaffolds based on in-situ formed polyaniline nanoparticle and polylactide for bone regeneration. J Colloid Interface Sci 514, 517–527 (2018).
24. Malvankar, N. S. et al. Tunable metallic-like conductivity in microbial nanowire networks. Nat Nanotechnol 6, 573–9 (2011).
25. Josberger, E. E. et al. Proton conductivity in ampullae of Lorenzini jelly. Sci. Adv. 2, e1600112 (2016).
26. Wünsche, J. et al. Protonic and Electronic Transport in Hydrated Thin Films of the Pigment Eumelanin. Chem. Mater. 27, 436–442 (2015).

Appendix 3: List of Protocols

A3.1 PBS PREPARATION

Materials/Reagent preparation

- Dulbecco's Phosphate-Buffered Saline powder (GIBCO #21600-044)
- Ultra-Pure (UP) water
- HCl (to lower pH)
- NaOH (to raise pH)
- Sterile filter 0.22 µm (Genesee #25-233)

Protocol steps

1. Dissolve 9.55 g of Dulbecco's Phosphate-Buffered Saline powder in 950 mL of UP water using a magnetic spin bar.
2. When dissolved, titrate with HCl or NaOH to achieve pH of 7.25±0.02 if used sterile or to 7.35±0.02 when planning to use non-sterile.
3. Top off to 1 L with UP water.
4. If required for cell culture or sterile culture, sterile filter under sterile conditions into an autoclaved 1 L glass bottle.

A3.2 MINIMUM ESSENTIAL MEDIA ALPHA MEDIUM (αMEM) PREPARATION

Materials/Reagent Preparation

- αMEM, 10% FBS, 1% P/S
- Minimum Essential Media Alpha Medium (αMEM) (GIBCO #12000-022)
- Ultra-pure (UP) water
- Sodium Bicarbonate ($NaHCO_3$) (Fisher Bioreagents #BP328-1)
- Fetal bovine Serum (FBS) (GenClone #25-514, Lot P110822)
- 10,000 U/mL Penicillin, 10 mg/mL Streptomycin (P/S) (Gemini Bio Products #400-109)
- HCl (to lower pH)
- NaOH (to raise pH)
- Sterile filter 0.22 µm (Genesee #25-233)

Protocol steps

1. Dissolve full media packet (α-MEM) in 850 mL of UP water.
   - Be sure to spray UP water within packet to get all the packet contents.
2. Add 2.2 g of sodium bicarbonate ($NaHCO_3$).
3. Add 100 mL of fetal bovine serum (FBS) to achieve 10 % in 1 L.
4. Add 10 mL of penicillin-Streptomycin (PS) to achieve 1% in 1 L.
5. Titrate with HCl or NaOH to achieve pH of 7.25±0.02.
6. Top off to 1 L with UP water.
7. Sterile filter under sterile conditions into an autoclaved 1 L glass bottle.
8. Keep in the fridge until use. Good for about 1 month.

A3.3 MSC CULTURE AND HANDLING

Materials/Reagent preparation

- Mesenchymal stem/stromal cells (MSC)
- Growth media (αMEM with 10% FBS + 1% P/S)
- PBS
- 0.25% Trypsin/0.1% EDTA, Corning™ 25053CI

Warm media (αMEM) and trypsin to 37ºC before starting.

Protocol steps

This protocol is written for cells with a fibroblast-like morphology (specifically mesenchymal stem/stromal cells, MSCs) cultured in T225 flasks. Volumes will have to be adjusted if a different cell type or flask size is used.

Passage cells when they reach 90-95% confluence.

1. Aspirate the media from the flask.
2. Rinse flask with sterile PBS to remove any remaining media which contains trypsin inhibitor. Aspirate.
3. Add 10 mL of Tryspin-EDTA solution to each flask.
4. Place flasks back in incubator (trypsin is a heat activated enzymatic solution).
5. Wait 5 min and check for cellular detachment.
   - Additional time can be added at 1 min intervals if a substantial number of cells remain adherent.
6. Add 10 mL media to each flask to neutralize the trypsin.
7. Pipette the trypsin + media + cell suspension out of the flask and into a 50 mL conical tube.
8. Count the cells using a Countess™ automated cell counter.
   - See Cell Countess™ protocol for cell counting instructions.
9. Pellet cell suspension via centrifugation (900 rpm for 8 min).
10. Aspirate the trypsin + media solution, taking care to not aspirate cell pellet.
11. Re-suspend cells in media at a concentration such that between 5×10^5 - 1×10^6 cells will be seeded per T225 flask.
    - T225 flasks seeded at 5×10^5 cells take ~1 week to reach confluency (donor and passage number dependent).
    - T225 flasks seeded at 1×10^6 cells take ~5 days to reach confluency (donor and passage number dependent).
12. Add media to the flask such that the total final volume will be 50 mL.
13. Add cell suspension at the desired seeding concentration to the flask using a micropipette.
14. Place flasks in incubator, change media every 2 to 3 days.

A3.4 CELL COUNTING WITH COUNTESS™ AUTOMATED CELL COUNTER

Materials/Reagent preparation

- Countess™ slides (Invitrogen #C10283) for cell counting are specific to the Countess™ cell counter and come with 0.4% trypan blue when purchased.
- The only additional materials needed are a sample of cell suspension, micropipettes, and pipette tips.

Protocol steps

1. Prepare the sample to be counted by adding 20 µL of your cell suspension to a microcentrifuge tube.
2. Add 20 µL of 0.4% trypan blue stain to the microcentrifuge tube.
3. Gently pipette up and down.
4. Load 10 µL of the sample mixture to each side of the Countess™ chamber slide.
5. Insert the slide, sample side up, into the slide port.
   - The instrument automatically illuminates the sample and focuses on the cells.
6. Press “Capture” and record the total cell number and percent viability.
7. To count the sample in the second chamber of the slide, remove and rotate the slide 180º, and reinsert the slide into the instrument. Repeat step 6.

Data analysis

1. If the viability was 90% or higher, average both total cell number counts.
2. Multiply this number by the volume of media you re-suspended your cells in before pelleting to calculate total cells.

A3.5 DULBECCO'S MODIFIED EAGLE MEDIUM (DMEM) PREPARATION

This protocol includes formulations to expand and differentiation myoblasts (*e.g.*, C2C12s)

Materials/Reagent preparation

Growth Medium (1L)

- Dulbecco's Modified Eagle Medium (DMEM) (GIBCO #12800-017)
- 890 mL ultra-pure (UP) water
- 3.7g sodium bicarbonate ($NaHCO_3$) (Fisher Bioreagents #BP328-1)
- 10 mL 10,000 Unit-10mg/mL Penicillin-Streptomycin (1%) (Gemini Bio Products #400-109)
- 100 mL Heat-inactivated Fetal Bovine Serum (FBS) (10%) (GenClone #25-514, Lot P110822)

Differentiation Medium (1L)

- Dulbecco's Modified Eagle Medium (DMEM)
- 970 mL UP water
- 3.7g sodium bicarbonate ($NaHCO_3$)
- 10 mL 10,000 Unit -10mg/mL Penicillin-Streptomycin (1%)
- 20 mL Heat-inactivated Horse Serum (2%), Thermo Cat.#26050088, Lot#2534240
    - Myotube formation is enhanced when the medium is supplemented with horse serum instead of FBS.

Note: To heat-inactivate serum, warm at 56°C for 30 min. Shake every 10 min or continuously.

Protocol steps

1. Dissolve full media packet (DMEM) in 850 mL of UP water.
    - Be sure to spray UP water within packet to get all the packet contents.
2. Add 3.7 g of sodium bicarbonate ($NaHCO_3$).
3. Add aliquots of Penicillin-Streptomycin and FBS or horse serum
4. Titrate with HCl or NaOH to achieve pH of 7.25±0.02.
5. Top off to 1 L with UP water.
6. Sterile filter under sterile conditions into an autoclaved 1 L glass bottle.
7. Keep in the fridge until use. Good for about 1 month.

A3.6 C2C12 CULTURE AND HANDLING

Materials/Reagent preparation

- Murine C2C12 myoblasts
- Growth media (DMEM with 10% FBS + 1% P/S)
- PBS
- 0.25% Trypsin/0.1% EDTA (Corning™ #25053CI)

Warm media (DMEM) and trypsin to 37°C before starting.

Protocol steps

- *IMPORTANT - DO NOT ALLOW CULTURES TO BECOME CONFLUENT
- This protocol is written for culture in a T225 flask.

Cell thawing

1. Thaw the vial in water bath at 37°C until just thawed (~2 min).
2. Transfer vial contents into a centrifuge tube with 9 mL of growth medium.
3. Spin at 125 × *g* for 7 min.
4. Discard the supernatant and resuspend the cell pellet in fresh growth medium.
5. Seed new flasks at cell concentration of 5×10^3 viable cells/cm^2.
   - This corresponds to about 3.75×10^5 viable cells for a T75 flask.
   - This corresponds to about 1.125×10^6 viable cells for a T225 flask.

Maintenance

1. Growth medium in the flask must be changed every 2-3 days after the initial seeding.
2. Split cells once the cells in the flask have reached 70% confluence.
   - Cultures must not be allowed to become confluent as this will deplete the myoblastic population in the culture.
   - Confluent C2C12 cultures will begin differentiation into myotubes.

Differentiation

1. Seed cells in a well plate at concentration of ~ 5×10^4 viable cells/cm^2.
    a. Seed cells at confluence to increase rate of differentiation.
    b. 6 well plate (Area = 9.5 cm^2) – ~47,500 cells
    c. 12 well plate (Area = 3.8 cm^2) – ~19,000 cells
    d. 24 well plate (Area = 1.9 cm^2) -- ~9,500 cells
2. Culture cells in differentiation medium to promote myogenic differentiation.
3. Change medium every other day.
4. After roughly 5-6 days in culture the myoblasts will differentiate into skeletal muscle myotubes.

Subculture

*Note: Passage >15 will have reduced proliferation/differentiation.

1. Aspirate the media from the flask.
2. Rinse flask with sterile PBS to remove any remaining media which contains trypsin inhibitor. Aspirate.
3. Add 10 mL of Tryspin-EDTA solution to each flask.
4. Place flasks back in incubator (trypsin is a heat activated enzymatic solution).
5. Wait 3-5 min and check for cellular detachment.
    - Additional time can be added at 1 min intervals if a substantial number of cells remain adherent.
    - To avoid clumping, do not agitate the cells by hitting or shaking the flask while waiting for the cells to detach.
6. Once cells have detached, add 20 mL media to each flask to neutralize the trypsin.
7. Pipette the trypsin + media + cell suspension out of the flask and into a 50 mL conical tube.
8. Count the cells using a Countess™ automated cell counter.
    - See Cell Countess™ protocol for cell counting instructions.
9. Pellet cell suspension via centrifugation (125 × *g* for 7 min).
10. Aspirate the trypsin + media solution, taking care to not aspirate cell pellet.
11. Seed new flasks at cell concentration of 5×10^3 viable cells/cm^2.
    - This corresponds to about 3.75×10^5 viable cells for a T75 flask.
    - This corresponds to about 1.125×10^6 viable cells for a T225 flask.
        a. 6 well plate (Area = 9.5 cm2) – ~47,500 cells
        b. 12 well plate (Area = 3.8 cm2) – ~19,000 cells
        c. 24 well plate (Area = 1.9 cm2) -- ~9,500 cells
12. Add media to the flask such that the total final volume will be 50 mL.

13. Add cell suspension at the desired seeding concentration to the flask using a micropipette.
14. Place flasks in incubator, change media every 2 to 3 days.

Cryopreservation

Cryopreservation Media is complete growth medium supplemented with 5 v/v% DMSO.

1. Based on cell count, calculate the number of vials needed for 1.125×10^6 viable cells in 950 µL for each vial.
2. Add freezing solution to cells for a resulting concentration of 1.125×10^6 cells/mL.
   - Note: add DMSO last, this is toxic to cells at room temperature.
   - Note: This means ~1.184×10^6 cells/mL before adding DMSO.
3. Pipette 1 mL of cell solution to each vial.
4. Place all vials in a cryopreservation vessel (*e.g.*, Mr. Frosty) and freeze at -80°C overnight.
5. Transfer all vials from -80°C to liquid nitrogen storage.

A3.7 PICOGREEN™ DNA ASSAY

This protocol is based on the Invitrogen™ Quant-iT™ PicoGreen™ dsDNA Assay Kit's (Thermo Fisher Scientific #P11496) instructions. Samples should be collected in an appropriate volume of 5X Passive Lysis Buffer (PLB) (Promega #E1910) diluted to 1X for this procedure.

Materials/Reagent preparation

- 1X TE Buffer
  - 2.5 mL of 20X stock solution in 47.5 mL of Ultra-pure H_2O
- Working strength PicoGreen™
  - 5 µL of 200x stock from freezer per 1 mL of TE buffer
  - MAKE FRESH AND PROTECT FROM LIGHT
- DNA standard

Protocol steps

1. This protocol is performed in a black opaque round-bottom 96-well plate
2. Prepare the DNA Standard Curve (1000, 100, 10, 1, 0 ng)
   - Add 6 µL of 50x λ-DNA standard to 294 µL of TE for a 1000 ng/mL standard. Mix well.
   - Add 225 µL of TE buffer to each of 3 additional tubes. Transfer 25 µL of 1000 ng/mL standard to the first tube and mix well. Repeat serial dilution for each of the following tubes.

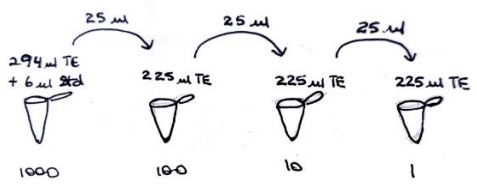

3. Transfer 100 µL of each DNA standard concentration to a 96-well plate in duplicate. Add 100 µL of TE buffer for the 0 ng standard.
4. Thaw samples in 1X PLB if necessary and sonicate for approximately 20 s at 40% power.
5. Spin down samples at 5000 × *g* for 5 min to pellet cell debris.
6. Add 75 µL of TE buffer to each sample well of the 96-well plate, and pipette 25 µL of each sample to the plate in triplicate.
7. Add 100 µL of working strength PicoGreen™ to each well of the plate containing DNA (both samples and standards).
8. Incubate in the dark for 5 min and quantify fluorescence at 528 nm excitation/485 nm emission on a plate reader.

Data analysis

1. Subtract the reagent's blank fluorescence reading from each sample. Plot a standard curve of DNA concentration against fluorescence (RFU).

			Avd Std F	Rel Std F
1000	43599	43162	43380.5	43291
100	4616	4536	4576	4486.5
10	662	632	647	557.5
1	154	152	153	63.5
0	93	86	89.5	0

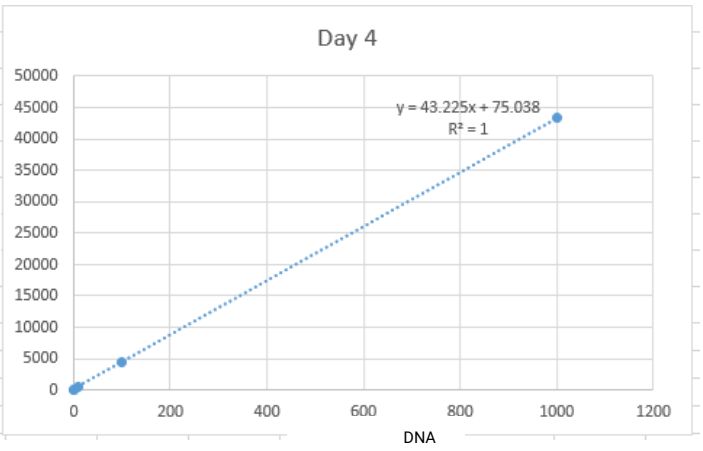

2. Using the standard curve, determine the DNA concentration of each unknown sample.
   - Concentration × 4 (*i.e.*, the sample was diluted 1:3 with TE buffer) × mL of solution sample collected in.

					Anything over 20% is out	x=(y-66753)/290016		(mulitply by volume of PLB used for collection)
Sample Numbe	Reading 1	2	AVERAGE	ST DEV	Cv (standard dev. Over avg	Concentration (ng/ml)	Concentration * 4 (based on dilutio	Total DNA (ng)
1	730696	748617	739656.5	12672.06063	0.017132359	2.320228884	9.280915536	3.712366214
2	743951	982200	863075.5	168467.4835	0.195194376	2.745788163	10.98315265	4.393261061
3	887057	885789	886423	896.6113985	0.001011494	2.826292342	11.30516937	4.522067748
4	745566	780737	763151.5	24869.6526	0.032588094	2.401241656	9.604966623	3.841986649

A3.8 RNA ISOLATION USING TRIZOL™ REAGENT

This protocol is based on the TRIzol™ Reagent (Thermo Fisher Scientific #15596018) instructions.

Materials/Reagent preparation

- TRIzol™ Reagent
- Chrolorform, molecular biology grade (Fisher Scientific # ICN19400290
- Isopropanol, molecular biology grade (Fisher Scientific #BP2618500)
- Ethanol, molecular biology grade (Millipore Sigma #E7023)
- Homogenizer (*e.g.*, Tissue Tearor)
- Nanodrop machine (*e.g.*, Nanodrop One©, Thermo Fisher Scientific)

Protocol steps

1. Lyse and homogenize samples in TRIzol™ Reagent according to your starting material.
- Tissues:
    i. Add 1 mL of TRIzol™ Reagent per 50–100 mg of tissue to the sample and homogenize using a homogenizer.
- Cell grown in monolayer:
    i. Remove growth media.
    ii. Add 0.3–0.4 mL of TRIzol™ Reagent per 1×10^5—10^7 cells directly to the culture dish to lyse the cells.
    iii. Pipet the lysate up and down several times to homogenize.
2. Incubate for 5 min to allow complete dissociation of the nucleoproteins complex.
3. Add 0.2 mL of chloroform per 1 mL of TRIzol™ Reagent used for lysis, securely cap the tube, then thoroughly mix by shaking.
4. Incubate for 2–3 min.
5. Centrifuge the sample for 15 min at 12,000 × *g* at 4°C.
    - The mixture separates into a lower red phenol-chloroform, an interphase, and a colorless upper aqueous phase.
6. Transfer the aqueous phase containing the RNA to a new tube by angling the tube at 45° and pipetting the solution out.
    - IMPORTANT! Avoid transferring any of the interphase or organic layer into the pipette when removing the aqueous phase.
7. (Optional) If the starting sample is small ($<10^6$ cells or <10 mg of tissue), add 5–10 µg of RNase-free glycogen as a carrier to the aqueous phase.
    - Note: The glycogen is co-precipitated with the RNA but does not interfere with subsequent applications.

8. Add 0.5 mL of isopropanol to the aqueous phase per 1 mL of TRIzol™ Reagent used for lysis.
9. Incubate for 10 min at 4°C.
10. Centrifuge for 10 min at 12,000 × *g* at 4°C.
    - Total RNA precipitate forms a white gel-like pellet at the bottom of the tube.
11. Discard the supernatant with a micropipettor.
12. Resuspend the pellet in 1 mL of 75% ethanol per 1 mL of TRIzol™ Reagent used for lysis.
    - Note: The RNA can be stored in 75% ethanol for at least 1 year at -20°C, or at least 1 week at 4°C.
13. Vortex the sample briefly then centrifuge for 5 min at 7500 × *g* at 4°C.
14. Discard the supernatant with a micropipettor.
15. Vacuum or air dry the RNA pellet for 5–10 min.
    - IMPORTANT! Do not dry the pellet by vacuum centrifuge. Do not let the RNA pellet dry, to ensure total solubilization of the RNA. Partially dissolved RNA samples have an A230/280 ratio <1.6.
16. Resuspend the pellet in 20–50 µL of RNase-free water, 0.1 mM EDTA, or 0.5% SDS solution by pipetting up and down.
    - IMPORTANT! Do not dissolve the RNA in 0.5% SDS if the RNA is to be used in subsequent enzymatic reactions.
17. Incubate in a water bath or heat block set at 55-60°C for 10-15 min.
18. Quantify RNA quality and quantity by reading 1 µL samples on a Nanodrop reader.
19. Proceed to downstream applications, or store the RNA at -70°C.

A3.9 RNA CONVERSION TO cDNA VIA REVERSE TRANSCRIPTION

This protocol is based on the QuantiTect Reverse Transcription Kit (Qiagen #205313) instructions.

Materials/Reagent preparation

- Two heat blocks that can accommodate microcentrifuge tubes. Set one heat block to 42°C and the other to 95°C.
- Thaw template RNA on ice.
- Thaw gDNA Wipeout Buffer, Quantiscript® Reverse Transcriptase, Quantiscript RT Buffer, RT Primer Mix and RNase-free water at room temperature (15–25°C).
- Mix each solution by flicking the tubes. Centrifuge briefly to collect residual liquid from the sides of the tubes, and then keep on ice.

Protocol steps

1. Prepare the genomic DNA elimination reaction on ice according to **Table A3.1** below. Mix and then keep on ice.

Table A3.7: Genomic DNA elimination reaction components.

Component	Volume/reaction
gDNA Wipeout Buffer, 7x	2 µl
Template RNA, up to 1 µg*	Variable
RNase-free water	Variable
Total reaction volume	14 µl

   - *This amount corresponds to the entire amount of RNA present, including any rRNA, mRNA, viral RNA and carrier RNA present, and regardless of the primers used or cDNA analyzed.
   - Use the variable volumes to reverse transcribe an equal mass of RNA in each reaction. This theoretically means the same mass of DNA will be used in each PCR reaction.
2. Incubate for 2 min at 42°C, then place immediately on ice.
   - Note: Do not incubate at 42°C for longer than 10 min.
3. Prepare the reverse-transcription master mix on ice according to **Table A3.2**. Mix and then keep on ice. The reverse-transcription master mix contains all components required for first-strand cDNA synthesis except template RNA.

- Note: If setting up more than one reaction, prepare a volume of master mix 10% greater than that required for the total number of reactions to be performed. Distribute the appropriate volume into individual tubes.
- Note: If using >1 µg RNA, scale up the reaction linearly. For example, if using 2 µg RNA, double the volumes of all reaction components for a final 40 µl reaction volume.

4. Add template RNA from step 3 (14 µl) to each tube containing reverse-transcription master mix. Mix and then store on ice.

Table A3.8: Reverse-transcription reaction components.

Component	Volume/reaction
Reverse-transcription master mix **Quantiscript Reverse Transcriptase***	1 µl
Quantiscript RT Buffer, 5x†	4 µl
RT Primer Mix	1 µl
Template RNA **Entire genomic DNA elimination reaction (step 3)**	14 µl (added at step 5)
Total reaction volume	20 µl

* Also contains RNase inhibitor.
† Includes Mg2+ and dNTPs.

5. Incubate for 15 min at 42°C.
   - Note: In some rare cases (*e.g.*, if the RT-PCR product is longer than 200 bp or if analyzing RNAs with a very high degree of secondary structure), increasing the incubation time up to 30 min may increase cDNA yields.
6. Incubate for 3 min at 95°C to inactivate Quantiscript Reverse Transcriptase.
7. Place the reverse-transcription reactions on ice and dilute cDNA with DNAse- and RNAse-free, ultra-pure water to achieve a concentration of 12.5 ng/µL.
8. Proceed directly with real-time PCR. For long-term storage, store reverse-transcription reactions at -20°C.

A3.10 POLYMERASE CHAIN REACTION (PCR)

This protocol is based on the *Taq* PCR Master Mix Kit's (Qiagen #201445) instructions.

Materials/Reagent preparation

- PCR thermocycler (*e.g.*, QuantStudio™ 6, Thermo Fisher Scientific)
- MicroAmp™ Fast Optical 96-well reaction plate, 0.1 mL (Thermo Fisher Scientific #4346907)
- MicroAmp™ Optical Adhesive Film (Thermo Fisher Scientific #4311971)
- Gene primers (Thermo Fisher Scientific #4331182)
- Thaw primer solutions and template nucleic acid. Keep on ice after complete thawing, and mix thoroughly before use.
- Thaw Taq PCR Master Mix and mix by vortexing briefly to avoid localized differences in salt concentration.

Protocol steps

1. Prepare a reaction mix according to **Table A3.3**.
   - Note: The reaction mix typically contains all the components required for PCR except the template DNA. Prepare a volume of reaction mix 10% greater than that required for the total number of reactions to be performed.

Table A3.9: Reaction setup using Taq PCR Master Mix.

Component	Volume/reaction
Reaction mix Taq PCR Master Mix, 2x	5 µl
10x primer mix (2 µM of each primer)	0.5 µl
RNAse-free water (provided)	2 µl
Template DNA (added at step 5)	2.5 µl (added at step 5)
Total reaction volume	10 µl

2. Mix the reaction mix gently but thoroughly, for example by pipetting up and down a few times. Dispense appropriate volumes into PCR tubes or the wells of a PCR plate.
3. Load diluted cDNA to each well.
4. Cover the plate with a plate sealer and seal each well.
   - First, remove any bubbles or wrinkles by scrubbing a crumpled Kim wipe all over the plate sealer surface. Next, run the thin edge of an implement around the entire plate seal (in a rectangle). Then run the implement between each row and each column.

5. Pull the side strips out from the plate (not up).
6. Centrifuge the plate at 900 rpm for 1 min.
7. Run the reaction using a thermocycle programmed according to the manufacturer's instructions. A typical PCR cycling program is outlined in **Table A3.4**.

Table A3.10: Optimized PCR cycling conditions.

Step	Time	Temperature
Initial denaturation	3 min	94°C
3-step cycling:		
1. Denaturation	30 s	94°C
2. Annealing	30 s	65
3. Extension	1 min	72°C
Number of cycles	40	
Final Extension	10	72°C

A3.11 PIERCE™ BCA ASSAY

This protocol is based on the Pierce™ BCA Protein Assay Kit (Thermo Fisher Scientific #23225) instructions.

Materials/Reagent preparation

- Preparation of diluted albumin (BSA) standards
    - Dilute the contents of one Albumin Standard (BSA) ampule into several clean vials, preferably using the same diluent as the samples.
    - Use the **Table A3.5** as a guide to prepare a set of protein standards.
    - Each 1 mL ampule of 2 mg/mL Albumin Standard is sufficient to prepare a set of diluted standards for either working range suggested in the table. There will be sufficient volume for three replications of each diluted standard.

Table A3.11: Preparation of diluted albumin (BSA) standards for the standard microplate procedure.

Vial	Volume of Diluent (µL)	Volume and Source of BSA (µL)	Final BSA Concentration (µg/mL)
A	0	300 of Stock	2000
B	125	375 of Stock	1500
C	325	325 of Stock	1000
D	175	175 of B	750
E	325	325 of C	500
F	325	325 of E	250
G	325	325 of F	125
H	400	100 of G	25
I	400	0	0

- Preparation of the BCA working reagent (WR)
    - Use the following formula to determine the total volume of WR required:
      (# standards + # unknowns) × (# replicates) × (volume of WR per sample) = total volume WR required
        - Example: for the standard test-tube procedure with 3 unknowns and 2 replicates of each sample:
          (9 standards + 3 unknowns) × (2 replicates) × (2 mL) = 48 mL WR required
        - Note: 2.0 mL of the WR is required for each sample in the test-tube procedure, while only 200 µl of WR reagent is required for each sample in the microplate procedure.

- Prepare WR by mixing 50 parts of BCA Reagent A with 1 part of BCA Reagent B (50:1, Reagent A:B). For the above example, combine 50 mL of Reagent A with 1 mL of Reagent B.
    - Note: When Reagent B is first added to Reagent A, turbidity is observed that quickly disappears upon mixing to yield a clear, green WR.
    - Prepare sufficient volume of WR based on the number of samples to be assayed. The WR is stable for several days when stored in a closed container at room temperature (RT).

Protocol steps

1. Pipette 25 µL of each standard or unknown sample replicate into a microplate well
    - Note: If sample size is limited, 10 µL of each unknown sample and standard can be used (sample to WR ratio = 1:20). However, the working range of the assay in this case is be limited to 125–2000 µg/mL.
2. Add 200 µL of the WR to each well and mix plate thoroughly on a plate shaker for 30 s.
3. Cover plate and incubate at 37°C for 30 min.
4. Cool plate to RT. Measure the absorbance at or near 562 nm on a plate reader.

Data analysis

1. Subtract the average 562 nm absorbance measurement of the Blank standard replicates from the 562 nm measurements of all other individual standard and unknown sample replicates.
2. Prepare a standard curve by plotting the average Blank - corrected 562 nm measurement for each BSA standard vs. its concentration in µg/mL. Use the standard curve to determine the protein concentration of each unknown sample.
    - Note: If using curve-fitting algorithms associated with a microplate reader, a four-parameter (quadratic) or best-fit curve provides more accurate results than a purely linear fit. If plotting results by hand, a point-to-point curve is preferable to a linear fit to the standard points.

A3.12 MICRO BCA™ ASSAY

This protocol is based on the Micro BCA™ Protein Assay Kit (Thermo Fisher Scientific #23235) instructions.

Materials/Reagent preparation

- Preparation of Diluted Albumin (BSA) Standards
    - Use **Table A3.6** as a guide to prepare a set of protein standards. Dilute the contents of one Albumin (BSA) Standard ampule into several clean vials, preferably using a diluent similar to the sample buffer.

Table A3.12: Preparation of diluted albumin (BSA) standards for the Micro BCA™ microplate procedure.

Vial	Volume of Diluent (mL)	Volume and Source of BSA (mL)	Final BSA Concentration (µg/mL)
A	4.5	0.5 of Stock	200
B	8.0	2.0 of A	40
C	4.0	4.0 of B	20
D	4.0	4.0 of C	10
E	4.0	4.0 of D	5
F	4.0	4.0 of E	2.5
G	4.8	3.2 of F	1
H	4.0	4.0 of G	0.5
I	8.0	0	0

- Preparation of the Micro BCA Working Reagent (WR)
    - Use the following formula to determine the total volume of WR required:
      (# standards + # unknowns) × (# replicates) × (volume of WR per sample) = total volume WR required
        - Example: for the standard Test Tube Procedure with 3 unknowns and 2 replicates of each sample:
          (9 standards + 3 unknowns) × (2 replicates) × (1 mL) = 24 mL WR required (round up to 25 mL)
        - Note: 1 mL of the WR is required for each sample in the Test Tube Procedure, while only 150 µL of WR is required for each sample in the Microplate Procedure.
    - Prepare WR by mixing 25 parts of Micro BCA Reagent MA and 24 parts Reagent MB with 1 part of Reagent MC (25:24:1, Reagent MA:MB:MC). For the above example, combine 12.5 mL of Reagent MA and 12.0 mL Reagent MB with 0.5 mL of Reagent MC.

- Note: When Reagent MC is initially added to Reagents MA and MB, turbidity occurs that quickly disappears upon mixing to yield a clear-green solution. Prepare sufficient volume of WR based on the number of samples to be assayed.
- The WR is stable for one day when stored in a closed container at room temperature (RT). It is not necessary to protect the solution from light.

Protocol steps

1. Pipette 150 µL of each standard or unknown sample replicate into a microplate well.
2. Add 150 µL of the WR to each well and mix plate thoroughly on a plate shaker for 30 seconds.
3. Cover plate using Sealing Tape for 96-Well Plates (Product No. 15036) and incubate at 37°C for 2 h.
   - Note: Limit incubations of microplate to less than or equal to 37°C, otherwise high background and aberrant color development may result. Most polystyrene assay plates deform, leach, and become cloudy at 60°C.
4. Cool plate to room temperature (RT).
5. Measure the absorbance at or near 562 nm on a plate reader.

Data analysis

1. Subtract the average 562 nm absorbance reading of the Blank standard replicates from the 562 nm reading of all other individual standard and unknown sample replicates.
2. Prepare a standard curve by plotting the average Blank-corrected 562 nm reading for each BSA standard vs. its concentration in µg/mL. Use the standard curve to determine the protein concentration of each unknown sample.
   - Note: If using curve-fitting software, use a best-fit polynomial equation rather than a linear equation for the standard curve. If plotting results by hand, a point-to-point fit is preferable to a linear fit to the standard points.

A3.13 LIVE/DEAD STAINING

Materials/Reagent preparation

- Fluorescent microscope (*e.g.*, Nikon Eclipse T32000U)
- Dimethyl sulfoxide (DMSO)
- Phosphate-Buffered Saline (PBS)
- Calcein AM (Thermo Fisher Scientific #C3100MP)
    - Stock from vendor = 50 µg in powder form
    - Add 25 µL DMSO to the powder in the stock vial to make a 2 mM solution.
    - 2 µM solution is needed for imaging.
        - For example: Add 25 µL of the 2 mM calcein AM solution to 25 mL of sterile PBS to make a 2 µM solution. This must be done in biological hood with the light off.
- Propidium Iodide (Thermo Fisher Scientific #P3566)
    - Stock solution from the vendor is 1 mg/mL = 1.5 mM
    - 5 µM solution is needed for imaging.
    - Add propidium iodide to the same PBS that to which the calcein AM was added.
        - For example if 25 mL of PBS used in previous section add 83 µL of 1.5 mM stock propidium iodide to the same 25 mL PBS in biological safety cabinet with the light off.

Protocol steps

1. Rinse cells or gels with sterile PBS.
2. Add previously prepared staining solution directly to wells.
    - Add solution in the biological hood with the light off.
    - Make sure that the cells are completely covered.
3. Return cells or gels to the incubator and incubate for 30-60 min.

Imaging

1. Turn on the microscope and ensure the fluorescent lamp is on.
2. Place cells on microscope stage and focus using bright-field.
3. Turn off the bright-field light, and set the filter wheel to “GFP”.
4. Open the fluorescent lamp shutter.
5. In imaging software (*e.g.*, NIS Elements), use the auto expose feature, making sure to select the “FITC” filter.
6. Set the exposure time to slightly lower than the auto expose recommended to better visualize your cells and lessen background fluorescence.
7. Select “capture”.

8. Save the image, indicating that this is the “live” stain.
9. Reset the filter wheel to “TRITC”.
10. Change the filter on the computer to “TRITC”.
11. Select auto exposure for the new TRITC filter.
12. Set the exposure time to slightly lower than the auto expose recommended to better visualize your cells and lessen background fluorescence.
13. Select “capture”.
14. Save the image, indicating that this is the “dead” stain.
    - The LIVE/DEAD images can be merged to visualize colocalization of the dyes.
15. To compare viability between groups, the exposure time on each channel must remain constant.
    - If a 200 ms exposure time is used for the FITC channel for the positive control then 200 ms must be used for all live images.
    - If a 100 ms exposure time is used for the TRITC channel for the negative control then 100 ms must be used for all dead images.
    - It is acceptable for the FITC and TRITC channels to have different exposure times.

A3.14 DAPI AND PHALLOIDIN STAIN

Materials/Reagent preparation

- Fluorescent microscope (*e.g.*, Leica Stellaris Confocal)
- 4% Paraformaldehyde
- Dimethyl sulfoxide (DMSO)
- Phosphate-Buffered Saline (PBS)
- Alexa Fluor Phalloidin 488 (Thermo Fisher Scientific #A12379)
    - Stock from vendor = 300 U in powder form
    - Dissolve the vial contents in 150 µL of anhydrous DMSO to yield a 400X stock solution, which is equivalent to approximately 66 µM.
    - Working concentration = 1:400
        - Sample calculation: 25 µL 400X Phalloidin in 10 mL PBS
- 4',6-Diamidino-2-Phenylindole, Dihydrochloride (DAPI) (Thermo Fisher Scientific #D1306)
    - Stock from vendor = 500X DAPI
    - Working concentration = 1:500
        - Sample calculation: 20 µL 500X DAPI in 10 mL PBS
- Triton X-100 (Sigma #X100)
    - Working concentration = 0.5%
        - Sample calculation: 10 mL DI Water + 50 µL of Triton X-100

Protocol steps

1. Fix cells/scaffolds in 4% Paraformaldehyde at room temperature (RT) for 1 h or at 4°C overnight.
2. Wash cells/scaffolds with 1X PBS twice.
3. Permeabilize cells with 0.5% Triton X-100 for 5 min at RT.
4. Wash with PBS once.
5. Stain with Phalloidin working solution for 1 h at RT.
6. Wash with PBS twice.
7. Stain nuclei with a working concentration of DAPI for 10 min at RT.
8. Wash three times with PBS.
9. Image using fluorescent microscope (absorbance/emission: 540 nm/564 nm).

A3.15 ELLMAN'S ASSAY

This protocol is based on the Ellman's Reagent (Thermo Fisher Scientific #22582) user instructions.

Materials/Reagent preparation

- DTNB (Ellman's Reagent) (5,5-dithio-bis-(2-nitrobenzoic acid)
- Reaction Buffer: 0.1 M sodium phosphate, pH 8.0, containing 1mM EDTA
- Cysteine Hydrochloride Monohydrate: M.W. = 175.6
- Ellman's Reagent Solution: Dissolve 4mg Ellman's Reagent in 1 mL of Reaction Buffer

Protocol steps

1. Prepare a set of cysteine standards by dissolving Cysteine Hydrochloride Monohydrate in Reaction Buffer according to **Table A3.7**.

Table A3.13: Preparation of standard curve using Cysteine Hydrochloride Monohydrate.

Standard	Volume of Reaction Buffer (mL)	Amount of Cysteine	Final Concentration (mM)
A	100	26.34 mg	1.5
B	5	25 mL of A	1.25
C	10	20 mL of A	1.0
D	15	15 mL of A	0.75
E	20	10 mL of A	0.5
F	25	5 mL of A	0.25
G	30	0	0

2. Prepare a set of test tubes, each containing 50 µL of Ellman's Reagent Solution and 2.5 mL of Reaction Buffer.
3. Add 250 µL of each standard or unknown to the separate test tubes prepared in step 2.
   - Note: For the unknown(s), make dilutions so that the 250 µL sample applied to the assay reaction has a sulfhydryl concentration in the working range of the standard curve (0.1-1.0 mM is ideal).
4. Mix and incubate at room temperature for 15 min.
5. Measure absorbance at 412 nm.

Data Analysis

Plot the values obtained for the standards to generate a standard curve. Determine the experimental sample concentrations from this curve.

- Note: The most accurate results are obtained from the linear portion of the standard curve (*i.e.*, the portion yielding an R^2 value equal to 1.0. One or more of the high standards may exceed the linear range).

A3.16 MEASURING THE RHEOLOGICAL PROPERTIES OF HYDROGELS

Materials/Reagent preparation

- 8-mm cross-hatched stainless-steel geometry
- Make hydrogels with 8 mm diameter to fit the geometry.
- In between testing hydrogels should be kept in media to remain hydrated.
- Gels cannot be tested more than once, as the rheometer tests them to failure.

Protocol steps

1. Turn on the air supply to the rheometer.
   - ➢ Pressure requirements for all DHR models: 30 psi.
2. Remove the black bearing lock by holding it in place while turning the draw rod knob at the top in a counter-clockwise direction. Once the bearing lock is removed, make sure that the spindle rotates freely.
   - ➢ NOTE: If air supply is interrupted while bearing lock is off, DO NOT TURN the DRIVE SHAFT; this will cause damage to the radial bearing. Locate another gas source, attach it to the gas port on the rheometer, and then attach bearing lock while the radial air bearing is floating.
3. Turn on the power to the rheometer.
4. Switch the power button, located on the rear of the electronics control box, to the ON position.
   - ➢ NOTE: If step 3 is performed before step 2, an alarm will sound and the instrument controller display will read “optical init. fail”. At this point, turn off the power and perform step 2.
5. When the instrument has finished the system check, start the instrument control software: Start>Programs>TA Instruments TRIOS>TRIOS. Then click “connect” to begin communication to your rheometer. You can also double-click on the TRIOS icon shortcut located on your PC desktop.
6. Determine the instrument inertia by selecting under the File Manager, the *Calibration tab* and then *Instrument*.

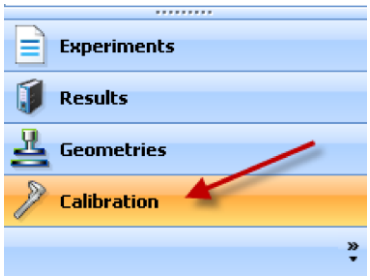

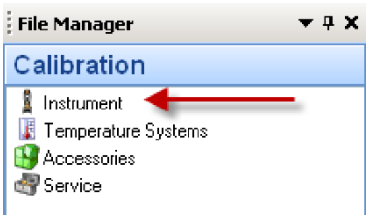

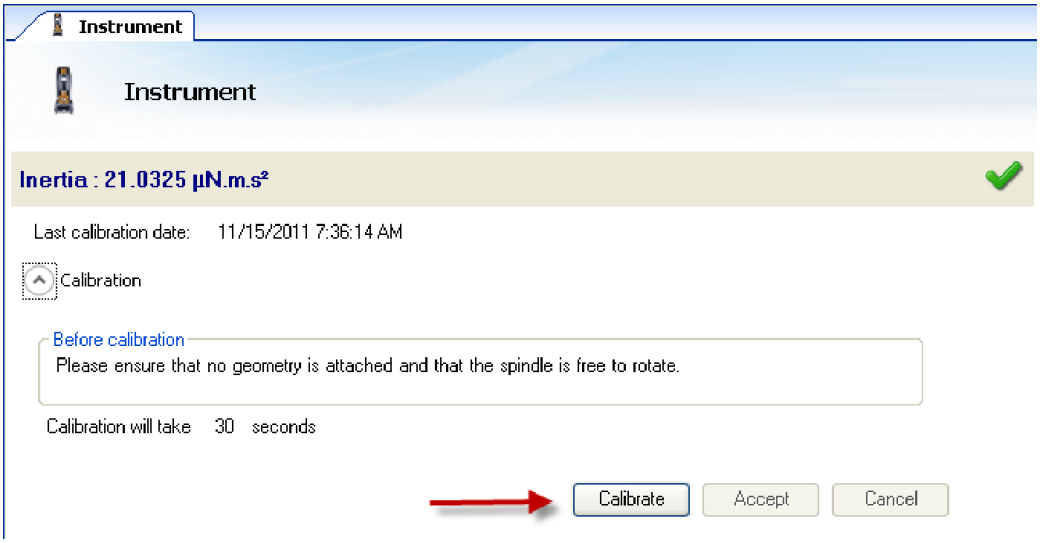

- This value is unique for each bearing assembly. An acceptable range for this value is ~21 – 22 µNms^2 for the DHR series. The value for the instrument should not change by more than 10% of the original Inertia value.
- NOTE: This calibration is recommended to be performed each time upon startup.

7. Attach test geometry by sliding it up the drive shaft and hold it stationary while turning the draw rod at the top in a clockwise direction. If the smart swap 3 geometry option "smart swap enabled" is selected, the appropriate geometry file is automatically applied to your experiment. If the smart swap geometry option is disabled, choose the appropriate geometry from the list of geometry files previously created, or create a new geometry by selecting NEW, and follow the New Geometry Wizard.

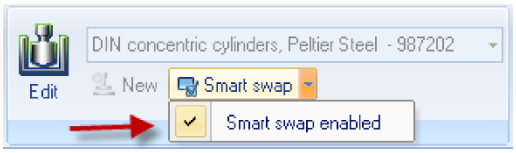

8. Determine the geometry inertia by selecting under the File Manager, the *Geometries* tab, *Calibrations* page, and then *Calibrate*.

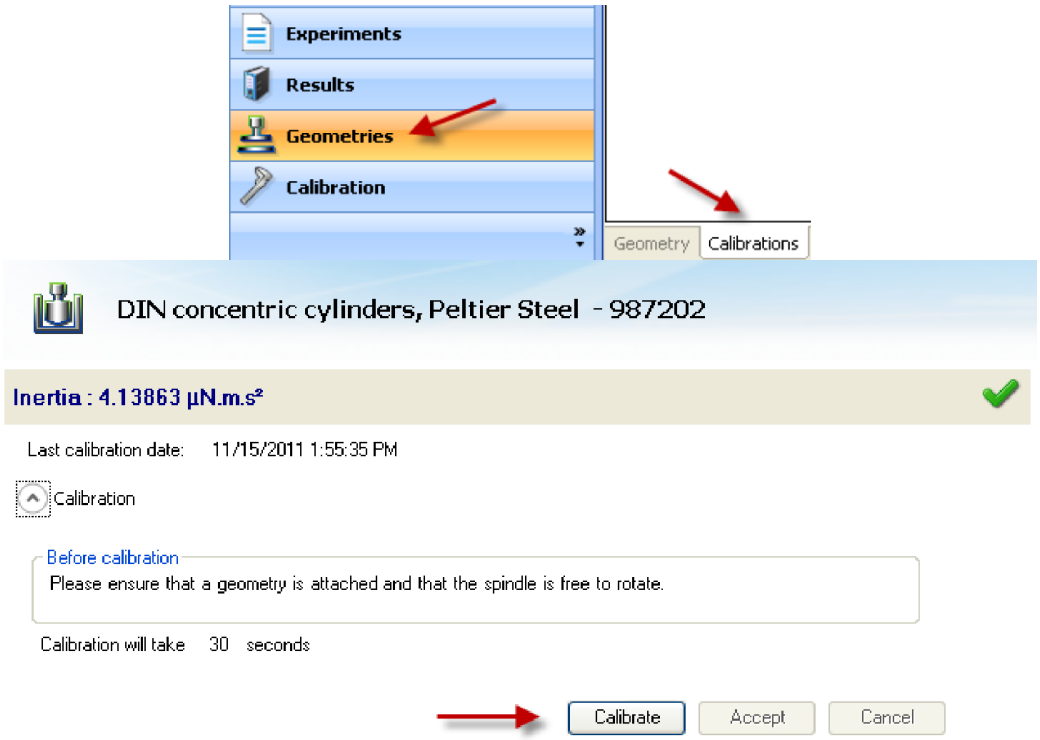

- The value of the inertia for each measuring system differs because they all have been uniquely engineered and have different masses. It is important to calibrate the inertia value for each geometry, particularly if high frequency oscillations are being used, or if low viscosity fluids are being measured.
- NOTE: This calibration is required when a new geometry file is first setup. For verification purpose, one can do it any time when changing geometry, but this is not required.

9. Calibrate bearing friction correction
   - A magnetic bearing is used to set the drive shaft afloat and provide virtually friction free application of torque to the sample. However, there will always be some residual friction. With most test materials, this is insignificant, but in about 1% of the low viscosity samples, this inherent friction causes inaccuracies in the final rheological data. To overcome this, the software has a bearing friction correction that should be activated. The bearing friction value without any geometry attached is ~0.25 – 0.3 µNm/(rad/s). With attaching a geometry, this value may raise up to about 0.3 – 0.5 µNm/(rad/s). Bearing friction correction can be found just below the Geometry Inertia calibration.

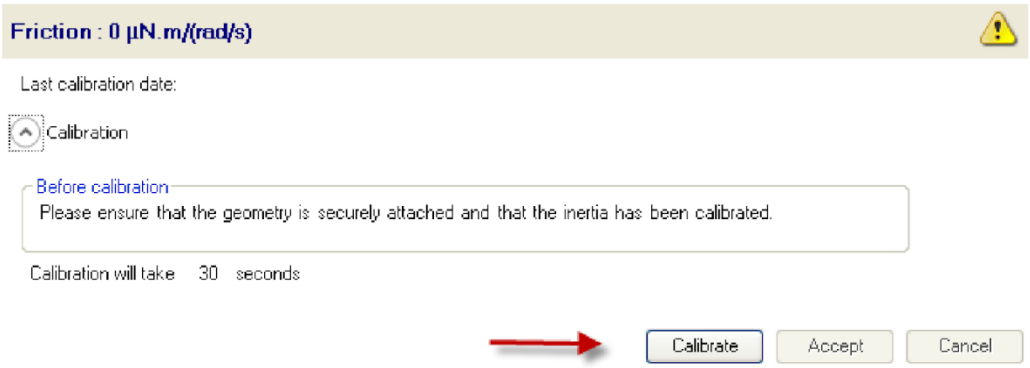

- NOTE: Please ensure that the Instrument Inertia (step 6) and Geometry Inertia (step 8) have been calibrated before determining the bearing friction correction value.
- NOTE: This calibration is required when a new geometry file is first setup. For verification purpose, one can do it any time when changing geometry, but this is not required.

10. Locate the zero gap icon located on the Front Control Panel of the DHR, or select GAP from the Control Panel and follow the directions on the screen.

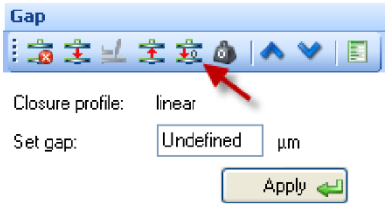

- NOTE: The upper geometry should be at the testing temperature before zeroing the gap. This will account for the change in dimensions due to the coefficient of thermal expansion of the testing geometry/system.
- NOTE: Zero gap needs to be performed every time when the geometry is removed or replaced. The gap closure profile options are located in Options> GAP

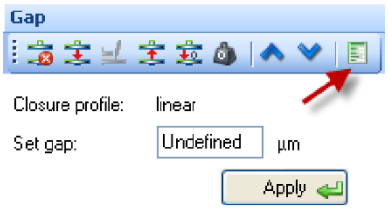

11. Perform a rotational mapping.
    - Due to the micron-level tolerances needed to make the magnetic bearing to work, any bearing will have small variations in torque behavior around one complete revolution of the shaft. They are consistent over time unless changes occur in the magnetic bearing.
    - By combining the absolute angular position data from the optical encoder with microprocessor control of the motor, these small variations can be mapped

automatically and stored in memory for subsequent real-time corrections in the test.

- To create a mapping, the software rotates the drive shaft at a fixed speed, monitoring the torque required to maintain this speed through a full 360° of rotation. These variations in torque can then be accounted for automatically by the microprocessor, which is in effect carrying out a baseline correction of the torque. This results in a very wide operating range of the bearing without operator intervention – a confidence check in bearing performance.
- Perform a rotational mapping on the geometry when the test procedure will be applying either a flow or transient (Creep or Stress Relaxation) mode of deformation.
- Hold the “Lock” button on the instrument control panel until you hear a beeping. This will lock the drive shaft to its “home” position. Then attach the geometry with the line on the side aligned with the maker on the bottom of the instrument head.

12. Begin the rotational mapping by going to the Geometries tab, *Calibrations* page, and then choose *Rotational Mapping*.

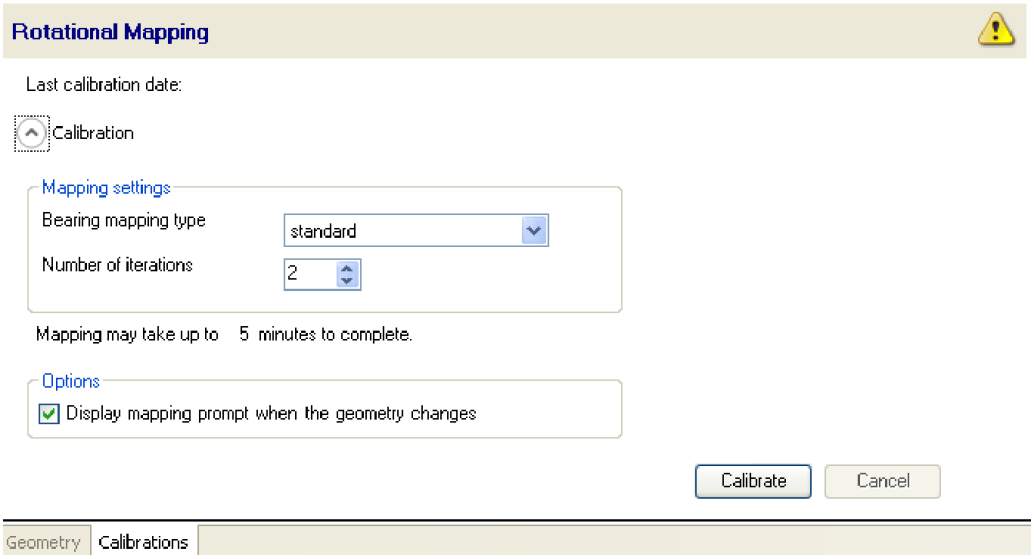

- The number of points in the map and the speed of rotation used are dependent upon the mapping type used. When mapping the geometry, the recommended settings are two iterations and standard type. For critical low-torque measurements, using < 1 µNm, precision mapping with two iterations is more suited. When using fast, standard or precision mapping the number of iterations should be set greater than one. If performing Creep procedure and using fast, standard or precision mapping, the number of iterations should be set to four, if the Recovery step is set to zero. Otherwise, setting the number of iterations greater than three has diminishing returns in the mapping performance.
- NOTE: This calibration is required when a new geometry file is first setup. The mapping history is recorded in each individual geometry file. If every time the geometry is loaded at the "home" position. There is no need for any additional mapping.

13. Create a new procedure by selecting Procedure from the Experiments tab or open a previously created procedure by selecting the appropriate file. The procedure can be viewed, edited, and adapted in the Procedure segments.

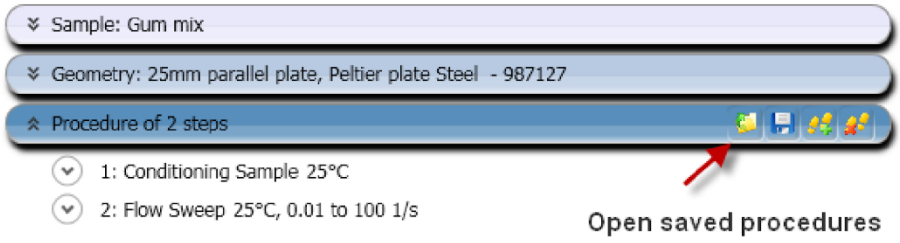

14. Select the directory/folder from File Path to save your data file. Experimental tests will auto-save directly to the designated folder. The name of the file can be the

same as your sample name or others by adding more Tokens. The sample information can be entered in the Notes box.

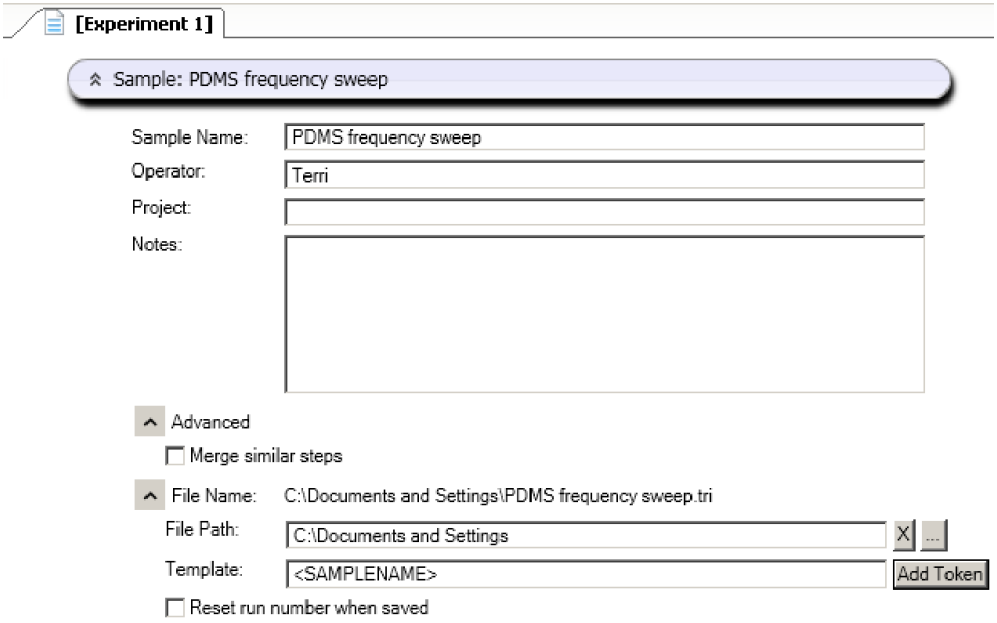

15. Load sample
    - The amount of sample volume that is required, based on the dimensions entered in the Geometry step for a cone, parallel plate and concentric cylinder systems, can be found in the Geometry Information step.
    - Avoid contact between a metal spatula used to transfer a sample and the metal stage.
16. Close the gap after loading a sample using one of three methods
    i. Manually enter the desired gap in the Control Panel – Gap window
    ii. Automatically have the instrument go to the gap value entered in the Geometry file information.
    iii. Manually raise or lower the gap by using the Front Control Panel arrows.
    - NOTE: The up and down arrows are also available in the Control Panel – Gap
    - NOTE: When using the cone geometry, the gap set must be equal to the truncation gap value that is scribed on the geometry shaft or stored in the smart swap file.
    - NOTE: When using the parallel plate geometry, the gap is variable, and should be between 500 microns and geometry diameter (microns)/10.
17. Trim the gap by loading extra material and close the gap to a value of 10% larger than the required gap, so that excess material is expelled from between the upper geometry and ower plate, (*i.e.*, overfilled state). Then lock the bearing with the bearing lock button on the Front Panel in order to keep the geometry from rotating, and trim the excess material using a right edged tool. Then lower the gap to the final test gap. The correct filling condition is shown in the following picture. You can also lower the gap until the axial force reads ~0.1 N.

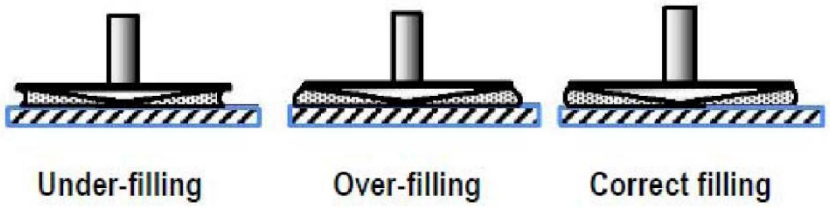

Proper loading of sample after closing the gap for cone and parallel plate geometry systems

18. Run a test by selecting the start experiment icon. 

Data analysis

Take the values at the horizontal linear region of the storage modulus and average these values to get the modulus.

A3.17 CHARACTERIZING HYDROGEL CONDUCTIVITY

Materials/Reagent preparation

- Power supply (*e.g.*, BK Precision #1735A)
- Digital multimeter (*e.g.*, SparkFun Electronics #VC830L)
    - Requires a 9V battery
- Angle vise (*e.g.*, Amazon # B0B4KM6CPG)
- Alligator clips
- 2 brass plates, each with an end bent at an angle
- Insulating material (*e.g.*, PDMS, silicone rubber, etc.)
- Calipers
    - Requires a coin 357 battery
- Spatula
- Something to record results (*e.g.*, pen and paper if you do not want to record directly into a digital spreadsheet).

*Allow adequate time for the power supply to warm up prior to testing per the manufacturer's instructions. If no instructions are provided, allow 2 hours.

Protocol steps

<u>Circuit setup</u>

1. Ensure all tools are dry before testing.
2. Use insulating materials as a layer between the brass plates and the jaws of the angle vise.
3. Slowly lower the top jaw of the angle vise to sandwich an insulating material between the brass plates.
4. Attach alligator clips to each brass plate.
5. Attach the free end of one clip to the red lead of the multimeter. Attach the free end of the other clip to the black lead of the power supply.
6. Use another alligator clip to connect the black lead of the multimeter to the red lead of the power supply.
7. Confirm you have set up your circuit correctly by switching the multimeter to the Continuity Buzzer setting (pink asterisk) and gently touch the plates together. The buzzer should sound, indicating a short circuit.
    - Note: If the buzzer does not sound, try connecting different leads within the system (*e.g.*, the red lead of the power supply to a brass plate or the black lead of the multimeter to the brass plate).

Material testing

1. Blot your material to remove excess storage liquid (*e.g.*, media, water) before testing.
2. Repeat steps 1-6 above, but instead of using an insulating material in step 3, use your test material.
3. Use a thin sheet of insulating material with a cutout to accommodate the material you are testing to prevent movement of your sample.
   - Note: This also creates a gap between the brass plates and ensures that the current measured is only what travels through the material
   - Tip: If your material is very thin, use labeling tape to create a thinner barrier between the brass plates.
4. Switch the multimeter to the lowest read setting in the current mode (*i.e.*, 20 µA, blue asterisk)
5. Use the course and fine knobs in the voltage section of the power supply to apply voltage to the material.
   - Note: The maximum voltage that should be applied to a water-based material (*i.e.*, hydrogels) is 500 mV. Higher voltages may result in electrolysis, which not only confounds results, it also destroys your material.

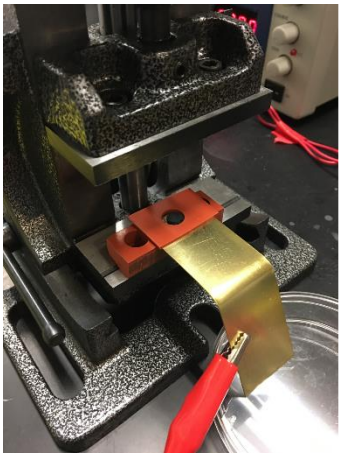
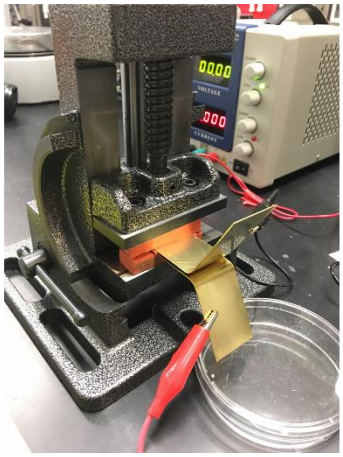
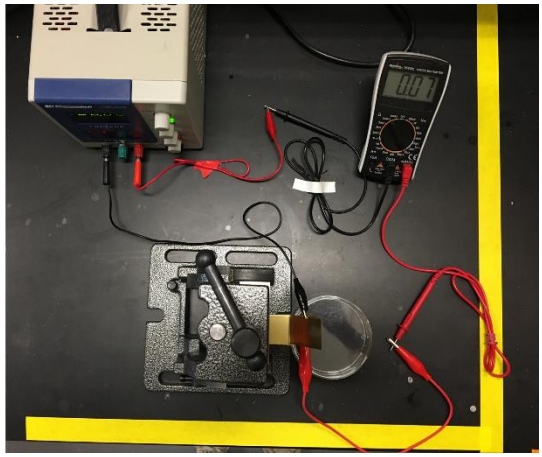

   - Tip: The course knob is VERY sensitive. If you are new to testing with this setup, practice using an insulating material (*i.e.*, a PDMS block).
6. For the first voltage tested, allow the system to equilibrate for 30 s. Record the current reading on the multimeter.
   - Note: Best results are achieved when the highest voltage in your chosen range is tested first. Then work towards the lowest voltage in your chosen range.
   - Tip: It is unlikely that the multimeter will settle on a number throughout testing. To ensure all samples are treated as equally as possible, use a timer (count-up mode) and record the reading on the multimeter as soon as the time is up (or a similarly consistent system that suits your needs).
7. After the first voltage is tested, use the knobs to apply the next voltage. Allow the circuit to equilibrate for 5 s. Record the current reading on the multimeter.

- Tip: Test a range of at least four voltages. This system is not very sensitive and water-based materials are difficult to characterize. That creates challenges for achieving a linear current-voltage curve (necessary for calculating resistance). At least 3 points are needed for a current voltage curve, so testing 4+ voltages allows you to delete 1 or 2 rogue data points.
- Note: Try to use the same current reading setting on the multimeter throughout testing. However, if the multimeter ever displays a 1 during testing, the maximum value for that range has been surpassed, and you will need to switch the dial to the left to increase the range. If the multimeter ever displays a 0 during testing, the minimum value for that range has been surpassed, and you will need to switch the dial to the right to decrease the range.

8. Repeat step 7 until all voltages in your chosen range have been tested.
9. Turn the power supply to 0 V and the multimeter to the lowest current reading setting.
10. Wait until the multimeter reads 0 μA before raising the jaws of the angle vise off your material. Support the top brass plate during this process, then move it to the side.
11. Use a spatula to slide your material off the bottom brass plate. Measure the material's diameter and thickness using calipers.
12. Repeat this process for each sample, making sure to wipe the brass plates dry before beginning a new round.

Data analysis

Use the accompanying spreadsheet for analyzing conductivity data. All formulas for calculations should be pre-populated.

1. Plot the current-voltage curves and analyze for linearity. R^2 values of ≥0.9 are acceptable. Plot voltage along the x-axis and current along the y-axis. Identify points whose removal improves the R^2 value of a linear curve fit.
2. Calculate the resistance (*R*) of your material using the following equation:

$$V = IR \rightarrow R = \frac{V}{I}$$

3. Note: Be sure to convert units. Voltage should be in volts (V) and current should be in amps (A).
4. Calculate the cross-sectional area (*A*) of your hydrogel and convert the units so they are in cm^2.
5. Convert thickness (*t*) to cm.
6. Calculate conductivity using the following relationship dictated by Pouillet's law:

$$\sigma = \frac{t}{RA} \left[\frac{S}{cm}\right]$$